Vehicle Ride Under Transient Conditions Using Combined On-Road Testing and Numerical Analysis

By

Mohd Azman Zainul Abidin
B.Eng, MSc

A thesis submitted in partial fulfillment of the requirement for the award of the Degree Doctor of Philosophy of Loughborough University

Wolfson School of Mechanical and Manufacturing Engineering
Loughborough University

Nov 2005

Loughborough University

CHAPTER TITLES ON THE TOP OF EACH PAGE THROUGHOUT THE BOOK ARE VERY PALE

Abstract

The thesis outlines a hierarchical modelling methodology for investigation in vehicle dynamics, in particular for combined ride and handling manoeuvres. The methodology involves the use of detailed multi-degrees of freedom models of vehicles with the inclusion of sources of non-linearity, using a multi-body approach, based on Lagrangian dynamics for constrained systems. It also includes the use of simpler and task-specific models, formulated in Newton-Euler approach. These simpler models with lower degrees of freedom, but with appropriate level of detail are more efficient in the study of specific, but non-trivial problems such as transient behaviour of vehicles in combined ride and handling, as encountered in many routine daily manoeuvres.

The modelling methodology is supported by careful vehicle testing, both for validation of the proposed approach, and assessment of the extent of applicability of simple, intermediate and multi-degrees of freedom full-vehicle models. Certain important vehicle handling and ride characteristics in pitch plane dynamics, roll behaviour, vehicle body bounce and combination of these have been studied, as well as the effectiveness of restraining action of chassis elements, such as the semi-leading and trailing arms for passive control of vehicle squat and dive motions, arising from acceleration from coast to drive and deceleration/brake of vehicle from drive to coast. Combined pitch and bounce motions have been studied when negotiating speed traps such as bumps, which also combine with significant body roll when single event obstacles of this kind are introduced.

The novelty of the research is in the detailed integrative numerical-experimental approach, and the development of intermediate models that adequately predict vehicle behaviour under steady and non-steady conditions for a wide range of ride and handling manoeuvres.

The investigations have culminated in a significant number of findings of practical use, particularly the ineffectiveness of anti-squat and dive features when combined pitch and bounce motions limit the usefulness of these devices. On the contrary, excessive roll dynamic behaviour of the vehicle is effectively palliated by the anti-roll bar, even under complex combined pitch, roll and body bounce such as those experienced in negotiating single event speed bumps.

Good agreement is found between the predictions of the intermediate model and those of the multi-body model and the actual vehicle tests, particularly for pitch and bounce dynamics.

Keywords: Vehicle dynamics, ride, transient motions, pitch plane and roll dynamics, intermediate modelling method, multi-body dynamics, vehicle testing

ACKNOWLEDGEMENT

The author wishes to express his sincere thanks to his supervisors, Professor Homer Rahnejat and Paul King for their support, guidance, help and motivation. Their invaluable suggestions and comments helped in preparation of journals, thesis and throughout the whole PhD research.

Sincere thanks are also due to SIRIM BERHAD for sponsorship of this research

The author is grateful to Professor T.J. Gordon (Michigan University) for his suggestions & contributions during early stages of intermediate vehicle model development.

I wish to thank my wife, Roshaiza and my two daughters, Maisarah & Diyanah for their support and their patience throughout my PhD research. I also would like to thank my parents, brother, and sisters who have consistently encouraged me to do my best in my PhD.

Finally, I would like to give special thanks to all my friends and colleagues for their support and encouragement.

TABLE OF CONTENTS

NOMENCLATURE

Symbol	Description
$A_{1...4}$	Matrix $M_{2...5}$ multiply by inverse M_1 respectively
$B_{1,2,3}$	Matrix M_6, M_7, M_8 multiply by inverse M_1
$\mathbf{F}_{aero}$	Aerodynamics force
$\mathbf{F}_{weight}$	Vehicle weight
$\mathbf{F}_{tyres}$	Tyre forces
$F_{x1}, \cdots, F_{x4}$	Longitudinal tyre forces
$F_{y1}, \cdots F_{y4}$	Lateral tyre forces
$F_{z1}, \cdots F_{z4}$	Vertical tyre forces
F_a	Actual tyre forces
$F_t^{\max}$	Nominal maximum 'rim contact' tyre force
G	Vehicle centre of gravity
H_0	Angular momentum
$\mathbf{I}_G$	Inertia matrix of vehicle
$\mathbf{I}_{xx,yy,zz}$	Roll ,pitch and yaw moment of inertia about mass centre
$\mathbf{I}_{xz}$	Product of inertia
$\mathbf{I}_3$	$n \times n$ identity matrix
KI,KP	Integral and propotional gains
$\mathbf{M}_{tyres}$	Moment about G from tyre forces
$\mathbf{M}_1$	Generalised mass matrix
$\mathbf{M}_2, \mathbf{M}_3, \mathbf{M}_4$	Matrix coefficients arising from the bilinear gyroscopic terms
$\mathbf{M}_5$	Matrix coefficient from aerodynamic drag
$\mathbf{M}_6$	Matrix consisting the sum of all the applied forces and body dimensions and gives the main contributions from the tyre force inputs
$\mathbf{M}_7$	Matrix containing the moment effect of dynamic suspension deflections $\tilde{\mathbf{z}}$
$\mathbf{M}_8$	Matrix containing gravity term
M_0	Moment of inertia
M	Vehicle mass
P	Nominal contact patch centre
Q	New position of P obtained by translating Q in body-z axes
R	Actual vehicle orientation
$R_{1,2,3}$	Orientation matrix in roll, pitch and yaw axis
$R^{\{B \to G\}}$	Passive rotation matrix that converts from the body to the global coordinates, using Euler angles
T_d	Drive torque (assumed to be generated from an inboard differential)

U, V	Longitudinal and lateral velocity
ε_1	Deviation of actual speed from desired speed
ε_2	Directional error between where the car is pointing and where it should be going
e_2	y-axis base vector for the tyre coordinate system
e_3	Unit vector(upward) normal to the road surface at *S*
g	Gravity
$\mathbf{k}$	Unit vector of the global z direction, relative to the vehicle coordinates
k_{aero}	Aerodynamics drag coefficient
$\mathbf{n}_S$	Unit vector(upward) normal to the road surface at *S*
$\mathbf{n}_B$	Unit vector in body-z
p, q, r	Angular velocity in x, y and z-axis respectively
$\mathbf{r}_G$	Distance of the contact patches from center of gravity
$\mathbf{r}_P$	Position of the nominal contact patch centre in global coordinate
$\mathbf{r}_P^{\{B\}}$	Position of the nominal contact patch centre in the vehicle body coordinates based at *G*
$\mathbf{r}_S$	Position of the nominal contact patch on road surface
$\mathbf{r}_A(z_{sus})$	Kinematics term which account for steering torque
$\mathbf{v}$	Unit vector normal to the wheel-plane
$\mathbf{v}_G$	3 components of translational velocity
$\mathbf{v}_Q$	Velocity of point Q moving within the plane (road surface)
$x, \dot{x}$	State and state derivative variables
$\mathbf{x}_4$	Set of x-coordinates at the four tyre contact patches
x_P, y_P	Position of point *P* from center of gravity in x-y plane
y_1	Acceleration/brake command
y_2	Steering angle
z_4	Set of z-coordinates at the four tyre contact patches from cg
z_s	Suspension deflection
z_t	Tyre deflection
$z_t^{\min}$	Maximum tyre compression
$z_t^{\max}$	Loss of tyre contact, where $F_t \to 0$
$\tilde{\mathbf{z}}$	Suspension deflections
S, S_{ref}	Actual and desired speed
β	Vehicle direction (yaw angle)
θ_v	Angle of the reference vector of vehicle in global coordinate;
$\boldsymbol{\omega}$	3 components of angular velocity
$\theta_1, \theta_2, \theta_3$	Roll angle, pitch angle and yaw angle respectively
$\dot{\theta}_1, \dot{\theta}_2, \dot{\theta}_3$	Derivative of roll angle, pitch angle and yaw angle respectively
φ, θ, ψ	Roll angle, pitch angle and yaw angle respectively

$\omega_1, \omega_2, \omega_3$	Body angular velocity, roll axis, pitch axis and yaw axis respectively
λ	Sum of the suspension and tyre deflections
μ	Expansion velocity of the suspension-tyre combination
$\delta x, \delta y$	Contact patch forward progression and lateral scrub respectively
$\delta\nu$	The change in the caster angle
δz	Suspension vertical changes
ϕ	Actual steer angle
ν, ρ	Caster and camber angle
γ	Lateral inclination angle
δ	Static toe angle
$\delta_k(z_{sus})$	Kinematics term which accounts for bump-steer
$\rho(z_{sus})$	Kinematics term which accounts for bump-camber

GLOSSARY OF TERMS

Terms	Description
ABS	Antilock Braking System
ADAMS	Automatic Dynamics Analysis of Mechanical System
CAE	Computer Added Engineering
CPM	Cycle per Minute
DAQ	Data Acquisition
DNS	Dynamics Non-linear Spatial
DOF	Degree of Freedom
DYC	Direct Yaw Control
FEM	Finite Element Modal
GPS	Global Positioning System
INS	Inertial Navigation System
LHS	Left Hand Side
LLTF	Lateral Load Transfer
LPM	Lump Parameter Mass
LVDT	Linear Variable Differential Transducer
MBF	Multi-Body Formulation
NVH	Noise, Vibration & Harshness
RHS	Right Hand Side
SAE	Society of Automotive Engineering
SVC	Static Vehicle Characteristic
TCS	Traction Control System
4WS	4 Wheel Steering

LIST OF FIGURES

Chapter 3

Chapter 5

Chapter 5

Chapter 6

LIST OF TABLES

Chapter 4

Chapter 5

CHAPTER 1
Introduction

1.1 Preamble

Modelling and simulation of vehicle dynamic behaviour plays an important role in its development for good ride and handling performance characteristics. The main objective for modelling and simulation is to reduce vehicle development time and the associated costs. Modifications and subsequent testing of computer models can be achieved faster and can be assessed in a more repeatable manner, using simulation techniques than relying on physical prototyping alone. There is also the potential benefit that a vehicle may not even have to be built for the initial conceptual design studies.

Current practice tends to promote the use of highly detailed modelling techniques, which include nearly all the vehicle parts that are thought to be significant in its dynamic behaviour. The implication is that, although still more efficient than using prototype vehicles, setting up a computer simulation can be a very time consuming and costly exercise. Besides, the complexity of large models can sometimes reduce the reliability of their predictions, especially when the model is constructed during the hectic process of development and design (Willumeit et al., 1992). Such circumstances often result in simulation projects, which can only confirm the design and measurement, but seldom contribute to a better design, before various test vehicles are built. Part of the problem lies with the large requirement for input data from a diverse range of sources, including dynamic tests (for inertia data), technical drawings and component data sheets. Due to these problems there is a strong case to be made for a simplified modelling approach. Sayer (Sayers and Han, 1996) have suggested that one can use a basic vehicle model with sufficient detail from sub-systems to deliver realistic simulation results.

1.2 Problem Definition

There has been considerable interest in recent years among large motor manufacturers to try to quantify vehicle responses to particular manoeuvres through the construction of complex multi-body models such as those usually constructed in ADAMS. These packages offer a comprehensive modelling environment, which suits all scenarios and allows the design engineer to predict the effect of component level modifications on the system performance. However, this approach is very time consuming, and many interactions can lead to erroneous conclusions. Detailed component geometry, material specifications, etc are often required to build a competent model, where in most situations it is extremely difficult or sometimes even impossible to collect the numerous data from a vehicle. In many cases the data is estimated or, even worse, incorrectly measured. This can lead to fundamental inaccuracies that can be difficult to detect.

Even though packages like ADAMS have become an industry standard (mainly to reduced non-compatibility between organisations), they often represent an overkill in many instances. Although programs like ADAMS will always be required, other computational tools with subtly different architecture do have their place, and in some instances, are more acceptable for specific applications, where more complexity only serves to detract from the analysis process.

More versatile programs would exhibit a modular structure, where the engineer chooses the parameters, which are most influential on the vehicle's performance using engineering judgement. This allows computational efficiency to be increased so that the engineer may focus upon the most significant results. Also if a program has open architecture then a model can evolve to a relevant level of sophistication.

Therefore, an aim of this research is to create a hierarchical modelling philosophy in which a combination of a complex multi-body model and a simpler intermediate one can be used to deal with a range of vehicle dynamic problems, where the level of complexity determines the use of one or the other, as well as the interactions between the two. In some ways this approach may appear to be a step backward, but the simpler models provide some of the answers to the problems created by the

more complex modelling software. While too much complexity has its own set of problems, too simple a model also limits the type of analysis, which can be conducted. Therefore, the work carried out in this thesis is intended to bridge this gap and introduce an intermediate vehicle model.

In line with the main aim and specific objectives, outlined in section 1.3, the requirements for the envisaged model are:

i) It has to be based on an open platform software
ii) The software must be widely available and reasonably inexpensive
iii) It must be easy to be modified for future revisions for specific developments on vehicle sub-system problems

Generally, the overall success of any simulation model depends upon:

i) The model formulation
ii) The input parameters
iii) The precision in programming
iv) Numerical accuracy and stability

For the work carried out in this thesis, model formulation represents an important focus. The model will have large angular movement with sufficient representation of driver input, driveline model, steering model, tyre model, suspension model and road profile. Special attention will be paid to the representation of the model of the suspension (especially the kinematics/compliance characteristics), since this sub-system is as equally important as the tyre model for realistic movements of the wheels.

Using this model several types of vehicle dynamic tests are to be investigated. The study is focused on real-world scenarios, where the vehicle is subjected to intermittent driving conditions in an urban area, where 'speed bumps' are deployed as a traffic calming measure. The effectiveness of anti-squat, anti-dive and anti-roll bar geometry on the pitch and roll plane dynamics of the vehicle are investigated under such complex manoeuvres.

The accuracy of the results achieved (the very reason for increasing the model complexity) would still be in question. Any model needs to be interrogated against measurements obtained from real vehicle tests and existing software solutions to verify the extent of accuracy of its predictions, or at least highlight areas that require further development.

1.3 Aim and Specific Objectives

The main aim is to develop an intermediate vehicle dynamic model, which is neither too simple nor too complex and is suitable for various types of vehicle combined ride and handling studies intended in this thesis. Moreover, this high-fidelity vehicle model can also form an effective basic model for future work, especially in the area of control system performance. The development of this model will be preceded by initial studies, where several simple vehicle models will be developed in order to give a better understanding of the actual work.

Basically there are 3 fundamental objectives in order to establish the proposed modelling strategy:

i) To establish simple vehicle models with different assumptions and levels of complexity.

ii) To establish a rigid six-degree-of freedom (6DOF) vehicle model that incorporates a steering system, a suspension system, representation of driver input, a driveline model, a tyre model and different road profile effects.

iii) To establish a suspension system that features:
   a) Kinematics due to the suspension geometry (camber changes, caster changes, toe changes, wheel centre displacements; in lateral and longitudinal directions).
   b) Compliance bushing effects
   c) Anti-roll bar effects
   d) Anti-dive and anti-squat effects

In order to establish a high fidelity intermediate vehicle model several more objectives need to be achieved:

i) To establish a virtual suspension test rig for the extraction of suspension characteristic information from a detailed multi-body non-linear model

ii) To investigate the effect of a "speed bump" on the pitch plane dynamics of a vehicle with anti-dive/squat features

iii) To investigate the effect of a "speed bump" on the roll dynamics of a vehicle with an anti-roll bar system

iv) To conduct on-road vehicle testing for verification purposes

v) To analyse and compare the results from actual vehicle testing with those from the detailed multi-body and the intermediate models

1.4 Structure of the Thesis

This thesis consists of eight chapters with appendices laid out as follows:

Chapter 1: A introductory chapter which provides a brief overview of vehicle development, especially that concerning the development of the vehicle modelling. It also defines the problems, the aims, the objectives and the structure of the thesis.

Chapter 2: Provides a literature review of the work carried out elsewhere, relevant to the research work carried out in this thesis.

Chapter 3: Describes the development of an intermediate vehicle model, including how the intermediate model is constructed in a Matlab/Simulink environment

Chapter 4: Describes the more complex vehicle model and the virtual test rig for extraction of suspension compliances.

Chapter 5: Describes the on-road vehicle testing conducted, under various manoeuvres.

Chapter 6: Presents the results of simulation studies and the vehicle tests

Chapter 7: Presents the overall conclusions of the research, a critical assessment of the results and suggestions for future work.

Chapter 2
Literature Review

2.1 Introduction

This chapter provides a review of literature in the area of vehicle dynamics and the various modelling approaches. In sub-system modelling, however, the emphasis will be given to assessment of vehicle chassis, suspension, tyre and steering system. A list of related publications is given in the list of references at the end of the thesis, while some of the most relevant topics are highlighted in the following sections.

This chapter first describes the two main modelling approaches used in the area of vehicle dynamics, and benchmarks them against one another. Both these modelling methods have been employed later in the thesis. Subsequently, a comprehensive review of literature in modelling of ride and handling issues is given, which are relevant to specific problems tackled in the later chapters.

2.2 Overview of vehicle dynamics modelling

Development of vehicle models was first introduced in the early 1950's after research into tyre dynamics led to a better understanding of how forces were generated. These early models were derived and solved using hand calculations and, therefore, had only a few degrees of freedom (DOF)(Gillespie, 1992). Nowadays, due to increased availability of computational tools, the development of vehicle modelling has become slightly easier and more widely studied. Models developed vary greatly in their capability, complexity, number of degrees of freedom, and the amount of input data required for simulation. There are many software packages available and the approach also can vary depending on the requirement or facilities available to the analyst

2.2.1 Modelling approaches

Two main methods (Sayers and Han, 1996, Segel, 1956) have been used in the development of vehicle dynamic models, the first of which uses a traditional approach, which is sometimes called the lumped parameter mass approach (LPM). This involves derivation of a number of simultaneous differential equations of motion, using Newton-Euler formulation, leading to the solution of these by direct integration. The second method, which is referred to as multi-body formulation (MBF) uses a computer to generate the equations of motion for a system represented by a number of rigid bodies, connected together by joints and internal forces. The equations of motion are usually automatically generated, using constrained Lagrangian dynamics. An example of a modelling code that uses this technique is ADAMS. Overview of the application of this technique to vehicle modelling is explained by Rahnejat (Rahnejat, 1998) and Sayer (Sayers and Han, 1996). The technique attempts to generate a dynamic model of a vehicle that is as close as possible to the real system. This is conceptually appealing, but eventually becomes extremely complicated in terms of the input data requirement and the number of equations generated, some of which are never used due to the imposed constraints.

The specific differences between these two approaches are further discussed in the following section.

2.2.1.1 Efficiency

The LPM approach has the advantage of allowing the analyst to include or to ignore certain effects at the time of model development(Willumeit et al., 1992). These assumptions or simplifications, made during model development, include those made while discretizing the system, and have a direct bearing on the accuracy of the simulation results. The resulting models only contain as many degrees of freedom (DOF) as are judged to be needed. Also, since many of these are custom made, one can easily include particular forcing function, peculiar to a system under consideration.

In the MBF approach, the analyst does not have the luxury of selecting the number of DOF(Blundell, 1999). Generally, every body is assumed to have 6 DOF and later the unwanted DOF are constrained, using holonomic or non-holonomic functions, which are non-linear algebraic equations. As a result a mix of differential-algebraic equations are obtained. MBF requires huge matrix operations and iterative techniques to satisfy the kinematics constraints. Consequently, these codes are computationally not very efficient for simple vehicular investigations. They are, however, very useful in large investigations. This also limits the use of MBF simulation in real time applications, highly iterative design optimisation, or interactive use. However, recursive MBF based approach can be used in real-time when parallel processing is used (Allen and Rosenthal, 1994). In a study carried out by Anderson (Anderson and Hanna, 1989), it was found that the Jeep (the vehicle model used in that study) needed more than 500 equations, when modelled through ADAMS. The same vehicle model was modelled as a LPM with 10 DOF, thus requiring only 10 second-order differential equations.

2.2.1.2 Modification ability

In the LPM approach, the model is for a specific vehicle configuration. If the vehicle under consideration is constructional different, then an equivalent vehicle has to be defined to use the available equations of motion. This can be very labour intensive. However, within the specific vehicle configuration the LPM approach seems to have easier access and is simpler to modify. In the MBF approach(Neto, 1994), vehicles with different configuration or any major design changes can be easily accommodated, by modifying the input file that describes in detail every vehicle component and their connectivity. However, for the input data file for each component must first be developed.

2.2.1.3 Human effort

In the LPM approach, the analyst must put much effort in deriving the equations of motion, then coding and validating them. This process is error prone. However, software packages like Mathematica or Matlab can reduce this task and the

associated risk. In the MBF approach(Allen and Rosenthal, 1994), the codes are believed to function properly. Here, the analyst is relieved of derivations of equations of motion and the constraint functions for assembly of parts, but the main effort is now shifted to modelling every component in great detail, using a variety of predefined elements and in keeping track of the system DOF, those reduced by kinematics constraints, and special considerations due to joint axes and their intersections/orientations. Another factor, which relates to human effort is the amount of required input data which are needed to be collected before the model is ready for use in a simulation study. For the MBF approach, the input consists of component geometry and its inertial properties, reference frame definitions, body types, body compliance description, topological and analytical constraints, applied forces and motion actuators, and any employed control laws. The LPM approach requires parameters of discretized elements.

Another important human factor is proficiency. With only a basic understanding of dynamics, analyst can derive equations of motion for simple systems, putting the constraints automatically, whereas MBF requires advanced user training. On the other hand, for larger and more complex models the converse of this argument is likely to be true.

2.2.1.4 Potential use

In the LPM approach, by the way the model has been defined through composite parameters, it is easy to make comparison between different vehicles' performance. This allows changes in the design to be studied directly. For example, in the LPM approach of the investigation of the effect of rear suspension roll steer on the vehicle direction response only this parameter can be changed independently of other input parameters (Sayers and Han, 1996). In the MBF approach, to account for this change, suspension pickup points and suspension link lengths need also to be altered. After these changes are made, a check is necessary to determine that they have not affected other suspension characteristics. However, it should be pointed out that relating the composite parameter changes in the LPM approach to the physical component changes is not an easy task. MBF simulations are most useful in

determining structure loads, large motion analysis, while LPM approach is more suitable for small motion analysis(Willumeit et al., 1992).

Quite often, one of the main purposes of vehicle simulation is to provide a means of predicting the handling qualities in the design stage. The designer may use simulation results to rule out some of the many proposed prototype designs, and only those, which meet the design objectives, lead to physical prototypes for further testing. Until this stage, not all the required parameters for simulation can be estimated or calculated. Typically, the designer uses handbook values, as such a detailed vehicle model need not necessarily give better results than a less complex model, unless the former model is complemented by accurate input parameters. On the other hand, (Willumeit et al., 1992) argue that various problems concerning dynamics of vehicles can be reliably solved with comparatively simple models.

2.2.2 Simulation software

There are number of programs available on the market to support vehicle development. From the two approach described in the previous sections, the relevant software can also be divided into two classes. For modelling using traditional approach probably the most common software used are MATLAB, EASY5, ACSL, MATRIXx, MathCAD, Mathematica, DYMOLA, Maple and VHDL-AMS as mentioned by Valasek (Valasek et al., 1999). There is one program called CarSim (Sayers, 1989) , which is one of the products offered by AutoSim in the LISP programming language. This software is programming software but using MBF approach. The free version can easily be obtained from the Internet. It is in an executable format, so understandably, it is difficult to develop without obtaining the developer code from the designers. The details behind this program are shown in a paper written by Sayers (Sayers and Han, 1996). Another study conducted at the University of Leeds (Crolla et al., 1994), attempts to position these simpler models with respect to multi-body programming. The paper specifically describes the development of Vehicle Dynamics Analysis Software (VDAS), which is a design tool-kit for use in the prediction of vehicle ride and handling behaviour.

Other multi-body codes that have been developed include: ADAMS, Simpack, TruckSim VEDYNA, A'Gem, BAMMS, FASIM, LMS/ IMITIA, MADYMO, MEDYNA, 3D MCADA, MECANO, NEWEUL, NUSTAR, ALASKA, DADS, MESA VERDE, PAMCrash, FEDEM,. It should be noted, however, that many of these codes are not commercially developed. They may have been written solely for research purposes and would not, therefore, be inappropriate for commercial applications. Further information regarding multi-body computer codes can be found in reference (Kortum and Sharp, 1993). However, it is somewhat out of date, but can still be considered as a useful reference.

Although MATLAB is not strictly considered as a vehicle dynamics package, together with Simulink it offers all the necessary tools to mathematically define and produce ' simple vehicle models for ride and handling analysis. MATLAB offers a huge range of mathematical manipulation and computational analysis tools. It is an open platform software which is easy to alter and optimise. SIMULINK provides a graphical user interface for producing block diagram

The open architecture of the Simulink system allows a great deal of freedom in the optimisation of developed model.

2.3 Overview of vehicle ride and handling

Traditionally ride and handling characteristics of a vehicle have been considered to be different issues(Genta, 1997). Ride quality is concerned with the sensation or feel of the passenger in the vehicle. Ride comfort problems mainly arise from vibration of the vehicle body, which may be induced by a variety of sources including surface irregularities, aerodynamic forces, vibration of engine and driveline, and non-uniformities of the tyre/wheel assembly. In contrast, handling characteristics are associated with the ability to control the directional motion of the vehicle and the ability to stabilize it against external disturbances. Previously compromise needed to be established between these two issues for normal passenger cars. However, advanced technologies such as active suspension systems (Acker et al., 1991) or active anti-roll bars (Ottgen and Bertram, 2001)can integrate these two issues,

without losing any of the required qualities. Indeed ride and handling cannot be separated in the modern vehicle development. As most vehicles are subjected to all road conditions, involving an increasing demand on their manoeuvrability combined ride and handling performance cannot be ignored.

2.3.1 Ride Comfort

The quality referred to as "ride comfort" is affected by a variety of factors, including high frequency vibrations, body bounce, body roll and pitch, as well as the vertical spring action normally associated with a smooth ride (Happian-Smith, 2002). If the vehicle is noisy, if it rolls excessively in turns, or lurches and pitches during acceleration and braking, or if the body produces a bouncy resonance, occupants will experience an "uncomfortable ride." The ride quality normally associated with the vehicle's response to bumps is a factor of the relatively low frequency bounce and rebound movements of the suspension system. Ride is perceived as most comfortable when the natural frequency of the sprung mass (i.e. the vehicle body) is in the range of 60 to 90 cycles per minute (CPM), or about 1 Hz to 1.5 Hz(Gillespie, 1992). When the frequency approaches 120 CPM (2 Hz), occupants perceive the ride as rather harsh. Consequently, the suspension of the average family sedan will have a natural frequency of about 60 to 90 CPM. A high-performance sports car will have a stiffer suspension with a sprung mass natural frequency in the range: 120-150 CPM (i.e.2-2.5Hz). Note further that the natural frequency of the unsprung mass (the suspension system itself, in the range 15-20 Hz) is usually set an order of magnitude higher than the vehicle, in order to guard against possible resonance. A "good ride" depends on the overall design of the vehicle, rather than just the design of the suspension system. To produce a comfortable ride, the high-frequency vibrations of wind and drivetrain noise must be minimized and properly isolated, and the suspension must be set in appropriate rubber mountings to isolate high-frequency induced vibrations. However, the natural frequency of the suspension system is still considered the most important element in determining the ride comfort. It is also noteworthy that transmission of any relatively large amplitude motion in the frequency range 8-12 Hz for any prolonged period can lead to severe passenger discomfort as this represents the range of natural resonance of human gut, and

explains the reason for motion sickness suffered by some passengers, and particularly those aboard ships or aeroplanes under unsteady environmental effects.

To illustrate how important the effect of other sub-systems (than the suspension itself) can be upon ride comfort of vehicles, note that for most sedans throttle induced tip-in and back-out (fore and aft) motions with sudden throttle action is around 2.5-7 Hz, usually referred to as shunt. Another effect is the kangaroo type motion of a vehicle with sudden release of the clutch, known as take-up judder (at 7-10 Hz for most vehicles) (Matschinsky, 2000).

2.3.2 Handling

According to Newton's first law of motion, a moving body will continue in a straight line uniform motion, until it is acted upon by a disturbing force. Newton's second law refers to the balance that exists between the disturbing force and the reaction of the moving body. In the case of an automobile, whether the disturbing force is in the form of a wind-gust, an incline in the road, or the cornering forces produced by tyres, the force causing the turn and that resisting it will always balance. Vehicle "feel" and handling characteristics have to do with the way in which the vehicle's inertial forces and the cornering forces of the tyres equilibrate. The magnitude and vector of the inertial forces are established by the vehicle's weight and balance. In a turn, angular acceleration results in a force that is centred at the vehicle centre of gravity and acts in a direction away from the turn centre. The ability to overcome these forces and produce a controlled, stable turn depends upon the combined characteristics of the suspension and the tyres. The job of the suspension system is to support, turn, tilt and otherwise manage the tyre-road interactions and their relationship to the vehicle and the ground in a way that will maximize their capabilities. The primary motions associated with the handling behaviour of a vehicle are longitudinal , lateral and yaw motions. However, when considering the limits of handling characteristics, the roll, bounce and pitch motions will have to be taken into account, because this will eventually affect the steering response of the vehicle.

2.4 Vehicle Modelling

As mentioned in the previous section, there are two methods that can be used in modelling vehicles, and both of these can be employed at different levels of complexity. Both methods have been employed in this thesis.

The complexity of vehicle model can be generally divided into two categories, these being linear and non-linear models. For fundamental studies of vehicle dynamics, it is useful to develop a linear model as such a 2-DOF bicycle model. Examples have been described by (Ellis, 1994), (Abe and Kano, 1999), (Willumeit et al., 1992),(Kiencke and Daib, 1997), (Mokhiamar and Abe, 2001), (Pongsathorn et al., 2002) and (Tran, 1992, Pacejka, 2002, Genta, 1997). The simple linear model is useful for studying the basic steering and handling response of a vehicle without the complications introduced by suspension systems and non-linear tyre models. The useful range for linear models for passenger cars is assumed to be up to 0.3g as demonstrated by Segel (Segel, 1956). The following assumptions are generally used for development of linear models:

- Small steering angle
- Linear tyre behaviour
- Constant forward speed
- Smooth and flat roads
- All angles are small so that the cosines are equal to one.

At higher lateral accelerations(greater than 0.3g)(Abe et al., 1996, Pacejka, 2002), linear assumptions are no longer valid and non-linear behaviour has to be included in the model. Thus, these models must also consider:

- Tyre forces and moments
- Bump stop forces
- Rebound stop forces
- Suspension kinematics
- Steering characteristics
- Spring/damper characteristics
- Other features, such as anti-dive/squat, anti-roll bar, aerodynamics etc

Such level of complexity is used and described by various authors, such as (Willumeit et al., 1992), (Schuller et al., 2001), (Makita, 1999), (Zbigniew, 1994), (Lugner and Mittermayr, 1989), (Sayers, 1989), (Hegazy et al., 2000), (Rahnejat, 2000) and (Cooke et al., 1997),(Pacejka, 2002). Advanced models integrate proper steering system, suspension system, different level of complexity in tyre models, engine system, transmission system and control systems.

2.4.1 Chassis (Degrees of freedom)

The complexity of a mathematical model of a vehicle can vary greatly, depending upon the problem, which is to be investigated. However, the analyst must be aware of the limit of validity of the model, depending on the assumptions made. The simpler the model is, the less likely that it can be used for other types of analysis.

(Abe, 1999, Abe and Kano, 1999),(Mokhiamar and Abe, 2001) and (Esmailzadeh et al., 2003) have developed basic 2-DOF linear vehicle models for initial studies of improving handling and safety, using Direct Yaw Control (DYC). In these models, the vehicle forward speed is considered a major stability parameter and assumed to be constant. Other assumption is that the lateral acceleration remains small, where lateral tyre force is considered to be proportional to the steer angle. Similar models were also developed by (Tran, 1992),(Yamamoto et al., 1989) and (Abe, 1989) to study handling performance of vehicles with additional rear wheel steering systems. An interesting paper by (Ryu et al., 2002) proposes a 2-DOF model to estimate vehicle sideslip angle, using a Kalman filter integrated with a Global Positioning System (GPS) and an Inertial Navigation System (INS). The results were very promising, however, the test were still using linear tyre models and at low lateral accelerations. The 2-DOF models have proven satisfactory, where the vehicle behaves like a linear system, with constant forward speeds, low lateral acceleration and small amount of sideslip as also demonstrated by (Pongsathorn et al., 2002). Application of 2-DOF models can be further extended as suggested by(Shin et al., 2001). He recommended that by modifying the tyre cornering stiffness the 2-DOF models can be used in the non-linear region without losing the advantage of their simplicity.

In spite of inaccurate predictions in non-linear regions, the 2-DOF models are still widely used in many control applications, because of their simplicity and the minimum requirements for inclusion of vehicle parameters. The limit of validity of the 2-DOF models can be further increased by removing linear tyre models and replace them with non-linear tyre models as demonstrated by (Best and Gordon, 2002) and However, one of the conclusions made by (Uematsu and Gerdes, 2002) stresses that the relative merits of robustness and responsiveness cannot easily be judged in a simple model. Thus, more detailed vehicle models would probably be a sensible approach.

Slightly more complex models have 3 DOF, and were developed to include longitudinal direction by(Horiuchi et al., 1999a), (Roukieh and Titli, 1992) and (Rossetter and Gerdes, 2000). However, the 3-DOF models have their own limitation due to linear tyre models. (Horiuchi et al., 1999b)in their studies for investigation of 4 wheel steering system (4WS) noted that these model become less effective when the tyres approach their limits of adhesion. Other 3-DOF models were also used by (Chen et al., 1996), (Nagai et al., 1997) and (Shino and Nagai, 2001). However, they all use non-linear tyre models to increase the limits of the validity of their analysis. There are also 3-DOF models developed by (Sharp, 1999), (Li, 1992) and (Kleine and Niekerk, 1998). However, due to differences in objectives of the analyses the degrees of freedom introduced into the models were also different. (Sharp, 1999) and (Li, 1992) were more interested in the investigation of longitudinal manoeuvring, where vertical dynamics, longitudinal dynamics and pitch dynamics were the main parameters, while (Kleine and Niekerk, 1998) was more concerned with cornering analysis, thus, lateral, yaw and roll dynamics were of primary concern.

As already mentioned the simpler models tend to restrict the range of analyses, which can be conducted. Hence, establishing 4-DOF models can provide a greater degree of applicability. Such models were used by (Tandy et al., 1992), (Chu et al., 2001)and (Lukowski and Medeksza, 1992) for their studies on vehicle cornering behaviour and also by (Lin et al., 2004) and (Savkoor and Ausejo, 1999) for handling studies of driver-vehicle interactions. (Harada and Harada, 1999) used a 4-DOF model for slightly different purposes, where the work carried out was for integration

of steering system and suspension control, thus pitch plane dynamics were more important than the longitudinal motion.

(Doniselli et al., 1996) investigated aerodynamic effects on ride comfort and road holding of two types of vehicle model: a single-track vehicle and a two-track vehicle. The two- track vehicle, with 5-DOF was used as a complex model, where additional degrees of freedom in the vertical direction were introduced. A similar model was used by (Willumeit et al., 1992), also as complex model in comparing several levels of mathematical detail to study a vehicle's dynamic behaviour during its development.

Ultimately for lump mass parameter modelling, 6-DOF is regarded by most researchers to be the highest possible degree of freedom model, since the vehicle as a body can at most be represented by 6 degrees of freedom. For this level of complexity the model would normally deal with a huge range of analyses.(Pisu et al., 2003), (Li et al., 2001) and (Park et al., 2001)have used such models for vehicle chassis control monitoring studies, while (Minaker and Anderson, 1999), (Lozia, 1994) and (Plochl and Lugner, 1999) have developed their models for conducting studies on vehicle performance due to suspension system, and uneven road surfaces, as well as validating driver models. (Sayers and Han, 1996) and (Dickison and Yardley, 1993), however, have used their models for various types of analyses, which were closely related to ride and handling analysis.

2.4.2 Suspension Modelling

Suspension is one of the important systems in vehicle modelling and is probably the second most important element after the tyre model in vehicle handling. This is due to the fact that the movement of the wheels in lateral and longitudinal directions eventually affect the generation of forces on the tyre contact patch. Review of literature on suspension modelling, however, shows that there is a considerable volume of literature, which tend to omit the effect of suspension systems (Abe et al., 2001, Terry et al., 2001, Gordon et al., 1991, Savkoor and Ausejo, 1999) to simplify the analysis, especially those involved in study of control issues. There are also some who rather prefer to use simple representations of suspension systems, where

the wheel is just moving up and down with selection of linear or non-linear spring/damper characteristics, based on the type of analysis required (Chu et al., 2001, Esmailzadeh et al., 2003, Best and Gordon, 1998, Harada and Harada, 1999, Horiuchi et al., 1999a, Horiuchi et al., 1999b, Nagai et al., 2002) (Nagai et al., 2002, Savkoor and Ausejo, 1999, Uematsu and Gerdes, 2002, Shino and Nagai, 2001, Kiencke and Daib, 1997, Pongsathorn et al., 2002, Ryu et al., 2002, Rossetter and Gerdes, 2000)These approaches, in reality, do not represent the true movements of the wheels. The components in suspension system introduce movements at the contact patch and these have a direct implication on the generation of forces at the tyre contact patch. More detail in modelling of suspension system can be seen in other contributions, such as those by (Minaker and Anderson, 1999) and (Makita, 1999), where a linkage approach is used to represent characteristics of the suspension. (Sharp, 1999), however, has used different approaches, where suspension characteristics are represented by simple linear coefficients, which represent wheel caster and longitudinal changes relative to wheel vertical movements. Similar approach were also used by (Cooke et al., 1997) and (Willumeit et al., 1992). However, they included additional characteristics, which includes camber and steer effects. Other researchers such as (Yip et al., 1992),(Chen et al., 1996) and (Tandy et al., 1992) have used slightly different approaches, where instead of relying on wheel bump they have employed body roll as the relative reference.

Linear coefficients are easy to implement into the system. However, they may not be suitable for large displacement of wheels. In a notable paper (Watanabe and Sayer, 2004) investigated these issues, related to pitching and rolling dynamics of a car. He established two suspension models: one with linear representation of suspension kinematics and the other which was referred to as the full non-linear model, using tabulated functions for suspension stroke. The results for moderate levels of braking, acceleration, and cornering were in agreement using both these models. However, at higher suspension deflections, the non-linear model gave better predictions for roll and pitch behaviour. (Schuller et al., 2001)has also suggested the use of test data to represent suspension characteristics. Other features such as bump stop, kingpin inclination and anti-roll bar also play an important role as described by (Lozia, 1994) under lane change manoeuvres.

Embedding these characteristics in the vehicle model actually results in a rigid model of the suspension system. In other words, it is only a representation and does not simulate the actual suspension system. The more complex representation will have to include the elasto-kinematics of suspension systems. The elasto-kinematics effects are due to bushing deformation in the joints or even due to structural compliances. Such complex model have been used by(Schuller et al., 2001), (Plochl and Lugner, 1999, Dickison and Yardley, 1993), (Chen et al., 1996) and (Sayers and Han, 1996) and are discussed next.

2.4.2.1 Elasto-kinematics

By including characteristics such as camber, caster, steer and wheel centre changes, the model becomes virtually equivalent to having ball joints and rigid links in the suspension system. However for more realistic and complex representation of suspension systems, elasto-kinematics effects will have to be included in the model. Elasto-kinematics play a significant contribution to ride comfort of a vehicle. This is due to the fact that modern tyres have a high circumferential stiffness. Therefore, they respond minimally to circumferential force fluctuations (i.e. the disturbances generated in the tyres' circumferential forces) that may be of the same order as the wheel loading. Without elasto-kinematics effects of the suspension system, such as that introduced by the rubber bushes, the tyre forces can transmit to the vehicle body and to the passengers. This can cause ride discomfort. As noted by (Matschinsky, 2000) for vehicles intended to be comfortable, those force require a longitudinal compliance in the wheel suspension of as much as $\pm 15mm$. However, such compliance would cause unfavourable attitude change of the wheels. Based on the review of literature these effects are widely included in the MBS models, but not in the LPM models. Analysts using LPM models prefer to simplify the model rather than complicate them. However, the inclusion of elasto-kinematics can also be at different levels of complexity, based on the type of analysis to be conducted. (Chen et al., 1996) have included just one element of compliance, which is steering compliance for their work on handling behaviour.(Schuller et al., 2001), (Plochl and Lugner, 1999) and (Dickison and Yardley, 1993) have added one additional element, which is considered to be an important element for handling analysis, this being camber

compliance due to tyre lateral loads. (Dickison and Yardley, 1993) claim that for a more realistic representation of suspension model for ride and handling analysis, a complete hub compliance should be established, which should include longitudinal and lateral displacements of the wheel centre, steer, camber and caster compliance due to the tyre forces.

Thus far all the compliance effects, mentioned above, use linear coefficients, which are based only on tyre forces, and the suspension position does not contribute to this overall compliance effect. However, in reality the suspension is moving up and down, thus the torques acting on the bushing alter. However, this still requires further investigation to ascertain how far the vertical movement of the suspension affects the compliance of the suspension system.

2.4.2.2 Anti-dive/squat

Anti-dive is a suspension parameter that affects the amount of suspension deflection when the brakes are applied. When a car is decelerating due to braking, there is a load transfer from the rear axle onto the front axle proportional to the centre of gravity height and the rate of deceleration, and inversely proportional to the wheelbase (Happian-Smith, 2002). If there is no anti-dive element (feature) present, the vehicle suspension will deflect purely as a function of the wheel rate. This means that the spring rate only controls the forward dive of the vehicle. When anti-dive features are added, they will resist a portion of the transferred load to the front. The spring and the suspension arms are sharing the load in some proportion. If a point is reached, called the "100-percent anti-dive," the suspension arms resist the entire transferred load and nothing is carried through to the spring. When this happens, there is no suspension deflection due to braking and no visible brake dive occurs. There is still load transfer onto the wheels, but the chassis does not pitch nose down. On passenger cars, anti-dive is added to make the pitch motions under braking more tolerable for the occupants, because of the typical soft spring rates. The anti-dive is made the same for both sides of the car, because most people brake in a straight line, and there is no directional preference on the street or in road racing for that matter. Generally to achieve the above characteristics, a combination of two basic constituents is required. One involves the wheel centre being constrained to move

longitudinally, when it moves vertically on its suspension's freedom. This is called "translational anti-dive". The other involves the hub carrier (or the steering knuckle) rotating in pitch, when the wheel moves vertically. This will be referred to as "rotational anti-dive" as explained by (Sharp, 1999). These two parameters are the derivative elements in modelling anti-dive.

Anti-squat is actually similar in principal to anti-dive. However, it is not for braking, but for accelerating events. The objective is to prevent the rear end of the car from squatting under power as it accelerates and causes a rearward weight transfer. This is usually resisted by the introduction of semi-trailing arms.

2.4.3 Steering Modelling

Steering system is considered as an important sub-system in vehicle modelling. Steering causes camber at the tyre contact patch. Even though this sub-system plays a significant relationship with the wheel motions, many analysts have preferred the use of simplified steering models (Chu et al., 2001, Park et al., 2001, Shino and Nagai, 2001, Pisu et al., 2003, Esmailzadeh et al., 2003, Harada and Harada, 1999, Horiuchi et al., 1999b, Kiencke and Daib, 1997, Ryu et al., 2002, Horiuchi et al., 1999a) rather than complex multi-body-type mechanism models. These simple models use a steering ratio to represent the steering system in a vehicle model. More realistic steering models are mentioned by (Yip et al., 1992), (Cooke et al., 1997), (Lukowski and Medeksza, 1992), (Lozia, 1994) and(Pisu et al., 2003), where elastic properties and geometry of the steering system have been included. Basically, there are four components in establishing a steering system model as explained by (Willumeit et al., 1992). These are "the kinematics steering angle", static toe in/out, toe in/out as a function of compression and "elastic steering angle" under the effect of self-aligning torque. Another approach for modelling steering system is by separate components such as column, gearbox and linkage system, which is described by (Plochl and Lugner, 1999). This paper considers the dynamics response of the steering system in a realistic way, where inertial effects, as well as elasticity and damping are taken into account for steering column and the steering linkage. The steering gear-box is modelled as a power steering unit with a constant transmission ratio. The connection to the vehicle is achieved by the moments and

the angle at the spatially inclined steering axes of the wheel. Thus, the driver input finally results in time delayed steering angles of each of the front wheels.

2.4.4 Tyre

Tyre is the most important component of the vehicle system, due to the fact that it interacts between the vehicle and the road surface. There are three forces and three moments acting on the tyre from the road surface. These are normal (vertical), longitudinal and lateral forces, and the self-aligning, overturning and rolling resistance moments. A good estimation of these forces can yield an accurate simulation result.

2.4.4.1 Type of tyre model

During the past half-century, there have been several types of mathematical models of the tyre developed, each with its own specific purpose, accuracy and complexity. As mentioned by Pacejka (Pacejka and Bakker, 1993), (Pacejka, 2002)the approach can range from purely empirical, which is based on test data to purely theoretical through complex physical model such as using brush type models(Mavros, 2004, Svendenius and Gafvert, 2004) and finite element methods. A very simple approach for the tyre model is a spring constant for vertical deflection (As used with quarter car multi-body models) and a linear relation between slip angle and lateral force generation (as used with 2DOF model). With a cut-off at the lateral force limits, almost realistic handling behaviour with two-wheel vehicle can be achieved. Mixed longitudinal and lateral slip can be taken into consideration by characteristic curves, groups of curves, or by suitable approximation functions(Bakker et al., 1987). However, to simulate more realistic dynamic tyre characteristics, further detail representation of the model such as SWIFT tyre (Oosten and Pacejka, 2000) would be required. The swift model represents only part-physical data. Thus, further refinement to suit conditions, such as short-wave road unevenness and durability study, for example for frequencies up to 150Hz can be found in the F-tyre (ADAMS/Pre, 2002) Investigations of extreme situation can even require a detail non-linear dynamics FEM model like DNS (Dynamics Nonlinear Spatial)-Tyre.

In general, tyre model can be categories in 4 approaches(Pacejka, 2002):

i) Mathematical model which describe measured tyre characteristics(test data) through tables or Mathematical formulae and certain interpolation schemes. Example Magic Formula tyre model(Pacejka and Bakker, 1993)

ii) Based on part-physical modelling. Through distortion, rescaling and multiplication, new relationship are obtained to describ certain off-nominal condition. This approach is very useful for vehicle simulation models that required rapid computations. Example HSRI model develop by Dugoff(Dugoff, 1970)

iii) Simple representation of physical models especially useful to get better understanding of tyre behaviour. Example brush tyre model (Mavros, 2004, Svendenius and Gafvert, 2004).

iv) The model is based on the physical approach(FEM model) a very fine detailed structure of the tyre. This class of models is mostly used for tyre analysis only under difficult situations. The application for vehicle simulation would be too time consuming. Example SWIFT-Tire(Van Oosten and Pacejka, 2000)

2.4.4.2 Tyre modelling

Tyre models play a significant role in vehicle simulation analysis. (Willumeit et al., 1992) used 3 different levels of complexity in vehicle modelling, concluding that a good estimation of tyre forces under various steady and transient vehicle manoeuvres is a pre-requisite for a realistic overall vehicle ride and handling simulation. However, based on the review of literature it seems that many of the analysts, especially in the field of vehicle dynamic control for handling analysis have preferred to use rather simple linear tyre models, where the vehicle (Single track model) undergoes low lateral acceleration and small steering angle. Such a tyre model has been used in references(Willumeit et al., 1992, Abe, 1989, Harada and Harada, 1999, Kiencke and Daib, 1997, Ryu et al., 2002, Pongsathorn et al., 2002, Shino et al., 2002, Horiuchi et al., 1999a, Lukowski and Medeksza, 1992, Appel et al., 1992). One reason behind the use of simpler models, as mentioned by(Kim and Ro, 2002), is that any inaccuracy in the model can cause an undesirable tuning

process, when a controller is incorporated into the vehicle system. Similarly, for analysis of ride only, the cushioning characteristics of a pneumatic tyre may only be represented. The most widely used and simplest model, representing the fundamental mode of vibration of the pneumatic tyre consists of a mass element and a linear spring in parallel with a viscous damping element as explained by Wong (Wong, 2001).However, these simple tyre models are very limited in their application as concluded by (Shiiba and Suda, 2002).

For more complex applications, for example at higher lateral acceleration, the linear tyre model is no longer valid as demonstrated by (Willumeit et al., 1992). As explained in previous section there are many non-linear tyre models, the most widely used being the "Magic Formula" tyre model. (Lin et al., 2003) and (Savkoor and Ausejo, 1999) incorporate this tyre model in their work on driver-vehicle interactions for vehicle handling analysis. (Best and Gordon, 2002) in his 2-DOF vehicle-handling model has also employed combined slip magic formula tyre model to impose realistic friction limits on the optimisation of vehicle parameter (vehicle centre of gravity and yaw inertia) and control action (steer and torque). (Chen et al., 1996) have provided a comprehensive review for subjective and objective tests for vehicle handling behaviour, using two different tyre types for both the front and rear wheels. The lateral forces and moments characteristics for the tyres were measured by the manufacturer and supplied as "Magic Formula". (Doniselli et al., 1996) and (Yip et al., 1992) in their work on aerodynamic effects on vehicle body for ride and handling analysis have used two types of vehicle model (with different levels of complexity) and two types of tyre model (linear and non-linear). In their more complex vehicle model, the Magic formula tyre model was used to generate forces at the contact patch. However, due to the importance of vertical movement for ride analysis, authors have included an additional degree of freedom for each tyre to represent the vertical deformation. However, since tyre damping is several orders of magnitude less than suspension damping, it has little impact on the ride performance and is usually neglected. Similar approach were also used by (Sharp, 1999) , (Cooke et al., 1997), (Dickison and Yardley, 1993), (Sayers and Han, 1996), and(Schuller et al., 2001). Even though they all use magic formula tyre model for horizontal elasticity, all of them added simple linear spring for vertical elasticity of the tyre. This is purely to accommodate the wide range of analysis conducted on the vehicle, such as

analysis concerning roll and pitch plane dynamics and also the inclusion of different road profile effects. (Keiyu et al., 2003) presented their work on suspension and braking control, stressing the main difficulty in the control of yaw rate through suspension as the result of the tyre-road interactions. They noted that in order to test the controller, realistic tyre models must be employed thus non-linear Magic formula tyre model was chosen. However, the magic formula tyre model was simplified to limit the complexity and uncertainty due to Tyre-road contact.

Beside Magic formula tyre there also other non-linear tyre models used by the analyst such as the Unified tyre model (Guo et al., 2001)used by Xiao-pei Lu (Lu et al., 2003) in his work on camber effect on tyre force and moment properties. Uemastu (Uematsu and Gerdes, 2002), however, have preferred to use another model, called Dugoff tyre model (Dugoff, 1970) for their work on stability control.
There are also commonly used tyre models, which are called Brush tyre models (Svendenius and Gafvert, 2004), which were used by(Chu et al., 2001), (Shino and Nagai, 2001), (Mavros, 2004) and(Park et al., 2001).

Chapter 3
Development of an Intermediate Vehicle Dynamics Model

3.1 Introduction

During the past decade improvements in computer capabilities and commercial multi-body simulation software have led to a tendency to develop detailed models of vehicle systems. The models are based on physical representations, usually requiring large quantities of input data(Willumeit et al., 1992, Dickison and Yardley, 1993). This is not always readily available to all engineering analysts. Even when the full set of input parameters is available, the simulation studies run considerably slower than the customised programs, which are less complex, but in many cases adequate for the purpose of investigation. The complexity of large models can sometimes reduce the reliability of simulation, especially when the model is constructed during the hectic process of development and design(Dickison and Yardley, 1993) . Such circumstances often result in simulation projects that can only confirm the design and measurement, but seldom contribute to a better design before various test vehicles are built. As reported in (Dickison and Yardley, 1993, Sayers and Han, 1996), various problems concerning the dynamics of a vehicle can be reliably solved with comparatively simple models of the real system. However, simple models have their limits and are only suitable for certain types of tests. The work carried out in this thesis is to establish a functional vehicle model which is capable of evaluating handling analysis as well as ride comfort, such as bump riding events. These simpler multi-body models are regarded as intermediate models (Sharp, 1999).

3.2 Kinematics and dynamics equations for vehicle dynamics application

The mathematical modelling for vehicle ride and handling can be performed using various methods with different levels of complexity, from a linear model to a highly complex non-linear one. However, not all analyses require highly complex vehicle models to obtain fairly accurate results(Sayers and Han, 1996). In order to form a

good understanding of vehicle behaviour, it is always helpful to start with a simple model, taking the 'Ladder of Abstraction' approach described by Milliken and Milliken (Milliken and Milliken, 1995). If the basic concepts can be clarified at a simple level they will carry through to a more realistic level. For the initial development work, which is to develop an understanding of how to model a vehicle, three models were built.

i) A bicycle model, having two degrees of freedom (DOF), which are essentially lateral and yaw degrees of freedom (the 2-DOF model)

ii) A vehicle model, having three degrees of freedom: lateral, yaw and roll dynamics with a simple suspension system (the 3-DOF model)

iii) A vehicle model, having four degrees of freedom: lateral, yaw dynamic, roll and longitudinal degrees of freedom with a simple suspension system and the 'Magic Formula' tyre model (the 4-DOF model)

Each model has different assumptions, different levels of complexity and different input requirements (See appendix 1).

Understanding the basic theory of three-dimensional rigid body kinematics constitutes the first step in understanding how the rigid body vehicle models work. Understanding of relative velocity, relative acceleration, rotating reference frame and relative transformation is very important for vehicle modelling development. Fortunately these information are widely available in books such as (Meriam and Kraige, 1993, Genta, 1997, Huston and Lui, 2001, Rahnejat, 1998).

Based on Newton second law and due to the assumption that the vehicle is symmetrical(left & right) and the centre of gravity is coincide with roll, pitch and yaw axes. The components of the translational dynamics in the direction of the moving axes can be written as:(Dickison and Yardley, 1993),(Willumeit,1992),(Genta, 1997), Mavros,2004):

$$\Sigma F_x = M \cdot \left(\frac{\partial}{\partial t}(U) - Vr + Wq \right) \tag{3.1}$$

$$\Sigma F_y = M \cdot \left(\frac{\partial}{\partial t}(V) - Wp + Ur \right) \tag{3.2}$$

$$\Sigma F_z = M \cdot \left(\frac{\partial}{\partial t}(W) - Uq + Vp \right) \tag{3.3}$$

and using standard angular momentum equation (3.4) and moment of inertia equation (3.5) below , (Meriam and Kraige, 1993, Huston and Lui, 2001, Mavros, 2004, Ellis, 1994).

$$\frac{d}{dt}(H_0) = \frac{d}{dt}(I_0 \omega) + (\Omega \times H_0) \tag{3.4}$$

$$\sum M_0 = \frac{d}{dt}(I_0 \omega) + (r_G \times M a_0) \tag{3.5}$$

where:

$$I_0 \omega = \begin{bmatrix} I_{xx} & -I_{xy} & -I_{xz} \\ -I_{yx} & I_{yy} & -I_{yz} \\ -I_{zx} & -I_{zy} & I_{zz} \end{bmatrix} \begin{bmatrix} p \\ q \\ r \end{bmatrix}$$

$$I_0 \omega = \begin{bmatrix} I_{xx}p - I_{xy}q - I_{xz}r \\ -I_{yx}p + I_{yy}q - I_{yz}r \\ -I_{zx}p - I_{zy}q + I_{zz}r \end{bmatrix} \tag{3.6}$$

Differentiating and substituting equation (3.5) into equation (3.6) yields:

$$\frac{d}{dt}(H_0) = \begin{bmatrix} I_{xx}\dot{p} - I_{xy}\dot{q} - I_{xz}\dot{r} \\ -I_{yx}\dot{p} + I_{yy}\dot{q} - I_{yz}\dot{r} \\ -I_{zx}\dot{p} - I_{zy}\dot{q} + I_{zz}\dot{r} \end{bmatrix} + \begin{bmatrix} p \\ q \\ r \end{bmatrix} \times \begin{bmatrix} I_{xx}p - I_{xy}q - I_{xz}r \\ -I_{yx}p + I_{yy}q - I_{yz}r \\ -I_{zx}p - I_{zy}q + I_{zz}r \end{bmatrix}$$

Assuming from equation (3.6) that :

$$\begin{bmatrix} T_x = I_{xx}p - I_{xy}q - I_{xz}r \\ T_y = -I_{yx}p + I_{yy}q - I_{yz}r \\ T_z = -I_{zx}p - I_{zy}q + I_{zz}r \end{bmatrix}$$

equation (3.5) can be written as:

$$\frac{d}{dt}(H_0) = \begin{bmatrix} I_{xx}\dot{p} - I_{xy}\dot{q} - I_{xz}\dot{r} \\ -I_{yx}\dot{p} + I_{yy}\dot{q} - I_{yz}\dot{r} \\ -I_{zx}\dot{p} - I_{zy}\dot{q} + I_{zz}\dot{r} \end{bmatrix} + \begin{bmatrix} qT_z - rT_y \\ rT_x - pT_z \\ pT_y - qT_x \end{bmatrix} \tag{3.7}$$

From equation (3.5), acceleration at the centre of the roll axis is:

$$a_0 = \begin{bmatrix} \dot{U} \\ \dot{V} \\ \dot{W} \end{bmatrix} + \begin{bmatrix} p \\ q \\ r \end{bmatrix} \times \begin{bmatrix} U \\ V \\ W \end{bmatrix} = \begin{bmatrix} \dot{U} + (qW - rV) \\ \dot{V} - (pW - rU) \\ \dot{W} + (pV - qU) \end{bmatrix}; \qquad r_G = \begin{bmatrix} x_G \\ y_G \\ z_G \end{bmatrix};$$

Thus: $$r_G \times Ma_0 = \begin{bmatrix} x_G \\ y_G \\ z_G \end{bmatrix} \times M \begin{bmatrix} \dot{U} + (qW - rV) \\ \dot{V} + (rU - pW) \\ \dot{W} + (pV - qU) \end{bmatrix};$$

And, finally, the equation for $\sum M_0$ becomes:

$$\sum M_0 = \begin{bmatrix} I_{xx}\dot{p} - I_{xy}\dot{q} - I_{xz}\dot{r} \\ -I_{yx}\dot{p} + I_{yy}\dot{q} - I_{yz}\dot{r} \\ -I_{zx}\dot{p} - I_{zy}\dot{q} + I_{zz}\dot{r} \end{bmatrix} + \begin{bmatrix} qT_z - rT_y \\ rT_x - pT_z \\ pT_y - qT_x \end{bmatrix} + \begin{bmatrix} x_G \\ y_G \\ z_G \end{bmatrix} \times M \begin{bmatrix} \dot{U} + (qW - rV) \\ \dot{V} + (rU - pW) \\ \dot{W} + (pV - qU) \end{bmatrix}$$

Due to the centre of gravity is coincide with vehicle axes and the vehicle is assume symmetric between left and right, the equation above can be summarise as below:

$$\Sigma M_x = I_{xx} \cdot \frac{\partial}{\partial t}(p) - (I_{yy} - I_{zz}) \cdot q \cdot r - I_{zx} \cdot \left(p \cdot q + \frac{\partial}{\partial t}(r) \right) \tag{3.8}$$

$$\Sigma M_y = I_{yy} \cdot \frac{\partial}{\partial t}(q) - (I_{zz} - I_{xx}) \cdot p \cdot r + I_{xz} \cdot (p^2 - r^2) \tag{3.9}$$

$$\Sigma M_z = I_{zz} \cdot \frac{\partial}{\partial t}(r) - (I_{xx} - I_{yy}) \cdot p \cdot q + I_{zx} \cdot \left(r \cdot q - \frac{\partial}{\partial t}(p) \right) \tag{3.10}$$

By having these 6 equations of motion eq(3.1, 3.2, 3.3, 3.8, 3.9, 3.10), the 6 degree of freedom rigid body vehicle model can be built.

3.3 Intermediate vehicle model

For acceleration, braking and cornering analyses it is sufficient to have one lumped mass located at the centre of gravity (CG) with appropriate mass and inertia properties. The standard SAE vehicle axis system is used as a reference for the model as shown in Figure 4.1.

The vehicle motions are defined with reference to a right-hand orthogonal coordinate system(SAE-J670e, 1976).

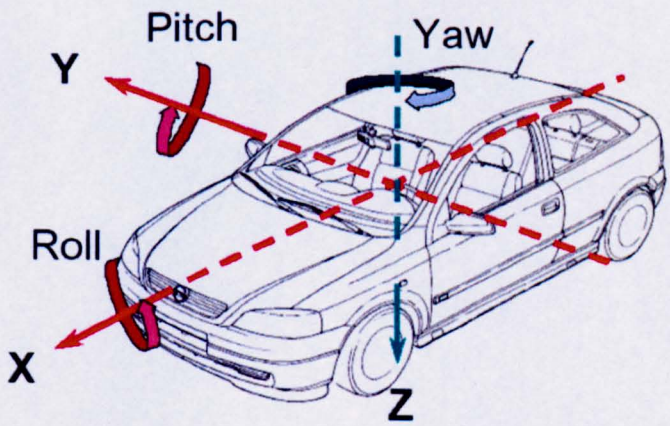

Figure 3.1: SAE Vehicle Axis Systems

The forces and moments acting on the vehicle follow the SAE vehicle axis. The force corresponding to the load on a tyre acts in the upward direction (negative in magnitude) and is called the vertical force.

The model described here has 6 degrees of freedom and also has a simplified generic representation of suspension kinematics that can represent the behaviour of most independent suspension systems.

The model also includes:

i) Large angular body motion.
ii) Three-dimensional and potentially long wavelength road surface undulations
iii) Linear spring and damper characteristics.
iv) Tyre vertical compliance (linear with maximum compression and also the potential for losing contact with the road).
v) Kinematics suspension bumps and rebound stops.
vi) Anti-dive and anti-squat suspension features for longitudinal and lateral dynamics
vii) Bump-steer effects
viii) Ackerman steering geometry
ix) Bump-camber effects.
x) Basic aerodynamic drag model
xi) Basic driveline model, based on torque demand and power limits
xii) Optional ABS/TCS features
xiii) Driver model and track definition
xiv) Suspension compliance (Camber, steer, caster, longitudinal and lateral)

The model is also developed so that one can perform a study of the vehicle on non-flat roads (e.g. speed bumps). The model at this stage excludes:

i) Structural flexibility.
ii) Unsprung mass dynamics (wheel-hop).

iii) Capability to deal with short-wavelength road profile features.

iv) Engine and transmission transients, assumes an infinitely variable transmission with only a maximum power limit

In section 4.7 this vehicle model, which is created in a MATLAB/SIMULINK environment, will be explained in more detail.

The vehicle model is divided into several main sections; that is, rigid body dynamics, vehicle kinematics, suspension and steering systems, driveline and tyre, and finally a driver model.

3.4 Rigid Body Dynamics

The model uses body-centred coordinates. The model inputs are the twelve input tyre forces

$$F_T = [F_{x1}, \cdots, F_{x4}, F_{y1}, \cdots F_{y4}, F_{z1}, \cdots F_{z4}]^T \tag{3.11}$$

and these are applied directly to the vehicle body. This is justified, because the unsprung mass is neglected and hence the resultant forces and moments on the unsprung mass are zero – hence the forces and moments are directly 'transmitted' to the vehicle body structure. The state variables are:

$$\mathbf{x} = [U, V, W, p, q, r]^T \tag{3.12}$$

(mass centre translational velocities and body angular velocities using body-fixed SAE axes). Other inputs are the aerodynamic force which is applied at the mass centre not at the centre of pressure point . This purely to simplified the model however this may contribute to additional error in overall vehicle movement:

$$\mathbf{F}_{aero} = -k_{aero} |\mathbf{v}_G| \mathbf{v}_G \tag{3.13}$$

where $\mathbf{v}_G = [U, V, W]^T$, and the vehicle weight is given as:

$$\mathbf{F}_{weight} = Mg\mathbf{k} \tag{3.14}$$

where **k** is the unit vector of the global z-direction, relative to vehicle coordinates. The anti-roll bar effect is based on vehicle body roll and also suspension deflection due road profile. Equations of motion are based on the standard Newton-Euler form as derived in Chapter 3. Thus:

$$M(\dot{\mathbf{v}}_G^{rel} + \boldsymbol{\omega} \times \mathbf{v}_G) = \mathbf{F}_{aero} + \Sigma\mathbf{F}_{tyres} + \mathbf{F}_{weight} + \mathbf{F}_{stabiliser} \tag{3.15}$$

Referring to Chapter 3 (Equation (3.1, 3.2, 3.3)), the translational dynamics can be divided into three translational elements as:

i) Longitudinal dynamics : $$m \cdot \left(\dot{U} - V \cdot r + W \cdot q \right) = F_x \tag{3.16}$$

ii) Lateral dynamics : $$m \cdot \left(\dot{V} - W \cdot p + U \cdot r \right) = F_y \tag{3.17}$$

iii) Vertical dynamics : $$m \cdot \left(\dot{W} - U \cdot q + V \cdot p \right) = F_z \tag{3.18}$$

For rotational dynamics the general equation is:

$$\mathbf{I}_G \dot{\boldsymbol{\omega}}^{rel} + \boldsymbol{\omega} \times (\mathbf{I}_G \boldsymbol{\omega}) = \Sigma\mathbf{M}_{tyres} \tag{3.19}$$

where, the inertia matrix assumes lateral symmetry(The vehicle is assumed symmetry between left and right) in the vehicle co-ordinates as:

$$\mathbf{I}_G = \begin{pmatrix} I_{xx} & 0 & -I_{xz} \\ 0 & I_{yy} & 0 \\ -I_{xz} & 0 & I_{zz} \end{pmatrix} \tag{3.20}$$

As derived earlier, the rotational equations can also be divided into three elements (L,M,N). These are:

i) Roll moment, L : $I_{xx}\dot{p} - I_{zx}\dot{r} - I_{yy}qr + I_{zz}qr - I_{zx}pq = L$ (3.21)

ii) Pitch moment, M : $I_{yy}\dot{q} - I_{zz}pr + I_{xx}pr + I_{xz}p^2 - I_{xz}r^2 = M$ (3.22)

iii) Yaw moment, N : $I_{zz}\dot{r} - I_{xz}\dot{p} - I_{xx}pq + I_{yy}pq + I_{xz}rq = N$ (3.23)

There are several ways of modelling vehicle dynamics. For basic vehicle model ,state-space approach can be use, However for higher level of complexity which includes non-linear elements, the approach is no longer suitable. A combination of Matlab and Simulink software are used, where $[U,V,W,p,q,r]$ are the states for the vehicle model.

U --- Longitudinal velocity
V --- Lateral velocity
W --- Vertical velocity
p --- Roll velocity
q --- Pitch velocity
r --- Yaw velocity

The input consists of the outputs from tyre forces, the aerodynamic force, the vehicle weight and also the vertical force from the suspension system. In order to establish the derivative equations, it is necessary to rearrange the equations of motion as follows:

Longitudinal dynamics : $M\dot{U} = F_x - M(Wq - rV)$ (3.24)

Lateral dynamics : $M\dot{V} = F_y - M(rU - pW)$ (3.25)

Vertical dynamics : $M\dot{W} = F_z - M(pV - qU)$ (3.26)

Roll moment : $I_{xx}\dot{p} - I_{zx}\dot{r} = M_x + (I_{yy} - I_{zz})qr + I_{zx}pq$ (3.27)

Pitch moment : $I_{yy}\dot{q} = M_y + (I_{zz} - I_{xx})pr - I_{xz}p^2 + I_{xz}r^2$ (3.28)

Yaw moment : $I_{zz}\dot{r} - I_{xz}\dot{p} = M_z + (I_{xx} - I_{yy})pq - I_{xz}rq$ (3.29)

Initially, the derivative equation can be written as shown below:

$$M_1\dot{X} = x_4 M_2 X + x_5 M_3 X + x_6 M_4 X + M_5 X + M_{\ldots n} F_{xyz} \quad (3.30)$$

From the above equations, left-hand-sides of the equations ($\dot{X}$) are:

$$LHS = M_1 = \begin{bmatrix} M & 0 & 0 & 0 & 0 & 0 \\ 0 & M & 0 & 0 & 0 & 0 \\ 0 & 0 & M & 0 & 0 & 0 \\ 0 & 0 & 0 & I_{xx} & 0 & -I_{zx} \\ 0 & 0 & 0 & 0 & I_{yy} & 0 \\ 0 & 0 & 0 & -I_{xz} & 0 & I_{zz} \end{bmatrix}$$

RHS of the equations have to be separated into five elements due to the existence of more than one state vector in one part of equation, thus:

$$M_2 = x_4 \begin{bmatrix} 0 & 0 & 0 & 0 & 0 & 0 \\ 0 & 0 & M & 0 & 0 & 0 \\ 0 & -M & 0 & 0 & 0 & 0 \\ 0 & 0 & 0 & 0 & I_{zx} & 0 \\ 0 & 0 & 0 & -I_{xz} & 0 & (I_{zz} - I_{xx}) \\ 0 & 0 & 0 & 0 & (I_{xx} - I_{yy}) & 0 \end{bmatrix} \quad M_3 = x_5 \begin{bmatrix} 0 & 0 & -M & 0 & 0 & 0 \\ 0 & 0 & 0 & 0 & 0 & 0 \\ M & 0 & 0 & 0 & 0 & 0 \\ 0 & 0 & 0 & 0 & 0 & (I_{yy} - I_{zz}) \\ 0 & 0 & 0 & 0 & 0 & 0 \\ 0 & 0 & 0 & 0 & 0 & -I_{xz} \end{bmatrix}$$

$$M_4 = x_6 \begin{bmatrix} 0 & M & 0 & 0 & 0 & 0 \\ -M & 0 & 0 & 0 & 0 & 0 \\ 0 & 0 & 0 & 0 & 0 & 0 \\ 0 & 0 & 0 & 0 & 0 & 0 \\ 0 & 0 & 0 & 0 & 0 & I_{xz} \\ 0 & 0 & 0 & 0 & 0 & 0 \end{bmatrix} \qquad M_5 = Aero\_coeff \begin{bmatrix} 1 & 0 & 0 & 0 & 0 & 0 \\ 0 & 1 & 0 & 0 & 0 & 0 \\ 0 & 0 & 1 & 0 & 0 & 0 \\ 0 & 0 & 0 & 0 & 0 & 0 \\ 0 & 0 & 0 & 0 & 0 & 0 \\ 0 & 0 & 0 & 0 & 0 & 0 \end{bmatrix}$$

Some of the terms on the right hand side of the equation contain products of two unknown values. Therefore, these values are calculated in the Simulink model. In order to establish the M_6 matrix, the moment of the vehicle body must be considered:

$$M_G = \sum r_i \times F_i \tag{3.31}$$

Where r is the distance between the tyre contact patch centre point and the vehicle C.G. Figure 3.2 below shows the notation used for each corner and the corresponding distance from each contact patch centre to the vehicle centre of gravity (CG).

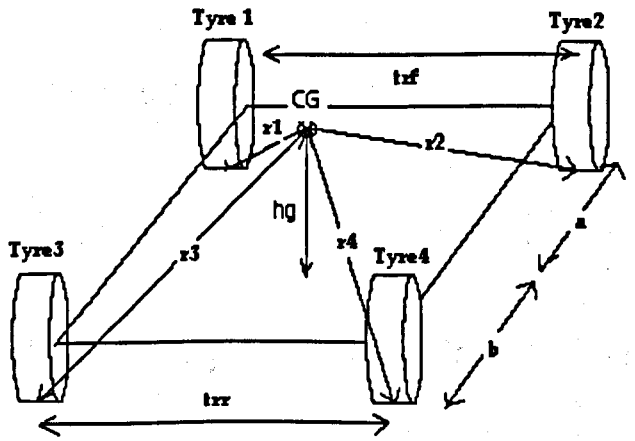

Figure 3.2: Notation used for each corner showing the distance from CG

a = longitudinal distance from the front axle to the centre of gravity (CG)

b = longitudinal distance from the rear axle to the centre of gravity (CG)

trf = front track width

trr = rear track width

hg = height of centre of gravity

For example (for Tyre 1):

$r_1 = r_{x1}i + r_{y1}j + r_{z1}k$ and $F_1 = F_{x1}i + F_{y1}j + F_{z1}k$, using

$M_G = \sum r_i \times F_i$, the equation for Tyre 1 becomes:

$$M_1 = \begin{bmatrix} r_{x1} \\ r_{y1} \\ r_{z1} \end{bmatrix} \times \begin{bmatrix} F_{x1} \\ F_{y1} \\ F_{z1} \end{bmatrix} = \begin{bmatrix} r_{y1}F_{z1} - r_{z1}F_{y1} \\ r_{z1}F_{x1} - r_{x1}F_{z1} \\ r_{x1}F_{y1} - r_{y1}F_{x1} \end{bmatrix} = \begin{bmatrix} 0 & -r_{z1} & r_{y1} \\ r_{z1} & 0 & -r_{x1} \\ -r_{y1} & r_{x1} & 0 \end{bmatrix} \begin{bmatrix} F_{x1} \\ F_{y1} \\ F_{z1} \end{bmatrix} = \begin{bmatrix} M_{x1} \\ M_{y1} \\ M_{z1} \end{bmatrix}$$

substitute the matrix with $r_1 = (a)i - \left(\frac{trf}{2}\right)j + (hg + z1)k$, where z1 is the vertical displacement of Tyre 1. Thus:

$$\begin{bmatrix} M_{x1} \\ M_{y1} \\ M_{z1} \end{bmatrix} = \begin{bmatrix} 0 & -(hg + z1) & -\left(\frac{trf}{2}\right) \\ (hg + z1) & 0 & -(a) \\ \left(\frac{trf}{2}\right) & (a) & 0 \end{bmatrix} \begin{bmatrix} F_{x1} \\ F_{y1} \\ F_{z1} \end{bmatrix}$$

Thus, all twelve moments are calculated as follows:

$$r_1 = (a)i - \left(\frac{trf}{2}\right)j + (hg + z1)k \qquad r_2 = (a)i + \left(\frac{trf}{2}\right)j + (hg + z2)k$$

$$r_3 = -(b)i - \left(\frac{trr}{2}\right)j + (hg + z3)k \qquad r_4 = -(b)i + \left(\frac{trr}{2}\right)j + (hg + z4)k$$

Roll Momenta (M_x):

$$M_{x1} = -(hg + z1)F_{y1} - \left(\frac{trf}{2}\right)F_{z1} \qquad M_{x2} = -(hg + z2)F_{y2} + \left(\frac{trf}{2}\right)F_{z2}$$

$$M_{x3} = -(hg + z3)F_{y3} - \left(\frac{trr}{2}\right)F_{z3} \qquad M_{x4} = -(hg + z4)F_{y4} + \left(\frac{trr}{2}\right)F_{z4}$$

Pitch Momenta (M_y):

$$M_{y1} = (hg + z1)F_{x1} - (a)\cdot F_{z1} \qquad M_{y2} = (hg + z2)F_{x2} - (a)\cdot F_{z2}$$

$$M_{y3} = (hg + z3)F_{x3} + (b)\cdot F_{z3} \qquad M_{y4} = (hg + z4)F_{x4} + (b)\cdot F_{z4}$$

Yaw Momenta (M_z):

$$M_{z1} = \left(\frac{trf}{2}\right)F_{x1} + (a)\cdot F_{y1} \qquad M_{z2} = -\left(\frac{trf}{2}\right)F_{x2} + (a)\cdot F_{y2}$$

$$M_{z3} = \left(\frac{trr}{2}\right)F_{x3} - (b)\cdot F_{y3} \qquad M_{z4} = -\left(\frac{trr}{2}\right)F_{x4} - (b)\cdot F_{y4}$$

Input = $\left[F_{x1}, F_{x2}, F_{x3}, F_{x4}, F_{y1}, F_{y2}, F_{y3}, F_{y4}, F_{z1}, F_{z2}, F_{z3}, F_{z4}\right]$

where $Total\_longitudinal\_forces = \left[F_{x1} + F_{x2} + F_{x3} + F_{x4}\right]$,

$Total\_lateral\_forces = \left[F_{y1} + F_{y2} + F_{y3} + F_{y4}\right]$

$Total\_vertical\_force = \left[F_{z1} + F_{z2} + F_{z3} + F_{z4}\right]$

Hence, the M_6 matrix is defined as follows (Vertical displacements are not included in this matrix):

$$M_6 = \begin{bmatrix} 1 & 1 & 1 & 1 & 0 & 0 & 0 & 0 & 0 & 0 & 0 & 0 \\ 0 & 0 & 0 & 0 & 1 & 1 & 1 & 1 & 0 & 0 & 0 & 0 \\ 0 & 0 & 0 & 0 & 0 & 0 & 0 & 0 & 1 & 1 & 1 & 1 \\ 0 & 0 & 0 & 0 & -hg & -hg & -hg & -hg & -\left(\frac{trf}{2}\right) & \left(\frac{trf}{2}\right) & -\left(\frac{trr}{2}\right) & \left(\frac{trr}{2}\right) \\ hg & hg & hg & hg & 0 & 0 & 0 & 0 & -a & -a & b & b \\ \frac{trf}{2} & \frac{trf}{2} & \frac{trr}{2} & \frac{trr}{2} & a & a & -b & -b & 0 & 0 & 0 & 0 \end{bmatrix} \begin{bmatrix} F_{x1} \\ F_{x2} \\ F_{x3} \\ F_{x4} \\ F_{y1} \\ F_{y2} \\ F_{y3} \\ F_{y4} \\ F_{z1} \\ F_{z2} \\ F_{z3} \\ F_{z4} \end{bmatrix}$$

An additional matrix, M_7, is created that includes the vertical tyre displacements in the moment calculations as shown below:

$$M_7 = \begin{bmatrix} 0 & 0 & 0 & 0 & 0 & 0 & 0 & 0 \\ 0 & 0 & 0 & 0 & 0 & 0 & 0 & 0 \\ 0 & 0 & 0 & 0 & 0 & 0 & 0 & 0 \\ 0 & 0 & 0 & 0 & -1 & -1 & -1 & -1 \\ 1 & 1 & 1 & 1 & 0 & 0 & 0 & 0 \\ 0 & 0 & 0 & 0 & 0 & 0 & 0 & 0 \end{bmatrix} \begin{bmatrix} F_{x1}z1 \\ F_{x2}z2 \\ F_{x3}z3 \\ F_{x4}z4 \\ F_{y1}z1 \\ F_{y2}z2 \\ F_{y3}z3 \\ F_{y4}z4 \end{bmatrix}$$

Matrix M_8, as shown below represents gravity effect on vehicle and finally matrix M_9 represents stabilizer bar effect on body roll.

$$M_8 = \begin{bmatrix} 1 & 0 & 0 \\ 0 & 1 & 0 \\ 0 & 0 & 1 \\ 0 & 0 & 0 \\ 0 & 0 & 0 \\ 0 & 0 & 0 \end{bmatrix} F_{weight} \qquad M_9 = Kroll\_coef \begin{bmatrix} 0 \\ 0 \\ 0 \\ 1 \\ 0 \\ 0 \end{bmatrix} X$$

The derivative of the state-space equation is now re-defined as:

$$\mathbf{M}_1\dot{\mathbf{x}} = (p\mathbf{M}_2 + q\mathbf{M}_3 + r\mathbf{M}_4 + \mathbf{M}_5|\mathbf{v}_G|_{aero})\mathbf{x} + \mathbf{M}_6\,\mathbf{F}_{Tyres} + \mathbf{M}_7\tilde{\mathbf{z}}\mathbf{F}_{xy} + \mathbf{M}_8\mathbf{F}_{weight} + \mathbf{M}_9\mathbf{x} \quad (3.32)$$

The effects of gravity, aerodynamics and stabilizer bar on the vehicle are also included as shown above in this final state-space equation

3.4.1 Aerodynamics forces

Aerodynamics forces have a major impact on the behaviour of a vehicle. Their effects include drag, lift, down force, lateral forces, moments in roll, pitch and yaw, and noise. These eventually influence the fuel economy, the handling and also the noise, vibration and harshness (NVH) characteristics of the vehicle. However, for this

model and at this stage to simplify the model, only two components of the drag are included, which are the longitudinal and lateral components. The aerodynamics force is expressed as:

$$F = \frac{1}{2}\rho V^2 A C_d \tag{3.33}$$

where, the force is assumed to be proportional to the dynamic pressure of the free current (i.e. $\frac{1}{2}\rho V^2$), to a reference surface area (A) and to a non-dimensional coefficient (C_d). For this model, the shape of the vehicle body is assumed to be a sphere; thus, the longitudinal and lateral drag forces are based on the above equation, however the forces will depend on the velocity in each direction and ρ, A and C_d are constant. Aerodynamic force always acts against the velocity vector of the vehicle travel and the lateral aerodynamics is assumed small relative to longitudinal aerodynamic force. Aerodynamics forces should be apply at the centre of pressure, However due to the type of analysis carried out in this thesis, the aerodynamics is assume small thus applied at centre of gravity for simplification reason.

3.4.2 Gravity forces

Transformation of the gravitational forces into vehicle body co-ordinates corresponds to a multiplication with the rotation matrix described in the previous chapter, with yaw angle being: $\psi = 0$.

The generic transformation matrix is expressed below (Rahnejat, 1998):

$$L(\theta,\varphi,\psi) = \begin{bmatrix} \cos\psi\cdot\cos\varphi & \sin\psi\cdot\cos\theta + \cos\psi\cdot\sin\varphi\cdot\sin\theta & \sin\psi\cdot\sin\theta - \cos\psi\cdot\sin\varphi\cdot\cos\theta \\ -\sin\psi\cdot\cos\varphi & \cos\psi\cdot\cos\theta - \sin\psi\cdot\sin\varphi\cdot\sin\theta & \cos\psi\cdot\sin\theta + \sin\psi\cdot\sin\varphi\cdot\cos\theta \\ \sin\varphi & -\cos\varphi\cdot\sin\theta & \cos\varphi\cdot\cos\theta \end{bmatrix}$$

But with zero yaw angle the above transformation matrix becomes:

$$\begin{bmatrix} \cos\varphi & \sin\varphi\sin\theta & -\sin\varphi\cos\theta \\ 0 & \cos\theta & \sin\theta \\ \sin\varphi & -\cos\varphi\sin\theta & \cos\varphi\cos\theta \end{bmatrix}$$

Thus, the forces generated due to gravitational effects are:

$$\begin{bmatrix} F_{GX} \\ F_{GY} \\ F_{GZ} \end{bmatrix} = \begin{bmatrix} \cos\varphi & \sin\varphi\sin\theta & -\sin\varphi\cos\theta \\ 0 & \cos\theta & \sin\theta \\ \sin\varphi & -\cos\varphi\sin\theta & \cos\varphi\cos\theta \end{bmatrix} \begin{bmatrix} 0 \\ 0 \\ mg \end{bmatrix}$$

3.5 Vehicle kinematics

The main purpose is to turn the local (i.e. vehicle-based) angular velocities into Euler angle derivatives and then integrate these to find roll, pitch and yaw angles. Following the equations given in (Katz, 1997, Rahnejat, 1998), the Euler angles are: $\theta_1 = \varphi, \theta_2 = \theta, \theta_3 = \psi$ (roll, pitch and yaw respectively). These are applied in the sequential order yaw- pitch-roll in body-fixed frame of reference to give the (active) transformation matrix from reference to actual vehicle orientation as:

$$R = R_3(\theta_3)R_2(\theta_2)R_1(\theta_1) \tag{3.34}$$

Note that the order is reversed here since each matrix is relative to the local body axes. Thus:

$$R_1(\theta_1) = \begin{pmatrix} 1 & 0 & 0 \\ 0 & \cos\theta_1 & -\sin\theta_1 \\ 0 & \sin\theta_1 & \cos\theta_1 \end{pmatrix}, R_2(\theta_2) = \begin{pmatrix} \cos\theta_2 & 0 & \sin\theta_2 \\ 0 & 1 & 0 \\ -\sin\theta_2 & 0 & \cos\theta_2 \end{pmatrix}, R_3(\theta_3) = \begin{pmatrix} \cos\theta_3 & -\sin\theta_3 & 0 \\ \sin\theta_3 & \cos\theta_3 & 0 \\ 0 & 0 & 1 \end{pmatrix}$$

R is also the passive transformation from the body to the global coordinates. Therefore, the Euler angle derivatives are found as (Katz, 1997)

$$\begin{aligned}\dot{\theta}_1 &= \omega_1 + (\omega_2 \sin\theta_1 + \omega_3 \cos\theta_1)\tan\theta_2 \\ \dot{\theta}_2 &= \omega_2 \cos\theta_1 - \omega_3 \sin\theta_1 \\ \dot{\theta}_3 &= (\omega_2 \sin\theta_1 + \omega_3 \cos\theta_1)/\cos\theta_2\end{aligned} \tag{3.35}$$

Euler angles are used to rotate the local mass centre velocity into globals that are then integrated to find the global x,y,z coordinates of *G* (the vehicle centre of gravity). Vehicle accelerations are also found in both the local and global coordinates, but only for post-processing purposes.

3.6 Suspensions and Steering

Nominal suspension deflections and velocities are found. These are considered as nominal, because bump and rebound stop forces are ignored at this stage, but will be included eventually. This is a non-trivial problem, because of the large-angle formulation highlighted here. Basically there are three stages to define suspension travel.

Firstly, one needs to find the nominal contact patch centre, point *P*, which translates and rotates with the vehicle body – based on the static 'trim' condition of the body, including static tyre deflection.
Using the mass centre *G* as a reference point:

$$\mathbf{r}_P = \mathbf{r}_G + R^{\{B\to G\}}\mathbf{r}_P^{\{B\}} \tag{3.36}$$

where the curly bracket superscripts denote the coordinate system used: $\mathbf{r}_P^{\{B\}}$ is the position of the nominal contact patch centre in the vehicle body coordinates, based at *G*, and $R^{\{B\to G\}}$ is the (passive) rotation matrix that converts from the body to the global coordinates using the Euler angles. In the remainder of this section it is assumed that similar transformations into globals have been carried out as necessary.

Secondly, one needs to find *Q*, the new position of *P* obtained by translating it in body-z axes – at this point no account is taken of the suspension geometry, including scrub effects, etc., as this has a negligible effect on the suspension vertical travel. This defines the nominal suspension deflection. Except where the wheel is out of contact with the road, one can expect the distance between *P* and *Q* to be small compared to the typical wavelength of the surface. If the surface is defined by $z = f(x, y)$, an initial approximation to *Q* is given by:

$$\mathbf{r}_S = [x_P, y_P, f(x_P, y_P)]^T \tag{3.37}$$

The approximation will be poor unless both the vehicle and the surface are considered to be close to the horizontal. *S* will be close in distance to the required point, so an improved approximation can be found by a planar representation of the road surface around *S*.

This is defined by $\mathbf{n}_S$, which is the unit (upward) normal to the road surface at *S*: (Huston and Lui, 2001)

$$(\mathbf{r} - \mathbf{r}_S) \cdot \mathbf{n}_S = 0 \tag{3.38}$$

Since *Q* is obtained by translating *P* parallel to the body-z unit vector $\mathbf{n}_B$, then:

$$\mathbf{r}_Q = \mathbf{r}_P + \lambda \mathbf{n}_B \tag{3.39}$$

Here λ is the sum of the suspension and tyre deflections (relative to the static equilibrium position, ignoring the actions of bump or rebound stops) and may be found by solving the above two equations to give:

$$\lambda = \frac{(\mathbf{r}_S - \mathbf{r}_P) \cdot \mathbf{n}_S}{\mathbf{n}_B \cdot \mathbf{n}_S} \tag{3.40}$$

In the model this is calculated in the global coordinates. Note that the estimation of suspension deflection can be refined via an iteration process on the choice of local surface normal and by including the suspension geometry effects, but the extra computational load is not justified.

The final step is to analyse the velocity of Q to determine the suspension velocity, and hence the overall velocity vector of the contact patch. As Q moves on the surface, its velocity is based on the rigid body motion of the vehicle, except for the addition of suspension velocity:

$$\mathbf{v}_Q = \mathbf{v}_G + \omega \times (\mathbf{r}_Q - \mathbf{r}_G) + \mu \mathbf{n}_B \tag{3.41}$$

where μ is the (expansion) velocity of the suspension-tyre combination. Since Q is moving within the plane, $\mathbf{v}_Q \cdot \mathbf{n}_S = 0$ and hence:

$$\mu = -\frac{\mathbf{n}_S \cdot \left(\mathbf{v}_G + \omega \times (\mathbf{r}_Q - \mathbf{r}_G)\right)}{\mathbf{n}_S \cdot \mathbf{n}_B} \tag{3.42}$$

Tyre vertical compliance is included in the suspension model. The unsprung mass is considered to be included with the vehicle body, so the 'massless' wheel constitutes a 'half degree of freedom' involving one state variable: the suspension deflection. In outline this works as follows. as above, the combined tyre/suspension displacement and velocities are known. The suspension deflection state z_s is used to determine the tyre deflection as $z_t = \lambda - z_s$ and both 'spring' forces acting on the wheel (see Figure 3.3) are known. After taking into account the geometry of the system and the in-plane forces, this assumption implies a required damper force and (via an inverse damper map) the required suspension velocity is used to update the suspension deflection state.

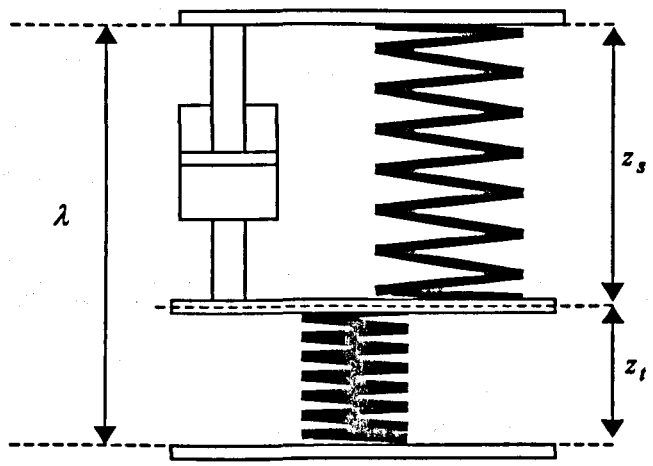

Figure 3.3: Tyre and suspension travel

Limits on tyre and suspension travel are implemented as simple modifications to the above:

$$z_t^{\min} \le z_t \le z_t^{\max}, \quad z_s^{\min} \le z_s \le z_s^{\max} \tag{3.43}$$

$z_t^{\min}$ represents the maximum tyre compression and a nominal maximum 'rim contact' tyre force $F_t^{\max}$ is applied. Alternatively, $z_t^{\max}$ represents loss of tyre contact, where: $F_t \to 0$.

When suspension end-stops are exceeded the damper force is overridden by virtual bump-stops and the calculated velocity is modified to prevent an excursion beyond the workspace limits as:

$$\dot{z}_s = \max\{\dot{z}_s^{calc}, \dot{z}_s^{small}\} \text{ if } z_s < z_s^{\min} \tag{3.44}$$

$$\dot{z}_s = \min\{\dot{z}_s^{calc}, -\dot{z}_s^{small}\} \text{ if } z_s > z_s^{\max} \tag{3.45}$$

Now, turning to the suspension geometry effects such as anti-dive characteristics and scrub effects, the balance is obtained via application of the *principle of virtual work* in the vehicle body coordinates. Consider the active forces and moments, acting on the wheel/hub assembly, when the body is fixed (see Figure 3.4), then virtual work takes the form:

$$F_x\,\delta x + F_y\,\delta y + F_z\,\delta z + F_s\,(-\delta z) + T_d\,\delta\nu = 0 \tag{3.46}$$

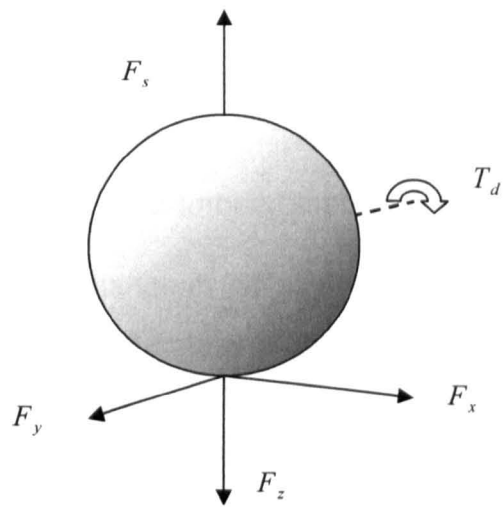

Figure 3.4: Forces and moments for the calculation of virtual work

Here all the forces are acting on the wheel/hub assembly and link reaction forces (ball-joints at the body connections) make no contribution. F_z increases with tyre extension, but carries a large negative component due to the static load. Overall, it is negative, tending to zero as the tyre lifts off the road surface. Similarly F_s would usually be negative, but increases as the suspension is expanded. The virtual work equation is based on the body-fixed coordinates and *z* is the suspension deflection (vertical height change of the contact patch centre) and is considered an independent variable. As the suspension is deflected, δx and δy (contact patch forward progression and lateral scrub respectively) follow from mapping the suspension geometry as:

$$\delta x = \left(\frac{dx}{dz}\right)\delta z \ , \ \delta y = \left(\frac{dy}{dz}\right)\delta z \tag{3.47}$$

F_s is the net suspension force, based on the vertical wheel travel. If the spring or damper is not directly aligned with the wheel vertical motion (as is typically the case) then the *principle of virtual work* can be used again to obtain $F_s(z)$. For example, if s is the spring deflection and $\widetilde{F}_s(s)$ is the variation of component of spring with deflection, then: $F_s(z) = \widetilde{F}_s(s)\dfrac{ds}{dz}$.

In the virtual work equation, T_d is the drive torque (assumed to be generated from an inboard differential) and $\delta\nu$ is the change in the caster angle. Brake torques do not contribute, because they are considered as internal to the wheel-hub assembly.

The virtual work equation can be written (in the body coordinates) as:

$$F_x d_x + F_y d_y + F_z - F_s + T_d d_\nu = 0 \tag{3.48}$$

Where: $d_x = \left(\dfrac{dx}{dz}\right)$ etc..

Defining: $$\mathbf{d} \equiv [d_x \, d_y \, 1]^T \tag{3.49}$$

The virtual work equation becomes:

$$\mathbf{F} \cdot \mathbf{d} = F_s - T_d d_\nu \tag{3.50}$$

This must now be transformed to the 'tyre' coordinates in order to find the unknown road-normal force. Leaving aside the details for now, let $R^{\{B \to T\}}$ be the (passive)

rotation matrix that transforms vector components from the body-fixed axes to the tyre axes. The dot product is the same in any coordinate system so transforming to tyre coordinates as:

$$\mathbf{F}^{\{T\}} = R^{\{B\to T\}}\mathbf{F}^{\{B\}},\ \mathbf{d}^{\{T\}} = R^{\{B\to T\}}\mathbf{d}^{\{B\}} \tag{3.51}$$

Making use of equation (27) yields:

$$F_s = F_x^{\{T\}} d_x^{\{T\}} + F_y^{\{T\}} d_y^{\{T\}} + F_z^{\{T\}} d_z^{\{T\}} + T_d\, d_v \tag{3.52}$$

With $F_z^{\{T\}}$ known from the tyre deflection and $F_x^{\{T\}}$ and $F_y^{\{T\}}$ are obtained as output from the tyre model. This determines F_S, the body-vertical suspension force. Subtracting the spring component (including static load) and inverting the damper map gives the suspension velocity as required above.

The transformation from body to tyre coordinates is now derived. In order to account for steering angle, steering axis geometry, toe, camber and caster change, Euler angles and road normal are also needed because the tyre-Z axis is normal to the road. Consider a general rotation through angle ϕ about an axis defined by a unit vector **n**(Huston and Lui, 2001). As an 'active' rotation, an arbitrary vector **v** is rotated and the coordinates are fixed, so $\mathbf{v}\to\mathbf{v}'$,with:

$$\mathbf{v}' = (\mathbf{v}\cdot\mathbf{n})\mathbf{n}(1-\cos\phi) + \mathbf{v}\cos\phi + (\mathbf{n}\times\mathbf{v})\sin\phi \tag{3.53}$$

So for steering rotation about the kingpin axis, for example, for *the right-front wheel*:

$$\mathbf{n} = \begin{pmatrix} \cos\gamma\sin\nu \\ \sin\gamma \\ \cos\gamma\cos\nu \end{pmatrix} \tag{3.54}$$

This is a unit vector pointing along the kingpin axis (ν = caster angle, γ = lateral inclination angle), and:

$$\phi = \delta_k(z_{sus}) + \delta \tag{3.55}$$

This is the actual steer angle plus a kinematics term $\delta_k(z_{sus})$, which accounts for bump-steer and the static toe angle. In equation (3.53) **v** is a unit vector normal to the wheel-plane and it is assumed that starting from the reference (trim) condition, the suspension is deflected first inducing bump-camber and bump-steer (these angles are small so the rotation sequence is unimportant and it is convenient to effect the camber first), then rotated by angle δ about the kingpin axis (see Figure 3.5).

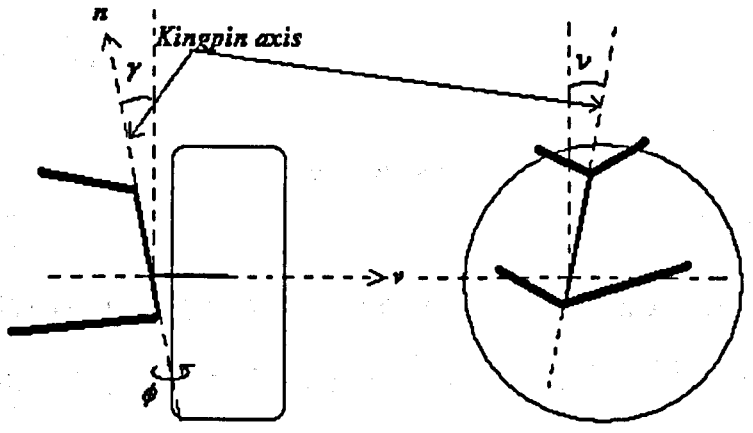

Figure 3.5: Virtual steering axis

Note that both caster and lateral inclination are considered constant in this model, but can easily be mapped as functions of suspension travel if required.

The overall rotation of the wheel plane normal using the body-fixed axes is:

$$\begin{pmatrix} 0 \\ 1 \\ 0 \end{pmatrix} \rightarrow \begin{pmatrix} 0 \\ \cos\rho \\ \sin\rho \end{pmatrix} = \mathbf{v} \rightarrow \mathbf{v}' \tag{3.56}$$

Working fully in the body-fixed coordinates requires the transformation of the road surface normal into the body coordinates in the following form:

$$\mathbf{n}_S = \mathbf{n}_S^{\{B\}} = R^{\{G\to B\}}\mathbf{n}_S^{\{G\}} \tag{3.57}$$

Removing the road-normal component from $\mathbf{v}'$ and rescaling gives the y-axis base vector for the tyre coordinate system as(Huston and Lui, 2001):

$$\mathbf{e}_2 = \frac{\mathbf{v}' - (\mathbf{v}'\cdot\mathbf{n}_S)\mathbf{n}_S}{\left|\mathbf{v}' - (\mathbf{v}'\cdot\mathbf{n}_S)\mathbf{n}_S\right|} \tag{3.58}$$

The z-axis vector is simply the road surface normal, $\mathbf{e}_3 = \mathbf{n}_S$, and the x-axis vector follows from the cross-product:

$$\mathbf{e}_1 = \mathbf{e}_2 \times \mathbf{e}_3 \tag{3.59}$$

If a vector $\mathbf{a} = [a_1\, a_2\, a_3]^T$ is given in the body-fixed coordinates and is multiplied by the matrix $R = [\mathbf{e}_1\, \mathbf{e}_2\, \mathbf{e}_3]$, formed from components of **e** (all in the body coordinates) with the following results:

$$\mathbf{a}' = a_1\mathbf{e}_1 + a_2\mathbf{e}_2 + a_3\mathbf{e}_3 \tag{3.60}$$

which is the vector 'actively' transformed from the body to the tyre axes. Hence *R* is also the passive rotation matrix from the tyre-coordinates to the body-coordinates:

$$R^{\{T\to B\}} = [\mathbf{e}_1\, \mathbf{e}_2\, \mathbf{e}_3] \tag{3.61}$$

For the front *left* wheel the above analysis is the same but the sign of λ is essentially reversed. If symmetry is assumed the look-up tables for $\delta_k(z_{sus})$ and $\rho(z_{sus})$ must also have negative signs applied; the model allows for independent left-right

suspension geometry. For the rear wheels the formulation is the same. Typically the commanded steer is zero, and the caster and lateral inclination angles are also assumed to be zero.

This essentially completes the suspension and steering analysis. It is noteworthy that the model is not currently set up to include steering torque output. The above steering geometry allows steering torque to be found quite simply via the inclusion of the mapped location $\mathbf{r}_A(z_{sus})$ of a reference point on the kingpin axis in the body-fixed coordinates (e.g. the outer ball-joint on the upper A-arm, or a body-fixed upper mount on a MacPherson strut).

3.6.1 Elasto-kinematics

The kinematics effects as functions of suspension travel are already contained in the model in the form of lookup tables for steer, camber, lateral deflection and longitudinal deflection, etc. This is equivalent to having ball joints and rigid links in the suspension system.

Additional changes in wheel position result from the forces and moments, which act at the contact patch. However, for simplicity up to this stage the forces acting on the contact patch are the main input to suspension elasto-kinematics. A linear approximation is taken in this approach, where a mapping method is used for additional wheel motion, resulting from these (steady-state) forces and moments.

For example:-

$$Change\_in\_steer = k_1(F_x) + k_2(F_y)$$

Thus, a matrix of coefficients k_1, k_2 is obtained for the induced changes, and these coefficients are determined from a more detailed model of the suspension as described later in Chapter 4.

A virtual test rig is developed in the ADAMS software to estimate the coefficients at a number of different suspension locations. The coefficients needed are:

i) Change in steer angle per unit change in F_x & F_y

ii) Change in camber angle per unit change in F_x & F_y

iii) Change in caster angle per unit change in F_x & F_y

iv) Change in the x-coordinate of wheel centre per unit change in F_x & F_y

v) Change in the y-coordinate of wheel centre per unit change in F_x & F_y

The idea is to carry out a virtual work calculation as though tyre compliance is absent and then add the compliance effects as "small perturbations". If the virtual work calculation is performed with the compliance effects included (i.e. changes in the contact patch), then the equation must also include the potential energy changes in the bushing.

If the bushing deformation is sufficiently small to have negligible effect on the position of the roll centre, for example, then the approximation should be reasonable. If the geometry changes due to bushing deflections, then the approximation is deemed as rather approximate or poor.

Under braking the bushes deform and cause small changes to the anti-feature geometries (this is in effect as though the 'ball joints' have moved), but provided these movements are small the anti-dive effect will hardly alter.

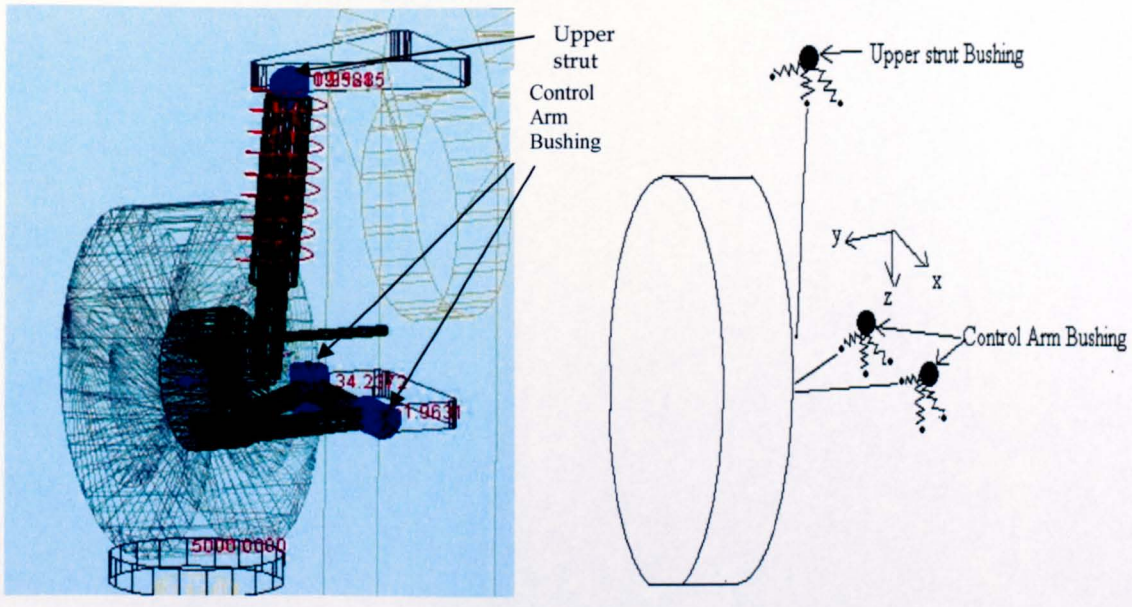

Figure 3.6: The McPherson Suspension system

Figure 3.6 shows the virtual test rig model of the McPherson suspension system that was developed using ADAMS software and a schematic diagram of the simplified compliance effects used in the intermediate model. For the virtual work approach, the schematic diagram above is better described in Figure 3.7. The effects of three bushes are combined into an equivalent bush.

When considering equilibrium of a certain system, it is often useful to consider the potential energy stored within the system. For simplicity, for the work carried out here a spring is used to represent the bushing components.

$$\text{Potential energy in spring}, V_e = \frac{kx^2}{2} \tag{3.62}$$

The work done on the body is the negative of the potential energy change in the equivalent spring.

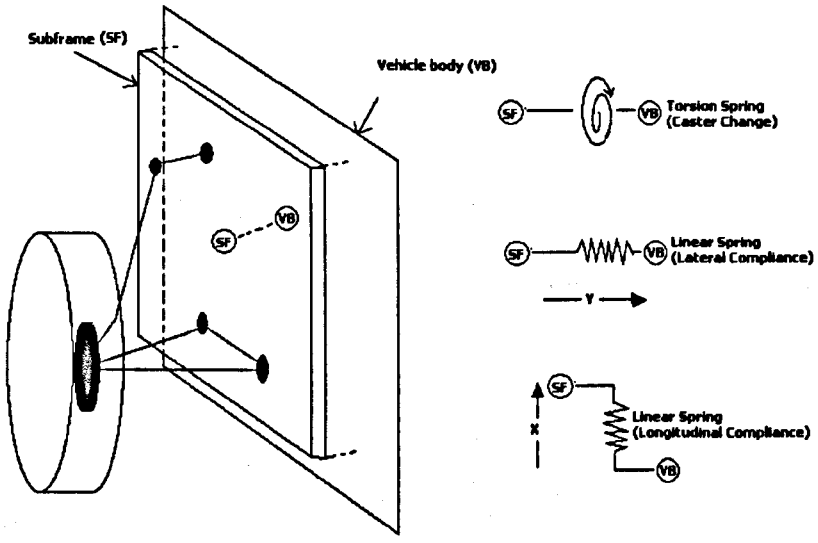

Figure 3.7: The simplified suspension compliance model

The principle of virtual work states that: $\delta W = 0$, when the system is in the state of equilibrium. This may be rephrased as: the virtual work done is equal to an increase in the stored potential energy. Thus:

$$\delta W = \delta V_e \tag{3.63}$$

Where: δW is the virtual work done by active forces other than the spring. For the existing 6-DOF model the virtual work equation is as below:

$$F_x \delta x + F_y \delta y + F_z \delta z + F_s(-\delta z) + T_d \delta \nu = 0 \tag{3.64}$$

In order to include the compliance effects in the model, one has to account for the potential energy generated due to the stiffness of the bushings. To represent the effect of compliance in the system, one may suppose:

Deformation of compliance element

$$V_e = \frac{k_x (x_c)^2}{2} + \ldots\ldots +$$

Then: $$\delta V_e = k_x x_c(\delta x_c) + k_y y_c(\delta y_c) + k_v v_c(\delta v) \quad (3.65)$$

Where: $\partial x_c, \partial y_c, \partial v_c$ are the deflections of the "equivalent spring" that models the effects of the various bushings and $k_{x,y,v}$ are the stiffness of these bushings in the system, thus:

$$\partial x_c = k_{cx1} F_x + k_{cx2} F_y$$
$$\partial y_c = k_{cy1} F_x + k_{cy2} F_y$$
$$\partial v_c = k_{cv1} F_x + k_{cv2} F_y$$

For simplicity, the coefficients $k_{cx1}, k_{cx2}, k_{cy1}, k_{cy2}, k_{cv1}, k_{cv2}$ are used to determine the bushing deformation as a constant value, regardless of the position of the vertical wheel travel. However, for better representation, these coefficients can be mapped from the data taken from the ADAMS virtual test rig.

Therefore, based on equations (3.62)-(3.65), the final virtual work equation becomes:

$$F_x \delta x + F_y \delta y + F_z \delta z + F_s(-\delta z) + T_d \delta \nu - \delta V_e = 0 \quad (3.66)$$

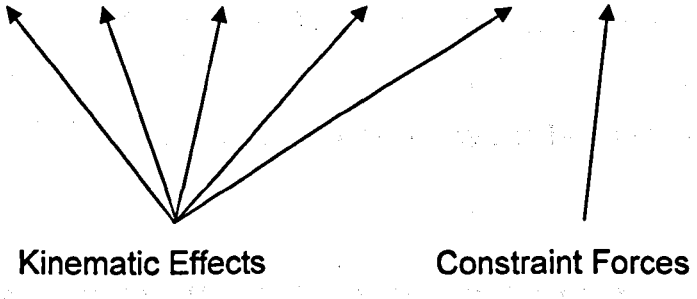

3.6.2 Anti-roll bar analysis

Generally, in order for body roll to occur, the suspension on the outside of the vehicle must compress while the suspension on the inside simultaneously extends (Hegazy et al., 2000). However, since the anti-roll bar is attached to both wheels, such movement is only possible if the anti-roll bar is allowed to twist. Therefore, the bar's torsional stiffness – or resistance to twist – determines its ability to reduce body roll. Less twisting of the bar results in lower movements in jounce and rebound by the opposite ends of the suspension, which result in reduced body roll. Reduction in roll angle helps in reducing lateral load transfer, which eventually enhances vehicle stability. Thus, it is important to include the anti-roll bar as a feature in the vehicle handling model as emphasised by (Ottgen and Bertram, 2001).

An elementary approach is used here to model the anti-roll bar.

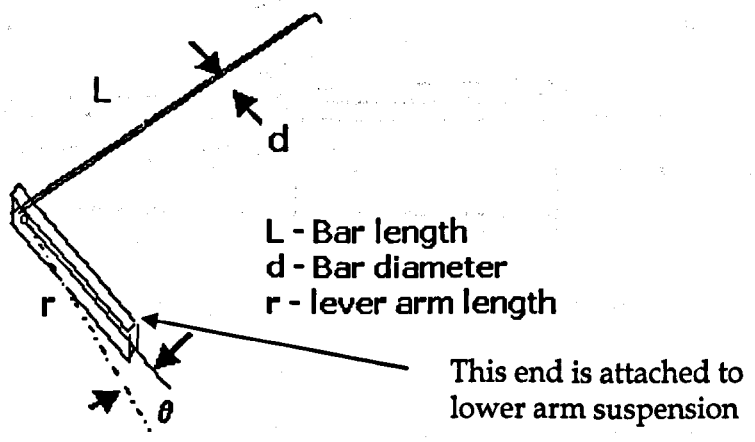

Figure 3.8: Twisting of the anti-roll bar

Based on Figure 3.8 above, the torsion bar rates can be found as:

Torsion angle is equal to , $\theta = \frac{TL}{JG}$ where for a solid rod: $J = \frac{\pi d^4}{64}$. From these two equations, it follows that:

$$\frac{T}{\theta} = \frac{\pi d^4 G}{64L} \tag{3.67}$$

Let the deflection at the end of the bar be equal to δ, where for a small twist angle: $\theta = \frac{\delta}{r}$. Now, the applied torque: $T = Fr$. Substituting this into equation (3.67) yields the deflection at the free end of the bar as:

$$\frac{F*r}{\frac{\delta}{r}} = \frac{\pi d^4 G}{64L} \Rightarrow \frac{F}{\delta} = \frac{\pi d^4 G}{64Lr^2} = k \tag{3.68}$$

However, to include the stabilizer bar's contribution to the overall roll stiffness of the vehicle, one has to consider the motion ratio of the suspension as explained below. From the simple lever system a number of relationships can be drawn as:

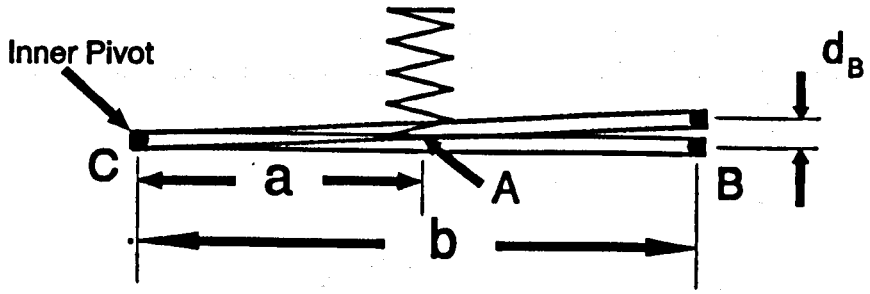

Figure 3.9: Suspension motion ratio

From Figure 3.9: $F_B = F_A\left[\frac{a}{b}\right]$ and $d_B = d_A\left[\frac{b}{a}\right]$.

Therefore:
$$\frac{F_B}{d_B} = k_B = \frac{F_A\left(\frac{a}{b}\right)}{d_A\left(\frac{b}{a}\right)} = k_A\left(\frac{a}{b}\right)^2 \tag{3.69}$$

The suspension roll stiffness (k_φ) can be determined, using elementary analysis techniques. If the wheel rates (k) are determined and the spring spacing (wheel track) (τ) is known, then the roll stiffness relationship to spring stiffness is as follows:

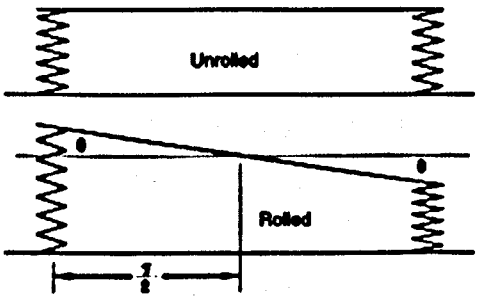

Figure 3.10: Vehicle body roll

The torque required to rotate the chassis about the roll axis is obtained as (see figure 3.10):

$$T = \frac{\tau^2}{4}(K_L + K_R)\theta$$

For equal spring rates, left and right, the above equation reduces to the following:

$$T = \frac{\tau^2}{2}(K)\theta$$

The roll stiffness is then:

$$K_\phi = \frac{T}{\theta} = \frac{\tau^2}{2}(K)$$

For roll stiffness in Nm/rad the equation becomes:

$$K_{\phi} = \frac{T}{\theta} = \frac{\tau^2 K}{(2 \bullet 57.3)} \tag{3.70}$$

where K is the individual wheel rate and τ is the wheel track.

From the above equations one can find the overall stabilizer bar contribution to the roll stiffness as:

$$k_{\phi\, bar} = \frac{\pi \;\; d^4 G}{64 \;\; L \;\; r^2} \left(\frac{r_2}{r_1} \right)^2 \left[\frac{\tau^2}{114.6} \right]$$

where r_1 is length of the attachment arm and r_2 is the pivot to the attachment arm.

Knowing the roll stiffness acting at the front or at the rear suspensions, one can evaluate the roll moment due to the anti-roll bar by multiply both the coefficients with the vehicle roll angle as described below.

$$\text{Roll moment due to the stabilizer bar} = Kroll\_coeff(\phi) \tag{3.71}$$

However, if the road profile is to be included in the model, the roll moment in equation (3.71) is no longer valid and must include the effect of suspension vertical travel due to the road profile.

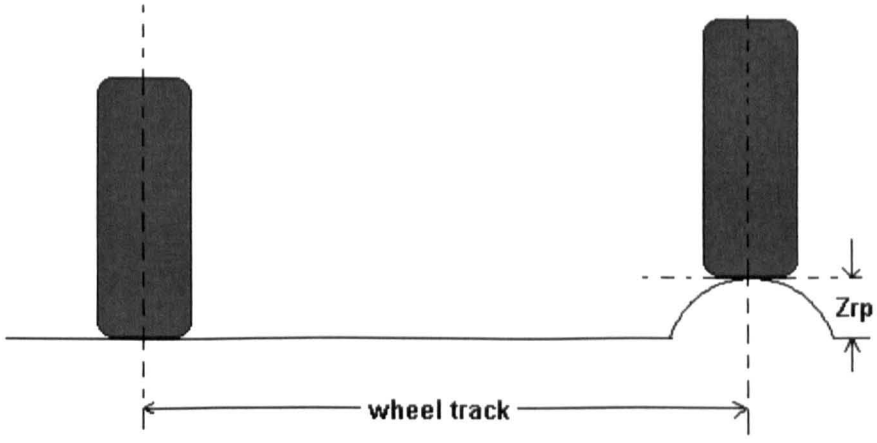

Figure 3.11: road profile effect on body roll

Additional roll deflections due to road profile for both front and rear can be represented in a general form as below (see figure 3.11):

$$\text{Additional roll angle,} \qquad d\phi = \tan^{-1}\left[\frac{Z_{rp}}{\text{wheel\_track}}\right] \tag{3.72}$$

Where: Z_{rp} is the height difference between the left and the right tyre contact patches. Thus, the moments generated by the anti-roll bars are obtained by adding to the body roll angle as shown below:

$$Kroll\_coeff[\phi - d\phi] \tag{3.73}$$

3.6.3 Calculation of longitudinal and lateral slip ratios

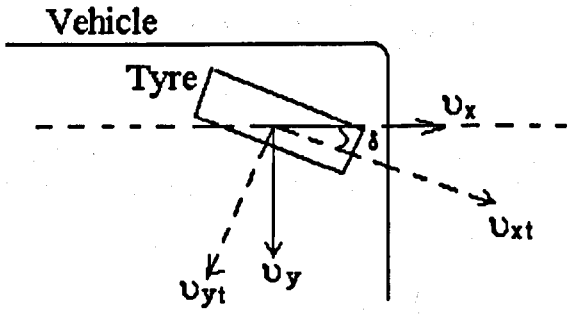

Figure 3.12: Velocity relative to the plane of vehicle

Referring to Figure 3.12: If S_x = slip at υ_{xt} direction and S_y = slip at υ_{yt} direction, then: Longitudinal slip ratio, $S_x = \dfrac{r\omega - \upsilon_{xt}}{\max(|\upsilon_{xt}|, \upsilon_0)}$ and Lateral slip ratio, $S_y = \dfrac{-\upsilon_{yt}}{\max(|\upsilon_{xt}|, \upsilon_0)}$,

where S_x - Longitudinal slip ratio S_y - Lateral slip ratio

υ_{xt} - Longitudinal velocity relative to wheel plane

υ_{yt} - Lateral velocity relative to wheel plane

3.6.4 The Ackerman Steer geometry effect

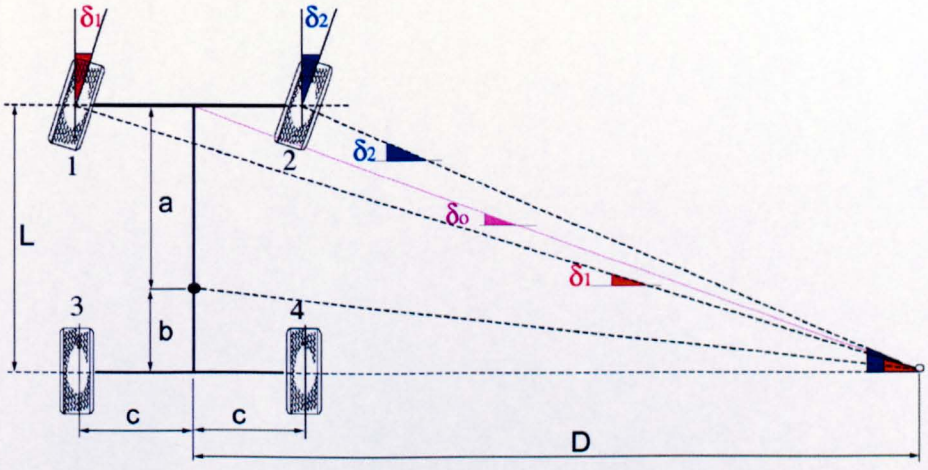

Figure 3.13: The Ackerman steering geometry

Referring to Figure 4.14, the steer angles at the rear wheels, δ3 = δ4, are zero if one assume no camber or steer effects in the rear suspension geometry. Also:

$$\tan\delta_0 = \frac{L}{D}, \quad \tan\delta_1 = \frac{L}{(D+c)} \quad \text{and} \quad \tan\delta_2 = \frac{L}{(D-c)}$$

So, if: $D = \frac{L}{\tan\delta_0}$, then: $D + c = \frac{L}{\tan\delta_1}$;

And:

$$\frac{L}{\tan\delta_0} + c = \frac{L}{\tan\delta_1};$$

$$\frac{L + c\tan\delta_0}{\tan\delta_0} = \frac{L}{\tan\delta_1};$$

$$\tan\delta_1 = \frac{L\tan\delta_0}{L + c\tan\delta_0} = \frac{\tan\delta_0}{1 + \frac{c}{L}\tan\delta_0} \quad \text{for small } \delta_0 \text{ and } \delta_1,$$

and using the binomial series:

$$(1+x)^n = 1+nx+\frac{n(n-1)x^2}{2!}+\frac{n(n-1)(n-2)x^3}{3!}+.....$$

then:

$$(1+x)^{-1} \cong 1-x$$

and, it becomes clear that:

$$\delta_1 = \frac{\delta_0}{1+\frac{c}{L}\delta_0} = \delta_0(1+\frac{c}{L}\delta_0)^{-1}$$

$$\delta_1 \approx \delta_0(1-\frac{c}{L}\delta_0) \text{ And } \delta_2 \approx \delta_0(1+\frac{c}{L}\delta_0)$$

and if Pa is the proportion of Ackerman then δ_1 and δ_2 become:

$$\delta_1 \approx \delta_0(1-\frac{Pa\times c}{L}\delta_0) \text{ and } \delta_2 \approx \delta_0(1+\frac{Pa\times c}{L}\delta_0)$$

Thus, in matrix form the correction for the steering input becomes:

$$\begin{bmatrix}\delta_1\\ \delta_2\\ \delta_3\\ \delta_4\end{bmatrix} = \begin{bmatrix}1 & -1\\ 1 & 1\\ 0 & 0\\ 0 & 0\end{bmatrix}\begin{bmatrix}\delta_0\\ \frac{Pa\times c}{L}\delta_0{}^2\end{bmatrix}$$

where: the steering correction coefficient are: Ksteer = $\begin{bmatrix}1 & -1\\ 1 & 1\\ 0 & 0\\ 0 & 0\end{bmatrix}$

3.6.5 Road profile

The 6-DOF model presented here requires a non-flat road surface, because the work carried out in this thesis involves the study of vehicle pitch and bounce. Therefore, having different (non-flat) road profiles included in the model enables a better understanding of the vehicle behaviour and helps establishing the reliability of the model for further work.

For these reasons, the following four types of road surface have been created:

i) Flat road
ii) Pure lateral slope
iii) A series of bumps in the longitudinal direction
iv) Data from file (i.e. the actual road profile)

There are two important parameters to be determined, which are required from all the road profiles, which are used for further analysis of the suspension system.

i) Height of the road surface , **z**
ii) Unit downward normal (n) as a function of the xy coordinates; **n**

3.6.5.1 Flat road

The road surface is considered flat and, therefore, **n** and **z** are rather simple, as shown below:

$$n = \begin{bmatrix} 0 \\ 0 \\ 1 \end{bmatrix} \text{ and } z = 0;$$

3.6.5.2 Pure lateral slope

The road surface, in this case, is considered tilted in a lateral direction to a certain extent, thus.

$$Slope = \eta\left(\frac{180}{\pi}\right) \tag{3.74}$$

where η (radians, see figure 3.14) is the required angle of the road surface (see figure below).

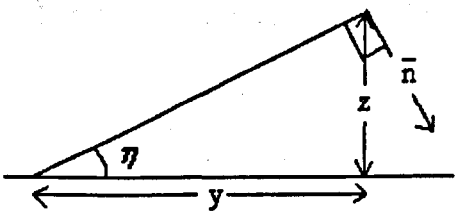

Figure 3.14: Pure lateral slope

The height of the road surface, z, is found as:

$$z = y\tan\eta \tag{3.75}$$

where y is the position of the contact point in the global y-coordinates and n is as below:

$$n = \begin{bmatrix} 0 \\ \sin(\eta) \\ \cos(\eta) \end{bmatrix}$$

3.6.5.3 A series of bumps in the longitudinal direction

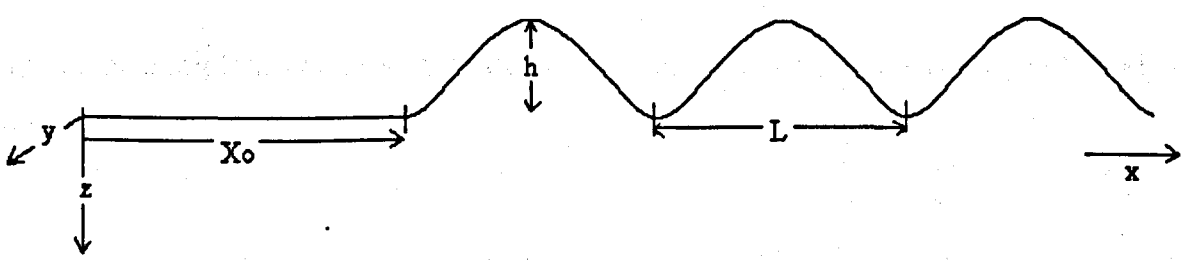

Figure 3.15: Road bump

In this case the road surface is divided into three sections (see figure 3.15). Firstly, an initial flat section followed. Secondly, a series of bumps are included. Thirdly, another flat section is incorporated. The first section is a flat surface before the first bump, where $z=0$ and $n=\begin{bmatrix}0\\0\\1\end{bmatrix}$. For the second section, the bumpy surface, z is a function of x where $z=-f(x)$, z being positive downwards. Here:

$$f(x)=\frac{h}{2}\left(1-\cos\frac{2\pi(x-x_0)}{L}\right)$$

and the gradient of the road is the derivative of $f(x)$, that is:

$$f'(x)=\frac{h}{2}\sin\frac{2\pi(x-x_0)}{L}\left(\frac{2\pi}{L}\right)$$

where $grad=f'(x)$ so $n=\begin{bmatrix}grad\\0\\1\end{bmatrix}$;

Note: *grad* is in term of vector in actual programming

In the third and last section, where the road goes flat again: $n=\begin{bmatrix}0\\0\\1\end{bmatrix}$, but z is:

$$f(x)=\frac{h}{2}(1-\cos(2\pi(nbump*L)))$$

Number of complete wavelengths are not necessarily an integer value, but road is flat thereafter.

3.6.5.4 Data from file

A similar approach is used in the case of an actually measured road profile as explained in previous section. However, in order to generate this road surface two inputs are required from the file: the x data and the z data. Based on these, the slope of the bump is estimated. The start and the end of this road profile are set to a flat road.

3.7 Driveline and tyre models

3.7.1 The driveline model

This aspect of the model deals with wheel spin dynamics (4 states) and a series of first order lags (with fixed time constants) for the build-up of engine torque (1 state), braking torques (4 states) and in-plane tyre forces (8 states). Overall, there are 17 states. The tyre *x*- and tyre *y*-components of velocity of the extended vehicle body, at the contact patches, including roll and pitch are used to find the longitudinal and lateral slip ratios. These are fed into the tyre model to obtain the 'pre-filtered' tyre forces F_p, which are lagged in the generation of the actual tyre forces F_a. This is schematically shown in figure 3.16.

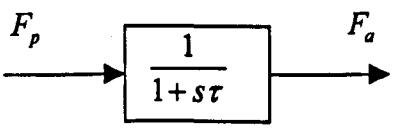

Figure 3.16: Lag in tyre forces

Subsequently, force/torque balance across the wheels determines the wheel acceleration and the wheel speeds. To prevent excessive wheel-spin and the associated numerical integration problems some additional non-linear damping is added to limit the maximum wheel accelerations. Optional simplified ABS/TCS functionality is also included to reduce the brake and drive-torque demands, when preset slip limits are exceeded.

3.7.2 Drive/Braking Force Calculation

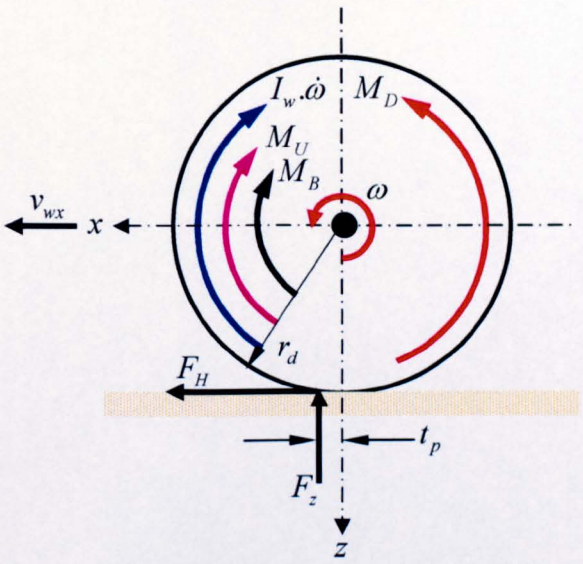

Figure 3.17: Drive/brake demand

Referring to figure 3.17, $I\dot{\omega} = T_d - T_b - F_x r$, or if drive/brake force equations are used, then this equation becomes: $I\dot{\omega} = (F_d - F_b - F_x)r$ So:

$$\dot{\omega} = \frac{(F_d - F_b - F_x)r}{I}$$

In the case where $\omega \rightarrow$ -ve, the sign of the brake force reverses and:

$$\dot{\omega} = \frac{(F_d - F_b sign(\omega) - F_x)r}{I}$$

3.8 Tyre Modelling

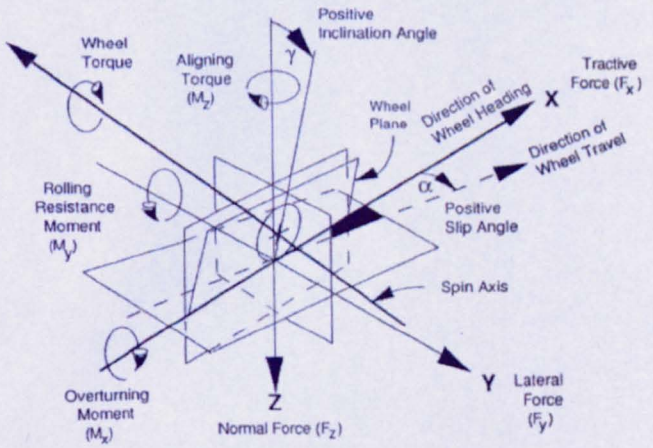

Figure 3.18: Tyre axes system(ADAMS/Pre, 2002)

Tyre characteristics play an important role in producing a good overall vehicle dynamics model (see figure 3.18). The tyre model can be simple or extremely complex, depending on the type of simulation test required. For the present study two types of tyre model were developed based on the 'Magic Formula' equation (Pacejka and Bakker, 1993). The one explained here is a rather simplified tyre model, based on the combined slip characteristics of slip angle and slip ratio as described in Milliken (Milliken and Milliken, 1995). The more complex tyre model will be explained later in this thesis (see Chapter 4).

Using a pure slip characteristic calculation of slip angle and vertical load, the normalized lateral force, $\overline{F}$, is defined as:

$$\overline{F} = \frac{F_y}{\mu_y Z} \tag{3.76}$$

where $\overline{F}$ - Nondimensional normalized lateral force

$\overline{F}$ F_y - Lateral force

$\mu_y Z$ - Peak force

Z - Vertical load

The peak force, μZ, is represented as a function of load and one may assume that $\mu_x Z$ is equal to $\mu_y Z$, thus:

$$Peak\_Force = \frac{\mu Z}{\left(1 + \left(1.5 * \frac{Z}{Mg}\right)^3\right)}$$

The normalized slip angle is defined as:

$$\overline{\alpha} = \frac{C \tan\alpha}{\mu_y Z} \tag{3.77}$$

where $\overline{\alpha}$ - nondimensional normalized slip angle

α - slip angle

C - cornering stiffness

$\mu_y Z$ - peak force

Cornering stiffness is also represented as a function of load and the lateral cornering stiffness C_α, and is assumed to be equal to the longitudinal cornering stiffness C_x.

$$\text{Cornering Stiffness} = a(1-\exp(-b*Z));$$

Where a=1200 - constant parameter
b=7.1670e-04 - constant parameter
Z - vertical load

Using the 'Magic Formula', the normalized lateral force, $\overline{F}$, is represented by:

$$\overline{F} = D'.\sin\left(C'.\arctan\left(B'.\left((1-E').\overline{\alpha} + \frac{E'}{B'}.\arctan(B'\overline{\alpha})\right)\right)\right) \tag{3.78}$$

where : B', C', D', E' : Parameters for solid curve for "Magic Formula"
$\overline{\alpha}$: Normalized slip angle
$\overline{F}$: Normalized lateral force

However, since the normalised slip angle is being replaced with the combined normalised slip variable, k, $\overline{F}$ becomes the normalised resultant force, R.

For the case of pure traction or braking with zero slip and camber angles, the normalised longitudinal force, $\overline{F}_x$, can be described as:

$$\overline{F}_x = \frac{F_x}{\mu_x Z} \tag{3.79}$$

and the normalised slip ratio, $\overline{S}$, as:

$$\overline{S} = \frac{C_x S}{\mu_x Z} \tag{3.80}$$

where F_x - traction or braking force
C_x - longitudinal cornering stiffness
S - Slip ratio, given by

$$S = \frac{\Omega R_0 - V\cos\alpha}{V\cos\alpha} \tag{3.81}$$

For zero slip angle S becomes:

$$S = \frac{\Omega R_0}{V} - 1$$

Using the combined slip characteristics, the calculation for slip ratio and slip angle for cases when traction or braking occur in a turn one would need a combined normalised slip variable as:

$$k = \sqrt{\overline{S}^2 + \overline{\alpha}^2}$$

and a normalised "resultant" force as:

$$R = \sqrt{\overline{F}^2 + \overline{F_x}^2} \tag{3.82}$$

Another necessary equation that is obtained from an analysis of measured data is;

$$\frac{\overline{F}}{\overline{F_x}} = \frac{\eta(k)\tan\alpha}{S} \tag{3.83}$$

where $\eta(k)$ - The multiplier necessary to hold for both small and large slip angles and the slip ratio

The $\eta(k)$ function is of the form: $\begin{Bmatrix} 0.5[1+\eta_0] - 0.5[1-\eta_0]\cos(0.5k), |k| \le 2\pi \\ 1, |k| > 2\pi \end{Bmatrix}$

At low slip, η is equal to η_0, where η_0 is determined from the cornering stiffness, longitudinal stiffness, lateral and longitudinal coefficients of friction. Thus:

$$\eta_0 = \frac{C_\alpha \mu_x}{C_x \mu_y}$$

By substituting into equation (4.77) one can separate the non-dimensional lateral and longitudinal forces as follows:

$$\overline{F} = \eta(k)R(k)\left[\frac{\tan\alpha}{\sqrt{S^2 + \eta^2 \tan^2\alpha}}\right] \tag{3.84}$$

$$\overline{F_x} = R(k)\left[\frac{S}{\sqrt{S^2 + \eta^2 \tan^2\alpha}}\right] \tag{3.85}$$

And by substituting these into equations (3.78) and (3.85) the final lateral and longitudinal forces generated at the tyre contact patch can be obtained.

3.8.1 Characteristics of the tyre model

Characteristics of the tyre model are shown in a series of plots below.

Tyre Characteristics 1: Lateral force vs. vertical load with different slip angle and A zero longitudinal slip ratio (see figure 3.19).

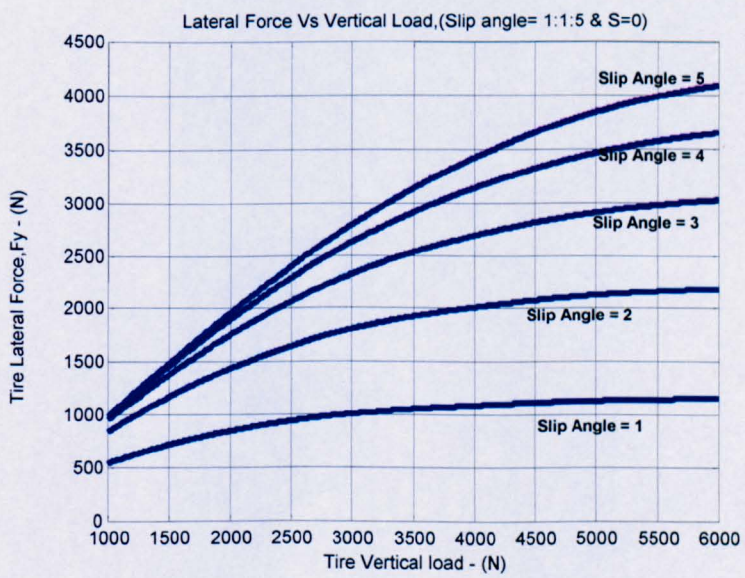

Figure 3.19: Lateral force Vs vertical load

Tyre characteristics 2: Lateral force vs. slip angle with different vertical load and a zero longitudinal slip ratio (see figure 3.20).

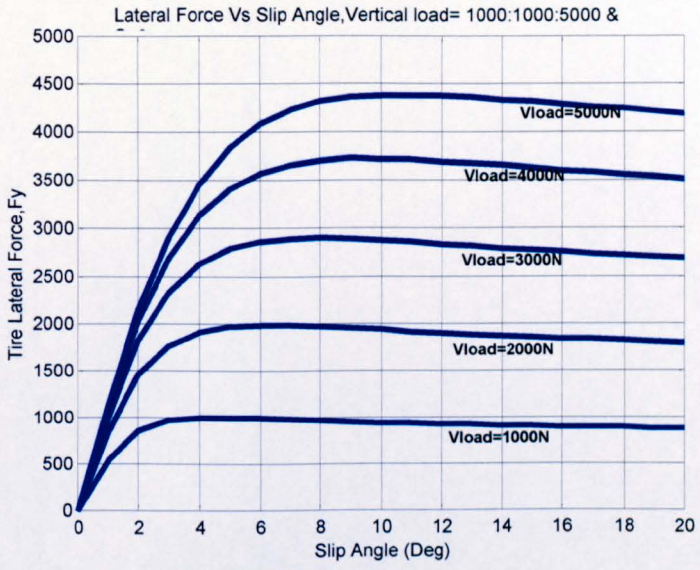

Figure 3.20: Lateral force Vs slip angle

Tire Characteristics 3: Lateral force vs. longitudinal slip ratio with a 2 deg slip angle and 3600N vertical load (see figure 3.21).

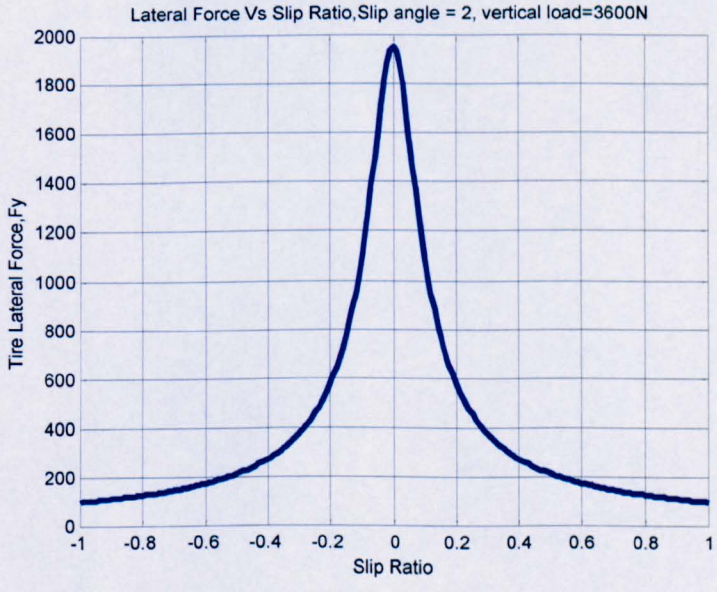

Figure 3.21: Lateral force Vs slip ratio

Tyre Characteristics 4: Lateral force vs. longitudinal force with 2 deg slip angle, 3600N vertical and longitudinal slip ratio between –1 to 1 (see figure 3.22)

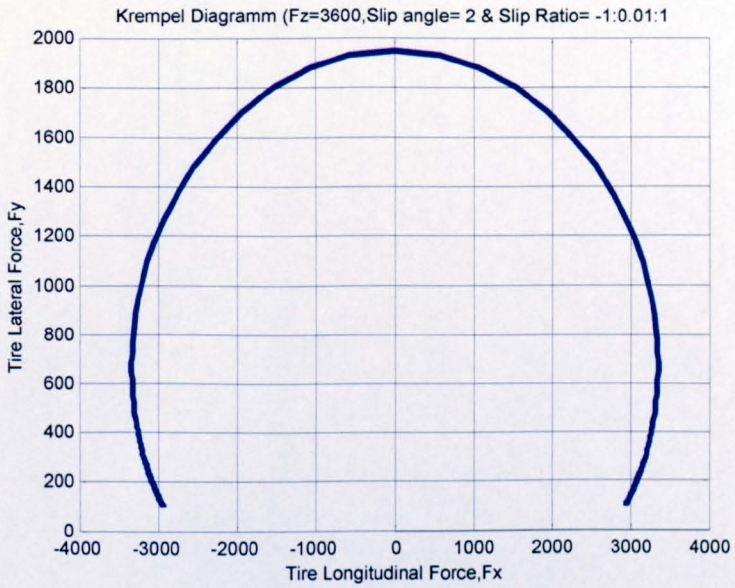

Figure 3.22: Lateral force Vs longitudinal force

Tyre characteristics 5: Longitudinal force vs longitudinal slip ratio with 2 deg slip angle and vertical load (1000N, 2000N, 3000N, 4000N, 5000N) (see figure 3.23).

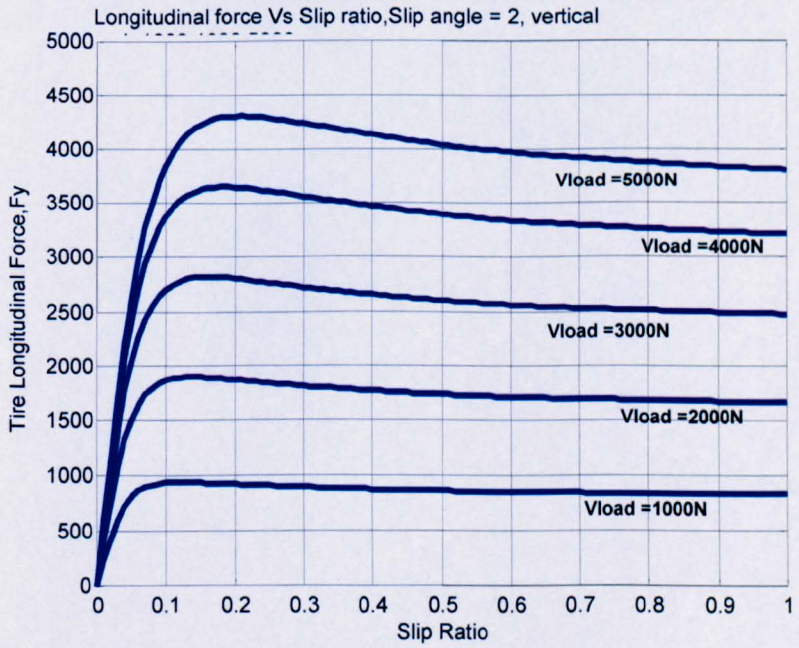

Figure 3.23 Longitudinal force Vs slip ratio

Tyre Characteristics 6: Cornering Stiffness vs. Vertical load (see figure 3.24).

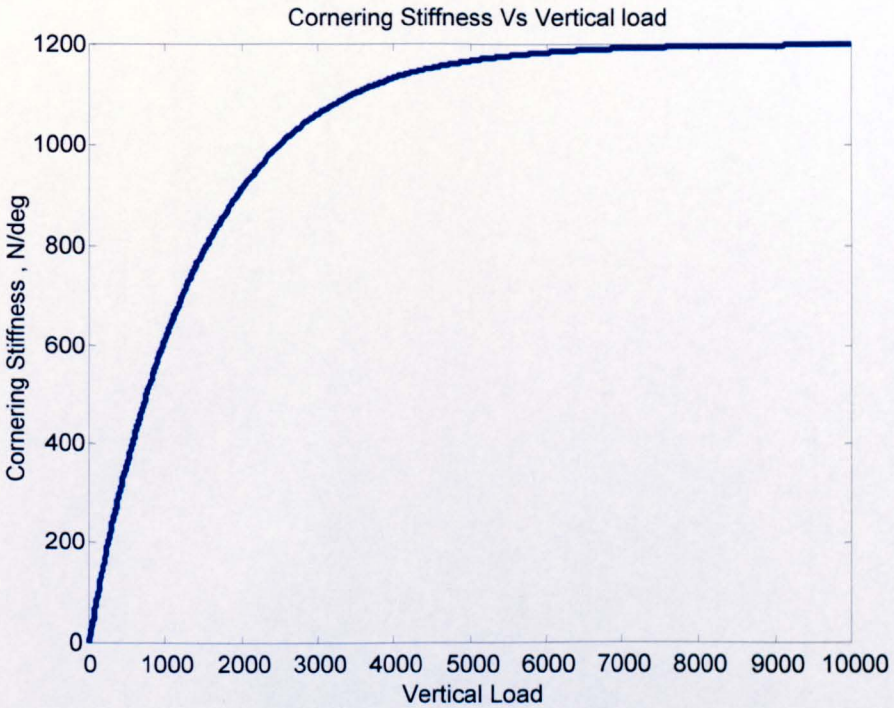

Figure 3.24: cornering stiffness Vs vertical load

Tyre Characteristics 7: Cornering Stiffness vs. Lateral force with zero longitudinal slip ratio and 5 deg slip angle (see figure 3.25).

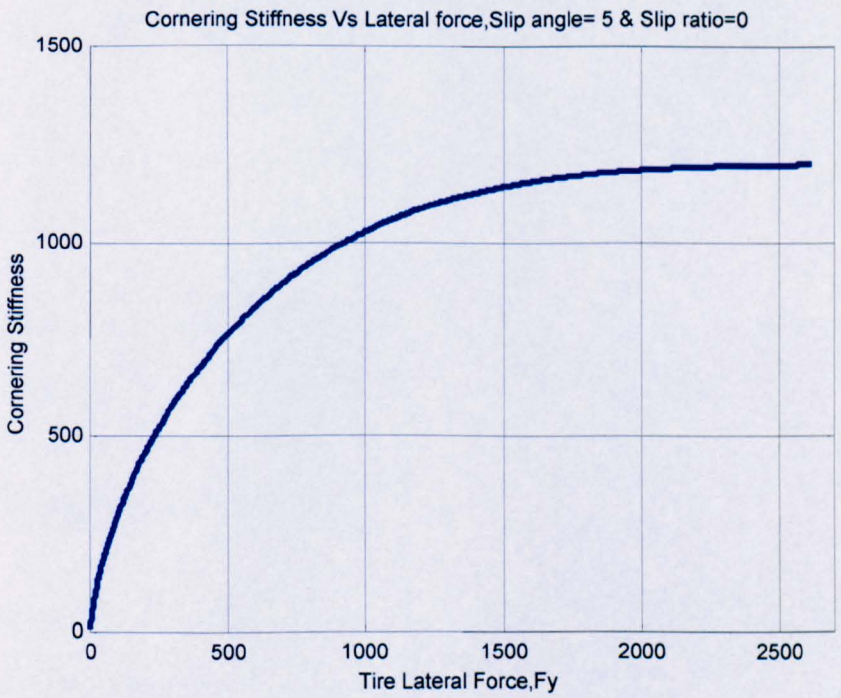

Figure 3.25: Cornering stiffness Vs Lateral force

3.9 Driver model

There is a choice of closed-loop (Gordon et al., 2002) or open-loop driver models. The closed-loop driver model depends on a reference vector field of target directions and speeds, which couples to simple proportional-plus-integral (PI) controllers for both steering and speed control. The vector field 'solves' the path and speed planning aspects of the driving task. An Ackerman steer provides a simple 'model' input for steering control and the remainder of the steering control is via PI feedback compensation. Tracking the speed reference control (S_{ref}) is done entirely via PI feedback. In more detail, the forward velocity (S) is the key parameter for speed control. The difference between the actual velocity (S) and the reference velocity (S_{ref}) generates an error (ε_1) that the PI controllers use to modify the command input to the model.

Deviation: $$\varepsilon_1 = \left(S - S_{ref}\right) \tag{3.86}$$

Speed Command: $$y_1 = \underbrace{-KI_1 \int \varepsilon_1}_{integral} \underbrace{-KP_1 \varepsilon_1}_{Proportional} \tag{3.87}$$

The deviation ε_1 of the actual speed from the desired value determines whether the output of the system would provide acceleration or a braking command. The output of the system, y_1, consists of two elements; an integral and a proportional element. The integral gain is KI and the proportional gain is KP.

The same approach is used for directional control. In this case a 3-element model of velocity is required: the longitudinal, lateral and yaw components of velocity. For directional control, θ_v, is the angle (in the global coordinates) of the reference vector within the reference vector field.

β is the yaw angle of the car and ε_2 represents a directional error between where the car is pointing and where it should be going: that is, ε_2 is the error between the vehicle's heading and the reference vector.

Deviation: $$\varepsilon_2 = (\beta - \theta_v) \tag{3.88}$$

Steering Angle Command; $$y_2 = \underbrace{-KI_2 \int \varepsilon_2}_{integral} \underbrace{-KP_2\varepsilon_2}_{Proportional} \tag{3.89}$$

The 'open-loop' driver is specified by desired steer angle and vehicle speed time-histories, but once again the speed control is feedback-based. However, since the desired speed is pre-computed a desired acceleration time-history is derived to provide an approximate input into the vehicle (equivalent torque demand), which is corrected by the PI feedback.

3.10 MATLAB/SIMULINK Model Structure

The Simulink model is structured in such a way that it is easy to understand. Basically there are 5 main subsystems as mentioned in an earlier section of this chapter. Each subsystem is further divided into yet more subsystems and these will be explained later. The five main subsystems (see Figure 3.26) are:

i) Body Dynamics
ii) Vehicle Kinematics
iii) Suspension and Steering
iv) Driveline and Tyre
v) Driver

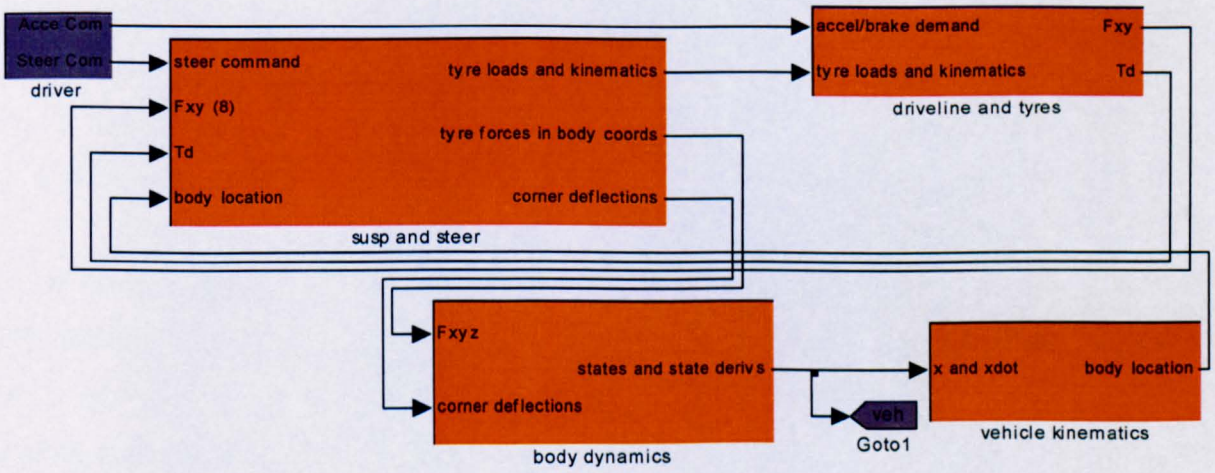

Figure 3.26 Overall vehicle dynamics model in MATLAB/SIMULINK environment

The model has closed-loop (Gordon et al., 2002)or open-loop modes. The closed-loop code is in a sub-folder that invokes a track definition and a resulting reference vector field. Here a fixed 20 m/s speed demand is used, and a simple look-ahead to the track centre-line. The programme file **trackgen.m** uses an initial set of control points that generate a reference path; it calls on the programme files **straight2.m** and **curve2.m** to generate more closely defined points and associated data, the format of which is an n × 8 matrix:

track = [s,points, tang, curv, r_centre]

- s = scalar distance from start point
- points = [x,y] coords of reference points
- tang = components of tangent vector along target path
- curv=curvature (= 1/radius) of the NEXT track section (zero for a straight line segment)
- r_centre = coordinates of track arc centre (or line segment centre for straight segments)

Run the program **map.m** to generate and plot the track, and also (two mouse clicks) to plot the target directions for the vehicle driver control.

The open-loop driver (again a separate sub-folder) contains functions such as **jturn.m** which define a time vector and driver demands for steering wheel angle and vehicle speed. There is a closed-loop aspect in that a target acceleration profile is generated and forward speed control attempts to track the desired speed using throttle and brakes. The name of the function specifying the particular manoeuvre is defined in **setic.m** (set initial conditions).

To switch between open-loop and closed-loop modes, the name of the s-function in **sixdof/driver** is changed as follows: **sfcont1** for closed-loop, and **sfcont2** for open-loop. The initial conditions also need to be defined and this is done in **setic.m**, which is fairly self-explanatory. Initial conditions are generally different for the open-loop and closed-loop modes.

In either open-loop or closed loop modes the road surface profile needs to be defined – here **roadsurface.m** contains a default flat road, but other cases can easily be defined.

The 'main programme' for running a simulation is **call.m** which contains calls to the setup m-files **modelsetup**, **lookup** (see below) and **setic.m** before running the model simulation **sixdof**. The programme file **call.m** also defines the simulation time-step and the stop time. Run **call.m** and give an optional file label to save results (e.g. 'run1' saves as **run1.mat**). If the file exists the data is simply re-loaded and no simulation is run. The exception is the default file label **temp.mat** which is over-written. Results may be viewed via **postprocess.m**, which again is fairly self-explanatory; and it can easily be edited and adapted according to the results required.

Note that both **setic.m** and **postprocess.m** use the names of states within **sixdof.mdl** and have to be updated if the state names (e.g. name of an integrator) are changed.

3.10.1 Vehicle and tyre data

Basic vehicle data is contained in **modelsetup.m** which also defines a number of matrices needed for the rigid body dynamics of the vehicle. These are explained in detail below. This m-file also calls **suspdat.m** (in subfolder **suspension data**), which further defines suspension data and tyre vertical stiffness.

The s-function **wheels.m** also contains some vehicle data: slip limits on ABS/TCS, time-constants for first-order lags in tyre force build-up, brake torque and drivetrain torque. Also the array *drive* defines FWD, RWD or 4WD, assuming open differentials in the current state of the model. The tyre model is also called using one command line in **wheels.m** which is of the form *[Fx,Fy]=magic(sx ,sy, vload)*.

The actual call is to the function **magic21.m** which sits in the sub-folder **tyre models**. Camber angles are available (variable name **gamma**) and can/should be used as the tyre model is refined further.

3.10.2 List of main sub-models and function used

3.10.2.1 Body dynamics

In this subsystem, the dynamics behaviour of the vehicle is constructed. All 6 equations of motion are modelled inside this subsystem. The effect of gravity and aerodynamics are also included here.

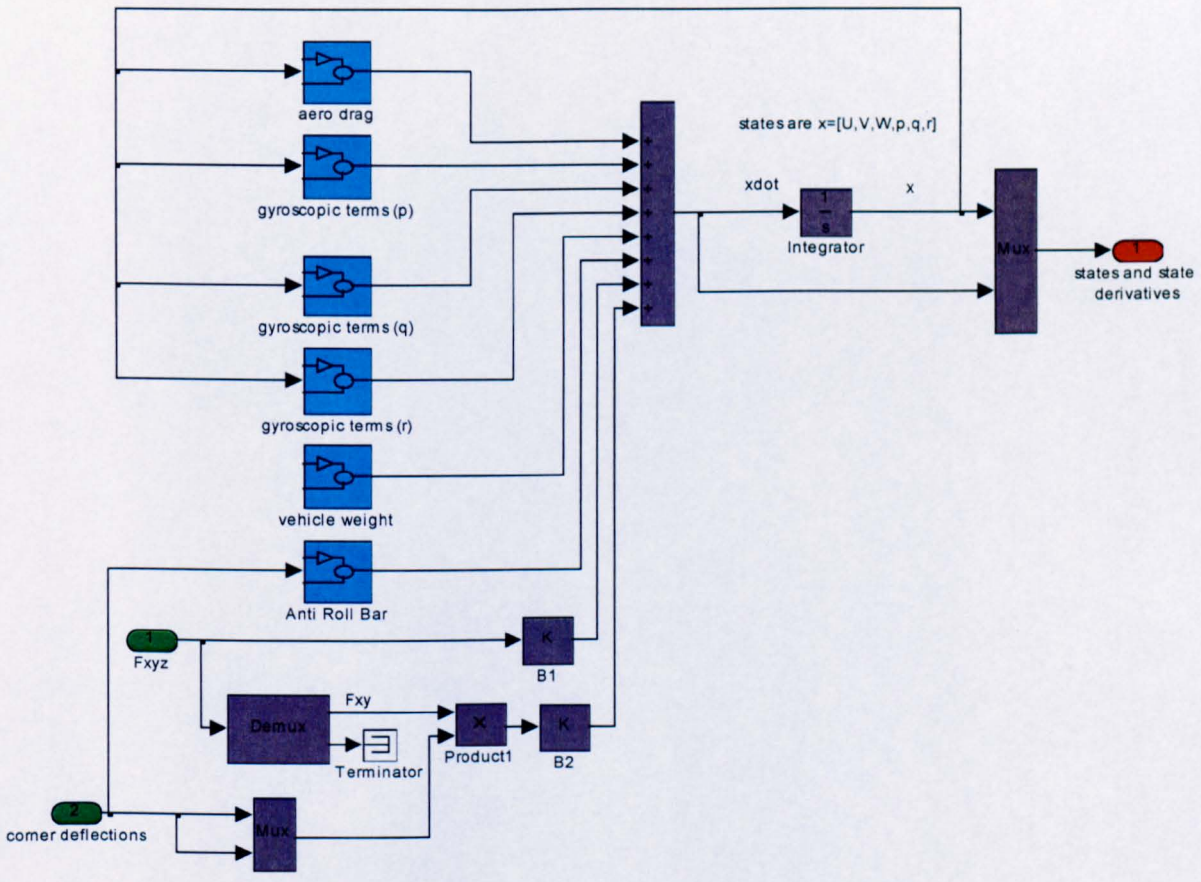

Figure 3.27 Body dynamics block

The inputs to the subsystem are F_x, F_y, vertical load and corner deflections. The output to this subsystem is the state and state derivative, which is then fed to the **Suspension & Steering** subsystem and also Matlab file. In this subsystem also the actual lateral and longitudinal accelerations are calculated. All calculations are in body coordinates and the sub-blocks are:

i) Aerodynamic drag

ii) Gyroscopic terms (p, q and r components)

iii) Vehicle weight (Gravitational effect)

3.10.2.2 Vehicle kinematics

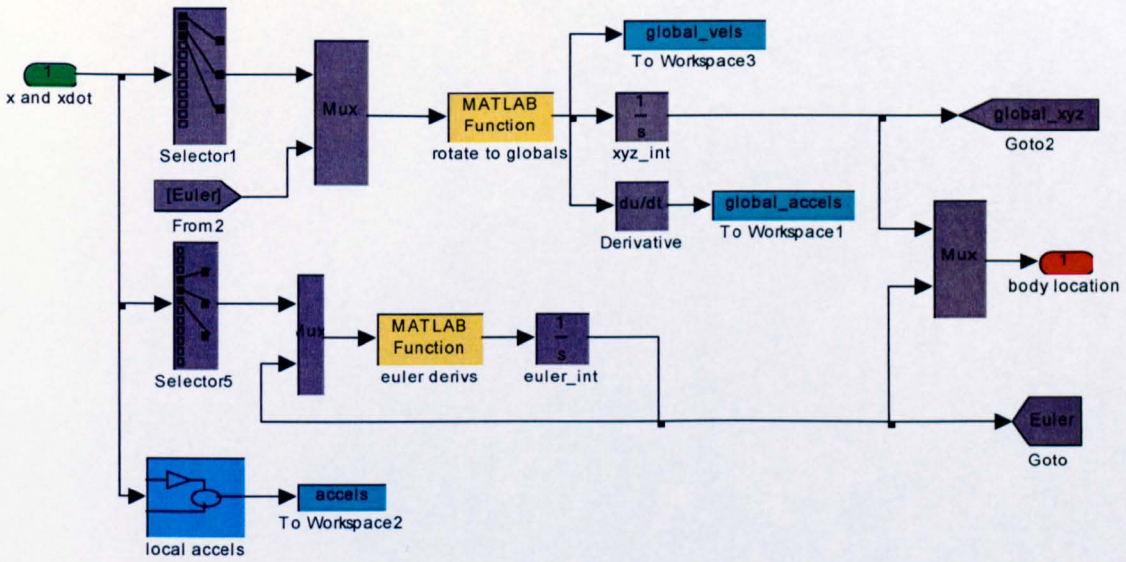

Figure 3.28 Vehicle kinematics block

This sub-system finds displacement and acceleration variables from the basic body motion variables. The inputs are in body coordinates and the outputs mainly in global coordinates. There are two sub-functions and one block in this sub-system, namely:

i) Euler derivatives – Compute vehicle angular velocity into 3 Euler Angle

ii) Local acceleration – Compute the actual vehicle acceleration

iii) Rotate to global – Rotate vehicle translational velocity from body coordinate to global coordinate

3.10.2.3 Suspension and steering

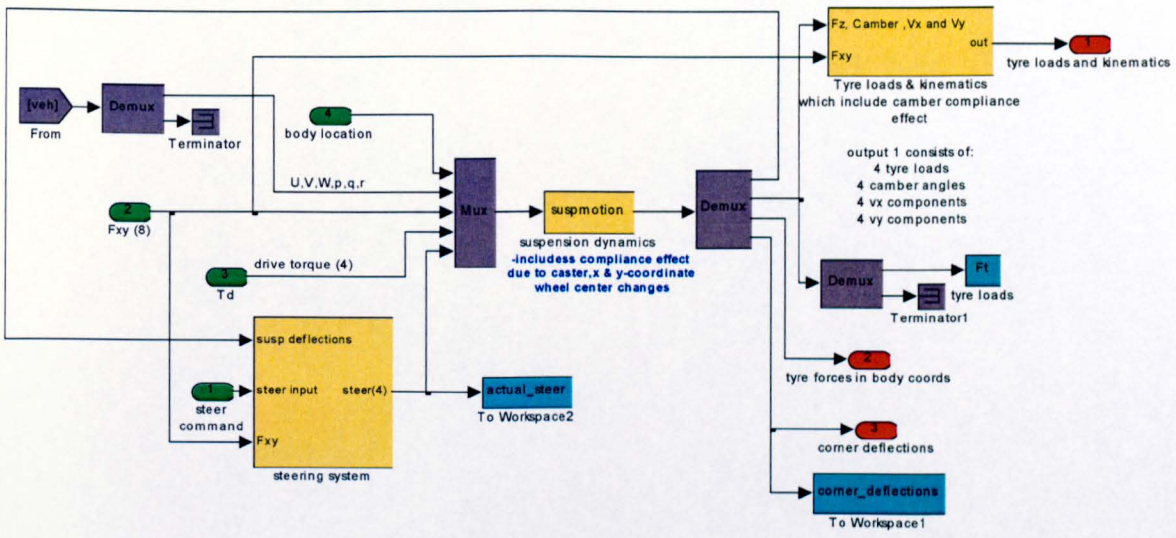

Figure 3.29 Suspension & steering system block

This block can be divided into two main parts. The first block is the steering correction calculation where the Ackerman method is use to make some adjustment to the steering input given by the driver model. Other inputs to the system are wheel travel and forces for the calculation of the compliance steer effect. The steering ratio for this model is 1:18, which is based on data, provided by FORD.

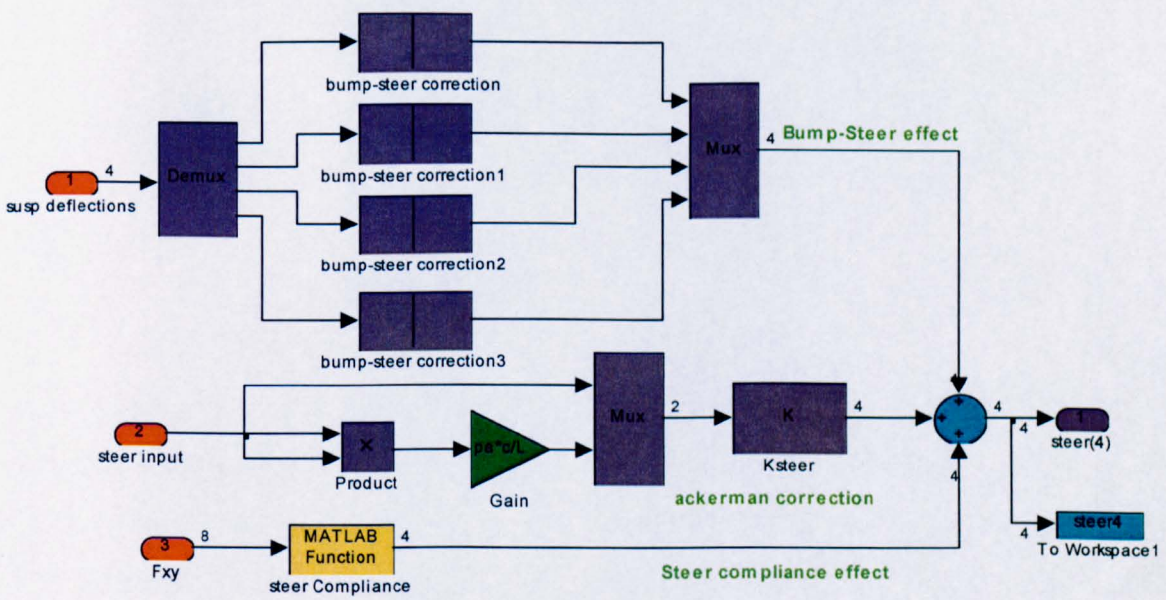

Figure 3.30 Suspension Motion Block

The second block, which is called 'Suspmotion' (refer to Figure 3.29), uses the S-function feature and inside it there are two more sub-functions associated with it:

i) Corner_kin.m – whose main purpose is to find the four corner deflections (suspension + tyre)

ii) Road_surface.m – whose main purposes are to find height of the road and unit downwards normal to the surface

Basically this block computes the suspension deflections and the tyre normal loads (relative to tyre/road coordinate). The s-function states are the four suspension deflections based on a massless wheel representation that includes suspension geometry effects, anti-roll bar, suspension compliance, bump stop and tyre lift.

3.10.2.4 Driveline and tyres

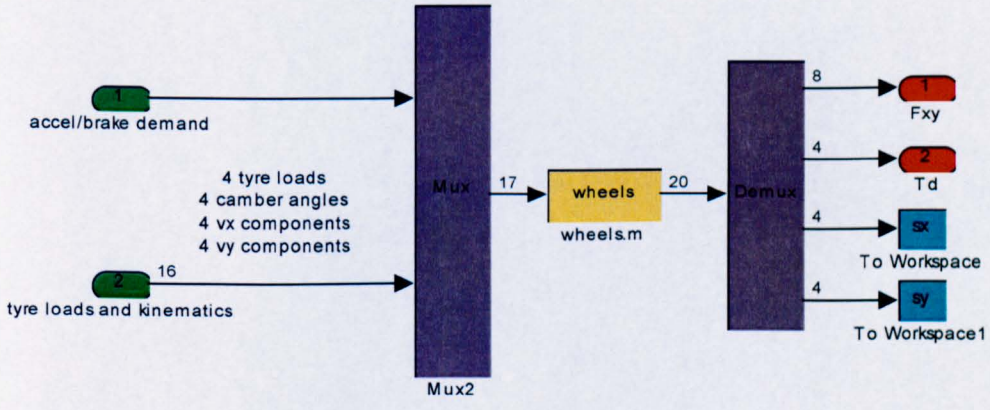

Figure 3.31 Wheel and tyre forces

This sub-system, which is called **wheel.m**, calculates tyre forces based on 17 state s-function inputs from the accel/brake demand, the tyre loads, the camber angles relative to the road and the in-plane vehicle velocities. There is only one sub-function under **wheel.m** which is called **Magic21.m** and it is used to calculate the lateral and longitudinal tyre forces (refer to the tyre modeling section).

3.10.2.5 Driver

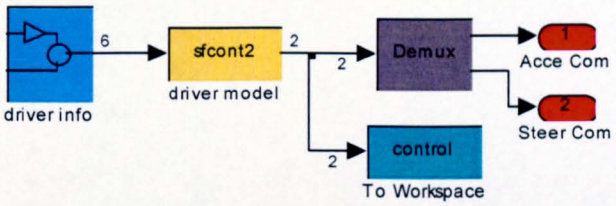

Figure 3.32 Driver model

There is a choice of closed-loop(Gordon et al., 2002) or open-loop driver modes for this sub-system. For the closed-loop driver, the inputs are the global x,y,z position, Euler angles, forward velocity, lateral velocity and yaw velocity to calculate steering and acceleration demand. However for open-loop driver mode the inputs are coming from a specific file which contains the desired steer angle, vehicle speed and time history. Different sub-function files are used to choose between driver modes. For the closed-loop driver mode the sub-function called **sfcont1.m** is used and for the open-loop driver mode the sub-function called **sfcont2.m** is used.

3.10.2.6 Other general-purpose routines

There are several general-purpose functions created in this model. These are:

i) **Matrix_b2g.m** – creates a rotation matrix, body to global

ii) **Rot_b2g.m** and **rot_g2b.m** – applies **matrix_b2g** or inverse to any input vector.

iii) **Mat_cam_t2b.m** – creates a rotation matrix (tyre to body) and also outputs the resultant camber angle

3.11 Closure

The Intermediate model described in this chapter can be further modify to include non-linear drag coefficient, non-linear damping coefficient and better representation of controller such as Anti-lock braking system or Traction control system.

For a high frequency ride comfort an analysis and for smaller speed bump at higher vehicle speed obviously the model need to be modify so to include unsprung mass element.

Chapter 4

Complex Vehicle Model and Suspension Test Rig

4.1 Introduction

One of the important objectives of this thesis is to conduct full vehicle analysis on a complex vehicle model and to acquire vehicle data, as well as suspension data from such a model to be used in the intermediate vehicle model. For this purposes, a complex vehicle multi-body model was established in the ADAMS/Pre environment (ADAMS/Pre, 2002) where all the data was provided courtesy of the Ford Motor Company based on a specific type of model.

The multi-body model was developed in ADAMS/Pre environment. ADAMS/Pre is one of the modules in the ADAMS suite of software, which is dedicated for designers or researchers to conduct studies related to vehicle analysis. Information about the overall capabilities of this module can be found in the MSC Software's website, which is: www.mscsoftware.com. Basically, there are 4 main data files, which are required to run simulation studies.

1. General vehicle information file (*.btt)
2. Front suspension system file (*.fst)
3. Rear suspension system file (*.rst)
4. Steering system file (*.sst)

There are also optional files: the powertrain system file, the brake system file and the control system file. However, for the work carried out in this thesis these optional files are not required.

Basically, *.btt file is for information such as tyre information, road profile information, rotational inertia, C.G of the vehicle, bushing related to chassis, aerodynamics forces, etc. All the related information regarding suspension data can be found in *.fst and *.rst files. For steering system information, the data is included in the *.sst file.

In all the above-mentioned files, at the end of the file one can include requested information to be available during the post-processing stages of the analysis.

If no option is selected, ADAMS automatically defaults to a standard control file (*.acf), which controls the steering, throttle and braking of the vehicle. Figure 4.1 shows a general process and relevant files in the ADAMS/Pre module.

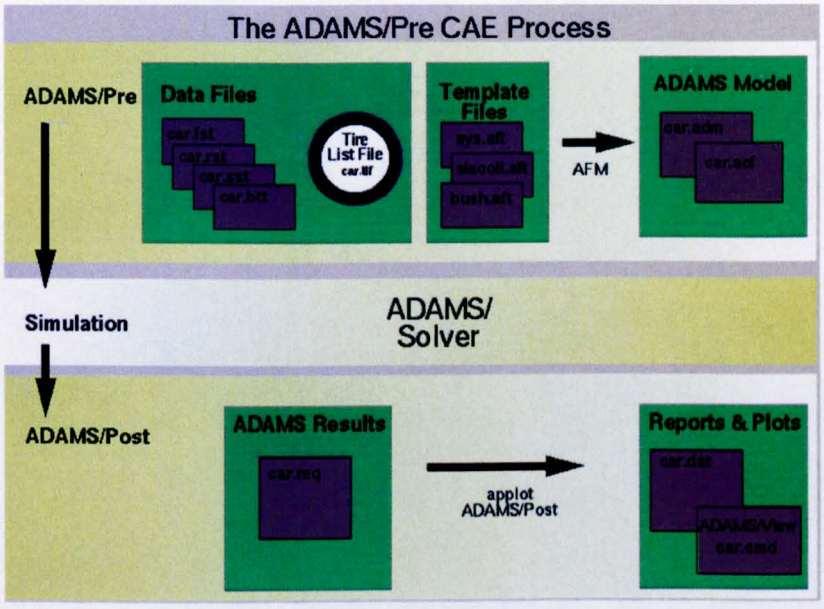

Figure 4.1: The ADAMS/Pre CAE process(ADAMS/Pre, 2002)

For the work carried out in this thesis, there are 5 important input files. These are:

i) Vehicle body
ii) Front suspension system
iii) Rear suspension system
iv) Steering System
v) Tyre model

The powertrain is not modelled in ADAMS/Pre. However, it is represented by the traction force acting directly on vehicle wheels, which is explained later in this chapter.

4.2 Vehicle Body

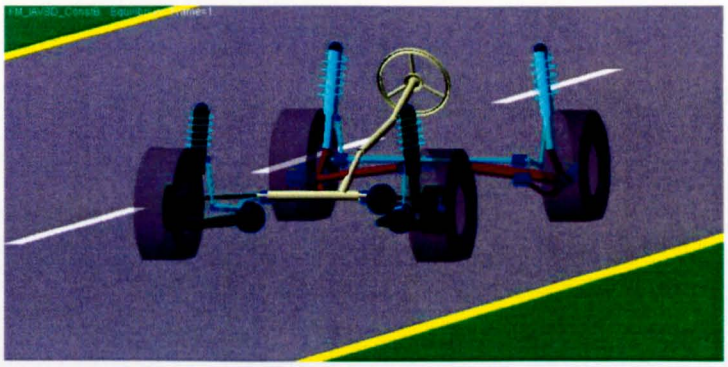

Figure 4.2: The ADAMS-base multi-body vehicle model

Body of the vehicle is considered to be rigid with general characteristics given in table 4.1 (also see figure 4.2).

General Characteristics		
Parameters	**Unit**	**Total**
Total weight	*N*	1.464E+04
Front ground reaction	*N*	8.795E+03
Rear ground reaction	*N*	5.849E+03
Total roll inertia	$kgmm^2$	5.129E+08
Total pitch inertia	$kgmm^2$	2.599E+09
Total yaw inertia	$kgmm^2$	2.769E+09
Total product Ixy	$kgmm^2$	1.269E+06
Total product Ixz	$kgmm^2$	-3.839E+06
Total product Iyz	$kgmm^2$	7.190E+04
Sprung mass	*Kg*	1.313E+03
Total c.g. height	*mm*	6.442E+02
Wheel track	*mm*	1.527 E+03
Wheelbase	*mm*	2.745E+03

Table 4.1: Vehicle Characteristics

The characteristics are obtained through SVC (Static Vehicle Characteristics) event. The characteristics computed by SVC are generally based upon the compliance matrix for a vehicle suspension. Loosely, this matrix is defined as the wheel centre deflections relative to the body due to unit forces and moments applied at the wheel centres. The compliance matrix is computed by inverting the Jacobian matrix formed

by ADAMS and then manipulating the resultant matrix to remove the body's six degrees of freedom and the effects of the tyres(ADAMS/Pre, 2002).

4.2.1 Aerodynamic Modelling in ADAMS

Other important input to the vehicle body is the aerodynamics forces, where the vehicle front section area is fixed to $2.130 m^2$ and the air density is taken as $1.220 kg/m^3$. In ADAMS/Pre, there is a routine, which models the aerodynamic forces and moments, which act on the vehicle. Aerodynamics modelling provides the sensitivities of a particular vehicle to wind gusts. This routine requires wind tunnel aerodynamic coefficient data for the vehicle being modelled and they must be taken according to the SAE J1594 conventions for Vehicle Aerodynamics Terminology. The user is provided an option of using two wind force points of application or only one. This option depends on the source and type of wind tunnel data. Europe tends to require two points, whereas the data in the U.S. is typically resolved to a single point. To apply aerodynamic forces at two positions on the body, the GFORCE statement (ADAMS/Pre, 2002) must be duplicated at both points.

A spline function for wind velocity versus angle of flow allows the modelers to simulate wind fans, chaotic wind forces, etc. The wind properties can be dependent on distance (useful for wind fan modeling) or on time (which allows the user to more easily investigate vehicle sensitivity versus speed). The wind velocity and angle are with respect to the ground frame of reference. The routine calculates relative wind speed and direction based on the vehicle velocity and yaw angle.

4.2.2 Powertrain/Traction controller

As mentioned earlier, for the work carried out in this thesis, the powertrain module is not necessary to be included in the vehicle model. The powertrain is merely represented by traction control directly to the vehicle wheels (see figure 4.3). The tyre routines allow for traction during a manoeuvre. This routine applies a force and a torque at the wheel centre for a given wheel. The torque is approximately equal to the force multiplied by the vertical distance of the wheel centre above the ground.

The tractive force is added to the tyre contact patch and transferred to the wheel centre with all of the other tyre forces.

To use traction, a corresponding SPLINE, ARRAY, and DIF statements are required (ADAMS/Pre, 2002). When using the traction controller, one should make sure that the appropriate longitudinal force ARRAY statements have been edited to allow for traction at the rear wheels for rear wheel drive vehicles and at the front wheels for front wheel drive vehicles. All wheel drive is also an option. As stated above, the traction ADAMS ARRAY statement must be specified. These statements provide the simulation with controller gains, as well as "on and off times" for the powertrain.

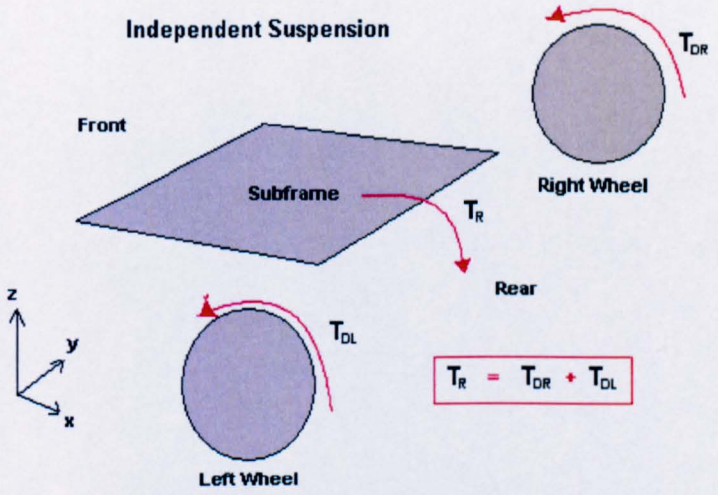

Figure 4.3: The Powertrain diagram

ADAMS/Pre models contain force elements for powertrain reaction torques, when the actual powertrain parts are absent. For an independent suspension the drive torques are reacted on the vehicle sub-frame or chassis. For a solid axle two sets of torques are modeled. The first set is a reaction on the axle housing part for the drive torques. These torques act about the vehicle Y-axis, and are opposite in direction to the drive torques on the rear wheels. The second torque is applied on the axle housing part about the vehicle X-axis, and reacted on the front engine mount part. The magnitude of the 2nd torque is the sum of the rear drive torques divided by the final drive ratio.

4.2.3 The Braking System

By default, ADAMS/Pre models the braking system by controlling torques at each of the 4 wheels. The brake proportioning spline controls the front/rear split. The brake controller applies torques as necessary to achieve the desired longitudinal deceleration. With the brake model, the brake controller controls the pedal force instead of the brake torques. However, for the work carried out in this thesis brake modeling is also not necessary. A similar approach to that for traction control is implemented for the brake control, where a standard PI (proportional-integral) controller is used to represent the braking system in the vehicle. The controller has brake proportioning for the front to rear, based on the longitudinal acceleration. It also has the ability to administer a side-to-side brake torque split. As with traction, braking requires corresponding SPLINE, ARRAY, and DIF statements. The ADAMS ARRAY statement provides the simulation with controller gains, as well as "on and off times" for the braking system.

4.3 Front suspension system

McPherson strut system is used in the model as shown in figure 4.4 below.

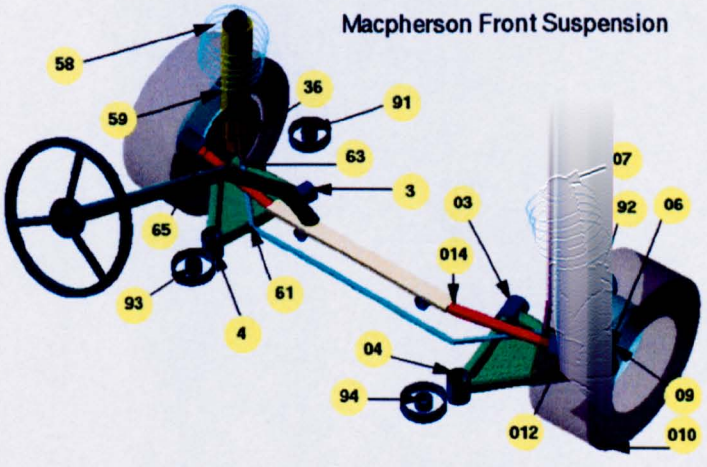

Figure 4.4: The Front Suspension System

Figure above shows the geometrical *hard-points* of all the joints in the suspension system. Not all hard-points use bushing to represent the joint between the two parts. The geometrical hard-points that use bushing are listed below in table 4.2.

Partname	Joint No
1. LCA Front Bushing	3
2. LCA Rear Bushing	4
3. Strut Mount Bushing	7
4. Tie Rod Ball Stud	12
5. Sta Bar Rotational	61
6. Sta Bar Link	63
7. Front Subframe	91-92
8. Rear Subframe	93-94

Table 4.2: Bushing locations in the front suspension

4.3.1 Front Suspension Characteristics

The suspension characteristics that ADAMS/Pre computes are based on the suspension geometry, the suspension compliance matrix, or both. Suspension geometry refers to the position and orientation of the suspension parts relative to the ground frame of reference as the suspension is articulated through its ride, roll, and steer motions. For example, the orientation of the wheel spindle axis is used to compute the toe and camber angles. The suspension compliance matrix refers to the incremental movements of the suspension due to the application of incremental forces at the wheel centres. ADAMS/Pre computes the suspension compliance matrix at each solution position as the suspension is articulated through its motion. Characteristics such as suspension ride rate and aligning torque camber compliance are computed based on the compliance matrix. The compliance matrix for a system, [C], is defined as the partial derivatives of displacements with respect to the applied forces:

$$[C] = [X/F]$$

If a system is assumed to be linear, the compliance matrix can be used to predict the system movements due to the input forces as:

$$\{X\} = [C]\{F\}$$

From this perspective, matrix element c_{ij} is the displacement of system degree of freedom i due to a unit force at degree of freedom j. ADAMS/Pre uses a 12 × 12 matrix relating the motion of the left and right wheel centres to unit forces and torques applied at the wheel centres. This matrix has the form:

$$\begin{Bmatrix} X\_Left\_wheel \\ Y \\ Z \\ AX \\ AY \\ AZ \\ X\_Right\_Whell \\ Y \\ Z \\ AX \\ AY \\ AZ \end{Bmatrix} \begin{Bmatrix} C(1,1), C(1,2) \ldots\ldots\ldots C(1,12) \\ C(2,1), C(2,2) \ldots\ldots\ldots C(2,12) \\ C(3,1), C(3,2) \ldots\ldots\ldots C(3,12) \\ \bullet \\ \bullet \\ \bullet \\ \bullet \\ \bullet \\ \bullet \\ \bullet \\ \bullet \\ C(12,1), C(12,2) \ldots\ldots\ldots C(12,12) \end{Bmatrix} \begin{Bmatrix} FX\_Left\_wheel \\ FY \\ FZ \\ TX \\ TY \\ TZ \\ FX\_Right\_wheel_x \\ FY \\ FZ \\ TX \\ TY \\ TZ \end{Bmatrix}$$

For example, element C(3,3) is the vertical motion of the left wheel centre due to a unit vertical force applied at the left wheel centre. Element C(3,9) is the vertical motion of the left wheel centre due to a unit vertical force applied at the right wheel centre. For an independent suspension without a stabilizer bar, C(3,9) is zero since a vertical force on the right wheel does not cause any motion of the left wheel.

ADAMS/Pre computes suspension wheel rate as the inverse of the z-axis displacement at the wheel centre due to the vertical forces applied at both the wheel centres simultaneously.

Left wheel rate = 1 / [C(3,3) + C(3,9)]

Right wheel rate = 1 / [C(9,3) + C(9,9)]

Detail explanation on how ADAMS/Pre calculates the suspension characteristics such as camber angle or caster angle is available in the ADAMS/Pre documentation(ADAMS/Pre, 2002).

For the suspension model used in the Ford Mondeo (vehicle studied in this thesis) the characteristics are as given in table 4.3 below:

Parameter	Unit	Average
Unsprung mass (total)	Kg	97.91
Roll centre height	mm	139.38
Wheel centre rise	mm	18.75
Static loaded tyre radius	mm	359.39
Track width	mm	1520.94
Axle distance from vehicle cg	mm	1096.42
Steer angle	Deg	0
Toe change	Deg/mm	-5.28E-03
Caster change	Deg/mm	8.09E-03
Camber change	Deg/mm	-1.48E-02
Roll camber coefficient	Deg/mm	7.39E-01
Percentage roll steer	%	3.40E+00
Single bump wheel rate	N/mm	3.97E+01
Roll rate	Nmm/deg	1.09E+06
Percent anti-dive/braking	%	1.80E+01
Percent anti-lift/accel	%	3.97E+00
Wheel hop natural freq.	Hz	1.09E+01

Table 4.3: Front suspension characteristics

Note: For more information on the compliance matrix, see *Definition of Compliance Matrix* in reference (ADAMS/Pre, 2002).

4.3.2 Kinematics Analysis (Left wheel)

As described in chapter 4, for the intermediate model to possess similar rigid suspension characteristics as the ADAMS/Pre model, kinematics analysis of the suspension system needs to be carried out on the complex multi-body model, so that the data obtained can be exported to the Matlab model for the virtual work calculations. For the approach undertaken in this thesis, there are several characteristics, which are required in the intermediate model:

a) Vertical wheel travel versus Longitudinal displacement of wheel center
b) Vertical wheel travel versus Lateral displacement of wheel center
c) Vertical wheel travel versus Camber angle displacement

d) Vertical wheel travel versus Caster angle displacement

e) Vertical wheel travel versus Toe angle displacement

Therefore, figure 4.5 through 4.7 are the output from suspension analysis conducted in the ADAMS/Pre software. These results are the standard plot retrieved from ADAMS/Pre post process

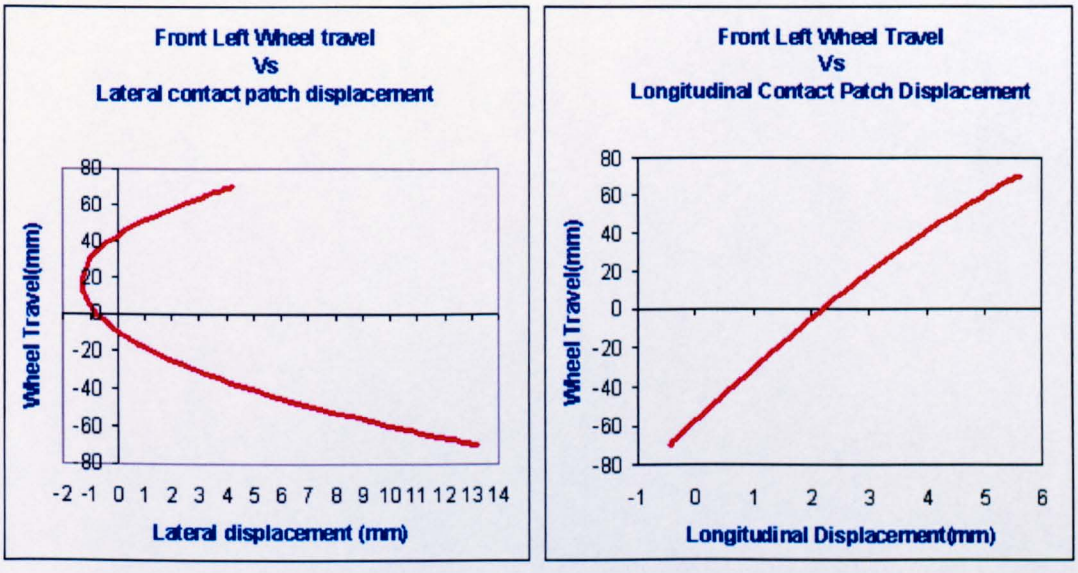

Figure 4.5: Wheel travel Vs Lateral/longitudinal displacement of at contact patch

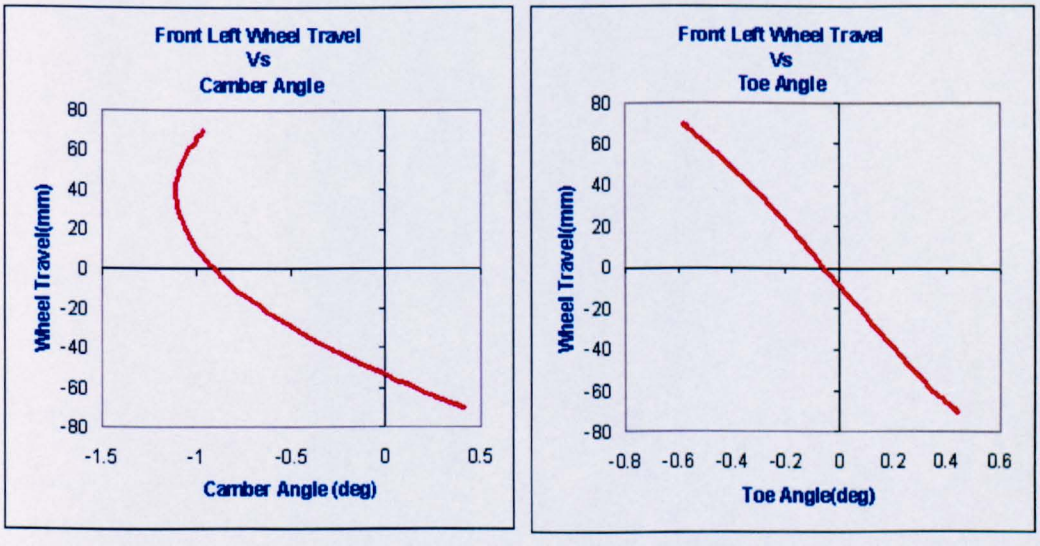

Figure 4.6: Vertical wheel travel Vs Camber/toe Angle

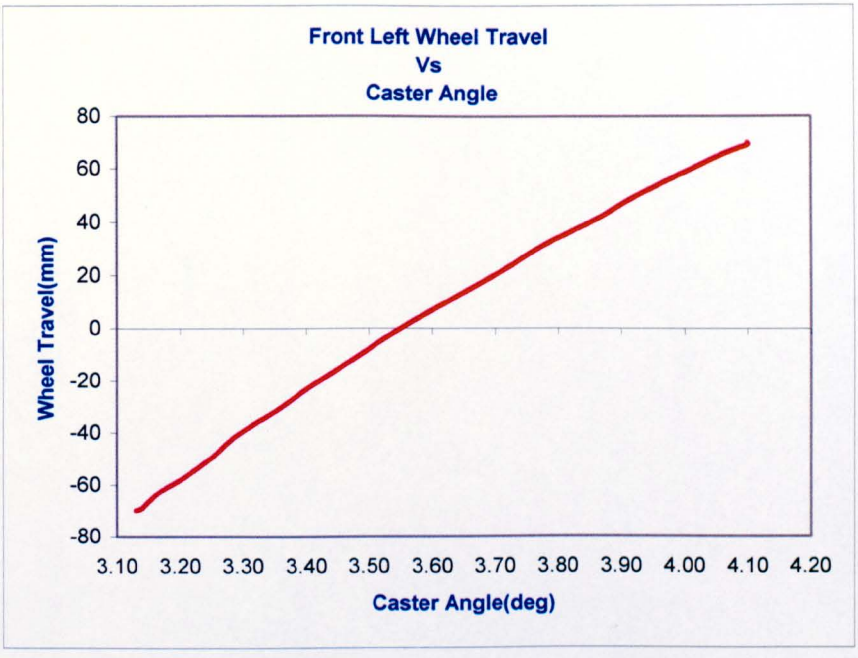

Figure 4.7: Vertical wheel travel Vs Caster Angle

These graphs are exported to the intermediate model, described in chapter 3. The imported data is given in table 4.4 below:

wheel travel	caster	toe	camber	longitudinal	lateral
70	4.1	-0.58	-0.962	5.63	4.24
69.1	4.1	-0.57	-0.968	5.57	4.07
66.6	4.07	-0.55	-0.989	5.40	3.58
62.4	4.03	-0.51	-1.02	5.14	2.79
56.6	3.98	-0.46	-1.06	4.82	1.82
49.5	3.92	-0.40	-1.09	4.44	0.79
41.1	3.86	-0.34	-1.11	4.02	-0.15
31.8	3.78	-0.27	-1.1	3.58	-0.88
21.6	3.71	-0.20	-1.06	3.11	-1.26
11	3.63	-0.12	-0.999	2.66	-1.25
0	3.55	-0.05	-0.9	2.20	-0.77
-11	3.48	0.02	-0.772	1.77	0.17
-21.6	3.41	0.09	-0.621	1.35	1.53
-31.8	3.35	0.16	-0.453	0.96	3.22
-41.1	3.29	0.22	-0.27	0.61	5.14
-49.5	3.25	0.28	-0.0903	0.30	7.14
-56.6	3.21	0.33	0.0747	0.03	9.06
-62.4	3.17	0.38	0.215	-0.18	10.75
-66.6	3.15	0.41	0.323	-0.33	12.07
-69.1	3.14	0.43	0.391	-0.42	12.91
-70	3.13	0.44	0.414	-0.45	13.20

Table 4.4: Front suspension kinematics data

4.3.3 Front anti-roll bar

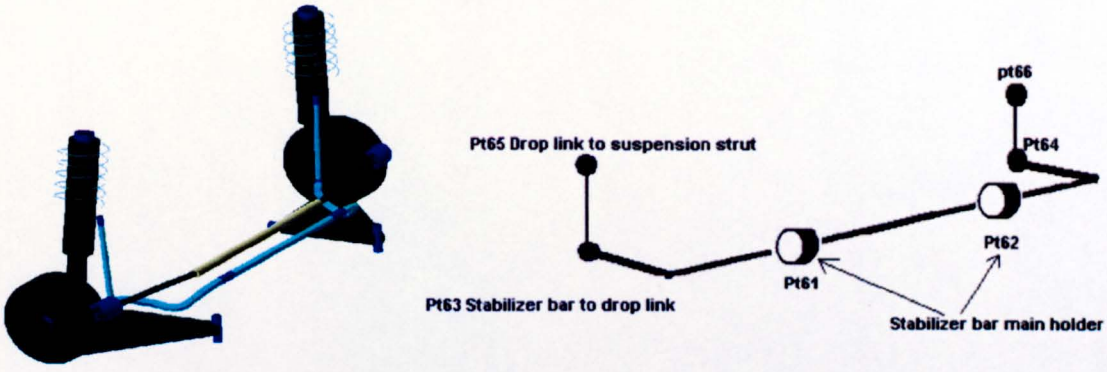

Figure 4.8: Front stabilizer bar

Beam element type of anti-roll bar model is used in complex vehicle model, which is more toward a realistic representation of actual physical of anti-roll bar.

Basically there are 26 points along the main strut of stabilizer where, each point is represented by rotational bushing, which as a spring rate and damping rate as mentioned in table below.

Spring rate of connection link (N/mm)	1.0E+05
Damping rate of connection link (N-s/rad)	2.5E+01
Modulus Young, E (N/mm^2)	2.07E+05
Modulus of rigidity, G (N/mm^2)	7.90E+04
Density (kg/mm^3)	7.86E-06

Table 4.5: Beam connection link data

Pt63, Pt64, Pt65 and Pt66 are joints, which are represented by bushing, and Pt61 & Pt62 are two joints, which hold the main stabilizer also represented by bushing. Bushing data are as shown in table 4.6 below.

Damping (N-sec/mm)	2.0E+01
Stiffness (N/mm)	2.0E+004
Tdamping (N-sec/deg)	3.49E-004
Tstiffness (N-mm/deg)	3.49E-01

Table 4.6: Bushing data

4.4 Rear suspension system

The model used is a Quadra-link strut system as shown below in figure 4.9.

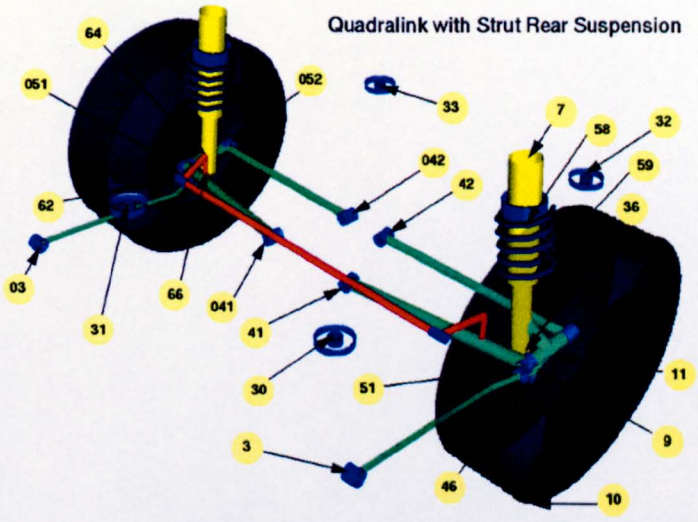

Figure 4.9: The Rear Suspension System

Figure 4.9 shows the geometrical *hard-points* of all the joints in the rear suspension system. Similar to the front suspension, not all the hard-points use bushing to represent the joint between the connected parts. The geometrical hard-points that use bushing are as listed below in table 4.5.

Partname	Part No
1. Strut Upper	7
2. Front Quad to Spindle	51
3. Front Quad to Subframe	41
4. Rear Quad to Spindle	52
5. Rear Quad to Subframe	42
6. Tension Strut to Spindle	46
7. Tension Strut to Frame	3
8. Stabilizer Bar to Frame	61-62
9. Front Subframe to Frame	30-31
10. Rear Subframe to Frame	32-33
11. Link to stabar bushing	63
12. Link to suspension bushing	65

Table 4.7: Part name and joint numbers

4.4.1 Rear Suspension Characteristics

A similar approach as described earlier for the front suspension characteristics is also used here. The rear suspension characteristics are listed below in table 4.6.

Parameter	Unit	Average
Unsprung mass (total)	Kg	8.252E+01
Roll center height	mm	1.787E+02
Static loaded tire radius	mm	3.667E+02
Track width	mm	1.527E+03
Axle distance from vehicle cg	mm	1.649E+03
Toe change	deg/mm	3.001E-03
Camber change	deg/mm	-1.764E-02
Wheel rate	N/mm	1.850E+01
Roll rate	N mm/deg	8.486E+05
Percent anti-lift/braking	%	3.167E+01
Percent anti-squat/accel	%	0.000E+00
Wheel hop natural freq	Hz	1.163E+01

Table 4.8: Rear suspension characteristics

4.4.2 Kinematics Analysis (left wheel)

Similar information as for the case of front suspension is also required here. The results from suspension analysis are shown in figures 4.9 through 4.11.

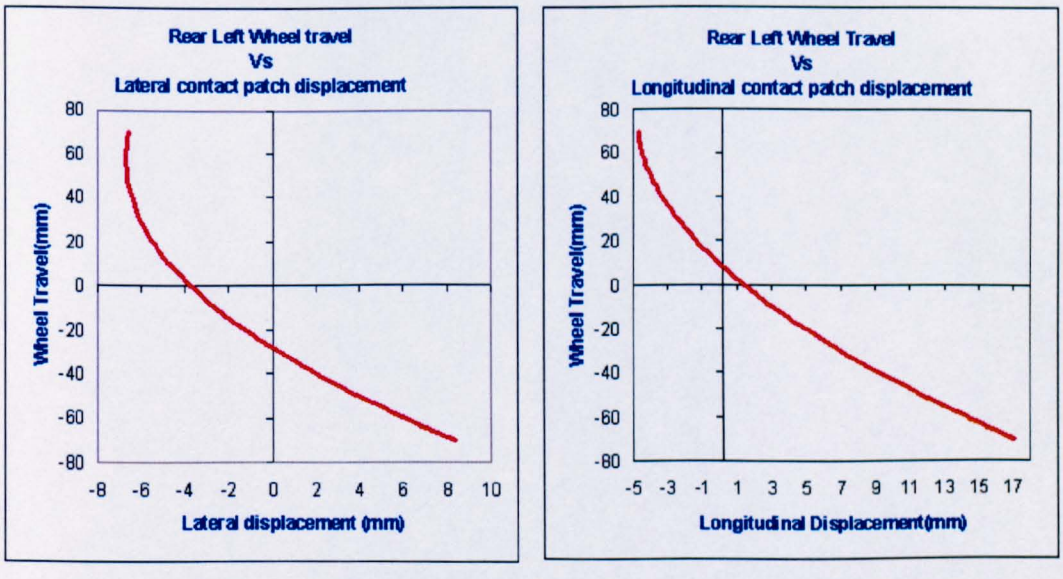

Figure 4.10: Vertical wheel travel Vs Lateral/longitudinal displacement at contact patch

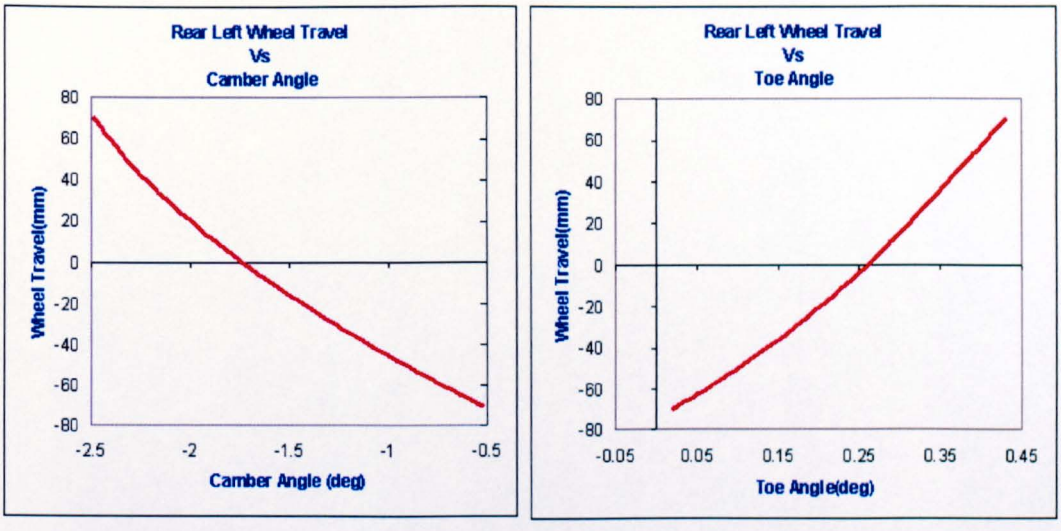

Figure 4.11: Vertical wheel travel Vs Camber / toe Angle

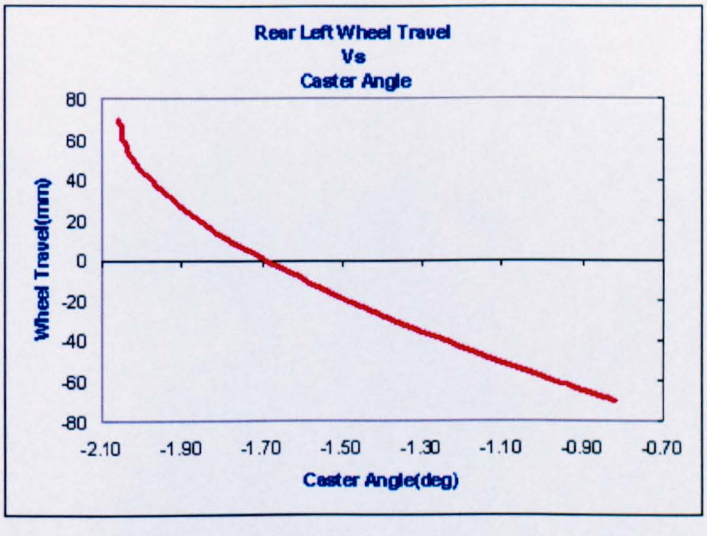

Figure 4.12: Vertical wheel travel Vs Caster Angle

These graphs are exported to the intermediate model in tabular form, with the data listed in table 4.9 below.

Wheel Travel	Caster	Toe	Camber	Longitudinal	Lateral
70	-2.06	0.43	-2.48	-4.65	-6.56
69.1	-2.06	0.43	-2.47	-4.64	-6.57
66.6	-2.05	0.42	-2.45	-4.61	-6.61
62.4	-2.05	0.41	-2.42	-4.51	-6.66
56.6	-2.04	0.40	-2.37	-4.31	-6.67
49.5	-2.02	0.38	-2.31	-3.95	-6.63
41.1	-1.98	0.36	-2.23	-3.37	-6.46
31.8	-1.93	0.34	-2.13	-2.56	-6.12
21.6	-1.87	0.32	-2.01	-1.49	-5.56
11	-1.79	0.29	-1.88	-0.15	-4.76
0	-1.69	0.26	-1.73	1.46	-3.71

-11	-1.58	0.23	-1.57	3.30	-2.45
-21.6	-1.47	0.20	-1.40	5.31	-1.00
-31.8	-1.35	0.17	-1.23	7.42	0.58
-41.1	-1.23	0.13	-1.07	9.53	2.22
-49.5	-1.12	0.10	-0.92	11.55	3.83
-56.6	-1.02	0.08	-0.78	13.37	5.31
-62.4	-0.933	0.05	-0.67	14.90	6.58
-66.6	-0.87	0.04	-0.59	16.06	7.56
-69.1	-0.832	0.02	-0.54	16.78	8.17
-70	-0.818	0.02	-0.52	17.02	8.37

Table 4.9: Rear suspension kinematics data

4.4.3 Rear anti-roll bar

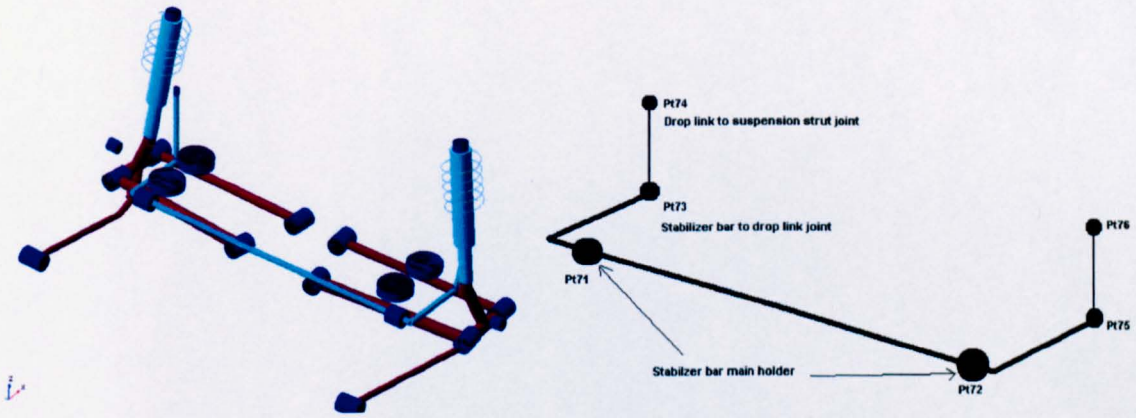

Figure 4.13: Rear anti-roll bar

Similar modeling approach is used to represent rear anti-roll bar however numbers of point along the main strut of stabilizer are reduce 8 points. This is due to the simple shape for rear anti-roll as can be seen in the figure 4.13 above.

Spring rate of connection link (N/mm)	1.0E+05
Damping rate of connection link (N-s/rad)	2.0E+02
Modulus Young, E (N/mm^2)	2.10E+05
Modulus of rigidity, G (N/mm^2)	8.0E+04
Density (kg/mm^3)	7.86E-06

Table 4.10: Beam connection link data

Pt73, Pt74, Pt75 and Pt76 are joints, which are represented by bushing, and Pt71 & Pt672 are two joints, which hold the main stabilizer also represented by bushing. Bushing data are as shown in table 4.11 below.

Damping (N-sec/mm)	2.0E+01
Stiffness (N/mm)	2.0E+004
Tdamping (N-sec/deg)	3.49E-004
Tstiffness (N-mm/deg)	3.49E-01

Table 4.11: Rear Bushing data

4.5 The complex tyre model

Tyre is one of the most important elements in any vehicle model. Reasonable tyre models can help to produce acceptable output for comparison with actual vehicle tests. Hence, the Magic Formula tyre model was chosen. The model is universally accepted in the industry. Since many ADAMS users have pre-existing tyre data from tyre suppliers and testing organizations in a format that is compatible with a special version of the Magic Formula tyre model cited in (ADAMS/Pre, 2002) and (Pacejka and Bakker, 1993), which is called "Pacejka tyre model", this model is used instead of the standard Magic Formula tyre model.

4.5.1 Magic Formula tyre model

For a given pneumatic tyre and road condition, the tyre forces, due to slip, follow a typical characteristic. The characteristics can be accurately approximated by a special mathematical function known as the Magic Formula. The parameters in the Magic Formula depend on the type of tyre and the road conditions. These parameters can be derived from experimental data obtained from tyre tests. The tyre is rolled over a road at various loads, orientations and motion conditions. The Magic Formula tyre model is, therefore, mainly of an empirical nature and contains a set of mathematical formulae, which are based on a physical background. The Magic

Formula calculates the forces (F_x, F_y) and moment $(M_x M_y M_z)$, acting on the tyre at pure and combined slip conditions, using longitudinal and/or lateral slip (κ, α), wheel camber (γ) and vertical force (*Fz*) as input quantities.

The general form (sine version) of the formula is written as follows:

$$Y(x) = D\sin[C\arctan\{Bx - E(Bx - \arctan(Bx))\}] \tag{4.1}$$

Where $Y(x)$ is either F_x or F_y. The self-aligning torque, M_z is calculated, using the lateral force F_y and the pneumatic trail *t*, which is based on a cosine type of Magic Formula (see figures 4.14 and 4.15):

$$Y(x) = D\cos[C\arctan\{Bx - E(Bx - \arctan(Bx))\}] \tag{4.2}$$

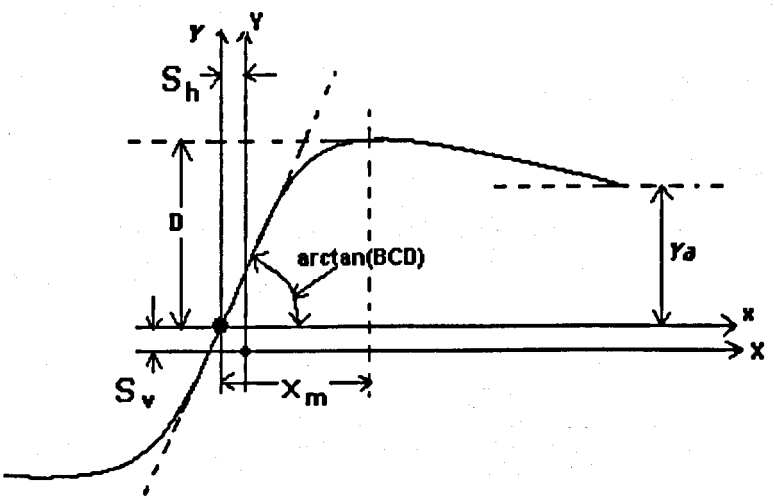

Figure 4.14: Some parameters in the tyre model (I)(ADAMS/Pre, 2002)

$$C = \frac{2}{\pi}\arcsin\frac{Ya}{D}; \qquad C = \frac{Bx_m - \tan(\pi/2C)}{Bx_m - \arctan(Bx_m)}; (C > 1)$$

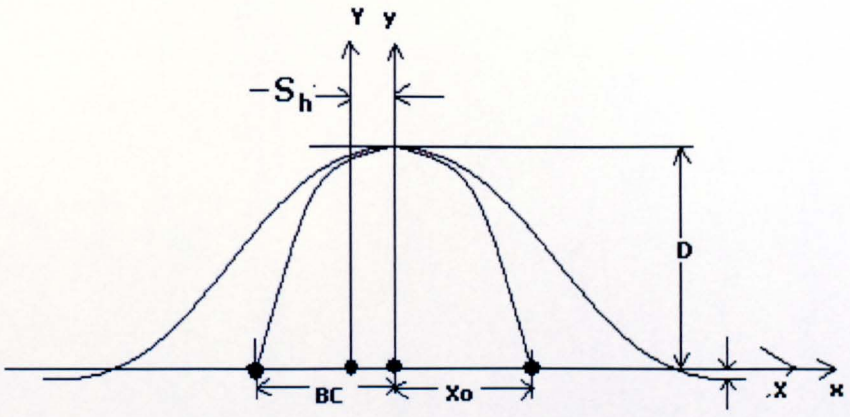

Figure 4.15: Some parameters in the tyre model (II)(ADAMS/Pre, 2002)

$$C = \frac{2}{\pi}\arcsin\frac{Ya}{D}; \qquad C = \frac{Bx_0 - \tan(\pi/2C)}{Bx_0 - \arctan(Bx_0)}; (C > 1)$$

Figures 4.14 and 4.15 show the curves produced by the sine and cosine versions of the Magic Formula respectively.

4.6 Steering System

A rack and pinion steering system is used in the Ford Mondeo car. The geometrical *hard-points* are listed in table 4.12.

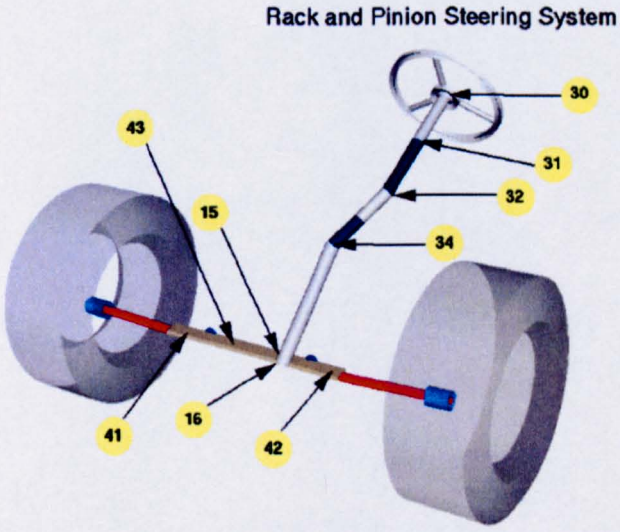

Figure 4.16: The Steering system

GEOMETRY HARDPOINTS

Steering Wheel	30	Tilt U-Joint	31
Upper U-Joint	32	Lower U-Joint	34
Bottom of Pinion	15	Center of Rack	16
Steering Gear Mount	41-42	Steering Gear Mount	43-44

Table 4.12: The hard-points in the steering system

4.7 Suspension Test Rig

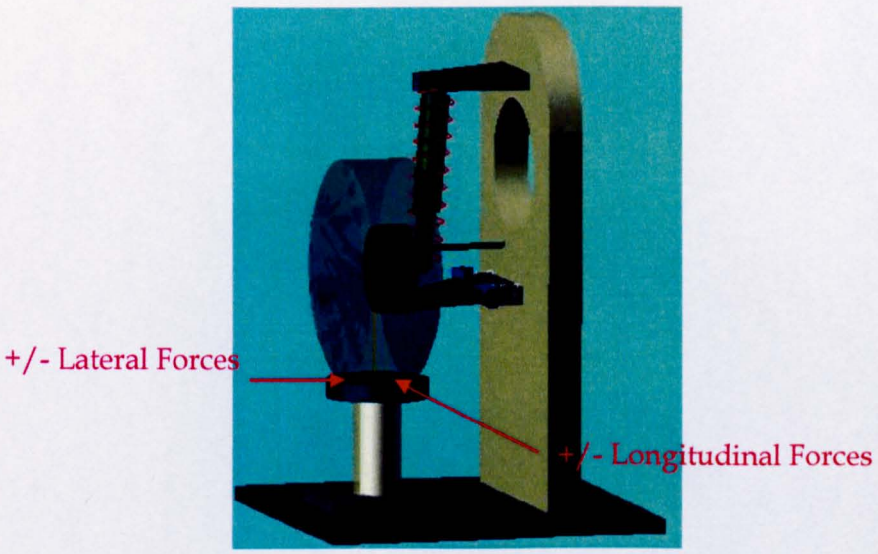

Figure 4.17: The virtual suspension test rig

As mentioned in chapter 1, one of the objectives of this work is to investigate the deformation of bushing in suspension due to forces acting on the contact patch. It is also important to ascertain the effect of wheel travel on the deformation of suspension system. This is for the purpose of noting the differences between simplified representation of suspension compliance in the intermediate model and complex compliance representation in the multi-body model.

The virtual test rig has to be built from basics (see figure 4.17), because the standard ADAMS/Pre module does not allow the user to simply model a "new" event, which is required for suspension deformation analysis. Thus, the virtual test rig had to be built in the core ADAMS/View environment. However, all geometrical detail, material properties, joints and the bushing associated with the suspension are exactly the same as the data exported from the ADAMS/Pre module.

The virtual test rig allows variable lateral and longitudinal forces to be applied to the suspension at different positions. For example, with specific lateral and longitudinal forces throughout the suspension jounce and rebound, the effect of these forces can be mapped as suspension compliance.

4.7.1 Suspension Compliance Characteristics

Using the virtual suspension test rig the steady state compliance effect due to forces acting at the contact patch and at the different position during wheel travel can be extracted as described in following section.

4.7.1.1 Contact patch deformation

Motions of contact patch in longitudinal and lateral directions are very important in the analysis, as they represent anti-dive/squat effects, as well as geometrical effect in suspension system. This information is then used in the virtual work calculations to determine the vertical loads acting on each wheel (see chapter 3). Due to this reason the work has been further extended to establish the extent to which bushing compliance contributes to the movements within the contact patch. These are rather simple analysis and the data were taken out from ADAMS/View standard Post Processor. The results are shown in figure 4.18.

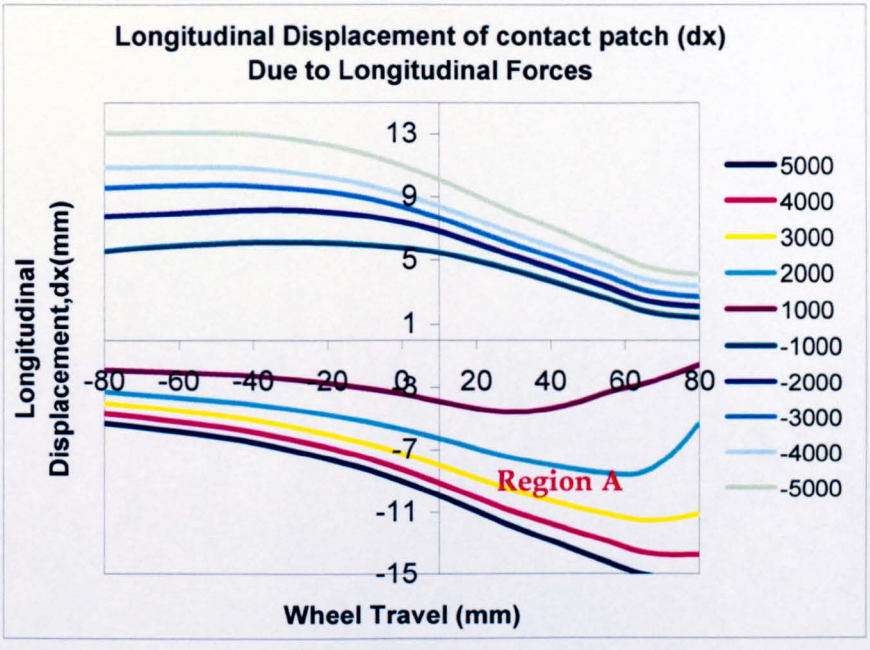

Figure 4.18a: Longitudinal deformation at contact patch due to Fx

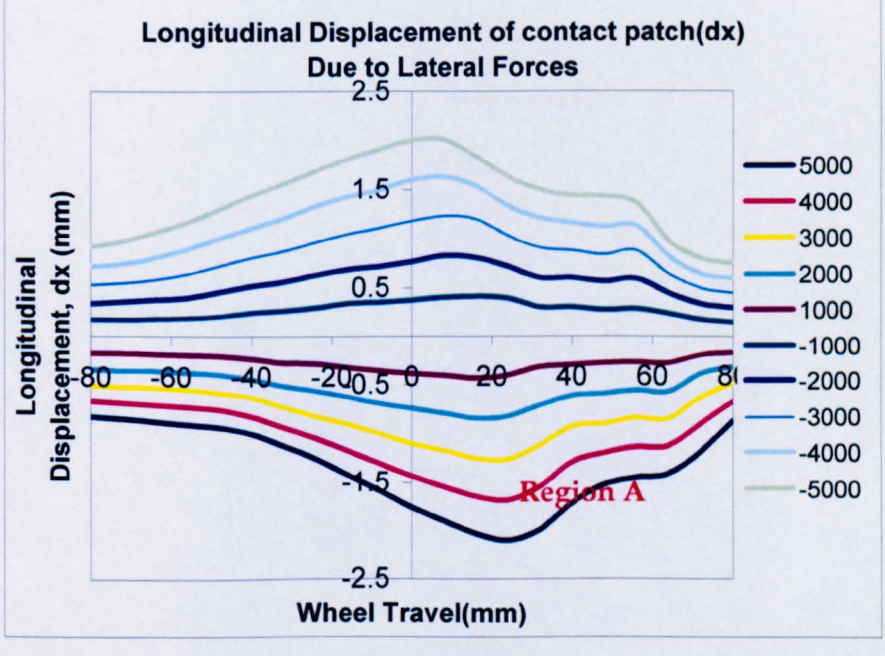

Figure 4.18b: Longitudinal deformation at contact patch due to Fy

The figure 4.18b shows the most important area is in region A, where the vehicle is subjected to braking or cornering, which means that the longitudinal force should be negative and the suspension is in a state of compression. The results show significant deformation, as much as 15mm, when the longitudinal force is at –5000N. Lateral forces also contribute to longitudinal deformation, but insignificantly, when compared to the longitudinal applied forces (see figure 4.19).

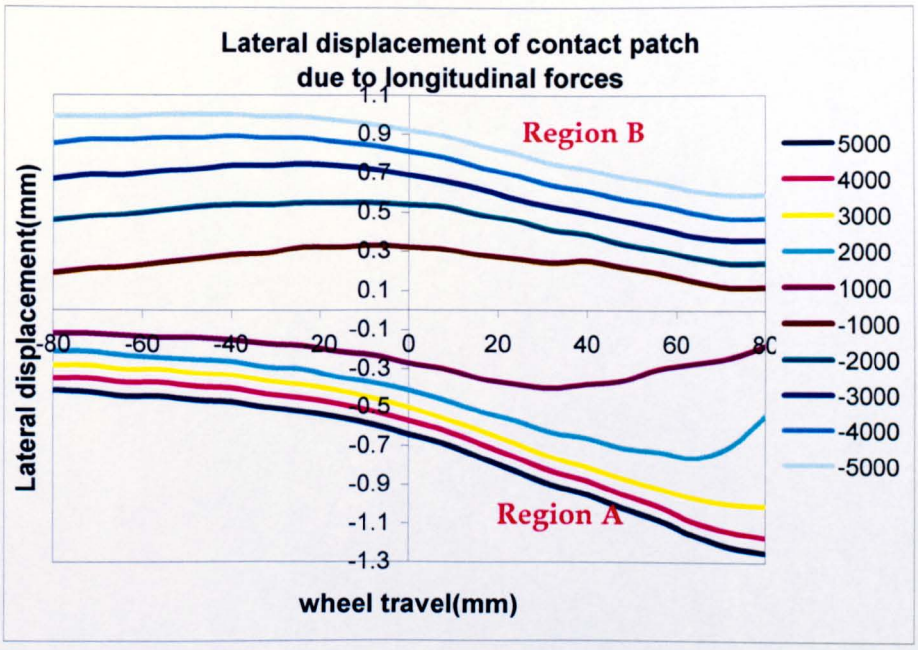

Figure 4.19a: Lateral deformation at contact patch due to Fx

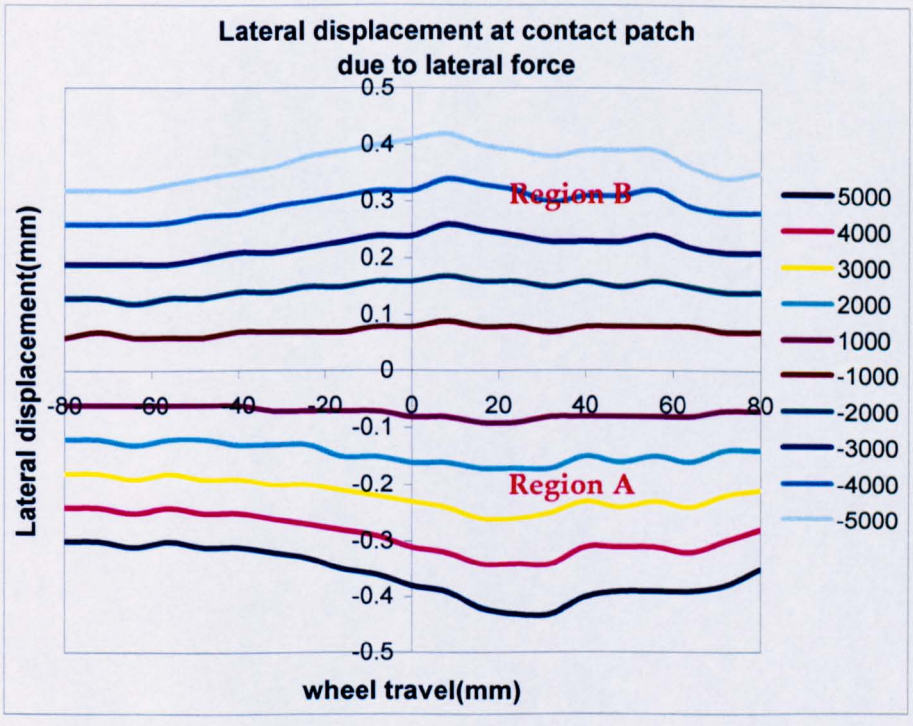

Figure 4.19b: Lateral deformation at contact patch due to Fy

For lateral deformation, regions A and B are the most important, because the vehicle can turn left or right, which means that the forces can be either positive or negative. The results show minimal deformation in lateral direction either due to lateral or longitudinal forces.

4.7.1.2 Wheel Camber deformation

Camber plays an important role, especially for vehicle handling. Negative camber can provide stability and also increase tyre contact patch area during cornering. Thus, it provides a better grip at the contact patch. However, this can lead to excessive tyre wear (Rahnejat, 1998). The analysis conducted here is to ascertain how far the suspension bushings contribute to the additional camber deformation. The results are shown in figure 4.20.

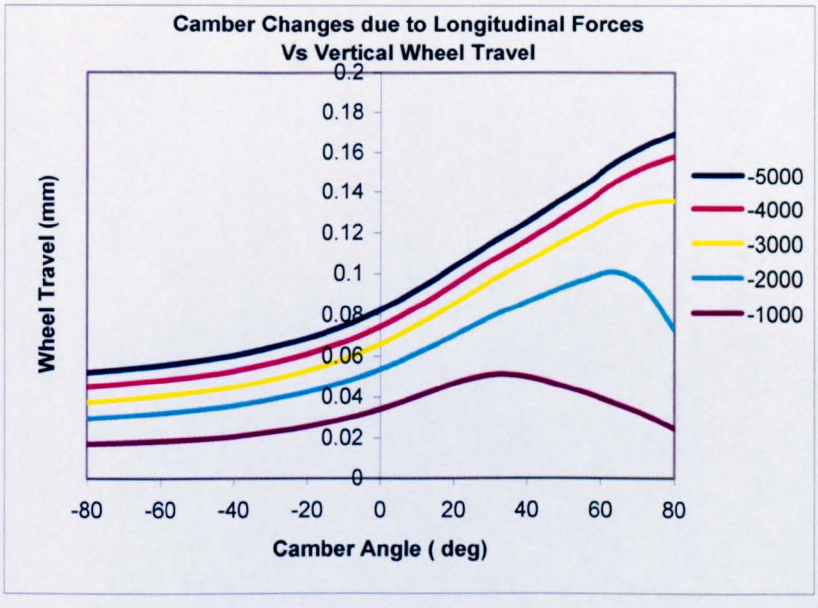

Figure 4.20a: Camber changes Vs vertical wheel travel due to longitudinal forces

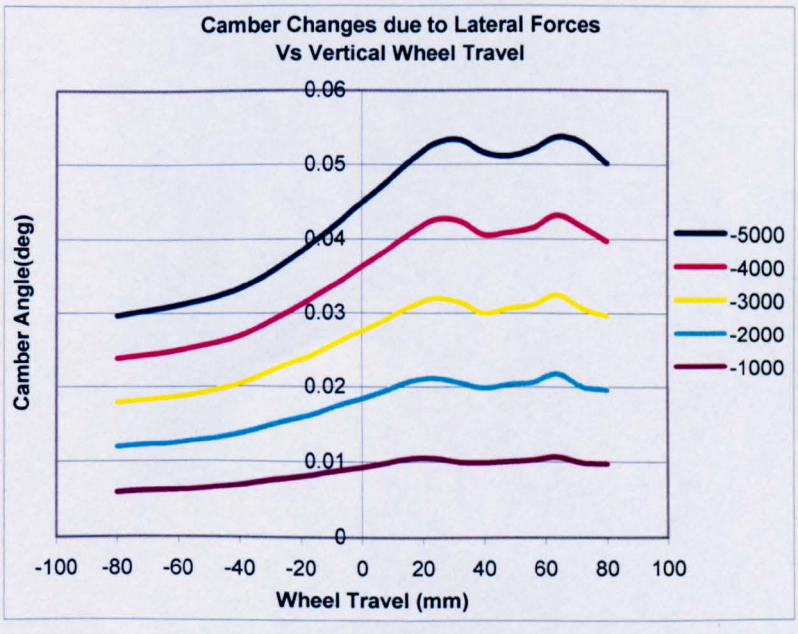

Figure 4.20b: Camber changes Vs vertical wheel travel due to lateral forces

From the results, it is clear that the camber deformation is quite small, and that the longitudinal force is the main parameter contributing towards camber deformation rather than the lateral force.

4.7.1.3 Wheel Caster Displacement

Most vehicles are not particularly sensitive to caster settings. Nevertheless, it is important to ensure that the caster is the same on both sides of the vehicle in order to avoid the tendency to pull to one side. While greater caster angles serve to improve straight-line stability, they also cause an increasing steering effort. Three to five degrees of positive caster is the typical range for its setting, with the lower angles being used on the heavier vehicles in order to keep the steering effort to a reasonable limit.

For the work carried out in this thesis caster change in the wheel is the most important rotational parameter compared to the toe or camber angles. This is because up to this stage only torque from caster change is included in suspension calculations. Thus, caster deformation is rather an important element , as well as to ascertain how far it affects deformation due to the tyre forces. The effect of wheel travel on caster change via tyre forces is shown in figure 4.21.

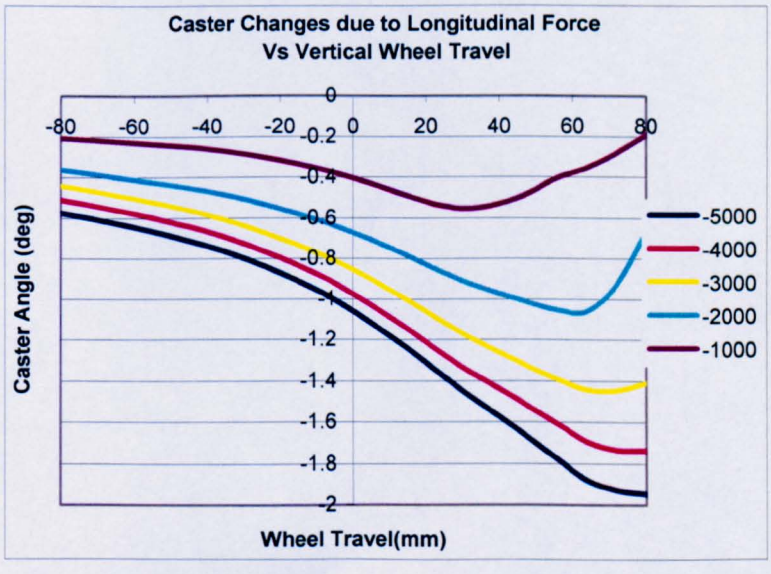

Figure 4.21a : Caster change Vs vertical wheel travel due to longitudinal forces

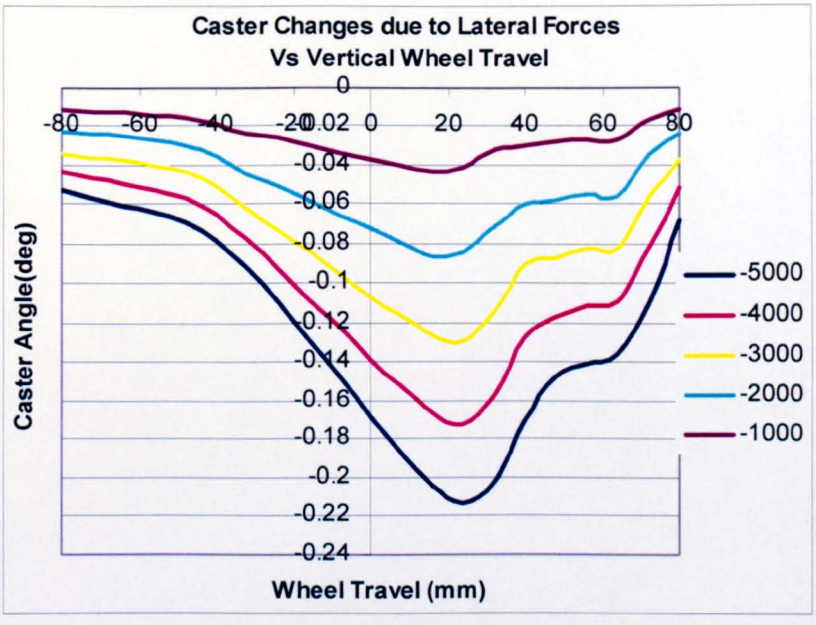

Figure 4.21b : Caster change Vs vertical wheel travel due to lateral forces

The result shows caster angle changes of up to 2 degree due to tyre longitudinal force variation. Even though the changes appear to be small in term of value, they actually are quite significant, since the caster change due to geometry as shown in figure 4.21, is also around 2 degree. Thus, bushing deformation can contribute significantly in term of percentage changes in caster angle.

4.7.1.4 Wheel Toe Displacement

Wheel toe is one of important elements in suspension characteristics. Toe settings affect three major areas of performance: tyre wear, straight-line stability and corner-entry handling characteristics. The toe setting on a particular car becomes a trade-off between the straight-line stability, afforded by toe-in and quick steering response promoted by toe-out. However, excessive toe can cause tyre wear, as well as power loss. The analysis conducted here is to understand the extent of bushing compliance upon toe displacement. The results are as shown in figure 4.22. The results show that bushing compliance can contribute up around 20% in toe change, if one compares it with toe change due to geometry alone.

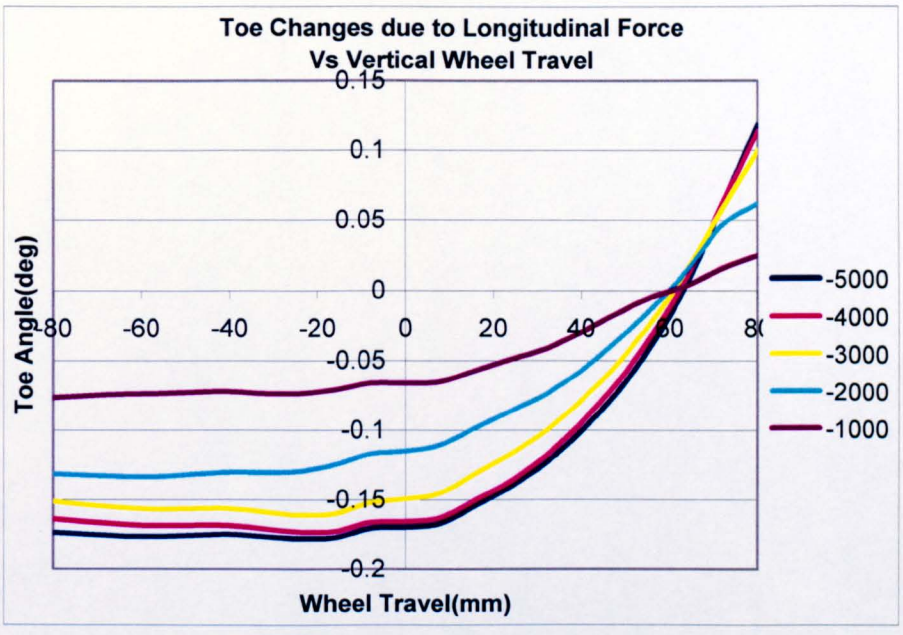

Figure 4.22a: Toe change Vs vertical wheel travel due to longitudinal forces

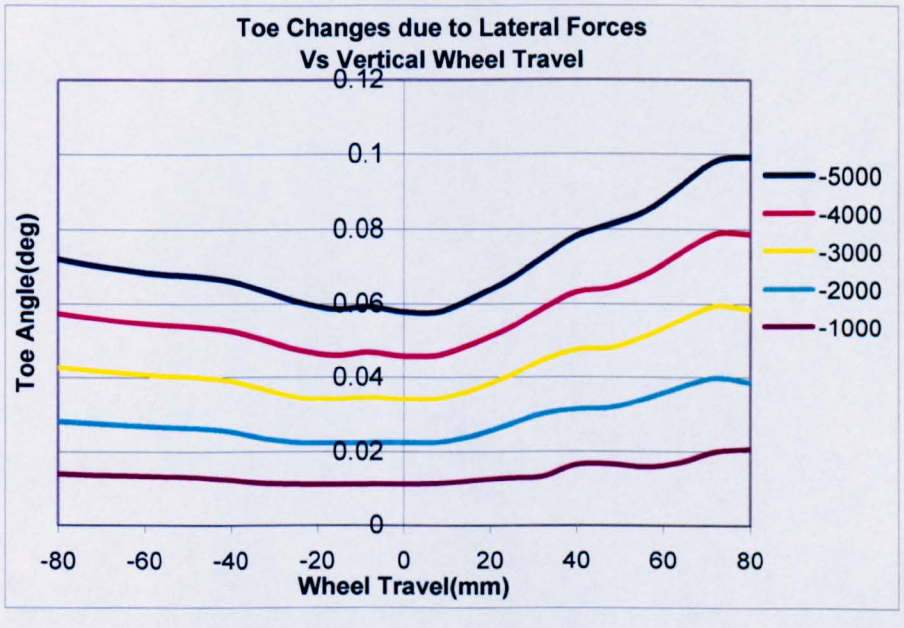

Figure 4.22b: Toe change Vs vertical wheel travel due to lateral forces

4.8 Closure

The ADAMS multi-body vehicle model presented here is a very complex model with a high degree of suspension system non-linearity, when compared to the intermediate model.

The characteristics of the suspension due to the geometry were retrieved to be used in the intermediate model.

The data from the virtual test rig provides good understanding of the effect of bushing compliance on contact patch behaviour, as well as variations on camber, caster and toe angles. A significant change in longitudinal displacement at the contact patch is observed compared to that in the lateral direction. Normal longitudinal force would be less than 3000N, which means that the corresponding deformation would be around 7mm. This represents around 50% changes compared to the kinematics effect. Lateral deformation is minimal, which is less than 5% of that due to kinematics effects.

Camber and toe induced deformations at the contact patch are considered small, and are within the range 10% to 20% of those due to kinematics effects. However, a significant change is observed in deformation due to caster changes. Even though the change is only about 2 degree, it is significant, when compared with kinematics effects, this being around 100%.

Chapter 5
On road vehicle testing

5.1 Introduction

In any vehicle modelling study, researchers always create a model to replicate the dynamics behaviour of actual vehicle as close as possible. Unfortunately, in order to make direct comparisons with computer model is always difficult to achieve, since there are so many parameters such as type of sensors (associated with cost), road condition or positioning of the sensor etc. However, these activities are very crucial since they determine whether the method and the assumptions used in building the model are produce sensible output.

An existing vehicle is used, which is equipped with data logging system and several sensors. All the sensors were calibrated.

In this chapter the main objective is to use the experimental data to verify the overall behaviour of both the ADAMS and the Intermediate models. However, special interest is paid to testing related to vehicle negotiating a speed bump and its effect on pitch and roll dynamics.

5.2 Experimental Set-up

This section provides the description of the test vehicle, the instrumentation used, the calibration method, and finally describe the data acquisition used for the tests. The following section explains the experimental procedure and finally presentation of several of the results retrieved from the test in raw format.

5.2.1 Description of the test vehicle

Figure 5.1: The test vehicle: Ford Mondeo

The test vehicle was a Ford Mondeo, shown in figure 5.1. This has a 2 litre, V6 4-stroke gasoline engine. It employs an independent front suspension, with a *Macpherson Strut*, and *Quadra-link type independent* rear suspension system, as shown in figure 5.2.

Figure 5.2: Front and rear suspension systems

The vehicle is a front wheel drive, using a rack and pinion steering system. Detailed physical and geometrical description of the vehicle is given in chapter 4, courtesy of Ford Motor Corporation.

5.2.2 Test Instrumentation

The instrumentation used in the vehicle tests were based on 11 sensors, as described below:

a) 3 accelerometers for measuring longitudinal, lateral and vertical accelerations
b) 3 rate gyros for measuring roll, pitch and yaw rates

c) A potentiometer for measuring steering angle
d) A magnetic pick-up sensor for measuring engine speed
e) A potentiometer to measure throttle pedal position
f) 2 magnetic pick-up sensors for measuring wheel speed at the rear wheels

All the sensors mentioned above are usually employed in all the standard vehicle handling tests. However, 4 additional linear variable differential transducers (LVDT) were also fitted to measure front and rear suspension deflection, which are crucial in ascertaining elasto-kinematic behaviour of suspensions, and used for overall comparison with the computer models.

5.2.2.1 Suspension deflection sensors

To make a direct comparison with suspension deflection or vertical displacement of the wheel obtained by simulation, appropriate sensors are required to be carefully placed either parallel to the McPherson suspension strut or purely in a vertical orientation. However, achieving this within a reasonable budget and given the tight available space proved to be a difficult undertaking.

There are two types of sensors selected as shown in figure 5.3 and 5.4 for measuring suspension deflection.

a) *Vishay Precision Linear Transducer* for rear suspension
b) *ASM WS10 Position Sensor* for the front suspension.

Figure 5.3: *Vishay Precision Linear Transducer*

Figure 5.4: *ASM WS10 Position Sensor*

Both sensors are linear displacement sensors, which are capable of measuring displacements up to $\pm 250mm$ for *ASM* sensor and $\pm 100mm$ for *Vishay* sensor respectively. Detail specifications of the sensors are attached in appendix 2.

5.2.2.2 Vehicle translational sensor

Figure 5.5: A215/220 series DC operated linear servo accelerometer

Three similar accelerometers were used to capture the translational motions of the vehicle along the three axes (longitudinal, lateral and vertical) (see figure 5.5). All of these were placed as closely as possible to the centre of gravity of the vehicle as shown in figure 5.6. Schaevitz DC-Operated accelerometers (see figure 5.5) are used, which are capable of measuring accelerations up to $\pm 2g$. Detail specifications of these accelerometers are given in appendix 2.

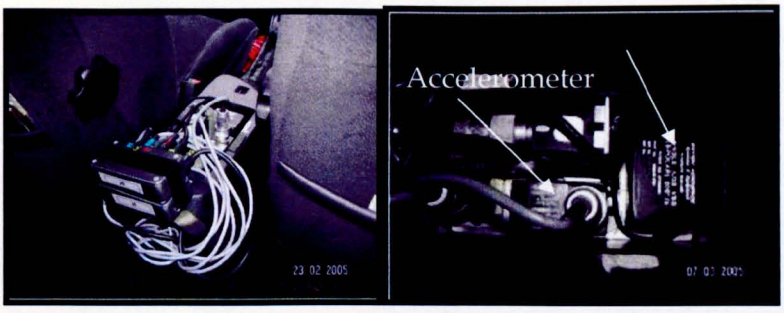

Figure 5.6: The positions of accelerometers and gyroscopes

5.2.2.3 Vehicle rotational sensor

Gyroscopes are instruments, which are used to measure angular motion. Vibrating Structure Gyroscopes are solid-state devices (see figure 5.7), which provide an output voltage proportional to the rate of turn applied to the sensitive axis. Three highly sensitive and expensive *British Aerospace* gyroscopes were used to capture rotational movements of the vehicle about all the three axes (roll, pitch and yaw motions). These were placed at nearly the same position as the accelerometers (see figure 5.6). Detailed specifications of the gyroscopes are given in appendix 2

Figure 5.7: Bipolar type single axis vibrating structure gyroscope

5.2.2.4 Vehicle steering angle sensor

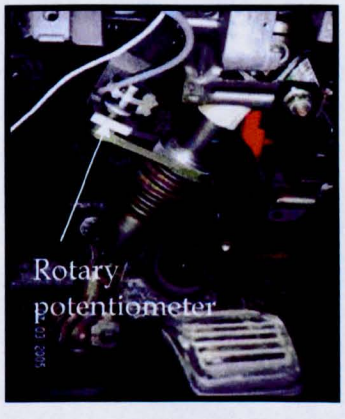

Figure 5.8: Potentiometer for measuring the steering angle

A linear rotary potentiometer was used to measure steering wheel angle. Basically, the sensor is positioned parallel to the steering column and connection between two components is made by using a belt. Since this is a linear potentiometer, calibration is rather straight forward. Increasing the steering wheel angle by a certain constant degree, the changes in the voltage can be plotted to get the estimated gain between steering angle and voltage output.

5.2.2.5 Vehicle wheel speed sensor

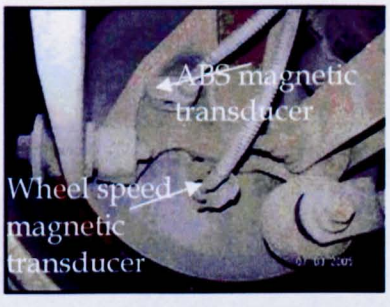

Figure 5.9: Magnetic "pick-up" transducer and it position at the rear wheel

Magnetic "pick-up" sensors were used for measuring left and right rear wheel speeds (see figure 5.9). Basically, the sensors are attached very closely to the brake disc cap, where 40 teeth are available to provide pulses per rotation, which can be used to calculate the actual wheel speed. The pulses are fed into a frequency-to-voltage converter system, which then generates a steady voltage output. By knowing the angular velocity of the wheel and its radius the vehicle forward speed can be determined as: $v = \omega r$.

5.2.2.6 Vehicle engine speed sensor

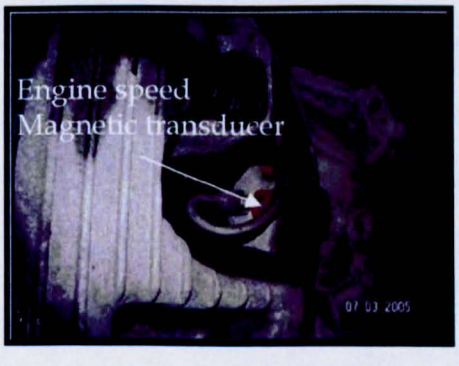

Figure 5.10: Location of magnetic "pick-up" transducer for engine speed sensor

A similar sensor as the wheel speed sensor is used to measure the engine speed (see figure 5.10). Basically, the sensor is attached very close to the flywheel, which has 135 teeth to pick up pulses as it rotates. The output pulses are fed into a frequency-to-voltage converter system, which then generates a steady voltage output.

5.2.2.7 Vehicle throttle pedal sensor

Figure 5.11: Potentiometer for throttle pedal sensor

A linear potentiometer was used to measure the displacement at the throttle pedal, which is similar to the rear suspension deflection sensor, but smaller in size. One end of the sensor is connected to vehicle chassis and the other end is connected to the top end of pedal plate as shown above. The sensor is capable of capturing displacements up to $\pm 50mm$.

5.2.3 Calibration

Calibration is an important step in any vehicle testing activity. A proper calibration can help in ensuring reliable outcome from the test data. Thus, all sensors used for the test were calibrated. For each sensor, a minimum of three samples of data sets were taken and the average values obtained. These are provided in the following sections.

5.2.3.1 Suspension deflection sensors

Suspension displacement sensors are very important in the study of combined ride and handling. Due to limited space around the suspension system, the tasks of installing all the sensors was found to be very difficult. The best position would have been to either install these parallel to the suspension strut or purely in a vertical orientation. However, this was difficult to achieve as one end of the sensor needed to be attached to the vehicle chassis and the other end should be attached to the suspension component. Since the suspension can move in vertical, lateral, longitudinal or caster directions, to obtain a purely parallel to the strut or a purely vertical alignment is almost impossible to achieve. Figure 5.12 shows the exact position and location of the suspension displacement sensors achieved in the installation.

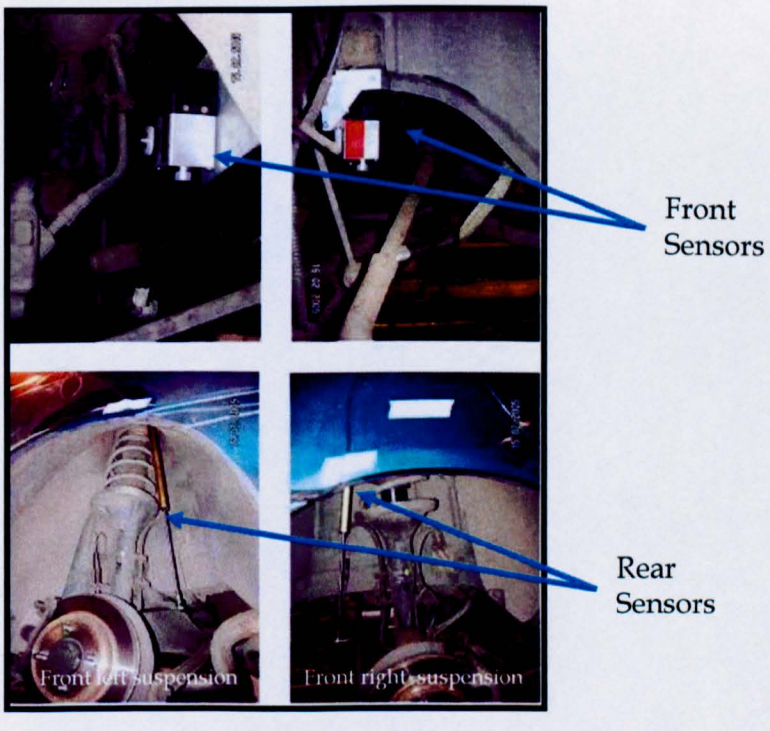

Figure 5.12: Installed front suspension displacement sensors

Due to the final installation positions of the sensors, a different approach in measuring suspension displacement had to be established for calibration purposes as shown in figure 5.13 below.

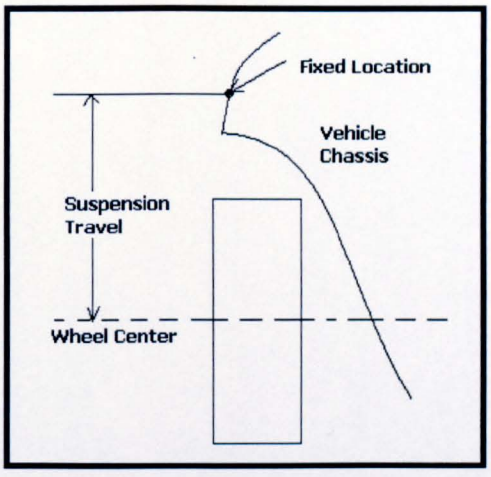

Figure 5.13: Measurement of suspension travel

A fixed location, vertically above the wheel centre on the vehicle chassis is selected and marked. This point from the wheel centre will be the zero reference position and the voltage output at this location is taken to be the base reference voltage.

Measurements are taken as the chassis is lifted and the suspension is allowed to gradually fall downwards, or alternatively more weight is applied directly on the suspension. Correlation between output voltage and suspension displacement can be made as shown in table 5.1. Several measurements were taken and the table provides the average value obtained for all the 4 installed sensors. Figure 5.14 shows that a linear variation was obtained during calibration.

	Front Left		Front Right		Rear Left		Rear Right	
	Position	Voltage	Position	Voltage	Position	Voltage	Position	Voltage
	34	2.02	34	2.93	35	1.09	34.5	1.06
	36.25	2.23	35.25	3.05	36	1.54	35.1	1.28
	37	2.32	36	3.14	37.25	1.91	36	1.7
	38.20	2.45	37.14	3.22	38.10	2.32	37.30	2.20
	39.00	2.54	38.00	3.29	39.00	2.70	38.10	2.54
Static equilibrium	40.00	2.62	39.00	3.39	40.00	3.08	39.00	2.90
	41.00	2.73	40.00	3.50	41.00	3.51	39.60	3.14
	42.00	2.84	41.25	3.61	41.50	3.71	40.50	3.47
	43.00	2.92	42.25	3.70	42.25	3.90	41.50	3.81
	44.00	2.99	43.00	3.77	43.00	4.16	42.50	4.00
	45.00	3.07	44.00	3.85	44.00	4.46	43.50	4.22
	45.50	3.13	45.00	3.93	45.00	4.77	44.25	4.41
	46.00	3.17	46.00	4.00	46.50	5.18	46.25	5.01
Average Step	1	0.091	1	0.087	0.77	0.34	1.05	0.35
Calibration Factor	0.091		0.087		0.44		0.33	

Table 5.1: suspension deflection Vs voltage

Note: all measurements are taken in cm and volt

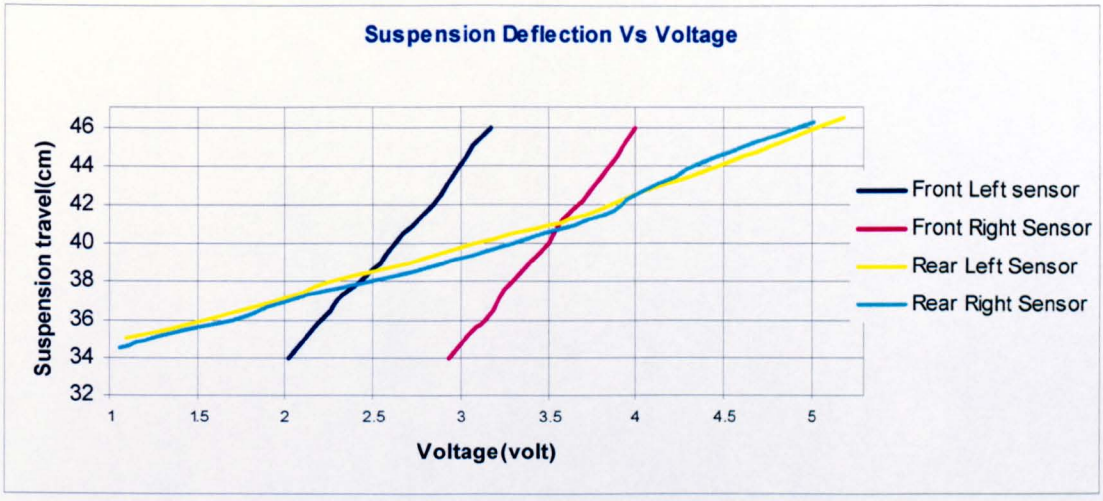

Figure 5.14: Suspension travel Vs voltage output (calibration curves)

5.2.3.2 Translational sensors (Accelerometers)

Calibration for all translational sensors was conducted by pointing the sensors both downward towards the ground, and upward away from it. By doing so one can measure the output voltage for $\pm 1g$. The measurement non-linearity was found to be less than $\pm 0.05\%$ for $10g$. The sensor output can thus be considered as almost linear for all the tests conducted. Table 5.2 lists the gains for each sensor:

Sensor	Gain
Longitudinal	**2.50965 V/g**
Lateral	**-2.4896 V/g**
Vertical	**-2.4942 V/g**

Table 5.2: Translational gains

5.2.3.3 Rotational sensors (Gyroscopes)

Original calibration was conducted by British Aerospace Systems & Equipment (refer to appendix 2 for sensor specification). However, since proper calibration is expensive, dismantling the sensor is not advisable. An alternative way to calibrate the sensor is required. The simplest approach is by driving the vehicle around a

constant radius with a constant speed and in a fixed number of circles. By knowing these information, one can calculate the speed (deg/sec) of vehicle going around a circle, which will relate to the voltage output. This procedure needs to be repeated so that the roll and pitch sensors can also take measurements. Table 5.3 below provides the gains for all the rotational sensors.

Sensor	Gain
Roll	0.09965 V/deg/sec
Pitch	0.09910 V/deg/sec
Yaw	0.0258 V/deg/sec

Table 5.3: Rotational gains

5.2.3.4 The steering wheel sensor

The calibration of the steering wheel sensor is rather simple. By turning the steering wheel to the left or right by 90 degrees per step, the change in the output voltage can be recorded. Since the sensor is a rotational linear transducer, the gain of the sensor can be obtained. The data listed below in table 5.4 is the results of calibration of the steering wheel motion of the test vehicle: the Ford Mondeo (see also figure 5.15).

Angle(deg)	Voltage(volt)
500	0.12
450	0.39
360	0.75
270	1.14
180	1.48
90	1.88
0	2.23
-90	2.62
-180	2.96
-270	3.37
-360	3.73
-450	4.13
-500	4.31
Average step	0.36
Calibration factor	0.004volt/deg

Table 5.4: Steering angle Vs voltage

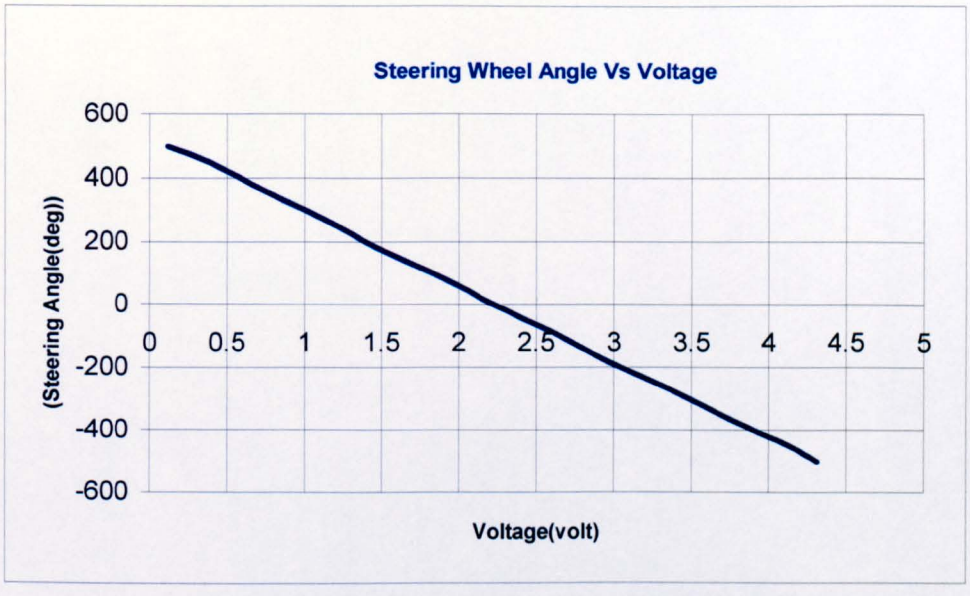

Figure 5.15: steering angle Vs voltage

5.2.3.5 Engine speed sensors

Calibration of the engine speed sensor was performed under given nominally steady engine speed at the intervals of 1000 rpm, and listed in table 5.5 below:

RPM	Voltage
0	0
1000	1
2000	2
3000	3
Calibration factor	1 mV/rpm

Table 5.5: Engine speed Vs sensor output voltage

5.2.3.6 Throttle pedal sensors

Throttle pedal position is difficult to measure due to location of the sensor (see figure 5.11). Since the sensor is linear, the calibration was performed by taking the voltage value at zero displacement and at the maximum position (at the bottom end).

Position	Voltage(Volts)
0%	0.45
100%	3.78
Calibration Factor	0.033

Table 5.6: The throttle pedal data

5.2.3.7 Wheel speed sensors

Calibration for these sensors was conducted by driving the vehicle at specific road speeds as shown in table 5.7. Good degree of linearity was observed (see figure 5.16). When the vehicle reached steady state condition at a particular speed, the voltage was recorded. This was carried out on a rolling road.

	Rear Left	Rear Right
Kph	Voltage	Voltage
0	0	0
10	0.19	0.2
20	0.41	0.43
30	0.63	0.65
40	0.85	0.88
50	1.07	1.10
60	1.29	1.32
70	1.50	1.55
80	1.72	1.77
90	1.93	1.99
100	2.15	2.21
Average step	0.22	0.22
Calibration factor	0.022volt/kph	

Table 5.7: Wheel speed Vs output voltage

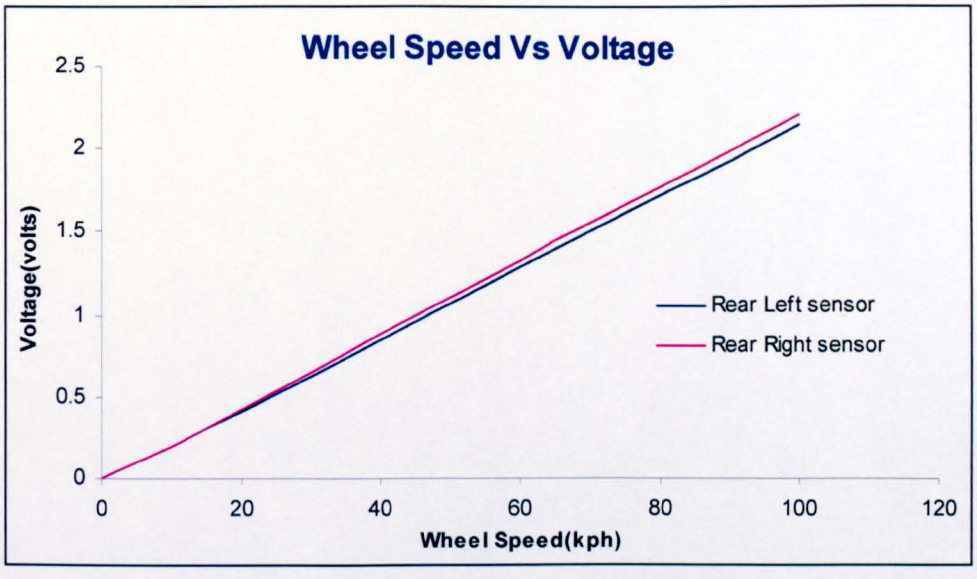

Figure 5.16: Wheel speed Vs voltage

5.2.4 Data Acquisition system

The mobile data acquisition (DAQ) system, fitted to the vehicle, is based around a 16 channel, 100 kHz DAQ board that is controlled by a laptop PC through its parallel port. Schematic diagram of the complete data logging system installed in the vehicle boot is shown below.

As shown in figures 5.17 and 5.18, there are 11 sensors. Two sensors (steering angle/Throttle pedal) were connected directly to the data collection unit. Wheel sensors and the engine sensor outputs have to be converted from pulses to voltage, using a frequency/voltage converter, before being transferred into the data collection unit. For the gyros and the accelerometers, each one requires amplification, thus the inputs are connected to a power distribution unit first before being transferred to the data collection unit. All the inputs go through an analogue filter unit, before being transferred to the Daqpad system.

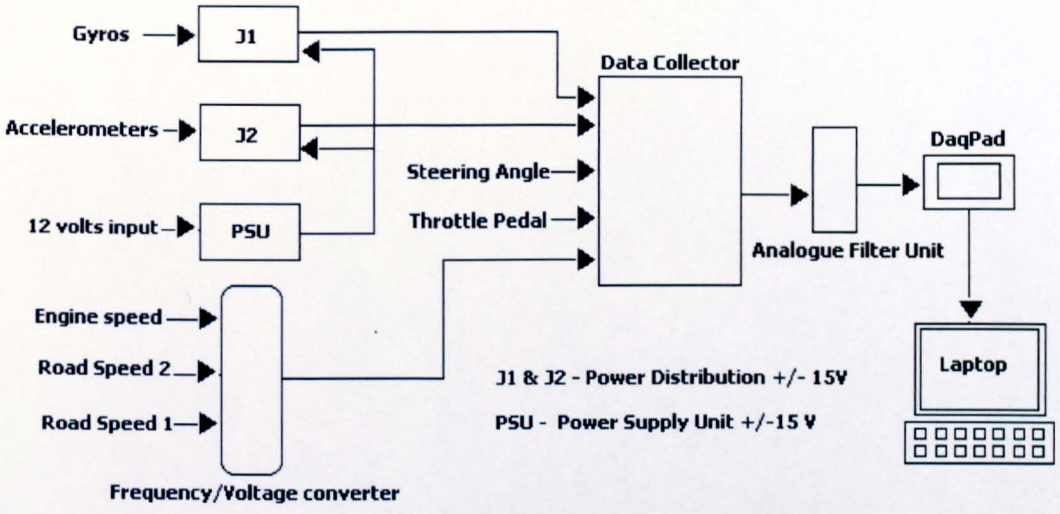

Figure 5.17: Schematic diagram of data logging system

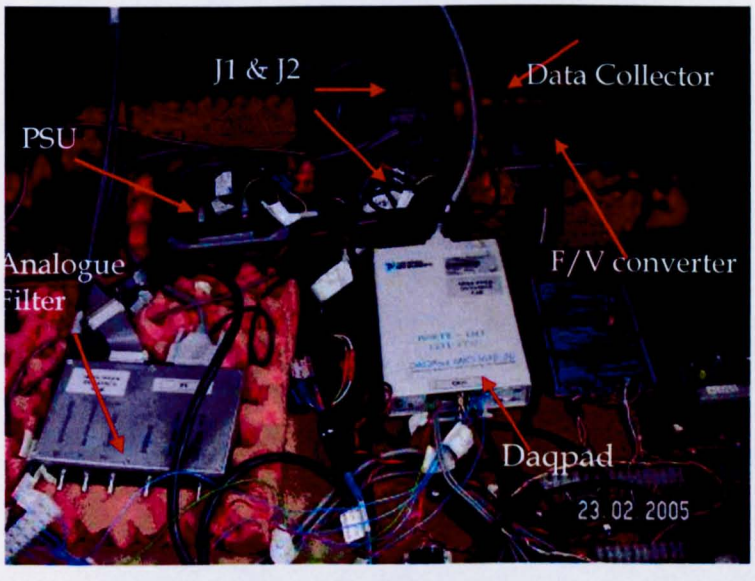

Figure 5.18: Data acquisition system located in the vehicle boot

LabView, version 5.1 software was used as the user-interface for logging the acquired signals, using a standard template file with a 200 Hz sampling rate.

5.3 Experimental Procedure and Result

For the work carried out in this thesis, the ideal testing condition would be to have a smooth flat road surface. However, this is not possible, thus, all the tests were conducted around Loughborough University's internal road-network and at several places outside the University.

5.3.1 Procedure for testing

The following road test procedures were adhered to for the various types of tests:

Test Name	Test description
Constant Braking	The straight-line deceleration event is used to evaluate vehicle during a simulated braking event. The vehicle was driven at constant speed (40kph) and suddenly subjected to constant braking, leading to constant 0.2g deceleration. Note: 0.2g deceleration was achieved when the driver applies the brake as fast and as hard as possible.
Constant acceleration	The straight-line acceleration event is used to evaluate vehicle during a simulated acceleration event. The vehicle was driven at constant speed of 10kph and suddenly subjected to a constant acceleration of 0.5g. Note: 0.5g acceleration was achieved, when the driver applies full throttle as fast as possible.
Speed bump 1	This event is for the vehicle going over a bump with a constant forward speed of 10kph and on a straight line.(The driver attempts to maintain the forward speed of the vehicle throughout the event)
Speed bump 2	This event is for the vehicle going over the bump with an initial constant forward speed of 40kph, but is given a constant braking rate of 0.2g at the onset of negotiating the bump. (The driver attempts to maintain the constant braking force applied to the pedal throughout the event)
One side speed bump	This event is for one side of the vehicle going over the bump with a constant forward speed of 10kph and on a straight line (The driver attempts to maintain the forward speed of the vehicle throughout the event).
Single lane change	This event is for the vehicle undergoing a lane-change manoeuvre, where the driver attempts to maintain a constant forward speed during the event. This test can run at any speed and any lateral acceleration level, but the lateral acceleration should be kept below a level, where the vehicle tends to over-steer.
Power-off in a turn	This event is similar to steady state cornering. However, during steady state condition the driver attempts a throttle back-out motion.
Braking in turn	This event is similar to the steady state cornering, however, during steady state condition, and while cornering the brake is applied.

5.8 Testing procedures

5.3.1.1 Road Profile Measurement

Figure 5.20: A speed bump

Accurate measurement of the road profile is an essential part of the vehicle testing activities, because the measured data will be used in the simulation studies with both the intermediate and ADAMS multi-body models in their comparative studies, and with the vehicle test dada. There are two types of speed bumps measured. These are: the normal speed bump and the split speed bump (for a single event action). These are shown in figure 5.20. Normal speed bump was used to study anti-squat/dive effects on the combined pitch plane and bounce dynamics of the vehicle, and the split speed bump was used to study the effect of anti-roll bar in combined pitch, roll and bounce dynamics of the vehicle.

The work carried out to measure the speed bump was conducted with the help of civil engineering department equipment. The equipment used was Surveyor Levelling (see figure 5.21) with an accuracy of $\pm 1mm$.

Figure 5.21: Surveyor Levelling

For the split speed bump, only one side of the bump was measured and three set of data were taken at the middle of the speed bump. Table 5.8 lists the average values obtained (also see figure 5.22).

Bump Length	Bump Height
0	0.0
20	1.8
40	17.0
60	39.0
80	60.0
100	78.0
120	80.0
140	80.0
160	77.5
180	55.0
200	35.0
220	16.0
240	1.0
260	0.0
280	0.0

Table 5.9: Single bump profile

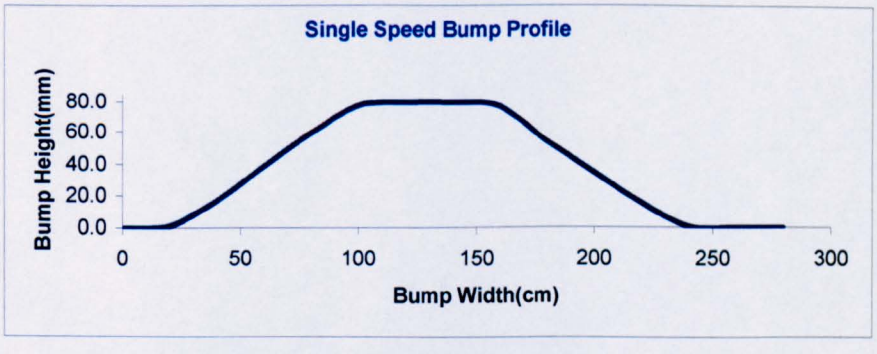

Figure 5.22:The single speed bump profile

For the normal speed bump, three set of data were also taken. However, since the profile is longer and it is not as straight as the single speed bump, a larger number of measurement steps was taken compared to those for the single speed bump. The resulting measured profile for the normal (full-width) speed bump is shown in figure 5.23.

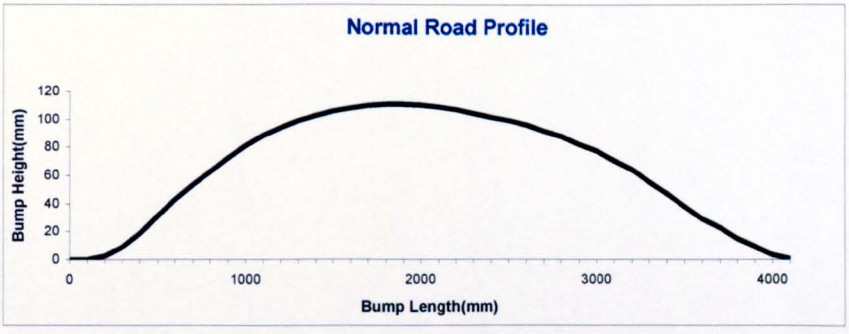

Figure 5.23: The normal speed bump profile

5.3.2 Presentation of raw acquired data

In this section some of the tests' results are presented. Most of the results are presented in chapter 6. Results presented here are raw data, taken directly from the data logger output and are, thus, given in terms of output voltage from the various sensors, described previously.

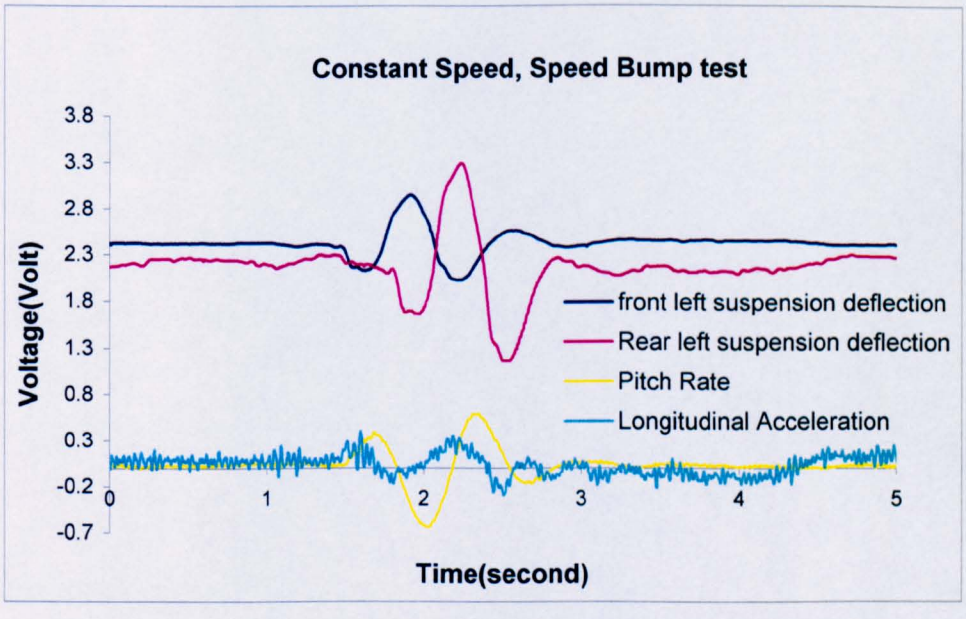

Figure 5.24: Speed Bump1 Test Results

The figure 5.24 shows slight changes in forward acceleration, when the vehicle is going over the speed bump. When the front suspension hits the speed bump a small compression at the rear suspension can be seen as expected. A good pitch angle characteristic can also be seen. Using the delay between the front suspension and rear suspension traversing the bump, a simple calculation can be made to confirm

the width of the speed bump or the speed of the vehicle. Based on the result here the time between those two suspensions is about 0.4sec, which confirmed the width of the speed bump (4m) and also the vehicle speed (10m/s).

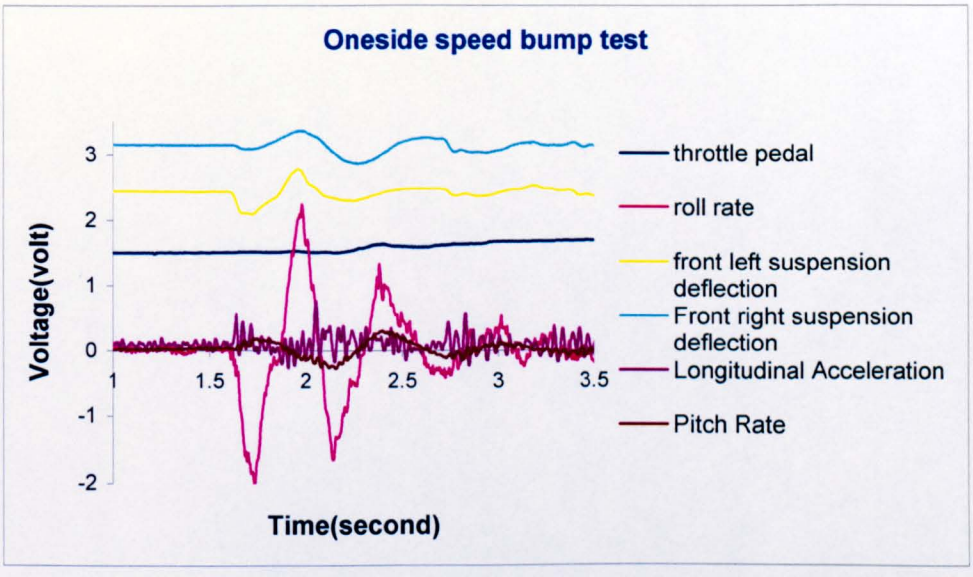

Figure 5.25: One side Speed Bump Test Result

In figure 5.25 shows the changes in vehicle pitch and vehicle forward velocity as expected. The roll angle characteristics can clearly be seen due to only one side of the vehicle going over the speed bump. Interesting suspension characteristic can be seen which suggests that when the left suspension is going over the speed bump the right suspension also suffers a small compression. This is because the speed bump is actually two-split speed bump in the middle of the road and obviously the driver has misjudged it and did not manage to avoid the bump on the opposing side of the split.

5.4 Additional observations

Initial problems encountered were the difficulties to place the suspension displacement sensor due the very limited package space available around the suspension compartment. For sensor installation at the rear suspension, the work was quite straight forward, however, an additional bar was required to act as a mount for one end of the sensors. For front suspension sensors, the installation work was more difficult, because the available area is very compact. A bracket was fabricated

so that the sensors could be attached to it. Due to these unique positions of the displacement sensors, the vertical suspension travel was measured slightly outside the suspension system itself.

Overall, all types of planned tests (listed above) were successfully conducted. However, for braking in turn and Power-off turn tests, the road condition was extremely poor for comparison purposes with the models. There were also a few setbacks during the testing activities, as two sensors for measuring pitch rate and vertical acceleration were somewhat malfunctioning. Due to this problem, the yaw rate and pitch rate sensors were swapped in places, based on the type of test conducted.

Chapter 6
Model Validation

6.1 Introduction

Validation of the Intermediate model is one of the important objectives of the thesis, as this is necessary for future research undertakings. In order to establish the model as a working and reliable vehicle model, validation is a prerequisite. Besides, validation will also help to acknowledge the approach and the assumptions used in the model. Furthermore, combined experimental and numerical investigations aid in fundamental understanding of observed behaviour of phenomena and performance of machines and mechanisms, in this case the combined ride and handling of vehicles.

Basically, the intermediate model is compared with the more complex computer model developed in the ADAMS multi-body dynamic environment, and also with the actual vehicle test data. However, vehicle tests are confined to certain manoeuvres only, given the considerable costs involved.

For the work carried out here the main objective is the overall performance of the vehicle in pitch plane dynamics, combined bounce and pitch, and combined roll, pitch and bounce dynamics, all typical of combined ride and handling manoeuvres of a non-trivial nature. A special interest is to investigate the effect of anti- dive/squat features and anti-roll bar behaviour under such manoeuvres, for example while negotiating a speed bump. The effect of suspension compliance is also investigated in the last section of this chapter.

This chapter is divided into three main sections: 1- Pitch plane dynamics, 2- roll dynamics and, 3- finally the investigation of elasto-kinematics behaviour of the suspension system.

All tests ascertain the response of the vehicle to sudden events, leading to transient conditions. Prior to the event the vehicle may be coasting under steady-state conditions or subject to transient accelerated motions.

6.2 Investigation of pitch plane dynamics

4 types of analyses were conducted to study vehicle's pitch plane dynamics. These included:

a) Constant acceleration on a flat road
b) Constant deceleration on a flat road
c) Constant speed, while negotiating a speed bump
d) Constant braking, while traversing the bump

Constant straight line deceleration and acceleration tests on a flat road were used to investigate pitch plane dynamics in isolation from the effect of other motions, such as vehicle bounce, as far as possible. Constant speed and braking tests, while negotiating the speed bump test were used to analyse the behaviour of vehicle under transient combined bounce and pitch motions.

To simplify the process of analysis, the elasto-kinematics effects in the intermediate model were not included at the initial stage. The effect will only be included in the ultimate section of this chapter. However, it should be noted that these effects are clearly present in the case of vehicle tests.

6.2.1 Constant acceleration analysis

For the vehicle tests carried out, the vehicle was initially driven at around 14km/h before the throttle was fully applied as instantaneously as possible. For this test several parameters were monitored:

a) Front suspension deflection
b) Rear suspension deflection
c) Pitch rate/angle
d) Longitudinal acceleration
e) Longitudinal velocity

In the case of simulations undertaken with the intermediate model, two sets of results were obtained:

a) Without Anti-squat/dive features (no suspension geometry effect)
b) With anti-squat/dive elements

However, for the ADAMS multi-body model and obviously for the actual vehicle, the results always included the anti-squat/dive features, as well as the elasto-kinematics effects of the suspension systems.

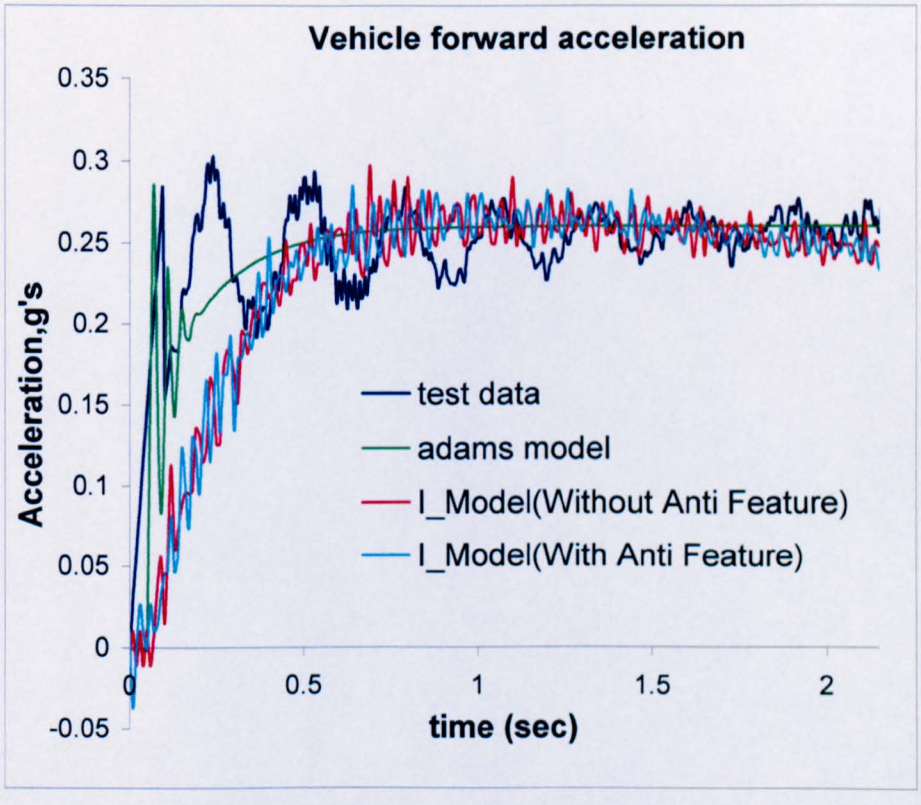

Figure 6.1a: Constant acceleration analysis, longitudinal accelerations

In the constant acceleration and deceleration studies, accelerations and the velocities of the vehicle are very important. Good correlation for these parameters is noted, as shown in figure 6.1. These give credence to the applied methodology, which is an important issue when one proceeds to investigate the more complex manoeuvres, described later.

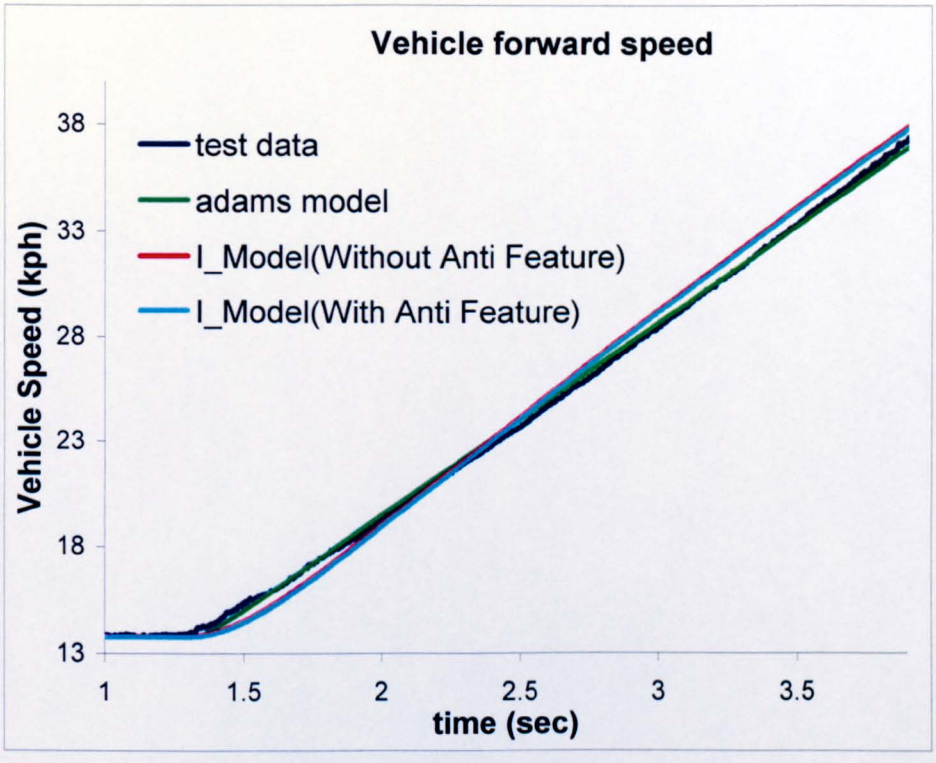

Figure 6.1b: Constant acceleration analysis, forward speed

Figure 6.1 shows that all the models predict nearly similar forward velocity time history as the actual vehicle test. However, the acceleration data under the transient condition shows some differences and a slight delay in the case of the predictions with the intermediate model. This is due to the fact that the intermediate model does not include the non-linear stiffness characteristics of the suspension bushings, which act almost instantaneously to resist the dive of the vehicle. This is evident from the actual test data, and is replicated well by the more complex multi-body model, which includes the longitudinal stiffness of all the suspension bushings. Under steady state condition the test data appears to be slightly unsteady. This is due to the drive by wire system that is pre-installed in the vehicle and cannot be disabled and is clearly not functioning properly.

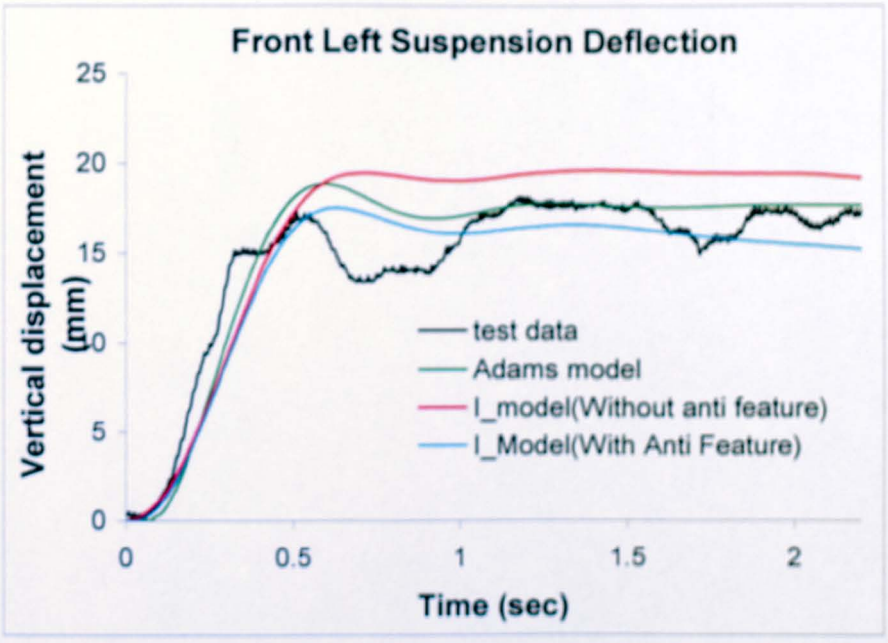

Figure 6.2a: Constant acceleration analysis, front left suspension deflection

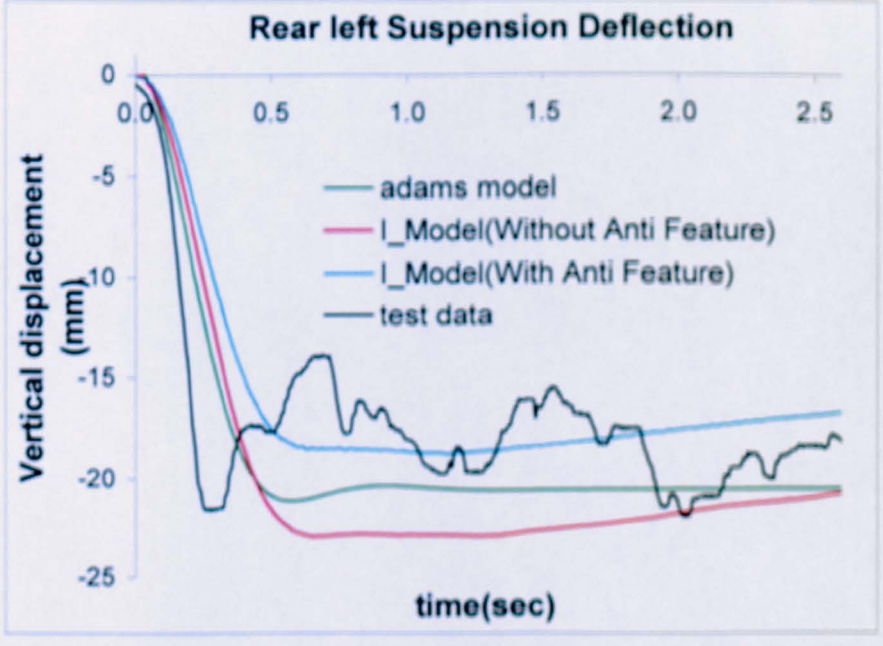

Figure 6.2b: Constant acceleration analysis, Rear left suspension deflection

Figure 6.2 shows the front and rear suspension deflections, where the models show reasonable correlations with the actual test data at steady state condition. This is probably due to flexibility of rear sensor which allows the sensor to have a small movement from original position during suspension travel. A good correlation is also found between the intermediate model, incorporating anti- dive and squat features

and the complex multi-body model with differences in a region of 5% for the front and rear suspensions. When these features are not included in the model a greater compliance exists and the vehicle is more prone to vertical displacements. It is clear that the inclusion of anti-dive elements in simple model contributes to a better correlation with a more complex model and the vehicle test data.

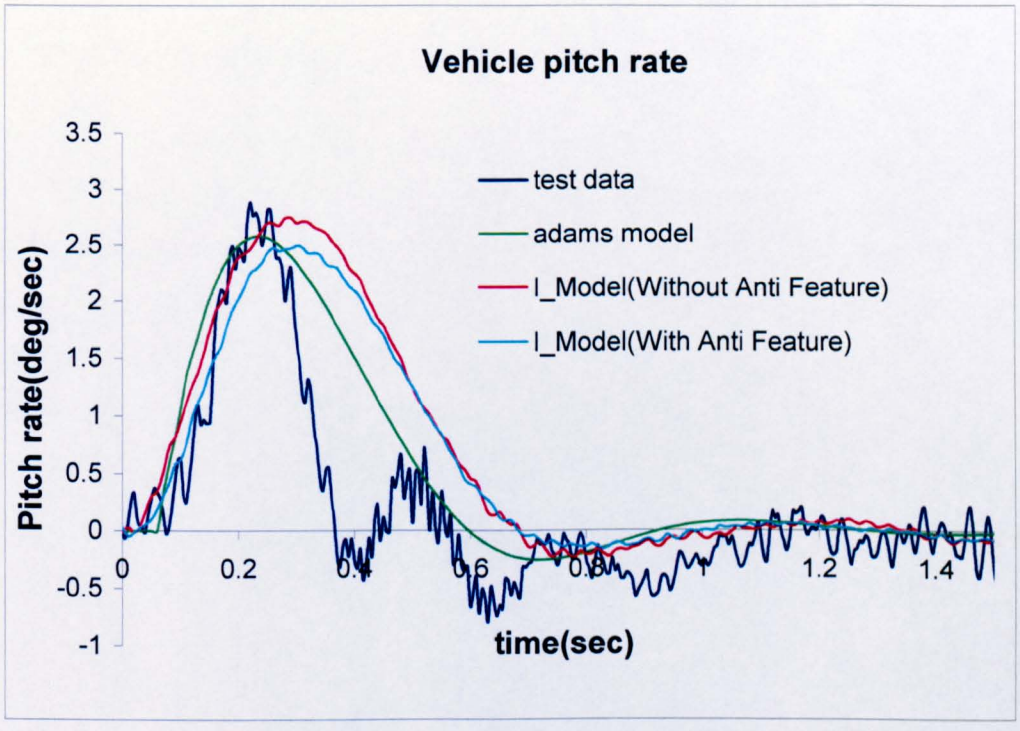

Figure 6.3a: Constant acceleration analysis, pitch rate

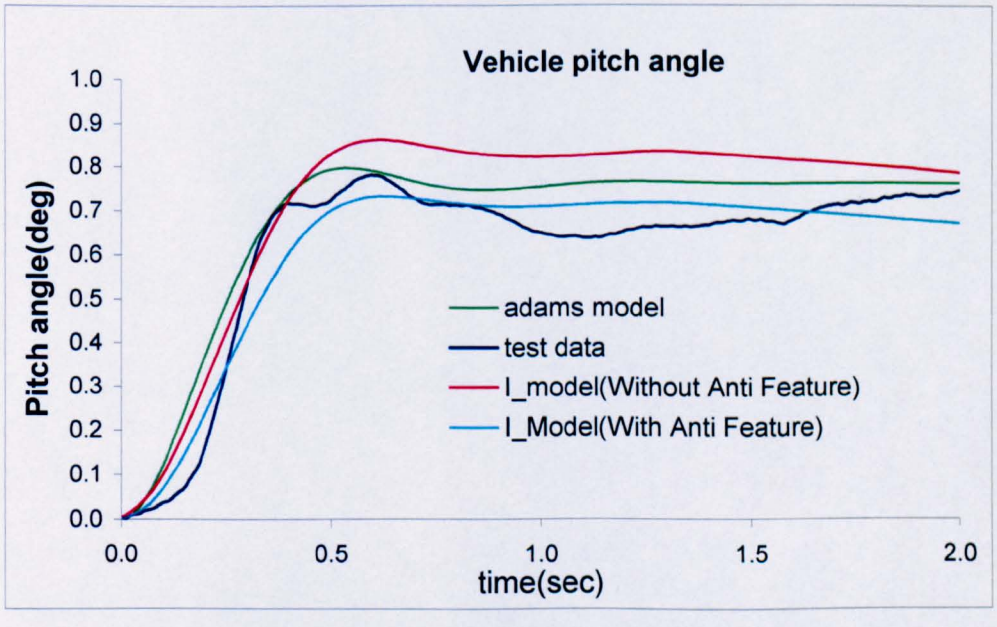

Figure 6.3b: Constant acceleration analysis, pitch angle

Vehicle pitch rate and pitch angle (see figure 6.3) also show good correlation between the various models and the vehicle test. The differences in the decay rate under transient condition are again due to the effect of suspension bushings' stiffness components. Additionally, the test data exhibits an oscillatory decay at around 2 Hz. This is probably due to the uneven road profile.

6.2.2 Constant deceleration analysis

For this event, the main target is to investigate the vehicle at steady state condition. The vehicle was driven at an initial speed of 35 kph, before a constant deceleration of 0.45g was applied through braking. Similar parameters as the case of constant acceleration analysis, described in the previous section, were monitored. However, some additional parameters to those measured in the actual vehicle tests were also compared between the complex multi-body model (see chapter 4) and the intermediate model (see chapter 3). These included force generated at all the tyre contact patches. The results are as follows of all these comparative studies are shown in figure 6.4.

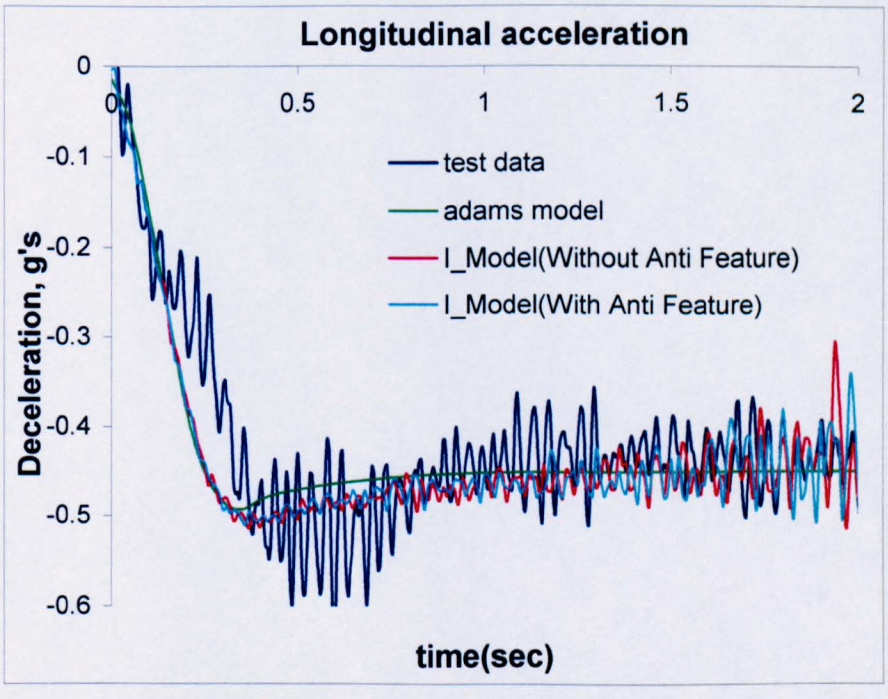

Figure 6.4a: Constant deceleration analysis , longitudinal deceleration

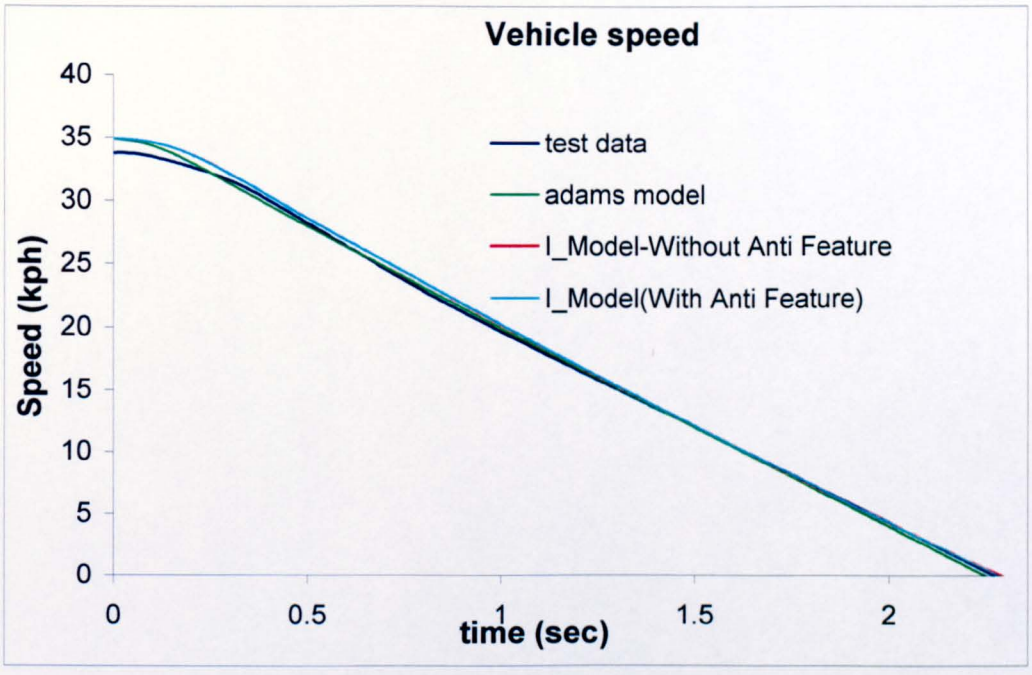

Figure 6.4b: Constant deceleration analysis , forward speed

Figure 6.4 shows a good correlation between the computer models and the actual vehicle test data. However, the test data seem to show an initial velocity slightly lower than the intended 35kph. This introduces a slight difference to the computed values.

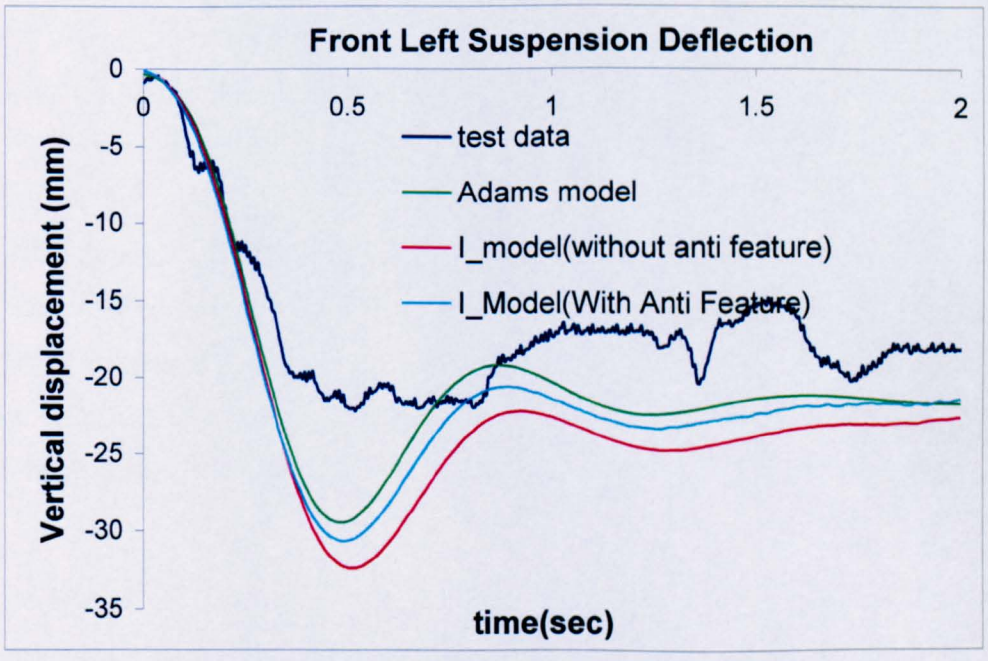

Figure 6.5a: Constant deceleration analysis, front left suspension deflection

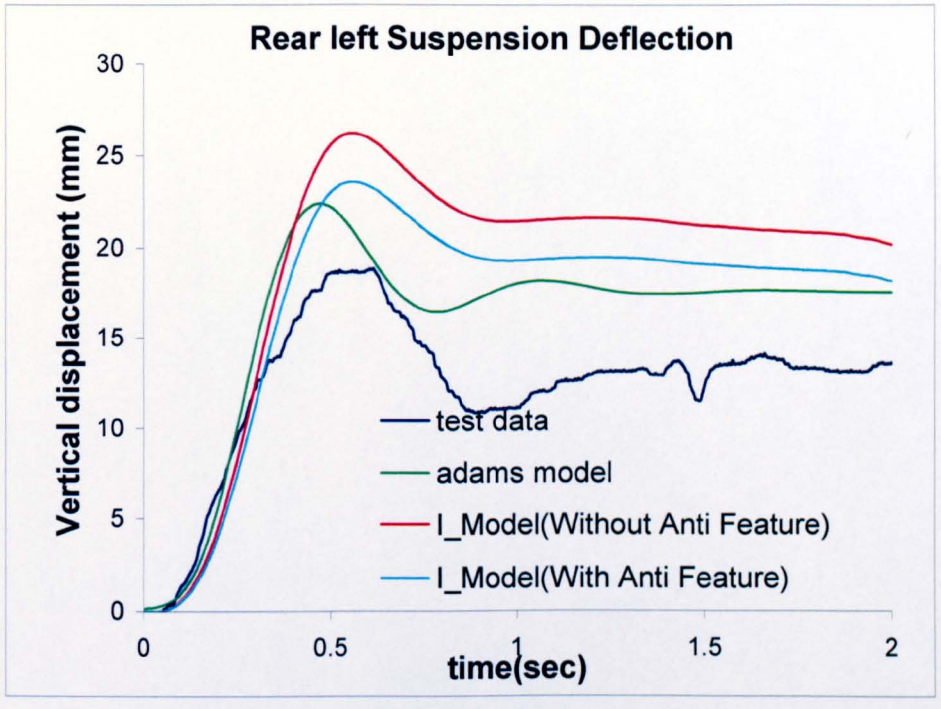

Figure 6.5b: Constant deceleration analysis, rear left suspension deflection

A much better correlation between the intermediate model predictions (with anti-features) and those by the complex multi-body model can be observed under this test than those under the constant acceleration test, where the intermediate model shows a better correlation with the test data. Suspension system without detailed geometry (i.e. anti-dive/squat features) exhibits a larger deflection similar to those in the constant acceleration test in the previous section (shown in figure 6.5). Therefore, it is clear that the multi-body ADAMS model, including the effect of anti-dive feature (in the case of constant deceleration) would agree better with the actual vehicle test. The intermediate model, having linearized suspension compliances conforms less to the actual vehicle data, particularly when anti-dive feature is omitted. Nevertheless, the overall trend is the same as for the vehicle data.

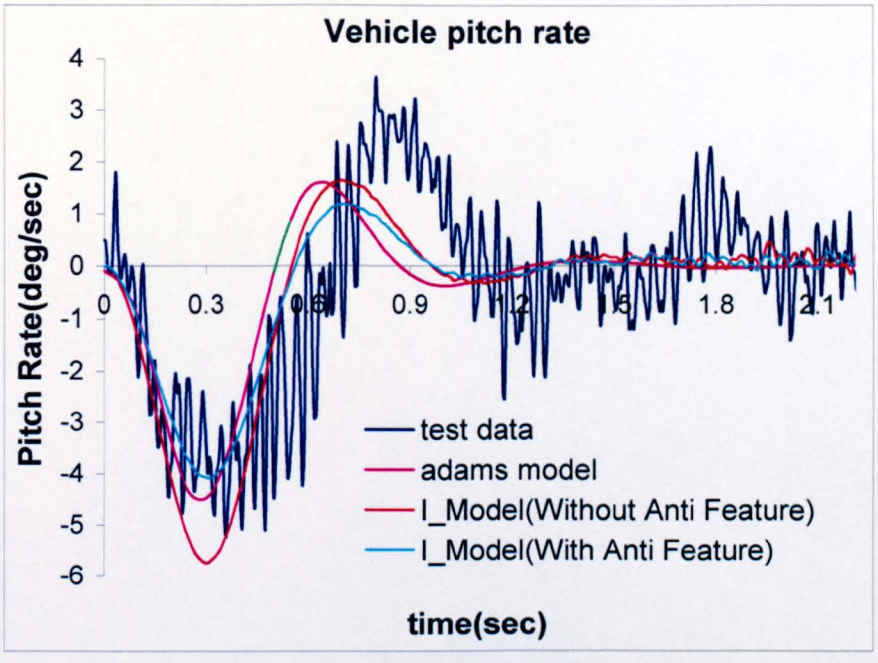

Figure 6.6a: Constant deceleration analysis, Vehicle pitch rate

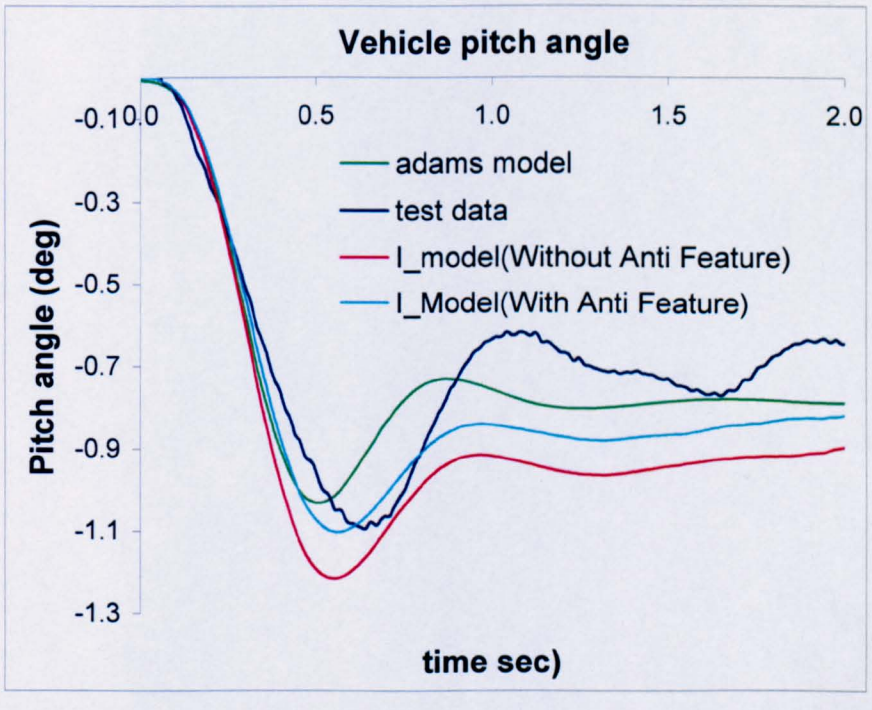

Figure 6.6b: Constant deceleration analysis, Vehicle pitch angle

Correlation between the complex model and the intermediate model with anti dive/squat feature is very good under steady state conditions, particularly for pitch-plane dynamics, as shown in figure 6.6. However, there are phase shifts between the two models and also with the vehicle data. This is probably due to the linear

versus the non-linear damping parameters used in the two models. An intermediate model without anti dive/squat feature provides the worse predictions as expected, where there is a deviation of 20% in pitch angle from the vehicle test data.

As mentioned earlier, additional parameters of importance include vertical and longitudinal tyre forces. These are important parameters, because of their relationship with suspension deflection and eventually with vehicle pitch dynamics.

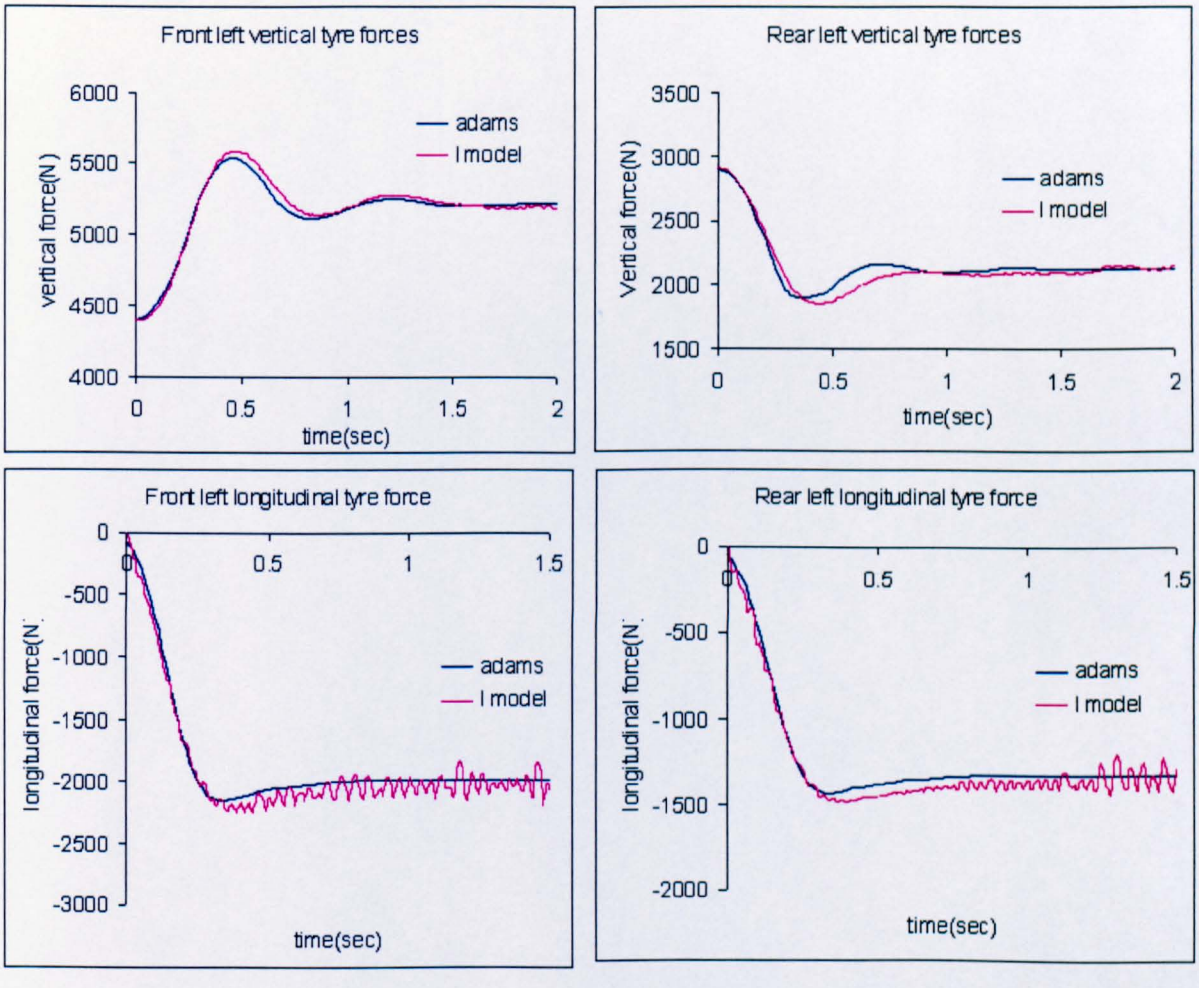

Figure 6.7: vertical and longitudinal tyre forces

Figure 6.7 shows good correlation between the ADAMS model and the intermediate model, including anti-dive/squat features, during transient and steady state manoeuvres. A direct comparison with the actual vehicle tests is not possible as monitoring of tyre forces is very difficult, if not impossible, to achieve.

6.2.3 Analysis for constant speed over a speed bump

This event is for the vehicle going over a measured speed bump (see chapter 5). The main target is to investigate the effect of anti-dive/squat features in combined pitch plane and bounce motions, as well as observing the vehicle response to short-lived transient conditions.

The initial forward speed of the vehicle was set at 25kph, before the vehicle met the speed bump. An attempt was made to maintain this speed, whilst negotiating the bump. The maintained kinematics conditions are indicated in figure 6.8. Note that for the case of vehicle test, there is a tendency for the driver to slightly back-out of the throttle as a natural reaction. This accounts for the larger perturbation in the time histories of the kinematics parameters under the actual vehicle tests. Similar parameters were monitored as in the previously mentioned tests. However, some additional parameters were also monitored, as described below.

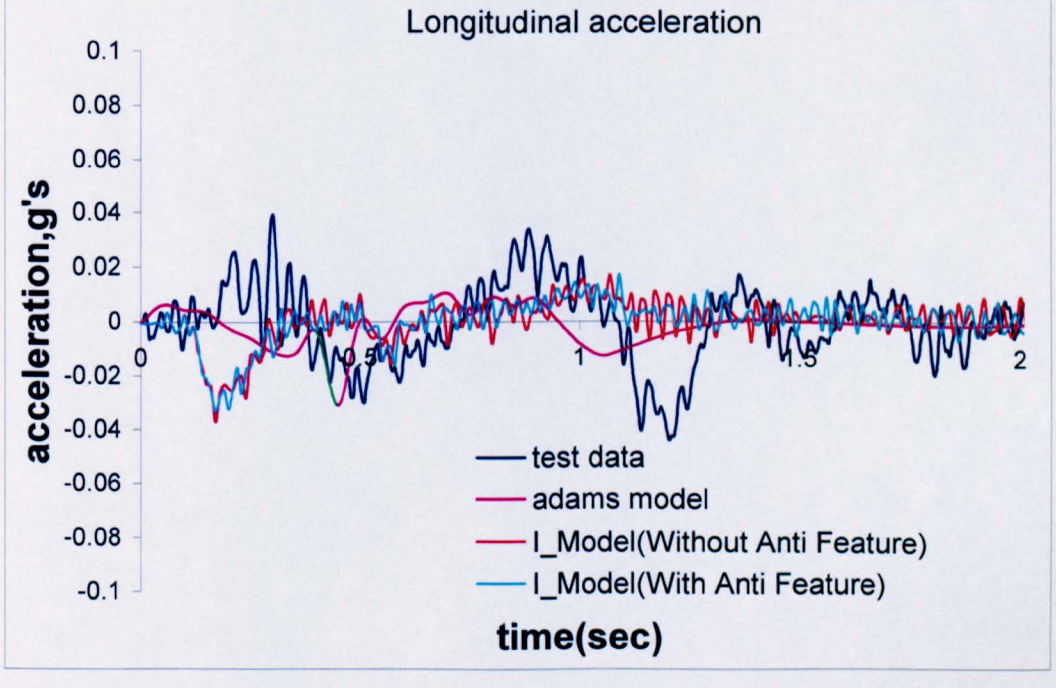

Figure 6.8a: Constant speed bump analysis, longitudinal acceleration

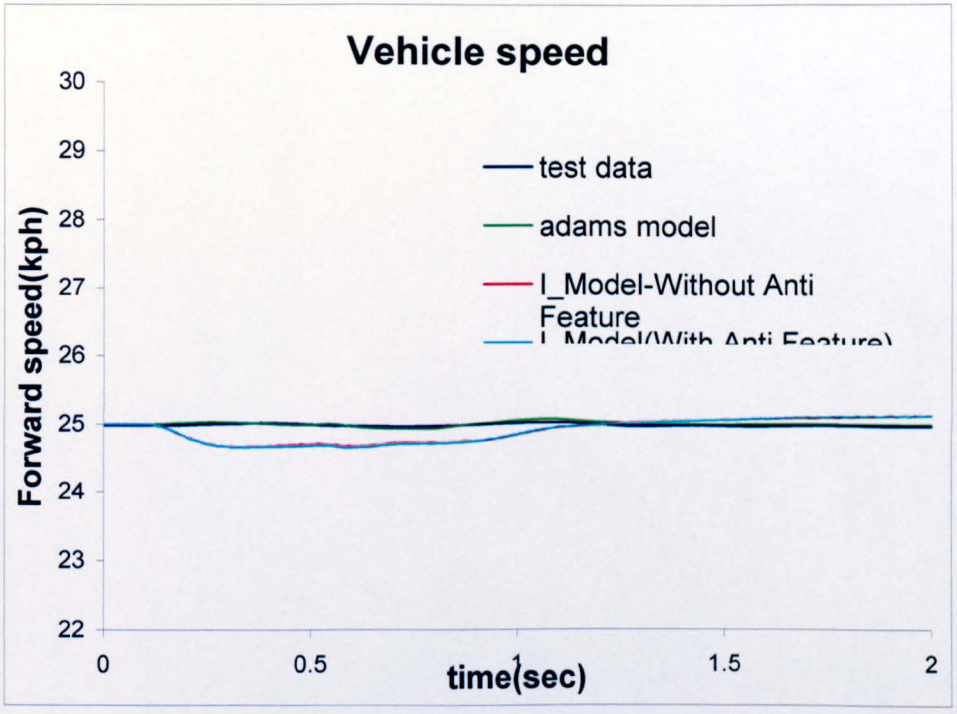

Figure 6.8b: Constant speedbump analysis, forward speed

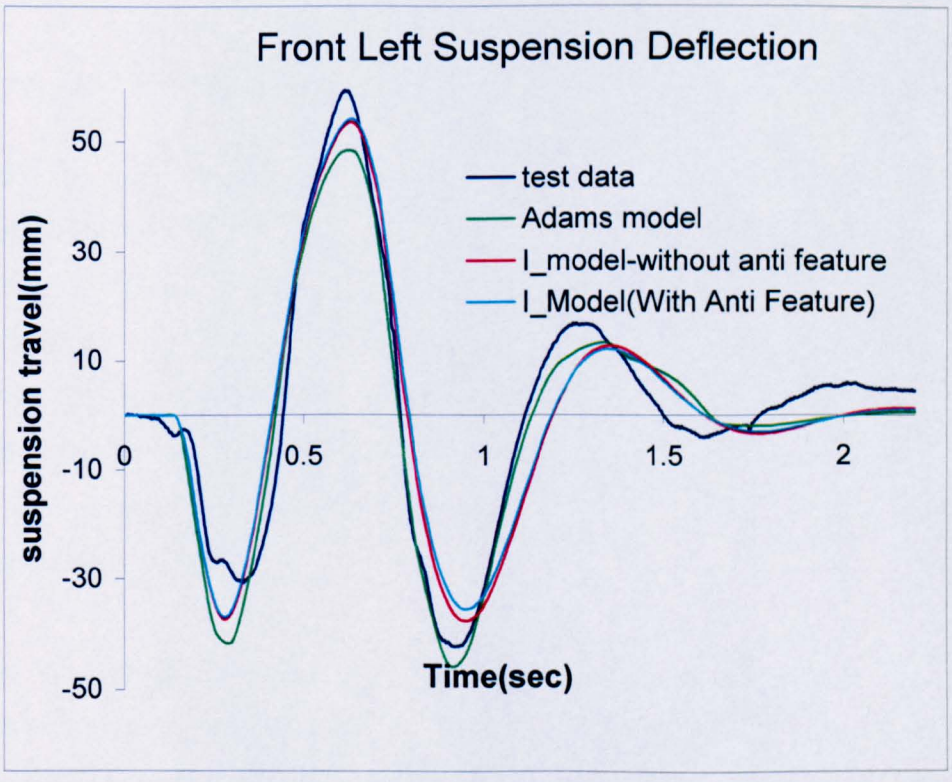

Figure 6.9a: Constant speedbump analysis, front left suspension deflection

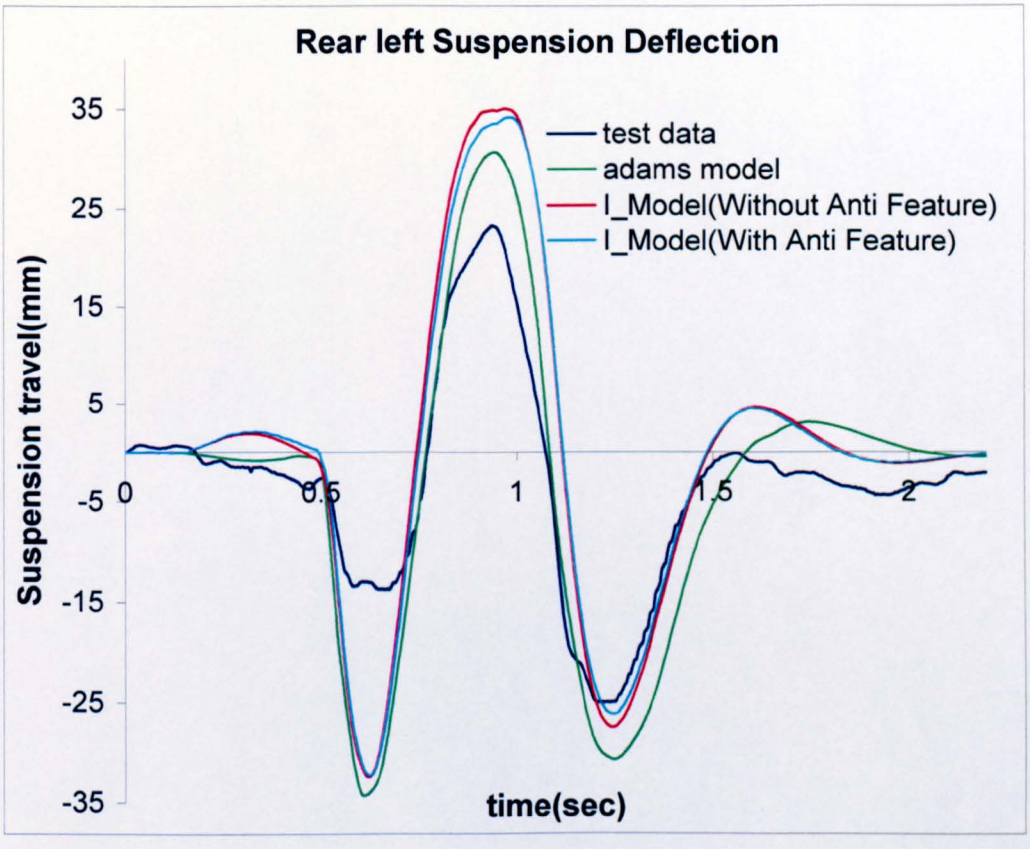

Figure 6.9b: Constant speed bump analysis, rear left suspension deflection

Overall, the suspension deflection in figure 6.9 shows good correlation between all the models and the vehicle test data. However, some significant differences during suspension compression at the rear left sensor can be observed. This can be possibly due to the road surface condition not accounted for properly in the initial measurement of the bump or the vehicle may have not traversed the bump square to it after the front suspension has already negotiated it. These conditions often occur in practice, but cannot be anticipated in numerical predictions. Nevertheless, this difference is merely 1 cm.

The figure also suggests that the anti-dive/squat features do not introduce any significant effect on suspension displacement. This is a find of practical importance, indicating that with any significant degree of bounce motion of the vehicle under transient conditions, the anti-dive and squat features have little time to react. This

can also be seen in figure 6.10, where pitch rate and pitch angle do not change significantly with or without anti-dive/squat features. A good correlation between predictions of the non-linear complex and the intermediate models can also be seen for both the front and the rear vertical tyre forces in figure 6.11.

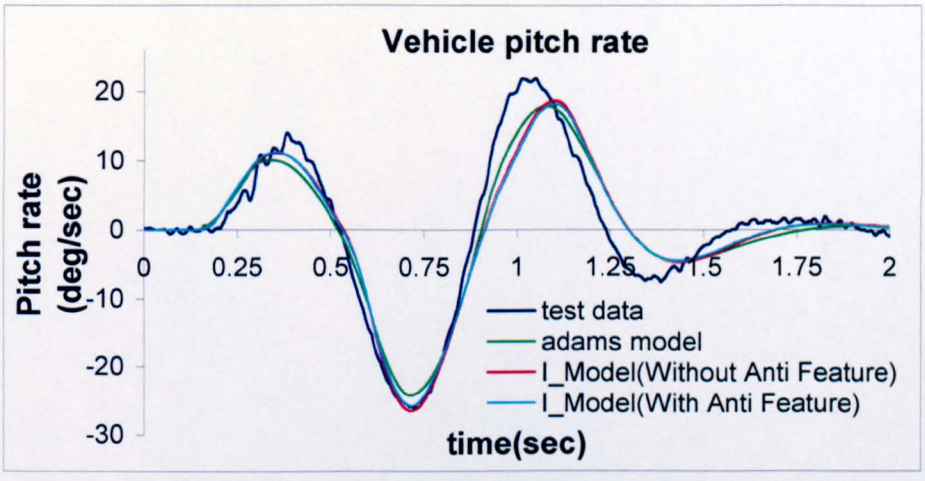

Figure 6.10a: Constant speedbump analysis, vehicle pitch rate

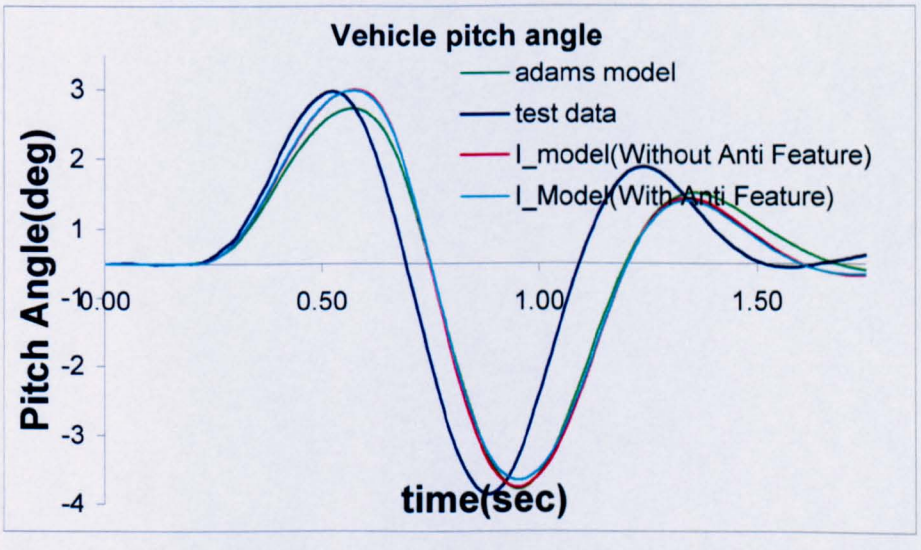

Figure 6.10b: Constant speedbump analysis, vehicle pitch angle

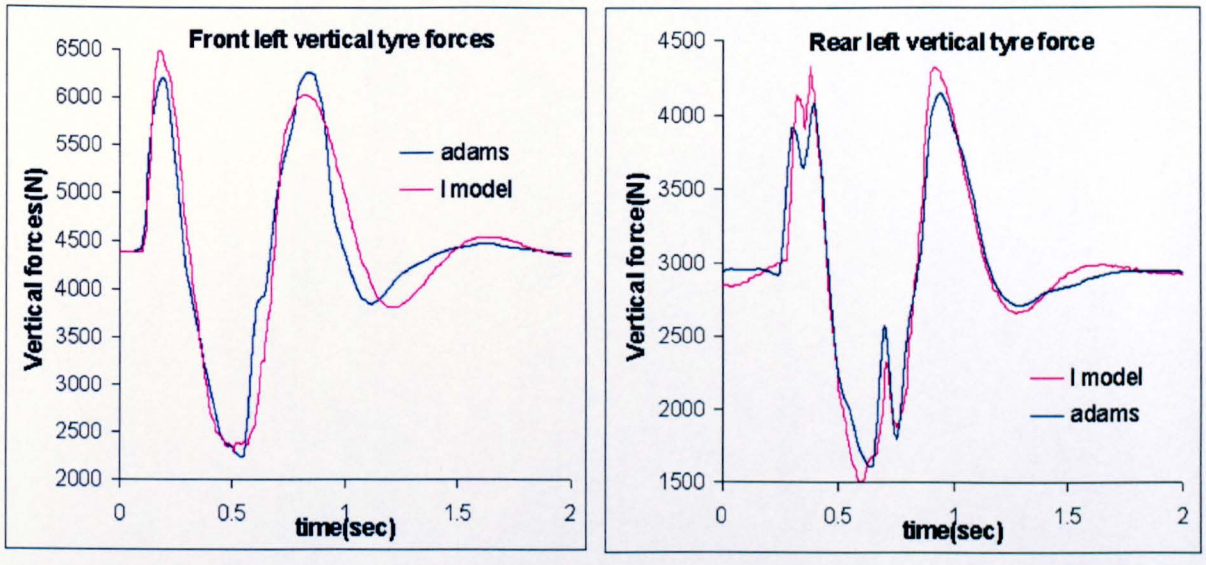

Figure 6.11: vertical tyre forces

In order to further analyse the effect of anti-dive/squat features, while negotiating a speed bump, several more tests were conducted with the intermediate model as shown in figure 6.12. Four different forward speeds were selected to note any variation in pitch plane dynamics. The results suggest that while negotiating the speed bump, the effect of anti-features are minimal due to vehicle bounce.

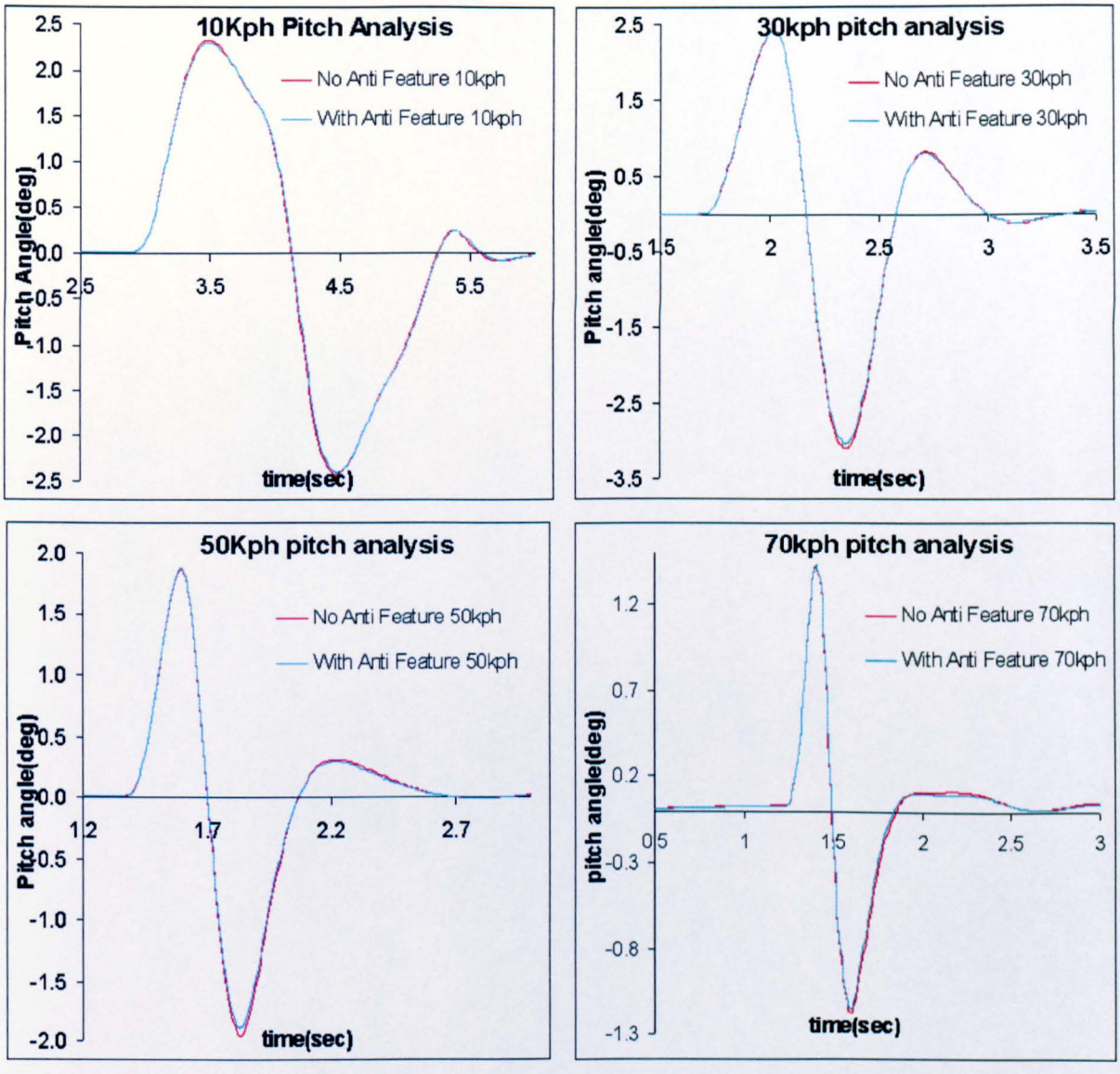

Figure 6.12: Pitch plane analysis with the Intermediate vehicle model

6.2.4 Analysis for Constant braking going over a speed bump

This event is for the vehicle negotiating a speed bump with an initial constant braking action. In this event, both steady state and transient conditions can be studied. This event is more representative of driver action under normal driving conditions, where a driver applies the brakes, before going over the bump. An initial speed of 20kph was set before a constant braking rate of 0.25g was applied to the vehicle. The results are shown in figure 6.13.

Figure 6.13 shows that under steady state conditions, the correlation is good between all the models. However, during transient periods the test data seems to

indicate a faster deceleration response (decay). The test data also has a slight anomaly in the forward velocity around 5 kph. This is due to the driver releasing the brake pedal, hence increasing the vehicle speed.

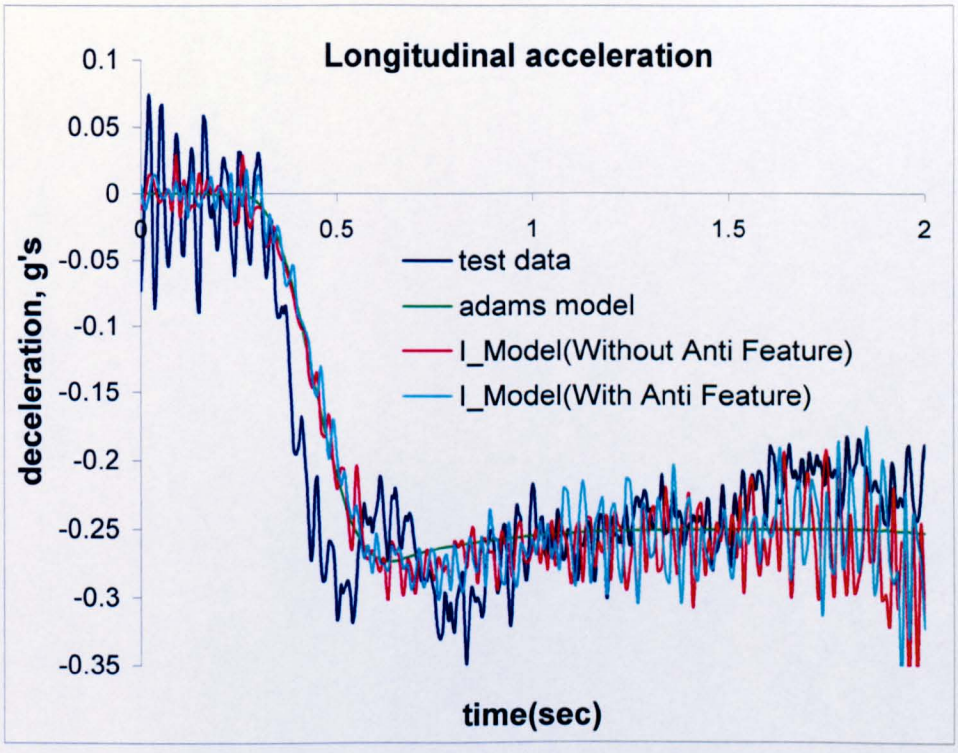

Figure 6.13a: Brake bump analysis, longitudinal deceleration

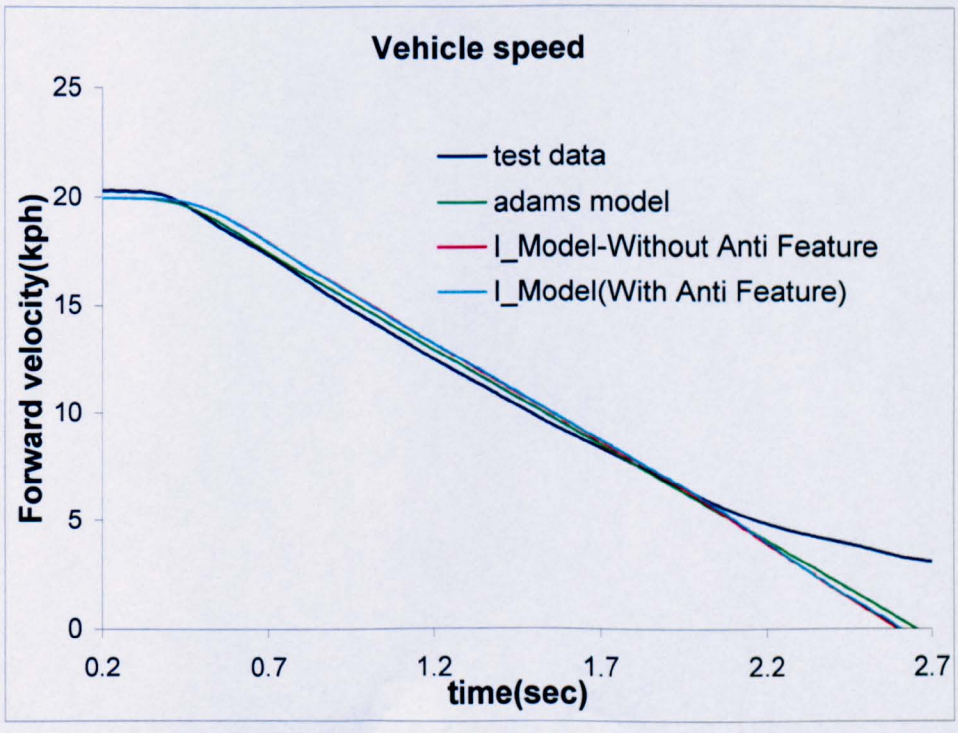

Figure 6.13b: Brake bump analysis, forward speed

This action leads to the rear axle negotiating the speed bump earlier as can be seen in figure 6.14.

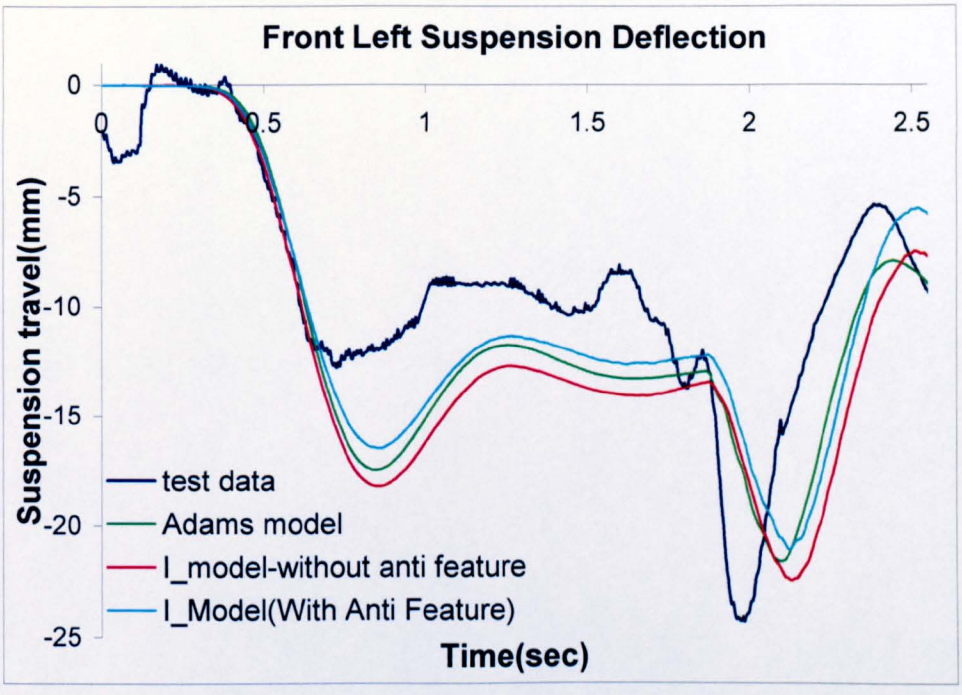

Figure 6.14a: Brake bump analysis, front left suspension deflection

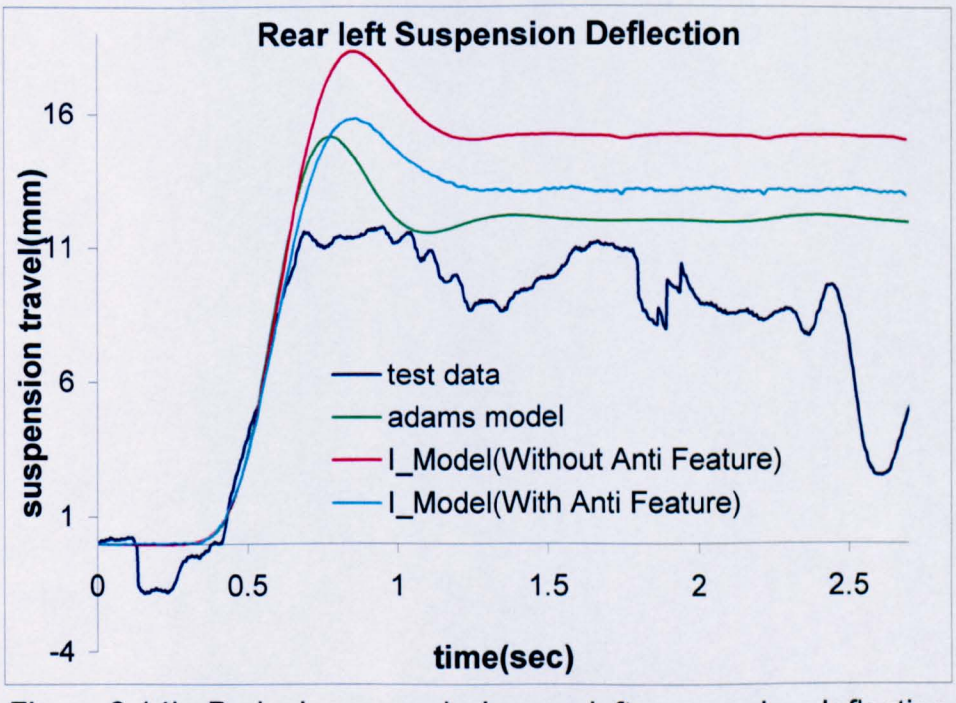

Figure 6.14b: Brake bump analysis, rear left suspension deflection

Figure 6.14 shows the front suspension, traversing the speed bump around 1.9 sec after braking and the rear suspension climbing the speed bump at 2.4 sec, which corresponds exactly to the right length for the vehicle wheel base. The deviations of

various models' predictions from the actual vehicle test are in line with the previously expounded explanations.

The observations at steady state conditions show that the model with no anti-dive/squat feature introduces larger suspension travels both at the front and the rear. This is also reflected in pitch angle in figure 6.15, although good agreement is generally noted. The effect is obviously more pronounced in pitch plane dynamics with vehicle bounce. Similar to the previous analysis, shown in figure 6.10, the effect of anti-features is important to investigate. Two different forward speeds were used with different decelerations to note their effects upon pitch plane dynamics.

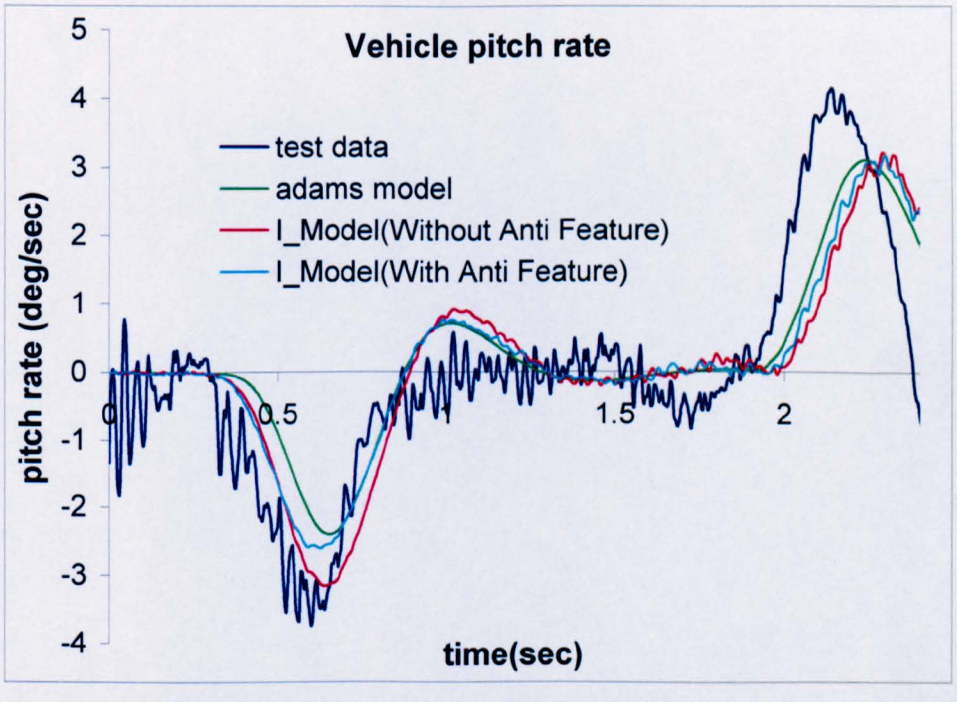

Figure 6.15a: Brake bump analysis, vehicle pitch rate

The results also suggest the same outcome as for the previous analysis (constant speed bump analysis), where with combined pitch and body bounce the effect of anti features seem to have diminished.

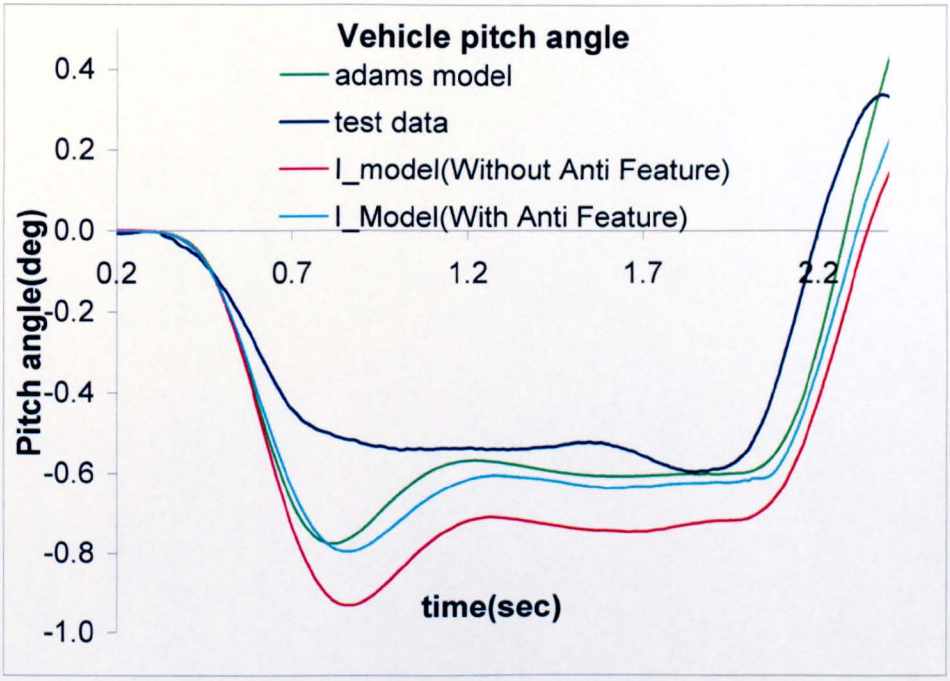

Figure 6.15b: Brake bump analysis, vehicle pitch angle

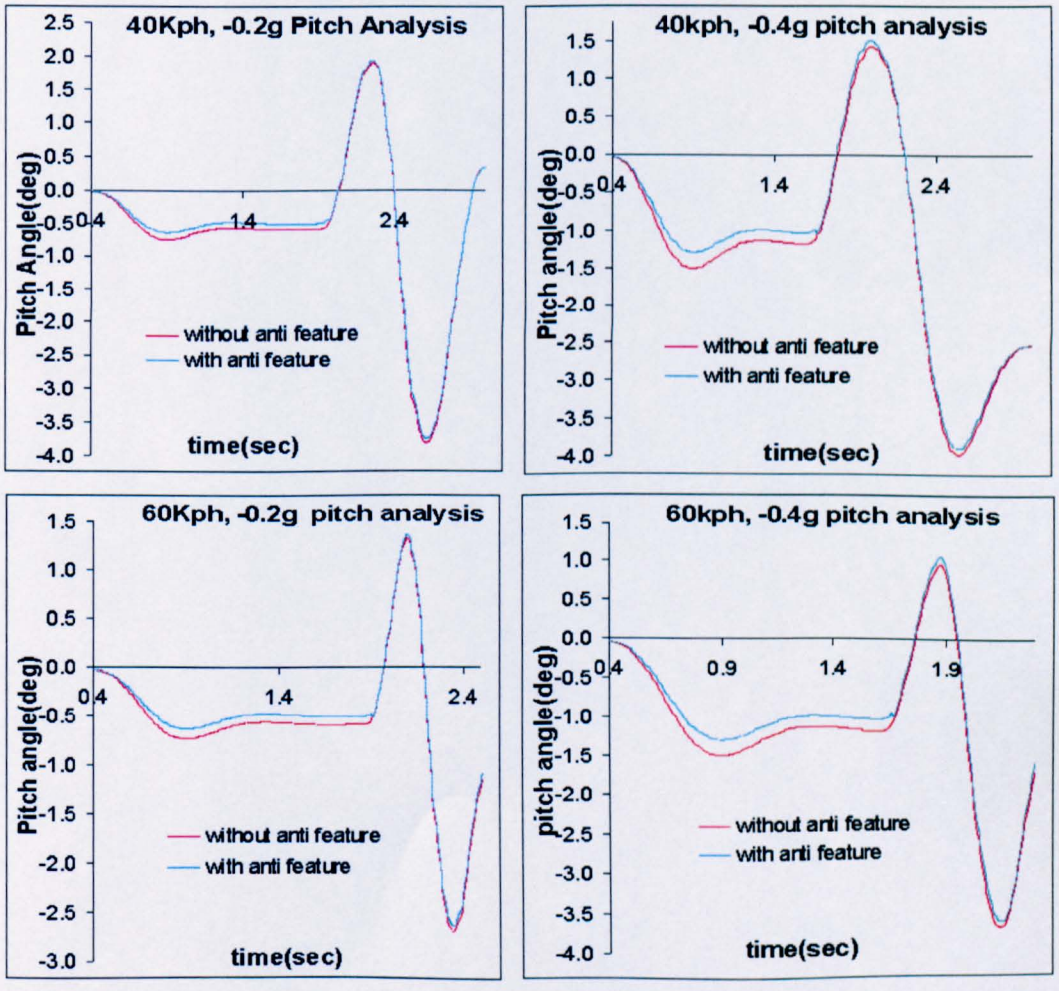

Figure 6.16: Pitch plane analysis for Intermediate vehicle model

6.3 Roll dynamics analysis

In this section the analysis is focused on correlation with vehicle tests subjected to roll motion due to single speed bump. Constant speed going over a single speed bump is made to ascertain the effect of the anti-roll bar feature upon vehicle roll dynamics.

6.3.1 Constant speed going over the a single speed bump analysis

This particular test was selected due to the increasing appearance of split speed bumps on the roads, especially around residential areas. Thus, this test is to investigate the effect of split speed bump upon combined body roll, pitch and bounce with and without an anti-roll bar system.

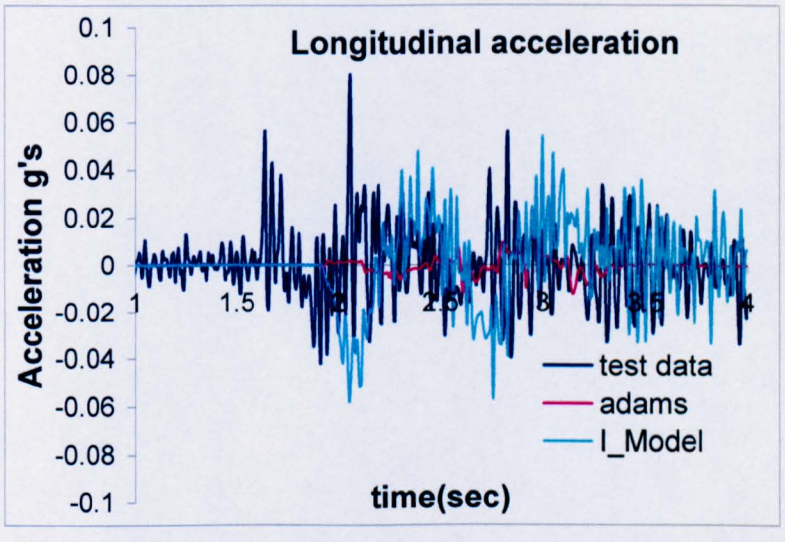

Figure 6.17a: Single speed bump analysis, longitudinal acceleration

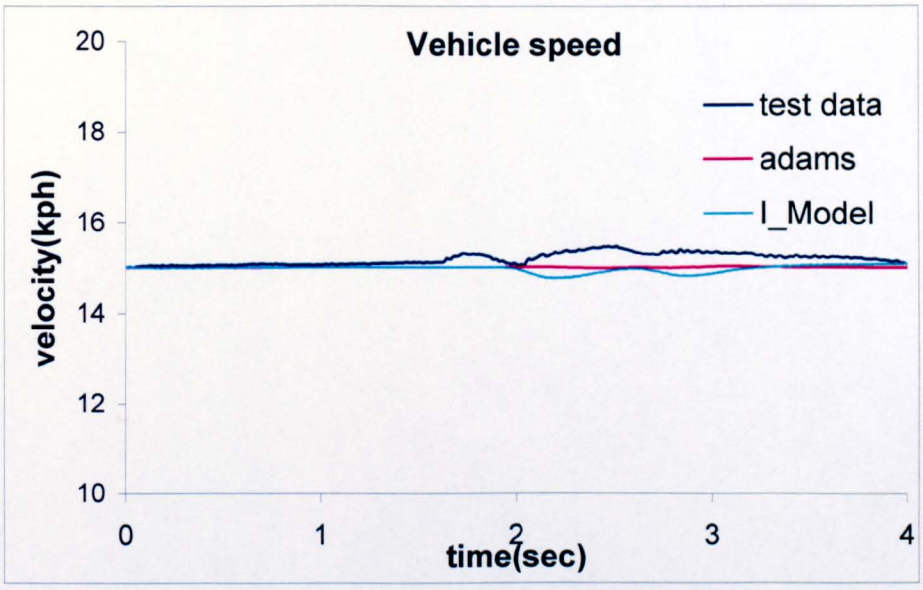

Figure 6.17b: Single speed bump analysis, forward speed

The speed of the vehicle was set at 15 kph, before it arrived at the speed bump and the results are shown in figure 6.17. Slight differences can be seen in the vehicle speed and acceleration as depicted in figure 6.17.

An interesting result can also be seen for the front suspension deflection (see figure 6.18). Without an anti-roll bar the front left suspension deflects more when going over the speed bump in comparison to the vehicle equipped with an anti-roll bar. However, the right suspension expands less with no anti roll-bar. The overall agreement between the two models' predictions is quite good, with only slight time delay between them. However, the lead in the time response in the vehicle test data when compared to the numerical predictions is quite large, although the characteristics and actual magnitudes are quite similar. This lead is due to the vehicle having a higher longitudinal acceleration, as well as noting that during the manoeuvre the right front wheel did not went between the two speed bump, instead it also hit the small potion of the right speed bump.

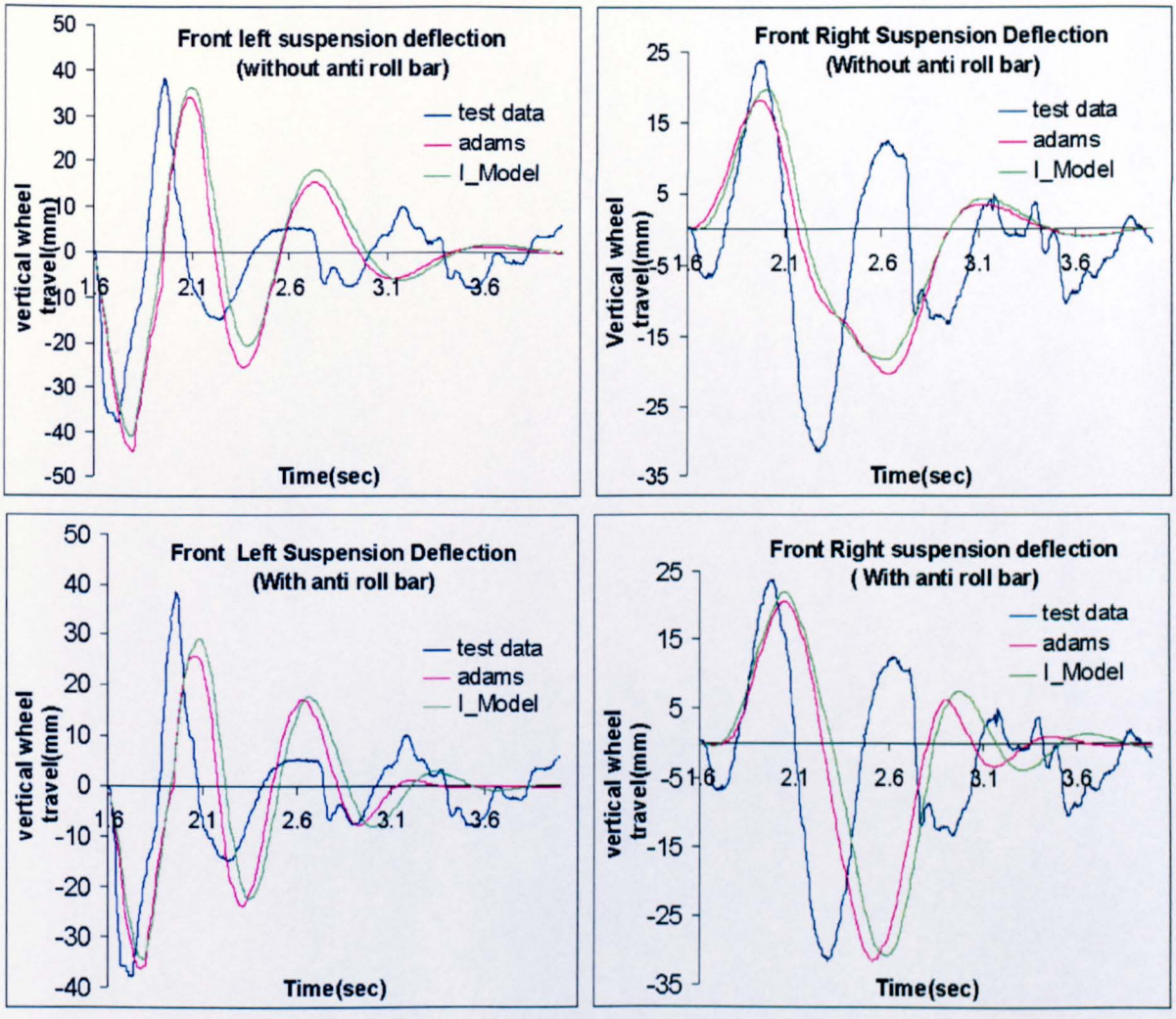

Figure 6.18: Front suspension deflection

The results for roll rate and the roll angle for vehicle configurations with and without an anti-roll bar indicate significant differences (see figure 6.18). Even though the suspension deflection reduces for the model with anti roll bar, but it produce higher roll angle and roll rate, which is not good for the vehicle ride and comfort. Thus, it is clear that the bump event is sufficient in its severity to properly activate the torsional response of the anti-roll bar.

Another important observation is the good conformity of the numerical prediction to experimental findings, except that the models do not include all sources of damping present in vehicle chassis. These include dissipation due to elastic distortions and source of dry friction in joints, which are very difficult to quantify for inclusion in the models

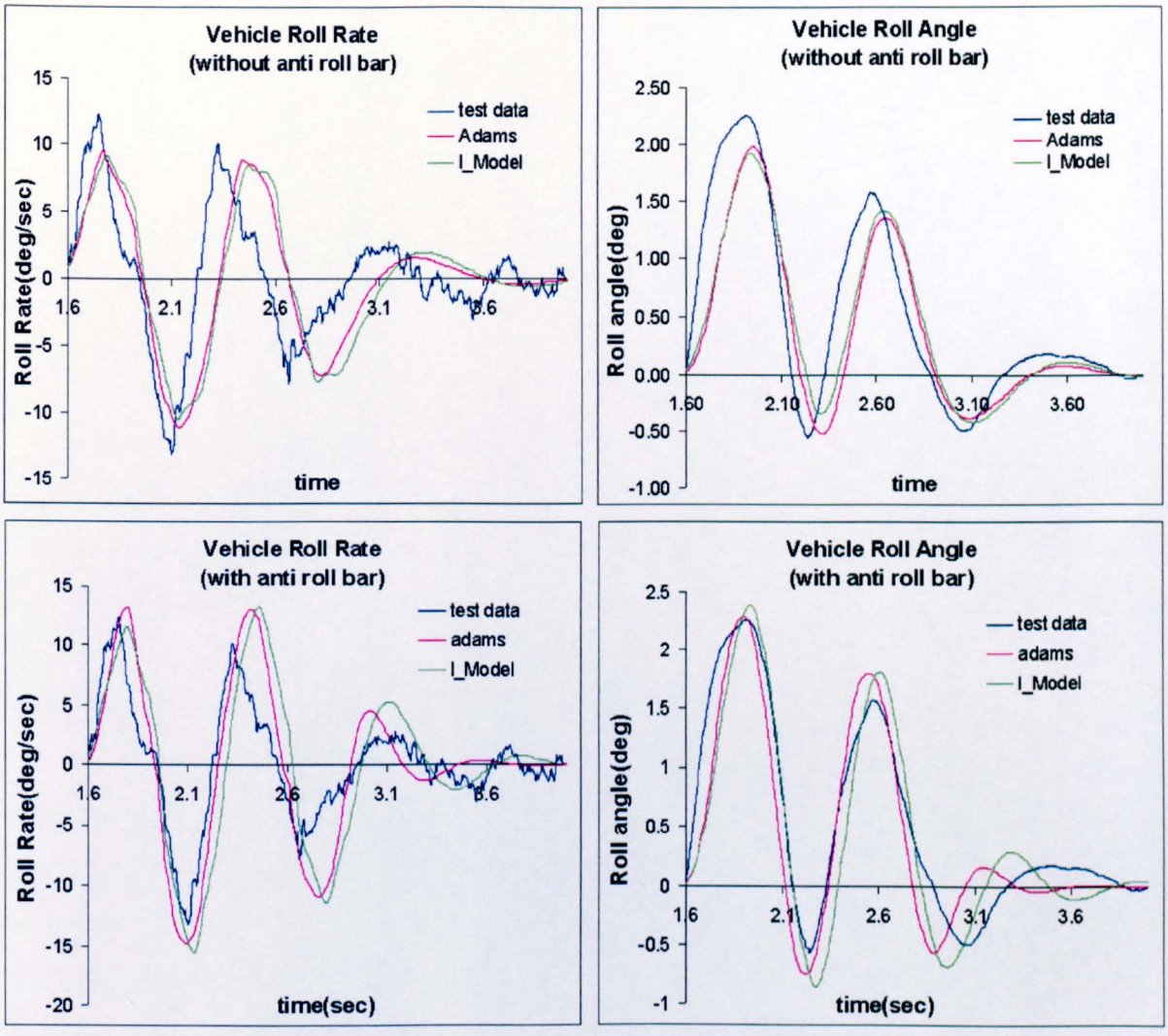

Figure 6.19: Variations in the roll rate and the roll angle

6.4 Elasto-kinematics effect on pitch plane dynamic

Elasto-kinematics plays a significant contribution to the ride comfort of a vehicle. As noted by (Matschinsky, 2000), for vehicles intended to be comfortable, the required longitudinal compliance in the wheel suspension should probably be of the order of $\pm 15mm$. However, such compliance would cause an unfavourable attitude change of the wheel. There are two elements, which can contribute to elasto-kinematics. One is the bushing component on the suspension system, and the other element is the structural deformation. However, up to this stage of the work the overall bushing effect on the suspension system has been ignored.

The work carried out in this section includes the elasto-kinematics effects on vehicle performance during steady state and transient conditions. The focus of research up to this stage has been vehicle pitch plane dynamics, rather than the overall effect of elasto-kinematics. Comparison is made between the ADAMS multi-body model and the intermediate model. Both models are represented here with and without the bushing effects. The important parameters to be measured are:

a) Longitudinal tyre forces
b) Lateral tyre forces
c) Suspension displacement/travel
d) Vehicle pitch rate
e) Vehicle pitch angle
f) Body bounce

6.4.1 Constant deceleration test for elasto-kinematics effect

Under braking, the suspension bushes deform to cause small changes to the anti-geometry (as though the 'ball joints' have moved), but provided these movements are small the anti-dive/squat effect hardly alters. However, if the changes are significant, the effect can be clearly seen in suspension deflection and eventually in the pitch angle variation or body bounce.

Note: WC – With Compliance & WOC – Without Compliance

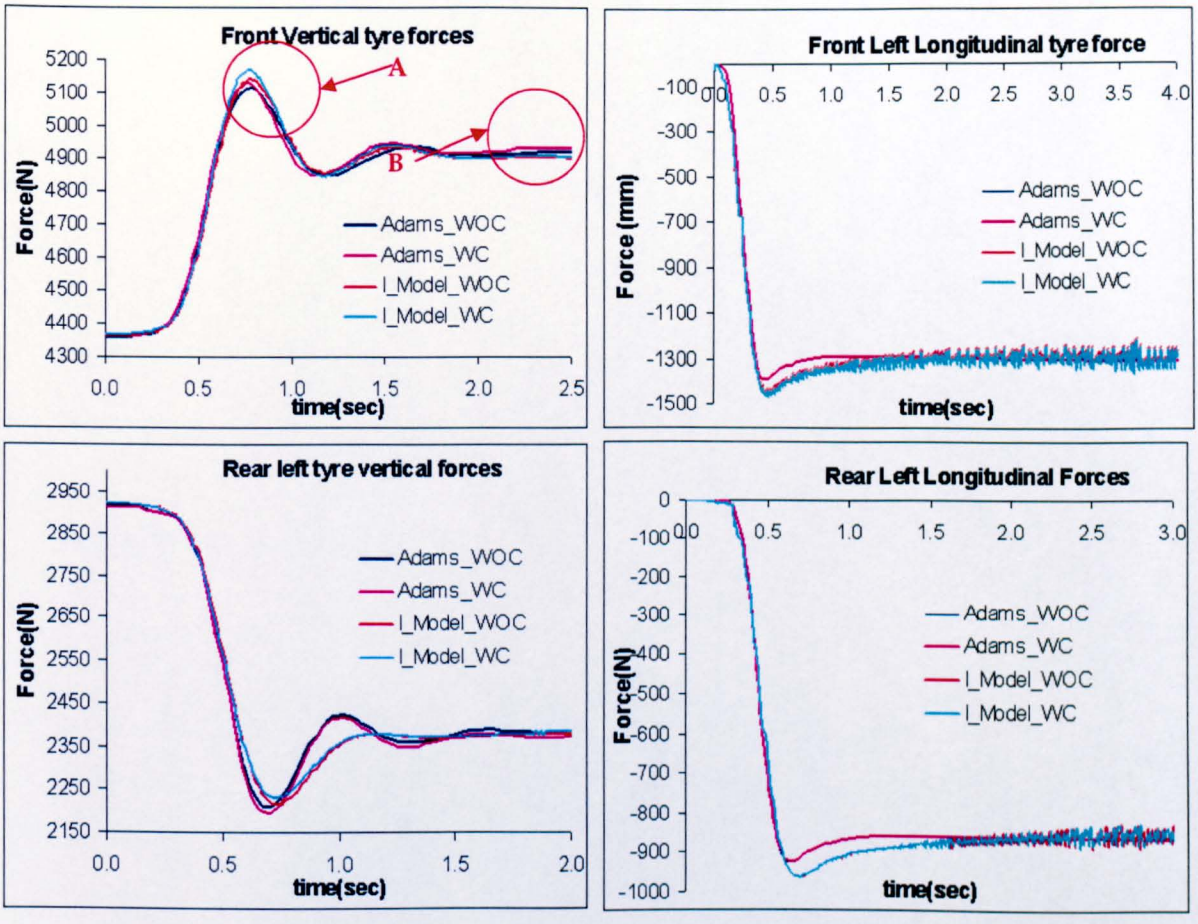

Figure 6.20: Front/Rear left vertical and longitudinal forces

Figure 6.20 shows very good correlation between the predictions of the two models for vertical and longitudinal tyre forces. The differences obtained with and without the bushing effect are still noticeable as can be seen in figure 6.20. During transient condition, the more detailed multi-body model (section A in figure 6.21) with the bushing effect shows a higher vertical force (about 20N) and with a higher corresponding frequency.

Similar case can also be seen for the intermediate model, however the intermediate predicts higher vertical forces during transience, but lower values during steady state conditions as depicted in section B (figure 6.22).

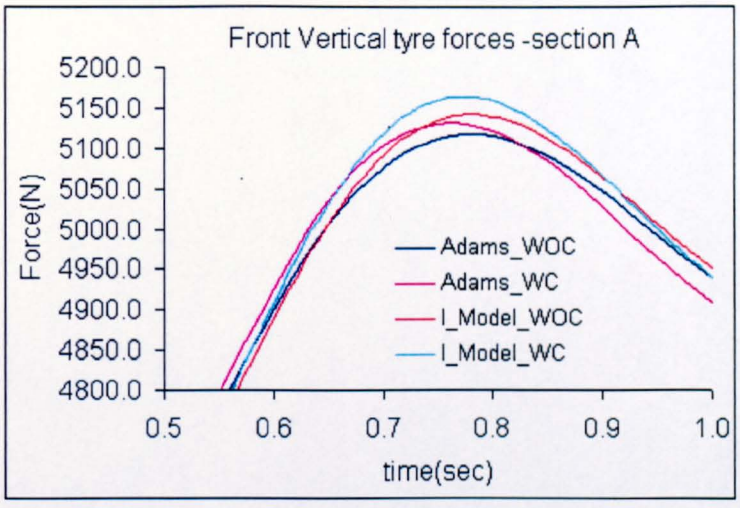

Figure 6.21: Section A – Front left vertical forces during transient condition

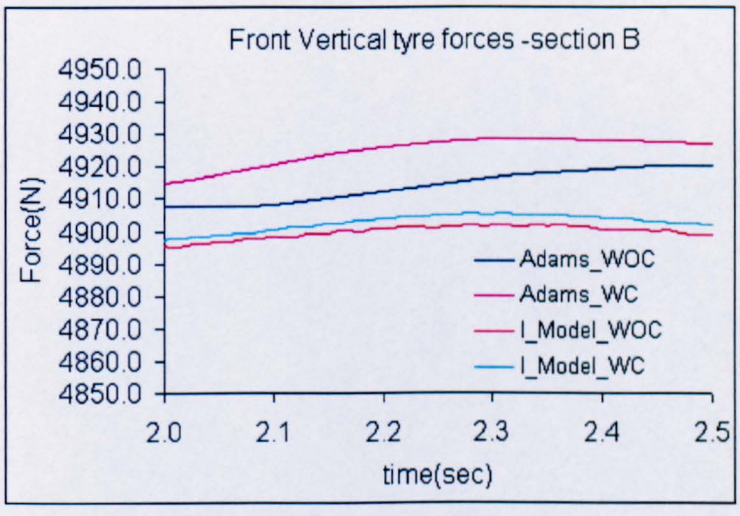

Figure 6.22: Section B – Front left vertical force during steady state condition

Interesting results can be seen for suspension deflection/travel analysis (see figure 6.23). At front suspension the effect of bushing on the multi-body model is about 3mm, when compared to that for the intermediate model, being 2mm difference between with and without the bushing effect. The bushing effect at the rear seems to be almost insignificant. This is understandable, because of the load transfer to the front under the decelerative motion. A similar situation can be observed, where with the included compliance effect the model seems to exhibit a higher frequency response and higher damping, which can be seen in the suspension deflection results (see figure 6.23). Front suspension deflection shows a very good correlation between the Adams model and the intermediate model with compliance. However, the rear deflection difference of 2 mm between them at steady state condition exists.

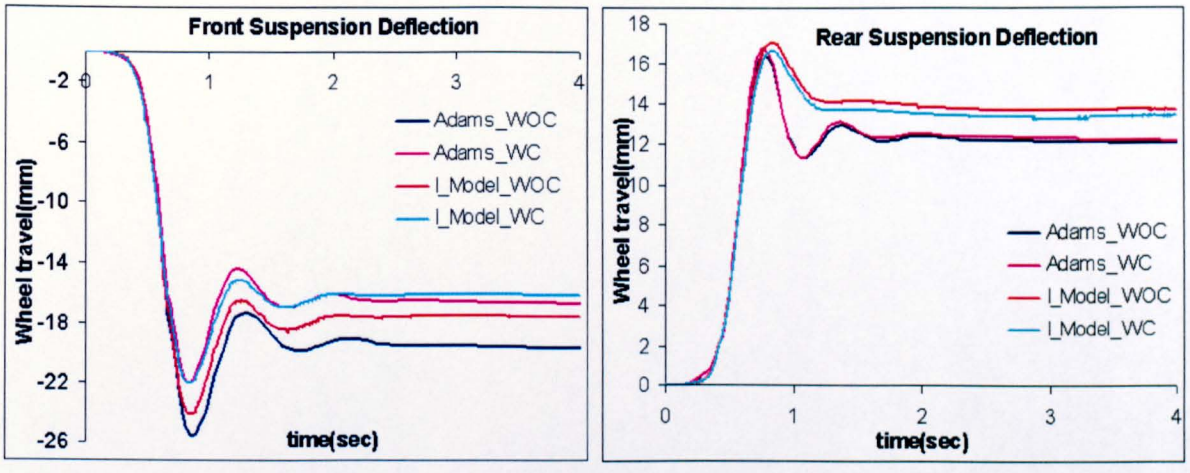

Figure 6.23: Suspension deflection

Figure 6.24 shows the variation of two important parameters in analysing the effect of bushing in pitch plane dynamics (these being the pitch angle and its rate of change). The result shows a noticeable difference in pitch rate, as well as the pitch angle with and without the elasto-kinematics of system compliances.

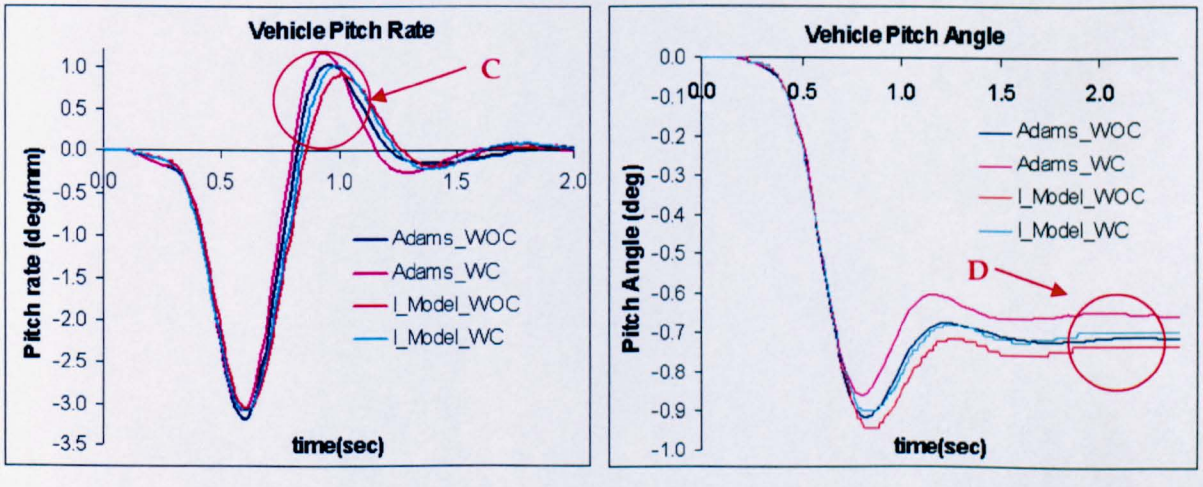

Figure 6.24: Vehicle pitch rate and pitch angle

The differences can be seen under both transient and steady state conditions as shown in sections C and D (see figure 6.25 and figure 6.26)

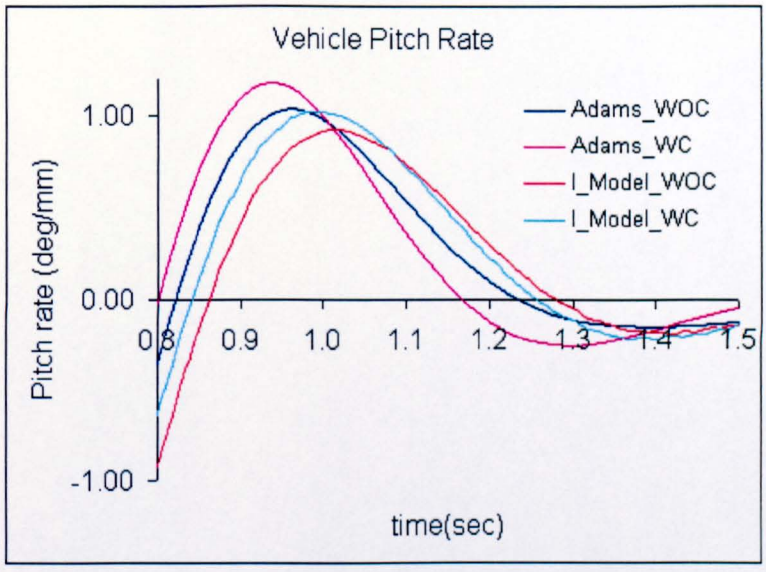

Figure 6.25: Section C: Vehicle pitch rate

Section C (figure 6.25) shows the vehicle pitch rate for the multi-body ADAMS model, where with the inclusion of compliance it exhibits a higher variation (amplitude), and a higher frequency response than without compliance. A similar situation situation also exists for the intermediate model.

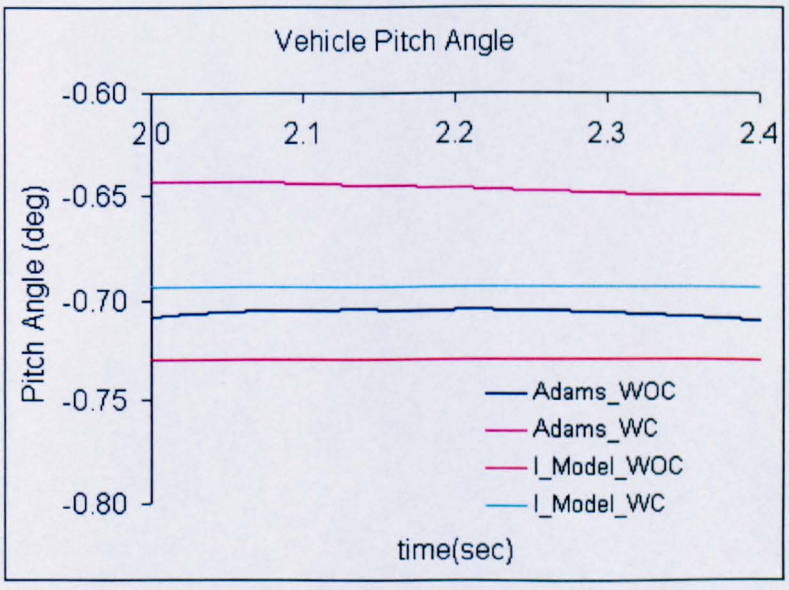

Figure 6.26: Section D of vehicle pitch angle

Section D (figure 6.26) illustrates that the vehicle pitch angle also differs with and without compliance as expected. Even though the difference is rather small, it clearly shows that bushing can provide an effect in the overall vehicle pitch plane dynamic

performance, not only under transient conditions, but also in steady state conditions. A significant effect can be seen in the vehicle vertical movement (see figure 6.27), where for the ADAMS model the difference between with and without bushing effect is around 2mm, which is a difference of nearly 25%. A similar characteristic can also be seen in the results from the intermediate model. However, the bushing effect is less pronounced; at about 15%.

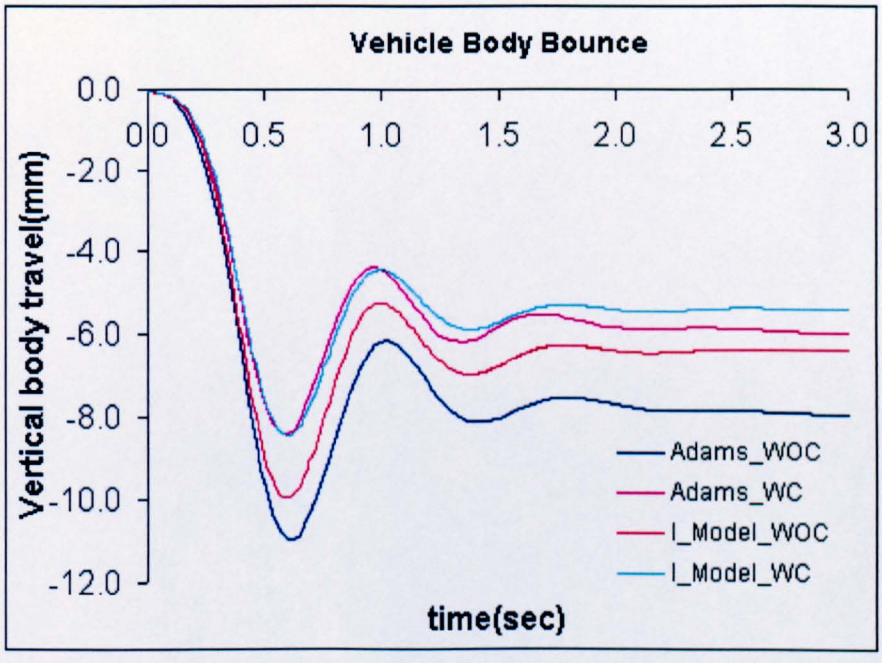

Figure 6.27: Vehicle body Bounce

6.5 Conclusion

A direct comparison with actual vehicle is quite difficult to achieve, because of the multiplicity of interactions of many parameters such as road profile and driver responses. Due to these interactions, the vehicle often experience unsteady motions due to unintended steering input, brake or forward acceleration and also in suspension deflection. These eventually affect its pitch or roll dynamic behaviour. There were 8 actual tests conducted, unfortunately 6 of which could be used for comparisons with computer models. The anomalies were due to the uneven road profile at the Donington Castle paddock area. Nevertheless, irrespective of the

problems encountered good correlation is noted between the models and most of the vehicle data.

Overall, the intermediate model has demonstrated a good correlation with the complex multi-body model and reasonable correlation with the vehicle test data. The current models demonstrate particularly good correlation in pure pitch plane dynamics, also in combination with significant body bounce. The correlations are less striking for roll dynamics, but still quite reasonable.

The anti-dive/squat analyses consistently show that these features play an important role in reducing pitching of the vehicle. The analysis, however, shows that with any abrupt bounce motion, for example while negotiating a speed bump, the effect of anti-pitch features can become insignificant.

The effect of an anti-roll bar is very important in vehicle handling, as it can reduce the body roll significantly. However, the analysis conducted shows that when the vehicle with an anti-roll bar is negotiating a single speed bump, it can actually suffer higher oscillatory roll dynamics at higher response frequency than the same vehicle without an anti-roll bar, if the elasto-kinematic properties of the bar are ill-chosen for an abrupt single event.

The elasto-kinematics analyses show that bushing can generate significant changes to the overall vehicle combined ride and handling characteristics during transient and steady state motions. Even though there are small changes in vertical and longitudinal forces, the bushing effect is still notable. It seem that the model with bushing compliance produces a higher frequency respond and magnitude during transient condition and also higher forces during steady state conditions. The bushing effect are much more obvious in suspension deflection characteristics, where the difference of 20% is noted between the predictions of the multi-body model and 15% for the intermediate model. Vehicle pitch plane dynamics also suggests similar results, where under transient conditions the vehicle with bushing compliance produces a higher pitch rate at higher frequency, but with a lower pitch angle during steady state conditions. This is due to provided compliance in the presence of introduced sudden inertial effects under transient conditions. A

significant difference is also seen in vehicle vertical deflection (body bounce), where the effect of bushing compliance changes the vertical displacement by around 20%.

A good correlation between the Adams model and the Intermediate model with similar pattern with and without bushing compliance strongly suggests that the approach used to generated compliance effect in the intermediate model is sensible.

CHAPTER 7

OVERALL CONCLUSIONS AND SUGGESTIONS FOR FUTURE WORK

7.1 Overall conclusions and contributions to knowledge

A number of findings have been highlighted in this thesis, which are considered as significant, and form the basis for an overall conclusion.

- The effect of anti-dive/squat features is important in vehicle pitch plane dynamics. The investigations show that when the vehicle is subjected to braking or acceleration, these features help in reducing vehicle dive and squat and pitch motions by resisting the generated inertial forces. The Intermediate model without these features produces a steady state error around 20%, whereas the intermediate model with these feature included shows results which conform closer to those obtained from the complex non-linear multi-body model and also agree better with the actual vehicle test data.

- Pitch plane dynamics, pitch and bounce motions are non-trivial problems that are often incorrectly regarded as simple. Some driver behavioural characteristics inhibit perceived ideal conditions such as failure to maintain a constant braking action, which is often easy to use in simulation studies. Some differences between vehicle data and simulation studies have been noted due to this problem. It is noteworthy that anti-dive and squat features play a role in pitch plane dynamics without significant body bounce. It is shown that their effect diminishes with any additional vehicle bounce, particularly at higher speeds. These conditions are often encountered in negotiation of speed bumps. Increasing vehicle speed over a barrier causes greater inertial imbalance, thus reducing the effect of anti-dive and squat features, which are designed essentially for normal pitch plane dynamics with

smaller vertical body bounce. This has been shown in the results of the vehicle negotiating speed bumps in the thesis.

- One other major finding, which was found during the research, shows that for pitch plane dynamics, one need not necessarily use a complex multi-body dynamics model, provided that a suitable representation of suspension kinematics is included in an intermediate model. The results in chapter 6 show a closer agreement between the intermediate vehicle model, with 18-DOF with the much more complicated ADAMS model with 396-DOF, when the suspension kinematics are included. The considerable difference in the level of complexity between these models points to a significant gain in the analysis time with the intermediate model. Thus, the performance of intermediate vehicle model is considered to be quite good in pitch plane dynamics, but not as accurate in combined pitch and bounce motions. This is because non-linearities in suspension spring/damper and bushing are not included in the intermediate model. However, good qualitative agreement is always found, including with the vehicle test data.

- Roll dynamics is very important parameter to be monitored, especially when conducting many vehicle manoeuvres, involving cornering, lane changing, and also rides of single event nature. An anti-roll bar is one of the major factors that contribute in overall vehicle roll stiffness. However, this feature has a disadvantage over ride and comfort analysis. The results for a single speed bump analysis clearly shows that when the vehicle model is incorporated with anti-roll bar system, it demonstrates a larger body roll rate at a higher frequency during transient conditions, compared to the vehicle model without an anti-roll bar negotiating the same speed bump.

- The anti-roll bar is a very important component to be included in vehicle modelling. Overall, in roll dynamics the intermediate model demonstrated a good correlation under steady state conditions with the complex model. However, during transient conditions, corresponding to sudden vehicle roll, the intermediate model did not performing as well. This is probably due to

non-linear spring/damper system in suspension system, as well as the beam type element used for the stabilizer bar, which introduces a non-linear effect in complex model, and not taken into account in the simpler intermediate model.

- From the virtual test rig analysis, it is clear that the position of wheel travel does play an important role on the actual deformation/travel of the suspension system. Even though this is a small effect in terms of the actual magnitude, it represents a significant percentage error. Based on the results obtained, it is shown that the longitudinal force is the dominant factor, compared to the lateral force in all translational or rotational deformation/travel in suspension system.

- The simplified approach, which was used to represent elasto-kinematics in an intermediate model, has demonstrated similar effect against the more complex multi-body model. When compliances are not included the vertical force increases about 50N in amplitude during transient condition and around 20N during steady state condition. Suspension deflection and pitch angle reduce, whilst the pitch rate increases during transience with higher damping characteristics (faster decay rate due to energy absorption by the deformation process). A similar effect can also be seen in the complex vehicle model, which replicates the results produced by the intermediate model.

- Based on the work carried out here, the overall performance of both computer models are quite goods against the vehicle test data, whilst it is clear that the complex model has a much greater degree of non-linearity and conforms better to the actual test data. Thus, for an initial evaluation of overall vehicle characteristics with certain deployed control system, a less complex vehicle model can be used, such as the intermediate model proposed in this thesis. However, for more detail overall vehicle characteristics, especially under transient conditions, the more complex vehicle model should be tried.

- Direct comparisons between the computer models and vehicle tests were found to be quite difficult to achieve, although this was realised for certain

parameters and manoeuvres. The difficulty is due to accurate inclusion of road surface conditions. However, if proper facility is made available or the road surface tends to good flatness, the quality of comparison would enhance considerably.

7.2 Critical Assessment of Approach

- Most of the vehicle models reported in literature (see chapter 2), especially those of a simplified construction assume that vehicle wheels are subject to pure vertical travel. However, in practice this is not the case. When the suspension articulates in vertical motion, the contact patch moves lateral and longitudinally due to the suspension geometry and compliance. To allow for these characteristics into the intermediate model, principle of virtual work approach was used, where any displacement at the contact patch contributes to work done in the suspension system. This eventually affects the actual suspension spring and damping forces.

- The assumptions used in the intermediate model so far yields reasonably good results. One of the main assumptions is the calculation of forces and moments based around the vehicle CG, and where roll, pitch and yaw axes are assumed always at the centre of gravity. In practice, the CG is always slightly above the roll or pitch axes. This can contribute to additional load transfer. However, to include this effect the vehicle dynamics equations will become extremely complex as demonstrate in chapter 3 and lead to considerable additional processing time.

- The investigations carried out in the thesis for ride analysis are limited to long-wavelength features due to the assumptions used for modelling of the sprung mass only. However, this can be improved upon by the inclusion of the unsprung mass into the suspension calculations, so that a wider range of ride analysis can be conducted, such as short-wavelength speed bumps and events leading to wheel hop motions.

- In the actual road vehicle testing, and especially in the university premises, budgetary constraints will always be a main limiting factor. Due to this reason, types of test, types of sensors, number of sensors and location of tests need to be carefully selected. Inclusion of more sensors and use of proper test tracks would be advantageous, for the reasons described above. The unavailability of measured suitably flat roads has resulted in incomplete validation of intermediate model for roll dynamics.

- Inclusion of elasto-kinematics effect in vehicle model is always perceived to increase the level of complexity of the vehicle model, and usually incorporated in complex vehicle model. It is believed that the inclusion of this effect in a simpler vehicle model, especially in those used to study control would probably provide a better picture of what to expect, rather than using complex models with many interactions.

7.3 Achievement of Aims

Several aims were highlighted in chapter 1. These included the following:

- Ascertaining the extent of usefulness of simple vehicle models, and establishing an intermediate vehicle modelling methodology. A higher degree of complexity was to be achieved in order to study integrated vehicle ride and comfort manoeuvres

- Establish a vehicle model with an open platform inexpensive software, which is widely available, yielding quicker processing times suitable for rapid scenario-building simulations, and a platform for subsequent development work for vehicle stability analysis and control.

- Develop a complex multi-body vehicle model in the ADAMS/Pre environment for validation of the intermediate vehicle model, the success of both being gauged against actual vehicle tests.

- Create a virtual suspension test rig in the ADAMS/View environment for the extraction of suspension characteristics and investigation of bushing deformation.

- Conducting on road vehicle testing for further validation of the intermediate model as well as complex model.

- Investigation of effectiveness of anti-dive/squat geometry, anti-roll bar and bushing compliance on the pitch and roll plane dynamics under real-world conditions.

All the above objectives of the thesis have been realised, with a critical assessment of some of the assumptions highlighted in the previous section.

Chapter 3 is basically report on the work carried out in achieving the first 4 objectives. Chapter 5 outlines the results of the various vehicle road tests, and chapter 6 provides the results of all the research undertaken, with comparisons between the numerical work and the experimental findings. The conclusions and major findings of the research are outlined in section 7.1.

7.4 Suggestions for Future Work

- An inclusion of unsprung mass in the intermediate model would probably be the first step for future improvement to the intermediate model, so that a more extensive range of analyses, especially in ride analysis can be carried out. The addition of extra degrees of freedom due to unsprung masses opens the way toward the study of off-road or all road vehicle combined ride and handling. Clearly, better tyre models for off-road work, based on soil mechanics will be required.

- With an extension of driveline model, the intermediate model can be used to introduce limited slip differentials or slip clutches to study vehicle transient

handling analysis for multi-axle vehicles or torque distribution control to wheels, studying wheel slipping and similar problems.

- For further validation of the intermediate model it would probably be of interest to include a control methodology such as Direct Yaw Control (DYC) into the intermediate model to see its effect on vehicle response, particularly under transient cornering manoeuvres. Of course a similar control system needs to be implemented in the complex vehicle model, as well as in the vehicle itself. The advantage of the intermediate model in "proving-out" of control strategies, before implementation into a more complex model can then be realised. In this context the model can be furnished with other features, using a similar approach as that already highlighted in this thesis, such as 4-wheel steer (4WS) or limited slip control, using anti-locking braking systems (ABS).

- Since the model is developed under Matlab/Simulink environment, a future extension of this research may be to link the model to the internet, thus using Matlab/Simulink web features. A user interface has to be developed for this purpose so that anyone on the internet can make any changes to the vehicle parameters, before submitting to the main server analysis.

The achievement of aims of the thesis has thus opened the way forward to study a range of topical issues in vehicle dynamics.

List of References

Abe, M. (1989) *Handling Characteristics of Four Wheel Active Steering Vehicles Over Full Manoeuvring Range of Lateral and Longitudinal Acceleration, Vehicle System Dynamics,* **18,** 87-101.

Abe, M. (1999) *Vehicle dynamics and control for improving handling and active safety: from 4-wheel steering to direct yaw moment control, Proceedings of the Institution of Mechanical Engineers Part K Journal of multi-body dynamics,* **213, Part K,** 87-101.

Abe, M. and Kano, Y. (1999) *Improvement of vehicle handling safety with vehicle side-slip control by direct yaw moment, Vehicle System Dynamics,* **Supplement 33,** pp 665-679.

Abe, M., Kanoa, Y., Suzukia, K., Shibahatab, Y. and Furukawab, Y. (2001) *Side-slip control to stabilize vehicle lateral motion by direct yaw moment, JSAE Review,* **22,** 413-419.

Abe, M., Ohkubo, N. and Kano, Y. (1996) *A direct yaw moment control for improving limit performance of vehicle handling - comparison and cooperation with 4WS, Vehicle System Dynamics,* **Supplement 33,** pp 33-54.

Acker, B., Darenburg, W. and Gall, H. (1991) *Active suspension for passenger cars., Dynamics of road vehicles, Proc. 11th IAVSD symp.*

ADAMS/Pre, M. A. s. (2002) *ADAMS/Pre User Reference Manual.*

Allen, R. W. and Rosenthal, T. J. (1994) *Requirements for Vehicle Dynamics Simulation Models, SAE Technical Papers, SAE 940175.*

Anderson, R. J. and Hanna, D. M. (1989) *Comparison of Three Vehicle Simulation Methodologies, Vehicle System Dynamics,* **18.**

Appel, H., Essers, U., Gohring, E., Povel, R., Glasner, E. C. and Tororvic, J. (1992) In *Total vehicle dynamics - FISITA 1992; Automotive technology serving society-Volume 1.,* Vol. 1 Mechanical Engineering Publications, pp. 247-255.

Bakker, E., Nyborg, L. and Pacejka, H. B. (1987) *Tyre modelling for use in vehicle dynamics studies, Society of Automotive Engineers,* pp 190-204.

Best, M. C. and Gordon, T. J. (1998) *Suspension system identification based on impulse-momentum equations, Vehicle System Dynamics,* **supplement 28,** pp 598-618.

Best, M. C. and Gordon, T. J. (2002) *Simultaneous Optimisation of Vehicle Parameter and Control Action to Examine the Validity of Handling Control Assumptions, Proceedings of the 6th International Symposium on Advanced Vehicle Control (AVEC),* pp 87-92.

Blundell, M. V. (1999) *The Modelling and Simulation of Vehicle Handling Part 1: Analysis Methods, Proceedings of the I MECH E Part K Journal of Multi-body Dynamics,* **213,** 103-118.

Chen, D. C., Crolla, D. A., Alstead, C. J. and Whitehead, J. P. (1996) *A comprehensive study of subjective and objective vehicle handling behaviour, Vehicle System Dynamics,* **Supplement 33,** pp 66-86.

Chu, T. W., Jones, R. P. and Whittaker, L. M. T. (2001) *A System Theoretic Analysis of Automotive Vehicle Dynamics and Control, Vehicle System Dynamics,* **37.**

Cooke, R., Crolla, D. A. and Abe, M. (1997) *Modelling combined ride and handling manoeuvres for a vehicle with slow-active suspension, Vehicle System Dynamics,* **27,** pp 458-475.

Crolla, D. A., Horton, D. N. L., Brooks, P. C., Firth, G. R., Shuttlewood, D. W., Woods, M. and Yip, C. K. (1994) *A Systematic Approach to Vehicle Design Using Vdas (Vehicle Dynamics Analysis Software), SAE Technical Papers, SAE 940230.*

Dickison, J. G. and Yardley, A. J. (1993) *Development and Application of a Functional Model to Vehicle Development, SAE Technical Papers, SAE 930835,* pp 221-230.

Doniselli, D., Mastinu, G. and Gobbi, M. (1996) *Aerodynamic effect on ride comfort and road holding of automobiles, Vehicle System Dynamics,* **Supplement 33,** pp 99-125.

Dugoff, H. (1970) *An Analysis of Tire Traction Properties and Their Influence on Vehicle Dynamics Performance, SAE paper 700377.*

Ellis, J. R. (1994) *Vehicle Handling Dynamics,* London : Mechanical Engineering Publications, 1994.

Esmailzadeh, E., Goodarzi, A. and Vossough, G. R. (2003) *Optimal Yaw Moment Control Law for Improved Vehicle Handling, Mechatronics,* **13,** 659-675.

Genta, G. (1997) *Motor vehicle dynamics: modeling and simulation.*

Gillespie, T. D. (1992) *Fundamentals of vehicle dynamics, SAE.*

Gordon, T. J., Best, M. C. and Dixon, J. (2002) *An automated driver based on convergent vector fields, Journal of Automobile Engineering,* **216,** pp 329 -347.

Gordon, T. J., March, C. and Milsted, M. G. (1991) *A comparison of adaptive LQG and nonlinear controllers for vehicle suspension systems, Vehicle System Dynamics,* **20,** pp 321-340.

Guo, K., Lu, D. and Ren, L. (2001) *A Unified Non-Steady Non-Linear Tyre Model Under Complex Wheel Motion Inputs Including Extreme Operating Conditions, JSAE Review 22(4),* pp 395 -402.

Happian-Smith, J. (2002) *An Introduction to Modern Vehicle Design, published by SAE and Butterworth-Heinemann.*

Harada, M. and Harada, H. (1999) *Analysis of Lateral Stability with Integrated Control of Suspension and Steering Systems,* 465-470.

Hegazy, S., Rahnejat, H. and Hussain, K. (2000) *Multi-body dynamics in full-vehicle handling analysis under transient manoeuvre, Vehicle System Dynamics,* **34,** 1-24.

Horiuchi, S., Okada, K. and Nohtomi, S. (1999a) *Effect of integrated control of active four wheel steering and indivitual wheel torque on vehicle handling and stability - A comparison of alternative control strategies, Vehicle System Dynamics,* **Supplement 33,** pp 680-691.

Horiuchi, S., Okada, K. and Nohtomi, S. (1999b) *Improvement of Vehicle Handling by Nonlinear Integrated Control of Four Wheel Steering and Four Wheel Torque, Elsevier,* 459-464.

Huston, R. L. and Lui, C. Q. (2001) *Formulas for dynamics analysis, Marcel Dekker ,ISBN 0824795644.*

Katz, A. (1997) *Computational rigid vehicle dynamics, Krieger, ISBN 1575240165.*

Keiyu, K., Osamu, Y. and Hiroyuki, U. (2003) *Enhancements in vehicle stability and steerability with slip control, JSAE Review,* **24,** 71-79.

Kiencke, U. and Daib, A. (1997) *Observation of Lateral Vehicle Dynamics, Control Engineering Practice,* **5,** 1145-1150.

Kim, C. and Ro, P. I. (2002) *An accurate full car ride model using model reducing techniques, Journal of Mechanical Design,* **Vol. 124,** pp 697-705.

Kleine, S. and Niekerk, J. L. V. (1998) *Modelling and control of a steer-by-wire vehicle, Vehicle System Dynamics,* **supplement 28.**

Kortum, W. and Sharp, R. S. (1993) *Multi-body Codes in Vehicle System Dynamics, Lisse, Swetz & Zeitlinger.*

Li, K., Bin, Y., Zhen, S. and Lian, X. (2001) *A modified nonlinear controller of vehicle longitudinal control system using VSC method.*

Li, S. (1992) *Optimal control of a three dimensional active vehicle suspension system, including servo-actuator dynamics, Society of Automotive Engineers*, pp 213-220.

Lin, M., Popov, A. A. and MCWilliam (2003) *Handling studies of driver-vehicle systems, Vehicle System Dynamics.*

Lin, M., Popov, A. A. and MCWilliam (2004) *Stability and performance studies of driver-vehicle systems with electronic chassis control, Vehicle System Dynamics,* **supplement 41,** pp 477-486.

Lozia, Z. (1994) *Behaviour during lane-change manoeuvre on an uneven road surface, Vehicle System Dynamics,* 417-422.

Lu, X.-p., Lu, D., Guo, K. and Tseng, F. (2003) *Camber effect on tire force and moment properties.*

Lugner, P. and Mittermayr, P. (1989) *Possibilities to Improve the Vehicle Cornering Dynamics by the Control of the Tire Forces, Vehicle System Dynamics,* **18.**

Lukowski, S. A. and Medeksza, L. (1992) *Vehicle cornering behaviour analysis using a general purpose simulation methodology, Society of Automotive Engineers,* pp 49-54.

Makita, M. (1999) *An Application of Suspension Kinematics for Intermediate Level Vehicle Handling Simulation, ELSEVIER,* 471-477.

Matschinsky, W. (2000) *Road Vehicle Suspensions, Professional Engineering Publishing, London and Bury St Edmunds.*

Mavros, G. (2004) In *Wolfson School of Mechanical and Manufacturing Engineering*Loughborough University, Loughborough.

Meriam, J. L. and Kraige, L. G. (1993) *Engineering Mechanics,* **Volume 2.**

Milliken, W. F. and Milliken, D. L. (1995) *Race Car Vehicle Dynamics,* SAE, Warrendale, PA, USA.

Minaker, B. and Anderson, R. J. (1999) *Modelling of dynamics of a vehicle with active geometry suspension, Vehicle System Dynamics,* **Supplement 33,** pp 716-727.

Mokhiamar, O. and Abe, M. (2001) *Combined Lateral Force and Yaw Moment Control to Maximize Stability as well as Vehicle Responsiveness during Evasive Manoeuvring for Active Vehicle Handling Safety, Vehicle System Dynamics,* **37.**

Nagai, M., Hirano, Y. and Yamanaka, S. (1997) *Integrated control of active rear wheel steering and direct yaw moment control, Vehicle System Dynamics,* **27,** 357-370.

Nagai, M., Shino, M. and Gao, F. (2002) *Study on integrated control of active front steer angle and direct yaw moment, JSAE Review,* **23,** 309-315.

Neto, A. C. (1994) *Application of Multibody Systems(MBS) Techniques to Vehicle Modelling.*

Oosten, J. J. M. V. and Pacejka, H. B. (2000) *SWIFT-Tyre- An accurate tyre model for ride and handling studies also at higher frequencies and short road wavelengths, ADAMS users' conference.*

Ottgen, O. and Bertram, T. (2001) *Influencing vehicle handling through active roll moment distribution, Vehicle System Dynamics.*

Pacejka, H. B. (2002b) *Tyre and vehicle dynamics.*

Pacejka, H. B. and Bakker, E. (1993) *The Magic formula tyre model, Vehicle System Dynamics, Proceedings of the 1st International Colloquium on Tyre Models for Vehicle Dynamics Analysis, Oct 21-22 1991,* **21,** 1-18.

Park, K., Heo, S. J. and Baek, I. (2001) *Controller Design for Improving Lateral Vehicle Dynamic Stability.*

Pisu, P., Soliman, A. and Rizzoni, G. (2003) *Vehicle Chassis Monitoring System, Control Engineering Practice,* **11,** 345-354.

Plochl, M. and Lugner, P. (1999) *A 3-level driver model and its application to driving simulations, Vehicle System Dynamics,* **supplement 33,** pp 71-82.

Pongsathorn, R., Mouri, H. and Nagai, M. (2002) *Vehicle Lane-Keeping Control by Four-Wheel-Steering System, AVEC,* 463-468.

Rahnejat, H. (1998) *Multi-Body Dynamics - Vehicles, Machines and Mechanisms,* Professional Engineering Publishing Limited.

Rahnejat, H. (2000) *Multi-body dynamics: historical evaluation and application, Proceedings of the I MECH E Part C Journal of Mechanical Engineering Science,* **214,** 149-173.

Rossetter, E. J. and Gerdes, J. C. (2000) *A study of lateral vehicle control under a virtual force framework.*

Roukieh, S. and Titli, T. (1992) *On the model-based design of semi-active and active suspension for private cars, Vehicle System Dynamics*, pp 305-318.

Ryu, J., Rossetter, E. J. and Gerdes, J. C. (2002) *Vehicle Sideslip and Roll Parameter Estimation Using GPS, Department of Mechanical Engineering, Stanford University.*

SAE-J670e (1976) *Vehicle Dynamics Terminology., SAE J670e.*

Savkoor, A. R. and Ausejo, S. (1999) *Analysis of driver's steering and speed control strategies in curve negotiation, Vehicle System Dynamics*, **Supplement 33,** pp 94-109.

Sayers, M. W. (1989) *Automated Formulation of Efficient Vehicle Simulation Codes by Symbolic Computation(AUTOSIM), Vehicle System Dynamics*, **18.**

Sayers, M. W. and Han, D. (1996) *A Generic multibody vehicle model for simulating handling and braking, Vehicle System Dynamics, Proceedings of the 1995 14th IAVSD Symposium on the Dynamics of Vehicles on Roads and Tracks, Aug 21-25 1995*, **25,** 599-613.

Schuller, J., Haque, I. and Eckel, M. (2001) *An Approach for Optimisation of Vehicle Handling Behaviour in Simulation, Vehicle System Dynamics*, **37.**

Segel, L. (1956) *Theoretical Prediction and experimental substantiation of the response of the automobile to steering control, Automobile Division, The Institute of Mechanical Engineers*, pp 26 - 46.

Sharp, R. S. (1999) *Influences of suspension kinematics on pitching dynamics of cars in longitudinal manoevring, Vehicle System Dynamics*, **supplement 33,** pp 23-36.

Shiiba, T. and Suda, Y. (2002) In *In Proceedings of AVEC2002, 6th International Symposium on Advanced Vehicle Control.*Hiroshima, Japan.

Shin, M., Bae, S., Lee, J. M., Heo, J. S. J. and Tak, T. O. (2001) *New Vehicle Dynamics Model for Yaw Rate Estimation, Vehicle System Dynamics*, **37.**

Shino, M. and Nagai, M. (2001) *Yaw-Moment Control of Electric Vehicle for Improving Handling and Stability, 2001 Society of Automotive Engineers of Japan, Inc.*

Shino, M., Raksincharoensak, P. and Nagai, M. (2002) In *AVEC 2002, 6th International Symposium on Advanced Vehicle Control*Hiroshima, pp. 25-31.

Svendenius, J. and Gafvert, M. (2004) *A brush-model based semi-empirical tire-model for combined slips, Society of Automotive Engineers, World Congress.*

Tandy, K., Heydinger, G. T., Christos, J. P. and Guenther, D. A. (1992) *Improving vehicle handling simulation via sensitivity analysis, Society of Automotive Engineers,* pp 1-10.

Terry, D. D., Roberts, S. G. and Allen, R. Y. (2001) *SIMON: A New Vehicle Simulation Model for Vehicle Design and Safety Research.*

Tran, V. T. (1992) *Handling Control with Additional Rear Wheel Steering, Total Vehicle Dynamics,* **1,** 75-86.

Uematsu, K. and Gerdes, J. C. (2002) In *In Proceedings of AVEC2002, 6th International Symposium on Advanced Vehicle Control.*Hiroshima, Japan.

Valasek, M., Breedveld, P., Sika, Z. and Vampola, T. (1999) *Software tools for mechatronic vehicle: Design through modelling and simulation, Vehicle System Dynamics,* **Supplement 33,** pp 214-230.

Van Oosten, J. J. M. and Pacejka, H. B. (2000) *SWIFT-Tyre- An accurate tyre model for ride and handling studies also at higher frequencies and short road wavelengths, ADAMS users' conference.*

Watanabe, Y. and Sayer, M. W. (2004) *The effect of non-linear suspension kinematics on the simulated pitching and rolling dynamic behavior of cars, The dynamics of vehicles on roads and on tracks,* **41,** 23-32.

Willumeit, H. P., Neculau, M., Vikas, A. and Wohler, A. (1992) *Mathematical models for the computation of vehicle dynamic behaviour during development, Total vehicle dynamics - FISITA 1992; Automotive technology serving society,* **1,** 41-48.

Wong, J. Y. (2001) *Theory of ground vehicles.,* John Wiley & Sons, Inc., New York.

Yamamoto, M., Harasa, H. and Yoshiaki (1989) *A Study on Active controlled Chassis System for Vehicle Dynamics, Vehicle System Dynamics,* **18.**

Yip, C. K., Crolla, D. A. and Horton, D. N. L. (1992) *The Influence of Aerodynamic Effect on Car Handling, Total Vehicle Dynamics,* **1,** 11-23.

Zbigniew, L. (1994) *Behaviour during lane-change manoeuvre on an uneven road surface, Vehicle System Dynamics,* 417-422.

Appendix 1

Theory & Assumption for 2DOF "Bicycle" Model

The two degrees of freedom of motion that are represented by the bicycle model are the vehicle's lateral and yaw dynamics. Basically this model is appropriate for study of steady-state cornering. The inputs to the system are the steering wheel angle and the vehicle forward velocity. A step change will be used as the steering input and forward velocity is assumed to be constant. A step steering input takes the vehicle through two distinct phases: the first is a transient phase, and the second is a steady state phase. (Gillespie, 1992), (Pacejka, 2002). (Milliken & Milliken, 1995)

The model derived below is only suitable for steady state low speed cornering (low lateral acceleration) due to the assumptions being made and the linear nature of the model. Higher lateral accelerations affect body roll, compliance effects, load transfer and tyre load sensitivity, thus the model becomes unsuitable for the analysis.

There are several assumptions made for this 2-DOF model. These are:

1. Linear tyre models
2. No rolling and pitching motions
3. No lateral load transfer
4. No longitudinal load transfer
5. No suspension compliance effects
6. Constant forward velocity (U)
7. A smooth road surface with no ride motions
8. Small angle assumption is used to simplify the equations of motion

Equations of motion

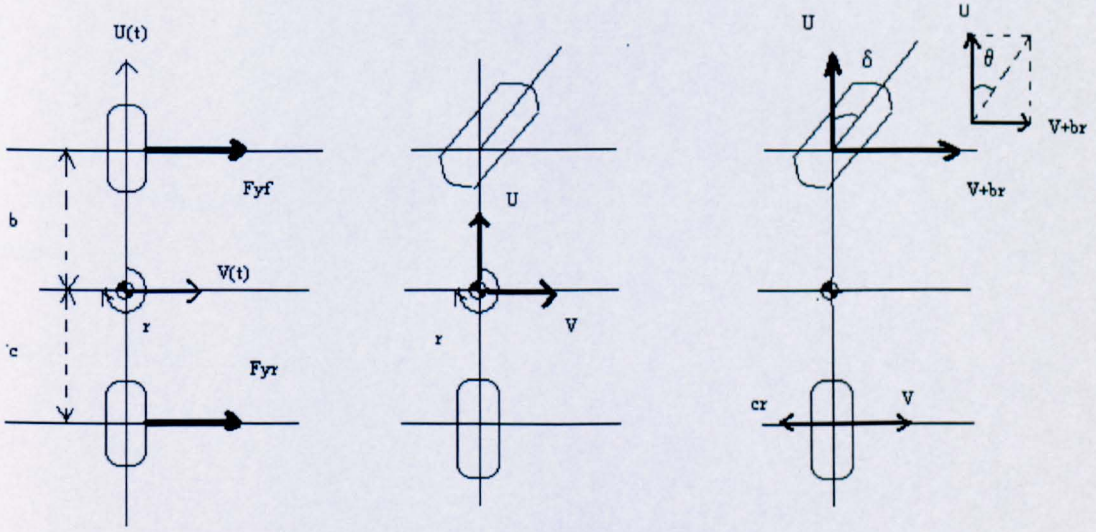

Figure 1.1: Free body diagram of the bicycle model

The equations of motion for the 2-DOF bicycle model, using Newton's second law are:

$$T = I\alpha \text{ and } F = ma$$

For this model, the above equations become: $N = I_{zz}\dot{r}$ and $Y = Ma_y$,

Where N is the yaw moment and Y is the side force, hence the lateral dynamics is described by:

$$F_{yf} + F_{yr} = M \times \left(Lateral\_Acceleration\right)$$

However, for total lateral acceleration, one has to include the rotational effect (Ur). Thus, the final lateral equation become:

$$F_{yf} + F_{yr} = M\left(\dot{V} + Ur\right) \tag{1.1}$$

For yaw rotation, the dynamic equation is:

$$bF_{yf} - cF_{yr} = I_{zz}\dot{r} \tag{1.2}$$

From Figure 1.1, slip angle, $\alpha_f = \delta - \theta$, where $Tan\theta = \dfrac{V + br}{U}$

For a small slip angle (α_f), $\theta \approx \dfrac{V + br}{U}$

So the front slip angle becomes: $\alpha_f = \delta - \dfrac{V + br}{U}$, and similarly, the rear slip angle becomes: $\alpha_r = -\dfrac{V - cr}{U}$. Hence, the front and rear linear tyre forces are :

$$F_{yf} = C_{\alpha f}\alpha_f = C_{\alpha f}\left(\delta - \frac{V + br}{U}\right) \text{ and } F_{yr} = C_{\alpha r}\alpha_r = C_{\alpha r}\left(-\frac{V - cr}{U}\right)$$

where, the tyre forces use the cornering stiffness coefficient, C_α which is only suitable for low speed and small slip angle analysis.

Thus, the *total side force* , $Y = F_{yf} + F_{yr}$

$$= C_{\alpha f}\alpha_f + C_{\alpha r}\alpha_r$$

$$= C_{\alpha f}\left(\delta - \frac{V + br}{U}\right) + C_{\alpha r}\left(-\frac{V - cr}{U}\right)$$

$$= \left[\frac{-C_{\alpha f} - C_{\alpha r}}{U}\right]V + \left[\frac{-bC_{\alpha f} + cC_{\alpha r}}{U}\right]r + \left[C_{\alpha f}\right]\delta$$

$$Y = Y_v V + Y_r r + Y_\delta \delta \tag{1.3}$$

where: Y_v is damping in the side-slip derivative

Y_r is the lateral force/yaw coupling derivative

Y_δ is the control force derivative

Total *Yaw Moment*, $N = bF_{yf} - cF_{yr}$

$$= bC_{\alpha f}\alpha_f + cC_{\alpha r}\alpha_r$$

$$= bC_{\alpha f}\left(\delta - \frac{V + br}{U}\right) + cC_{\alpha r}\left(-\frac{V - cr}{U}\right)$$

$$= \left[\frac{-bC_{\alpha f} + cC_{\alpha r}}{U}\right]V + \left[\frac{-b^2C_{\alpha f} - c^2C_{\alpha r}}{U}\right]r + \left[bC_{\alpha f}\right]\delta$$

$$N = N_v V + N_r r + N_\delta \delta \tag{1.4}$$

Where: N_v is the static directional stability derivative

N_r is the yaw damping derivative

N_δ is the control moment derivative

From equations (3.33) - (3.36) one can obtain the lateral and yaw accelerations in the form of state-space representation. The states' vector will be the lateral velocity *V* and the yaw velocity *r*. The input or control vector will be the steering wheel angle δ. Thus:

$$\dot{V} = \left[\frac{Y_v}{M}\right]V + \left[\frac{Y_r}{M} - U\right]r + \left[\frac{Y_\delta}{M}\right]\delta \quad \text{-------- Lateral Acceleration}$$

$$\dot{r} = \left[\frac{N_v}{I_{zz}}\right]V + \left[\frac{N_r}{I_{zz}}\right]r + \left[\frac{N_\delta}{I_{zz}}\right]\delta \quad \text{------- Yaw Acceleration}$$

Note that the total lateral acceleration is: $\dot{V} + Ur$

State space representation:

$$A = \begin{bmatrix} \frac{Y_v}{M} & \frac{Y_r}{M} - U \\ \frac{N_v}{I_{zz}} & \frac{N_r}{I_{zz}} \end{bmatrix}$$ ---- System Matrix ; $$B = \begin{bmatrix} \frac{Y_\delta}{M} & \frac{N_\delta}{I_{zz}} \end{bmatrix}$$ ----- Input Matrix

$$C = \begin{bmatrix} 1 & 0 \\ 0 & 1 \\ 1/U & 0 \\ Y_v/M & Y_r/M - U \end{bmatrix} \begin{matrix} Lateral\_Velocity \\ Yaw\_Velocity \\ Vehicle\_Slip\_Angle \\ Lateral\_Acceleration \end{matrix}$$ -------- Output Matrix

$$D = \begin{bmatrix} 0 \\ 0 \\ 0 \\ Y_\delta/M \end{bmatrix}$$ -------- Feed forward Matrix

For this particular state-space representation the output is set as mentioned above in the output matrix. The details of the Matlab code for this model is given in appendix2.

Nomenclature:

$C_{\alpha f}, C_{\alpha r}$ are the cornering stiffness from front & rear

α_f, α_r, Front slip angle

δ, Steering angle

θ, Vehicle direction angle

r, Yaw rate

U, Forward speed

V, Lateral speed

c, Rear wheelbase

b, Front wheelbase

F_{yf}, F_{yr}, Side force for front and rear

N, Total yaw moment

Y, Total side force

END

2. Theory & Assumption of 3DOF model

The 3-DOF model presented here is slightly more complex compared to the 2-DOF model, since it includes roll dynamics into the system model, and also a fixed horizontal roll axis. However, the model is still a linear model that describes lateral, yaw and roll motions of the vehicle with a constant forward velocity. Based on 2DOF model but with the inclusion of roll centre height (h_1) from CG, the lateral dynamics of the vehicle is as given below: (Pacejka, 2002), (Milliken & Milliken, 1995).

$$M\left(\dot{V}+\dot{p}\,h_1+rU\right)=Y \text{ (Lateral Force)} \tag{2.1}$$

For rotational dynamics there are two components, which are the roll and yaw moments. If L is the total roll moment and N is the total yaw moment, based on equations (2.1) and (2.3), but also with the inclusion of the roll centre height from the CG, the rotational dynamics becomes:

$$I_{xx}\dot{p}-I_{xz}\dot{r}+Mh_1\left(\dot{V}+rU\right)=L \text{ ; Roll moment} \tag{2.2}$$

$$I_{zz}\dot{r}-I_{xz}\dot{p}=N \text{ ; Yaw moment} \tag{2.3}$$

Calculation of Forces and Moments

Since the vehicle undergoes roll motion, the calculation of forces for this model also includes the effect of roll camber and roll steer. Lateral forces:-

$$Y=F_{yf}+F_{yr} \tag{2.4}$$

$$F_{yf}=C_{\alpha fL}\alpha_{fL}+C_{\alpha fR}\alpha_{fR}+\left(C_{\gamma fL}\frac{\partial\gamma}{\partial\phi_{fL}}+C_{\gamma fR}\frac{\partial\gamma}{\partial\phi_{fR}}\right)\phi$$

With linear approximation, one can average over the two front wheels. So the total axle force becomes:

$$F_{yf}=C_{\alpha f}\alpha_f+\left[C_{\gamma f}\frac{\partial\gamma}{\partial\phi_f}\right]\phi \text{ , (the front side force)} \tag{2.5}$$

where:

$$C_{\alpha f}=C_{\alpha fL}+C_{\alpha fR};\quad \alpha_f=\frac{1}{2}\left(\alpha_{fL}+\alpha_{fR}\right);\quad \frac{\partial\gamma}{\partial\phi_f}=\frac{1}{2}\left(\frac{\partial\gamma}{\partial\phi_{fL}}+\frac{\partial\gamma}{\partial\phi_{fR}}\right);$$

The same applies for the rear side force as:

$$F_{yr} = C_{\alpha r}\alpha_r + \left[C_{\gamma r}\frac{\partial \gamma}{\partial \phi_r}\right]\phi \quad \text{(the rear side force)} \tag{2.6}$$

And if: $\varepsilon_f = \dfrac{\partial \delta_f}{\partial \phi}$ —— (Front Roll steer Coefficient)

Then:

$$\delta_f = \delta + \varepsilon_f \phi \tag{2.7}$$

So the front slip angle becomes:

$$\alpha_f = \delta_f - \frac{V + br}{U} \tag{2.8}$$

Substituting equations (2.7) and (2.8) into equation (2.5), the front side forces become:

$$F_{yf} = C_{\alpha f}\left\{\delta + \varepsilon_f \phi - \left(\frac{V + br}{U}\right)\right\} + \left(C_{\gamma f}\frac{\partial \gamma}{\partial \phi_f}\right)\phi$$

For the *rear side force*: $\varepsilon_r = \dfrac{\partial \delta_r}{\partial \phi}$ due to geometry:

$$\delta_r = \varepsilon_r \phi \tag{2.9}$$

then, the rear slip angle is:

$$\alpha_r = \delta_r - \frac{(V - cr)}{U} \tag{2.10}$$

Substituting equations (2.9) and (2.10) into equation (2.6), the rear side forces becomes:

$$F_{yr} = C_{\alpha r}\left\{\varepsilon_r \phi - \frac{(V - cr)}{U}\right\} + \left[C_{\gamma r}\frac{\partial \gamma}{\partial \phi_r}\right]\phi \tag{2.11}$$

From equation (2.4), Y is equal to:

$$Y = \left\{C_{\alpha f}\left(\delta + \varepsilon_f \phi - \frac{(V + br)}{U}\right) + \left(C_{\gamma f}\frac{\partial \gamma}{\partial \phi_f}\right)\phi\right\} + \left\{C_{\alpha r}\left(\varepsilon_r \phi - \frac{(V - cr)}{U}\right) + \left(C_{\gamma r}\frac{\partial \gamma}{\partial \phi_r}\right)\phi\right\}$$

$$= \left[C_{\alpha f}\right]\delta + \left[C_{\alpha f}\varepsilon_f + C_{\gamma f}\frac{\partial \gamma}{\partial \phi_f} + C_{\alpha r}\varepsilon_r + C_{\gamma r}\frac{\partial \gamma}{\partial \phi_r}\right]\phi - \left[\frac{\left(C_{\alpha f} + C_{\alpha r}\right)}{U}\right]V + \left[\frac{\left(-bC_{\alpha f} + cC_{\alpha r}\right)}{U}\right]r$$

In order to simplify the equation, the lateral force and yaw moment equations can be represented in the form:

$$Y(Lateral\_force) = Y_v V + Y_r r + Y_\phi \phi + Y_p p + Y_\delta \delta \tag{2.12}$$

$$N(Yaw\_moment) = N_v V + N_r r + N_\phi \phi + N_p p + N_\delta \delta \qquad (2.13)$$

and the handling coefficients $Y_v, Y_r, Y_\phi, Y_p, Y_\delta, N_v, N_r, N_\phi, N_p, N_\delta$ are easily found to be as follows:

$$Y_v = -\frac{(C_{af} + C_{ar})}{U}; \qquad N_v = \frac{(-bC_{af} + cC_{ar})}{U};$$

$$Y_r = \frac{(-bC_{af} + cC_{ar})}{U}; \qquad N_r = -\frac{(b^2 C_{af} + c^2 C_{ar})}{U};$$

$$Y_\phi = C_{af}\varepsilon_f + C_{if}\frac{\partial \gamma}{\partial \phi_f} + C_{ar}\varepsilon_r + C_{ir}\frac{\partial \gamma}{\partial \phi_r}; \quad N_\phi = bC_{af}\varepsilon_f + bC_{if}\frac{\partial \gamma}{\partial \phi_f} - cC_{ar}\varepsilon_r - cC_{ir}\frac{\partial \gamma}{\partial \phi_r}$$

$$Y_p = 0; \qquad N_p = 0;$$

$$Y_\delta = C_{af}; \qquad Y_\delta = bC_{af};$$

The roll moment, L, is more easily obtained in term of suspension stiffness and damping. The roll moment due to front and rear suspension is:

$$L_{susp} = -(K_{\phi f} + K_{\phi r})\phi - (B_{\phi f} + B_{\phi r})p \qquad (2.14)$$

The negative sign is due to the fact that the moment acts against the roll deflection/ roll angular velocity. One must also add these to the moment due to the vehicle weight (see figure 2.1, note for small roll angle: $\sin\phi \approx \phi$), thus:

$$L_{weight} = Wh_1\phi \qquad (2.15)$$

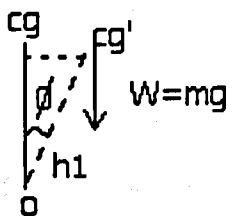

Figure 2.1: Moment due to vehicle weight

And hence:

$$L_v = 0;$$
$$L_r = 0;$$
$$L_\phi = -(K_{\phi f} + K_{\phi r}) + Wh_1;$$
$$L_p = -(B_{\phi f} + B_{\phi r});$$
$$L_\delta = 0;$$

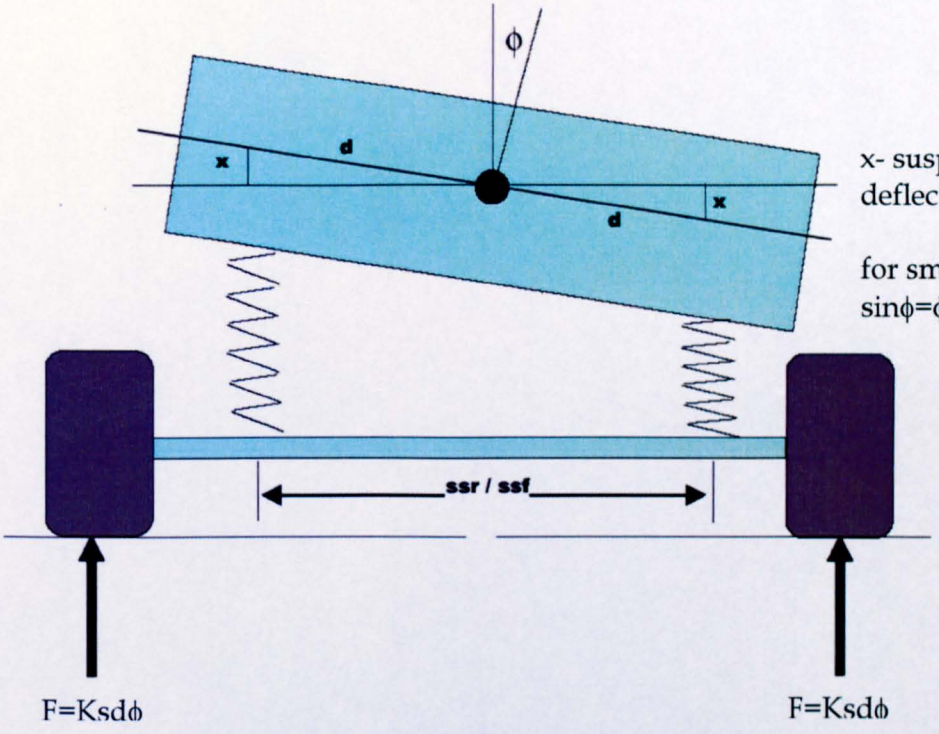

Figure 2.2: Suspension system for the 3-DOF model

Roll moment (see figure 2.2): $= 2Ksd\phi d = 2Ksd^2\phi$

$$= 2Ks\left(\frac{ssf}{2}\right)^2$$

$$= \frac{1}{2}Ks(ssf)^2$$

thus: $K_{\phi f} = \frac{1}{2}K_f(ssf)^2\phi$, $K_{\phi r} = \frac{1}{2}K_r(ssf)^2\phi$, $B_{\phi f} = \frac{1}{2}B_f(ssr)^2\phi$, $B_{\phi r} = \frac{1}{2}B_r(ssr)^2\phi$

State Space Representation:

$$M\dot{V} + \dot{p}h_1 + rU = Y_v V + Y_r r + Y_\phi \phi + Y_p p + Y_\delta \delta \tag{2.16}$$

$$I_{xx}\dot{p} - I_{xz}\dot{r} + Mh_1\left(\dot{V} + rU\right) = L_\phi \phi + L_p p + L_\delta \delta + L_v V + L_r r \tag{2.17}$$

$$I_{zz}\dot{r} - I_{xz}\dot{p} = N_v V + N_r r + N_\phi \phi + N_p p + N_\delta \delta \tag{2.18}$$

$$\dot{\phi} = p \tag{2.19}$$

$$\underbrace{\begin{bmatrix} M & Mh_1 & 0 & 0 \\ 0 & -I_{xz} & I_{zz} & 0 \\ Mh_1 & I_{xx} & -I_{xz} & 0 \\ 0 & 0 & 0 & 0 \end{bmatrix}}_{\mathbf{m1}} \begin{bmatrix} \dot{V} \\ \dot{p} \\ \dot{r} \\ \dot{\phi} \end{bmatrix} = \underbrace{\begin{bmatrix} Y_v & 0 & Y_r - MU & Y_\phi \\ N_v & 0 & N_r & N_\phi \\ 0 & L_p & L_r Mh_1 U & L_\phi \\ 0 & 1 & 0 & 0 \end{bmatrix}}_{\mathbf{m2}} \begin{bmatrix} V \\ p \\ r \\ \phi \end{bmatrix} + \underbrace{\begin{bmatrix} Y_\delta \\ N_\delta \\ L_\delta \\ 0 \end{bmatrix}}_{\mathbf{m3}} \delta$$

$$K = inv(m1);\ A = K * m2;\ B = K * m3;$$

$$\begin{bmatrix} \dot{V} \\ \dot{p} \\ \dot{r} \\ \dot{\phi} \end{bmatrix} = A \begin{bmatrix} V \\ p \\ r \\ \phi \end{bmatrix} + B\delta$$

B and D matrices are not shown, but they can be anything, depending on the required outputs. Details of the Matlab code for this model are included in the appendix 2.

Nomenclature:

$\frac{\partial \gamma}{\partial \phi}$, Roll camber coefficient

ϕ, Roll angle

$\varepsilon = \frac{\partial \delta}{\partial \phi}$, Roll steer coefficient

L, total roll moment

N, total yaw moment

K, Rotational suspension stiffness

B, Rotational suspension damping

p, Roll rate

h_1, CG height from roll axis

W, Vehicle weight, N

M, Vehicle weight, kg

Y, Lateral force

h_1, CG height from roll axis

U, Forward speed

V, Lateral velocity

r, Yaw rate

p, roll rate

ssf / ssr, Front & rear wheel track

END

3. Theory & Assumption for 4DOF Model (with incline roll axis)

The 2DOF & 3DOF models described earlier use a linear tyre model with a simple suspension system and a constant forward velocity. However, in 4DOF model, the complexity of the model is further increased by introducing an additional degree of freedom for longitudinal dynamics with an inclined roll axis. (Pacejka, 2002). (Milliken & Milliken, 1995), (Genta, 1997)

With the inclusion of the roll centre height (p_1), the longitudinal dynamics is represented as:

$$M(\dot{U} - rV - prh_1) = X \tag{3.1}$$

Other equations are the same as for the case of the 3-DOF model, but for roll and yaw moments the equations are slightly different due to the inclination of the roll axis. The new equations are given below:

$$(I_{xx} - \varepsilon I_{xz})\dot{p} - I_{xz}\dot{r} + M\dot{V}h_1 = -MUh_1 r + L_{susp} + Wh_1\phi \tag{3.2}$$

$$I_{zz}\dot{r} + (-I_{xz} + \varepsilon I_{zz})\dot{p} = N \tag{3.3}$$

And: $\dot{\phi} = p$ to complete the final set of equations.

For this 4-DOF model the generation of lateral and longitudinal tyre forces are further extended by introducing a simple tyre model, which is based on the "Magic Formula" tyre model (Pacejka and Bakker, 1993), which is explained in more detail in Chapter 3.

The state-space representation of this 4-DOF system becomes:

The state-vector is:

$x_1 = U$ – Longitudinal velocity,

$x_2 = V$ – Lateral velocity,

$x_3 = p$ – Roll velocity,

$x_4 = r$ – Yaw velocity,

$x_5 = \phi$ – Roll angle,

From the above equations, left hand sides of the equations ($\dot{X}$) are M_1

$$\text{LHS} = \begin{bmatrix} M & 0 & 0 & 0 & 0 \\ 0 & M & Mh_1 & 0 & 0 \\ 0 & Mh_1 & I_{xx} - \varepsilon I_{xz} & -I_{xz} & 0 \\ 0 & 0 & -I_{xz} - \varepsilon I_{zz} & I_{zz} & 0 \\ 0 & 0 & 0 & 0 & 1 \end{bmatrix} \dot{X}$$

The RHS of the equations must be separated into two terms due to there being more than one state vector. The M_2 matrix consists of no x_4 factor and the M_3 matrix consists of the x_4 factor, thus:

$$M_2 = \begin{bmatrix} 0 & 0 & 0 & 0 & 0 \\ 0 & 0 & 0 & 0 & 0 \\ 0 & 0 & 0 & 0 & Wh_1 \\ 0 & 0 & 0 & 0 & 0 \\ 0 & 0 & 1 & 0 & 0 \end{bmatrix} X$$

$$M_3 = x_4 \begin{bmatrix} 0 & M & Mh1 & 0 & 0 \\ -M & 0 & 0 & 0 & 0 \\ -Mh_1 & 0 & 0 & 0 & 0 \\ 0 & 0 & 0 & 0 & 0 \\ 0 & 0 & 0 & 0 & 0 \end{bmatrix} X$$

For inputs to the system refer to figure 3.1 below.

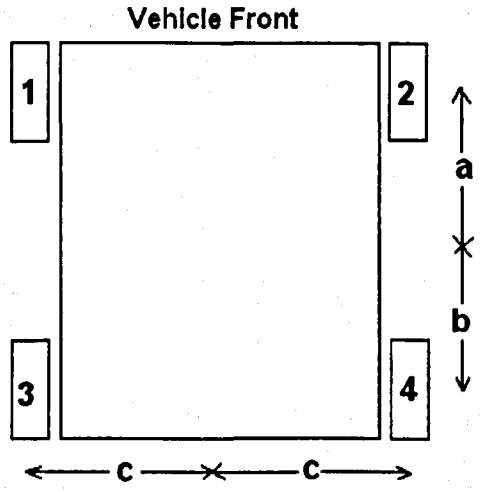

Figure 3.1: The vehicle block

Input, $U = [F_{x1}, F_{x2}, F_{x3}, F_{x4}][F_{y1}, F_{y2}, F_{y3}, F_{y4}][F_{z1}, F_{z2}, F_{z3}, F_{z4}]$

$X = F_{x1}, F_{x2}, F_{x3}, F_{x4};$

$$Y = F_{y1}, F_{y2}, F_{y3}, F_{y4};$$

$$L = F_{y1}(-h_0) + F_{y2}(-h_0) + F_{y3}(-h_0) + F_{y4}(-h_0) + F_{z1}c + F_{z2}(-c) + F_{z3}c + F_{x4}(-c)$$

$$N = F_{x1}c + F_{x2}(-c) + F_{x3}c + F_{x4}(-c) + F_{y1}a + F_{y2}a + F_{y3}(-b) + F_{y4}(-b);$$

$$O = 0;$$

$$M_4 = \begin{bmatrix} 1 & 1 & 1 & 1 & 0 & 0 & 0 & 0 & 0 & 0 & 0 & 0 \\ 0 & 0 & 0 & 0 & 1 & 1 & 1 & 1 & 0 & 0 & 0 & 0 \\ 0 & 0 & 0 & 0 & -h_0 & -h_0 & -h_0 & -h_0 & c & -c & c & -c \\ c & -c & c & -c & a & a & -b & -b & 0 & 0 & 0 & 0 \\ 0 & 0 & 0 & 0 & 0 & 0 & 0 & 0 & 0 & 0 & 0 & 0 \end{bmatrix} U$$

So the state-space representation becomes:

$$M_1 \dot{X} = M_2 X + M_3 X + M_4 U$$

where : $A_1 = M_1^{-1} M_2$

$$A_2 = M_1^{-1} M_3$$

$$B = M_1^{-1} M_4$$

$$\dot{X} = A_1 X + A_2 X + BU$$

Vertical load calculation

These are obtained using figure 3.2. For the front axle:

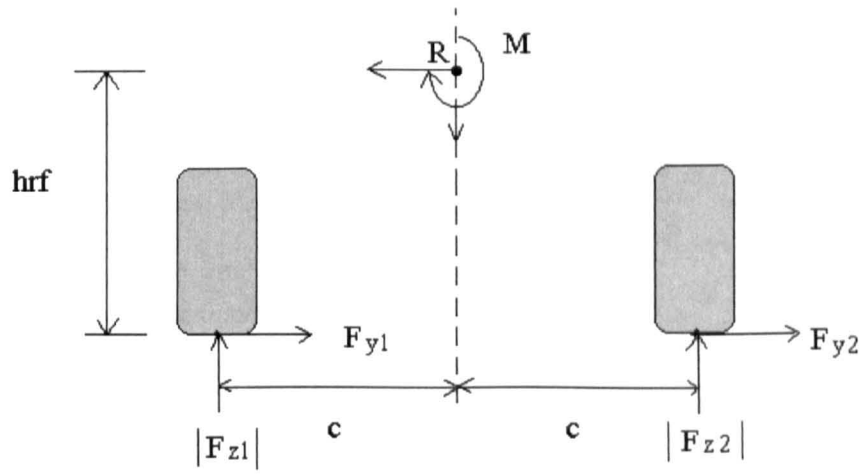

Figure 3.2: Vertical load

M is the roll moment of the suspension about point R (the front roll centre). The suspension roll stiffness and suspension roll damping are given below:

$$L_{susp} = K_{\phi}\phi + B_{\phi}p;$$

Based on Figure 3.7, the roll moment about the front roll centre becomes:

$$L_{susp} + c\left(\left|F_{z1}\right| - \left|F_{z2}\right|\right) - hrf\left(F_{y1} + F_{y2}\right) = 0;$$

$$\left|F_{z1}\right| - \left|F_{z2}\right| = \frac{hrf}{c}\left(F_{y1} + F_{y2}\right) - \frac{1}{c}\left(L_{susp}\right); \tag{3.4}$$

where: $\left|F_{z1}\right| + \left|F_{z2}\right| = W_f$ and W_f is the front load.

$$\left|F_{z2}\right| = W_f - \left|F_{z1}\right| \tag{3.5}$$

Substituting equation (3.57) into (3.58) yields:

$$2\left|F_{z1}\right| - W_f = \frac{hrf}{c}\left(F_{y1} + F_{y2}\right) - \frac{1}{c}\left(L_{susp}\right);$$

$$\left|F_{z1}\right| = \frac{hrf}{2c}\left(F_{y1} + F_{y2}\right) - \frac{1}{2c}\left(L_{susp}\right) + \frac{W_f}{2} \tag{3.6}$$

and:

$$\left|F_{z2}\right| = \frac{-hrf}{2c}\left(F_{y1} + F_{y2}\right) + \frac{1}{2c}\left(L_{susp}\right) + \frac{W_f}{2} \tag{3.7}$$

so the load transfer ($LLTF$) is:

$$LLTF = \frac{hrf}{2c}\left(F_{y1} + F_{y2}\right) - \frac{1}{2c}\left(L_{susp}\right);$$

and, therefore, $\left|F_{z1}\right| = \frac{W_f}{2} + LLTF$ and $\left|F_{z2}\right| = \frac{W_f}{2} - LLTF$

Thus, the total vertical load in matrix form is obtained as:

$$|F_z| = Kload \begin{bmatrix} \phi \\ p \\ F_{y1} \\ F_{y2} \\ F_{y3} \\ F_{y4} \\ W_f/2 \\ W_r/2 \end{bmatrix}$$

where :

$$F_{z1} = \frac{1}{2c}\left[-K_{\phi f}\phi - B_{\phi f}p + hrf\left(F_{y1} + F_{y2}\right)\right] + \frac{W_f}{2}$$

$$F_{z2} = \frac{1}{2c}\left[K_{\phi f}\phi + B_{\phi f}p - hrf\left(F_{y1} + F_{y2}\right)\right] + \frac{W_f}{2}$$

$$F_{z3} = \frac{1}{2c}\left[-K_{\phi r}\phi - B_{\phi r}p + hrr\left(F_{y3} + F_{y4}\right)\right] + \frac{W_r}{2}$$

$$F_{z4} = \frac{1}{2c}\left[K_{\phi r}\phi + B_{\phi r}p - hrr\left(F_{y3} + F_{y4}\right)\right] + \frac{W_r}{2}$$

Kload =

$$\begin{bmatrix} -K_{\phi f}/2c & -B_{\phi f}/2c & hrf/2c & hrf/2c & 0 & 0 & 1 & 0 \\ K_{\phi f}/2c & B_{\phi f}/2c & -hrf/2c & -hrf/2c & 0 & 0 & 1 & 0 \\ -K_{\phi r}/2c & -B_{\phi r}/2c & hrr/2c & hrr/2c & 0 & 0 & 0 & 1 \\ K_{\phi r}/2c & B_{\phi r}/2c & -hrr/2c & -hrr/2c & 0 & 0 & 0 & 1 \end{bmatrix}$$

Refer to Chapter 3 for the calculation of slip-angle, slip ratio, and drive/brake demand.

Nomenclature:

ϕ , Roll angle

ε , Incline roll axis

L , total roll moment

N , total yaw moment

K , Rotational suspension stiffness

B , Rotational suspension damping

h_1 , CG height from roll axis

W , Vehicle weight,N

h_1 , CG height from roll axis

ε , Incline roll axis angle

Appendix 2

Model WS10
with analog or SSI output

Compact sensor for industrial applications

- **Protection class IP65**
- **Measurement ranges:**
  0 ... 100 mm to 0 ... 1250 mm
- **Analog output 0 ... 10 V, 4 ... 20 mA, potentiometer or A/D converted synchronous serial output (SSI)**

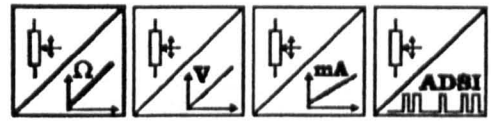

Specifications

Outputs	Potentiometer: 1 kΩ Voltage: 0...10 V Current: 4...20 mA, 2 or 3 wire Voltage and current output, adjustable A/D converted synchronous serial 16 bit max. (SSI)
Resolution	Essentially infinite / ADSI16: max. 16 bit full scale
Material	Aluminium and stainless steel. Cable: stainless steel
Sensing Device	Precision potentiometer
Connector	Male socket 8 pin (M12 or DIN 45326)
Linearity	Up to ±0.05 % full scale
Protection Class	IP65 (only when the electrical plug is correctly assembled and connected)
Weight	800 g approx.
Environmental	
EMC	Refer to output specification
Temperature	Refer to output specification

Order Code WS10 Analog or SSI

WS10 - □ - □ - □ - □ - □

Model Name

Measurement Range (in mm)
100 / 125 / 375 / 500 / 750 / 1000 / 1250

Outputs (see pages 57 ff.)

R1K	= Potentiometer 1 kΩ (other values on request)
10V	= With 0 ... 10 V signal conditioner
420A	= With 4 ... 20 mA signal conditioner (2 wire)
420T	= With 4 ... 20 mA signal conditioner (3 wire)
PMU	= With 0...10 V/4...20 mA signal conditioner, adjustable
ADSI16	= With A/D converted synchronous serial output 16 bit (option: 12, 14 bit)

Linearity
L10 = ±0.10 % option: L05 = ±0,05 % L25 = ±0.25 %

Cable fixing

M4	= M4 cable fixing
SB0	= Cable clip

Connection

M12	= 8 pin socket M12
D8	= 8 pin socket DIN 45326

Order Code Mating Connector (see accessories p. 82) **D8:** CONN-DIN-8F-W **M12:** CONN-M12-8F-G

Order Example: WS10 - 1250 - 10V - L10 - M4 - M12

Model WS10
with analog or SSI output

Cable Forces
typical at 20 °C

Range	Maximum pull-out force	Minimum pull-in force
mm	[N]	[N]
100	4.7	3.0
125	4.6	2.4
375	7.4	3.9
500	5.5	2.8
750	7.6	3.8
1000	5.3	2.9
1250	4.6	2.4

Outline drawing

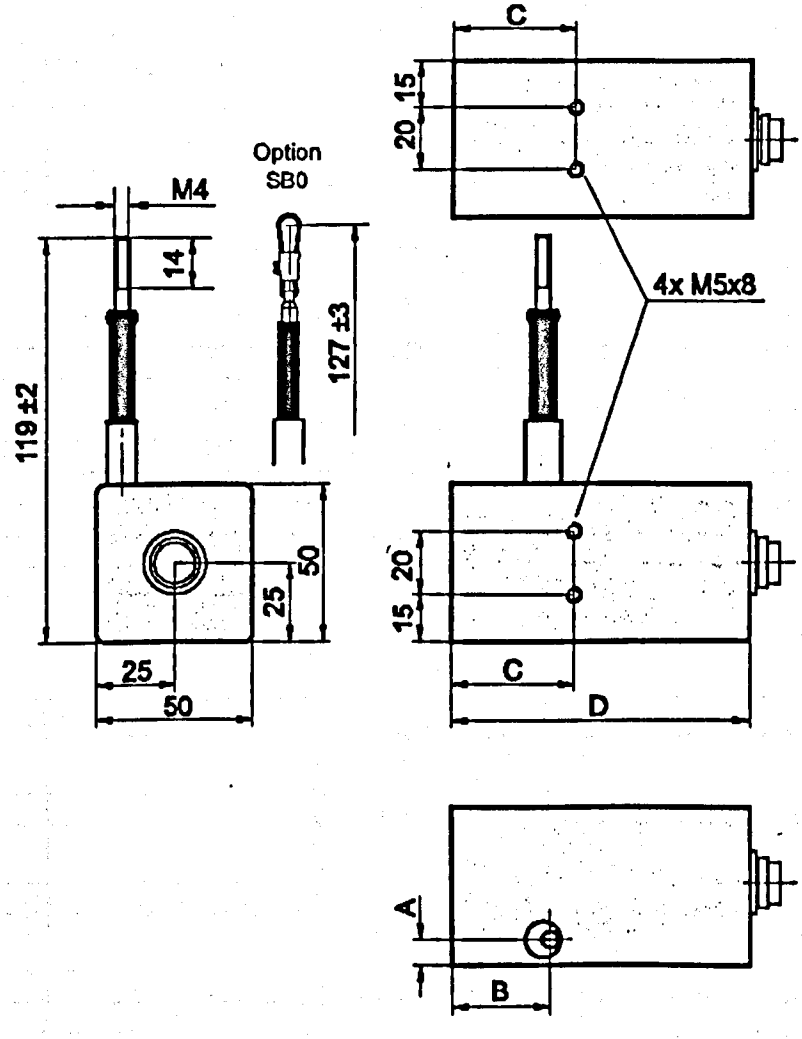

Dimensions informative only.
For guaranteed dimensions consult factory

Dimensions (mm)

Range	A	B, C	D (ADSI16)
375; 750	12.5	B=31, C=38.5	93.5 (120.5)
100; 125; 500	8.0		
1000; 1250	8.0		

50 L, 34 L

Vishay Sfernice

Precision Linear Transducers, Conductive Plastic (REC)

FEATURES

- Measurement Range 25mm to 450mm
- High accuracy ± 1% down to ± 0.025%
- Essentially infinite resolution
- Long life
- Sealed on request

The 50 L and 34 L are compact, accurate and adaptable motion transducers for both industrial and military markets.

ELECTRICAL SPECIFICATIONS		
	50 L	**34 L**
Theoretical electrical travel (TET = E) **in increments of 25mm**	25mm 300mm	25mm 450mm
Independent linearity (over TET) on request	≤ ±1% - ≤ ± 0.1% ≤ ± 0.05% for E ≥ 100mm ≤ ± 0.025% for E ≥ 200mm	
Actual electrical travel (AET)	see table 1	
Ohmic values (RT)	400Ω/cm to 2kΩ/cm	
Resistance tolerance at 20°C	± 20%	
Repeatability	≤ 0.01%	
Maximum power rating	0.05W/cm at 70°C, 0W at 125°C	
Wiper current	recommended: a few µA - 1mA max. continuous	
Load resistance	minimum 10^3 x R_T	
Number of tracks	1; on request 2	
Insulation resistance	≥ 1000MΩ	500VDC
Dielectric Strength	≥ 500VRMS 50Hz	≥ 750VRMS 50Hz

MECHANICAL SPECIFICATIONS		
	50 L	**34 L**
Mechanical travel	TET + 2mm min.	
Housing	anodized aluminium	
Operating force on request	0.35N typical (standard model)	2.50N typical (sealed model)
Shaft (free rotation)	stainless steel	
Termination on request	3 wires PTFE AWG-30 L = 300mm cable or connector	
Wiper	precious metal multifinger	
Sealing	IP65 on request	

PERFORMANCE	
Operating life	50 million cycles typical
Temperature range	- 55°C + 125°C
Sine vibration on 3 axes	1.5mm peak to peak or 15g - 10 Hz - 2000Hz
Mechanical shocks on 3 axes	50g - 11ms - half sine

STANDARD MODEL DIMENSIONS in millimeters, general tolerance ± 1mm

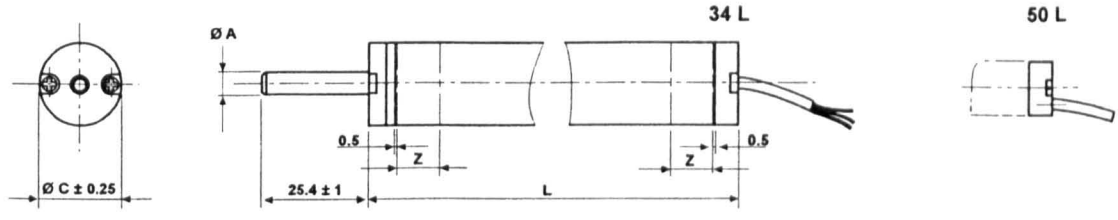

ELECTRICAL CONNECTIONS

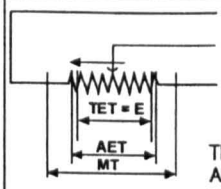

Terminals	wire	cable
3 Alim. (+):	green	blue
2 Wiper:	red	red
1 Alim. (-):	yellow	white

TET = Theoretical electrical travel
AET = Actual electrical travel
MT = Mechanical travel

Table 1

TET = E	AET	TOL.
25mm to 275mm	E + 1mm	± 0.5mm
300mm to 450mm	E + 1mm	± 0.8mm

Table 2

DIMENSIONS		50 L	34 L
Shaft	øA	- 0 3.175 - 0.025	- 0 5 - 0.025
Body	øC	12.7	19.05
Body Length	L	E + 41	E + 63
Tightening Zone	Z	7	12

ACCESSORIES ON REQUEST - DIMENSIONS in millimeters, general tolerance ± 3mm

Clamp for 34L
Vishay Reference: CQ00051

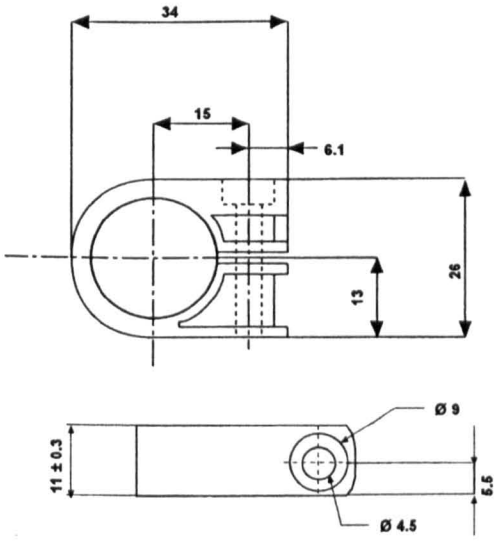

Clamp for 50L
Vishay Reference: CQ00050

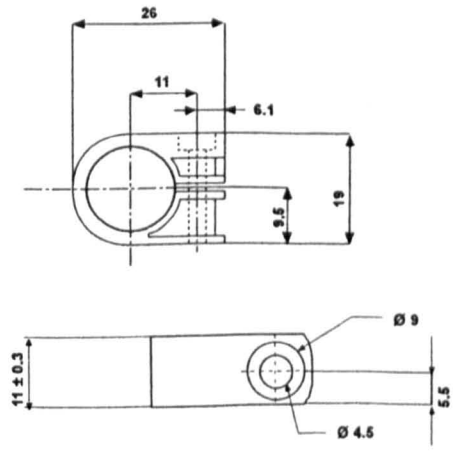

OPTIONS - DIMENSIONS in millimeters, general tolerance ± 1mm

OPTION 1: SEALED (IP65)

W03280 (34 L)
W03242 (50 L)

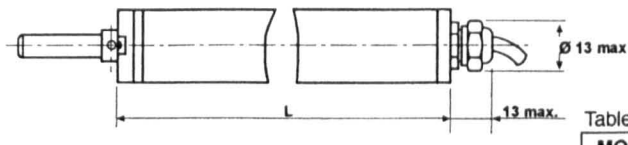

Table 3

MODEL	L
34 L	TET + 83.5
50 L	TET + 70.5

OPTION 2: DELIVERED WITH CLAMPS AND BINDER CONNECTOR 680

34 L ... W05013

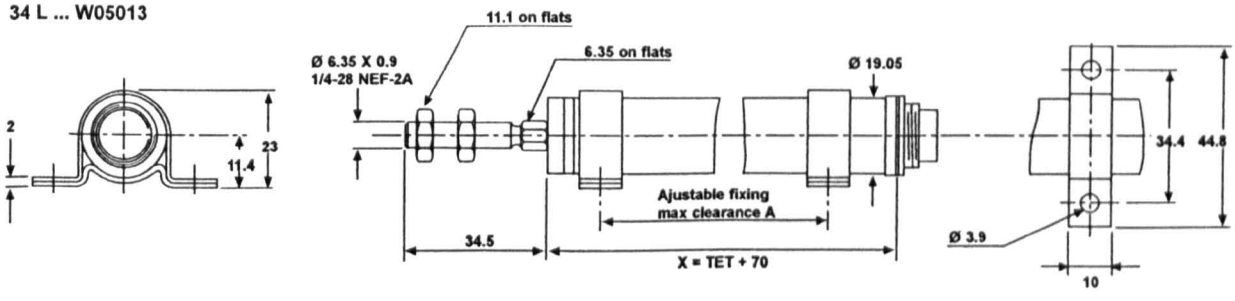

OPTION 3: SPRING LOADED SHAFT; OUTPUT BY SHIELDED CABLE

W01744 (34 L)
W01743 (50 L)

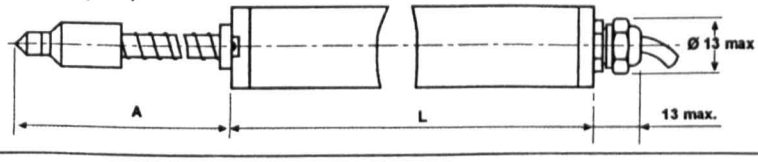

Table 4

MODEL	A	L
34 L1	61.4	TET + 119.5
34 L2	93.6	
34 L3	125.8	
34 L4	158	
50 L1	70	TET + 97.8
50 L2	116	
50 L3	162	
50 L4	208	

OPTION 4: DOUBLE BALL JOINT

W03263 (34 L)
W01565 (50 L)

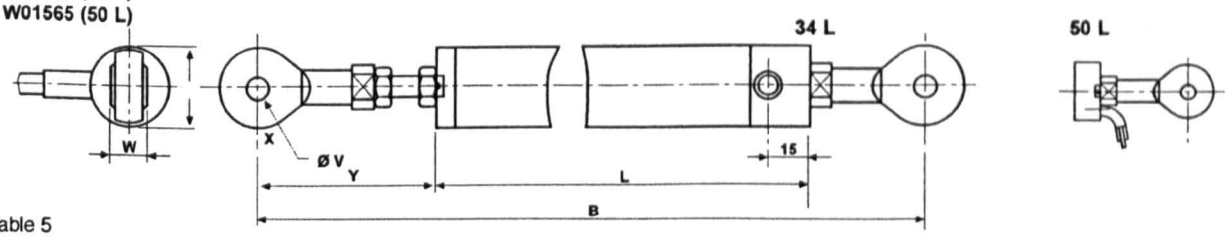

Table 5

MODEL CODE		B	L	øV	W	X	Y	TET
50 L W01565	L1 to L3	TET + 108.5	TET + 57.5	3	6	12	30 ± 2	25 to 75
	L4 to L6	TET + 133.5	TET + 82.5	3	6	12	30 ± 2	100 to 150
34 L W03263	L1 to L5	TET + 151.6	TET + 82.8	5	8	18	42 ± 2	25 to 125
	L6 to L10	TET + 173.6	TET + 104.8	5	8	18	42 ± 2	150 to 250
	L11 to L12	TET + 230	TET + 161.2	5	8	18	42 ± 2	275 to 300

ORDERING INFORMATION

REC	34	L	3	D	103	W...
SERIES	MODEL	NUMBER OF TRACKS	THEORETICAL ELECTRICAL TRAVEL	LINEARITY	OHMIC VALUE	MODIFICATIONS
		L = 1 track LL = 2 tracks	Times 25mm	A : ± 1 % D: ± 0.1% E: ± 0.05% F: ± 0.025%	First 2 digits are significant numbers 3rd digit indicates number of zeros	Special feature code number

Schaevitz™ Linear Servo Sensor Technology

DC-Operated Accelerometers

ATTN. RAY PINCHIN
FROM. JOHN CURIO

Features

- *Ranges ±0.25g to ±20g*
- *Closed loop force balance system*
- *Self test facility*
- *DC input – DC output*
- *High reliability*
- *Manufactured to ISO 9001 standards*
- *Flight qualified versions available*

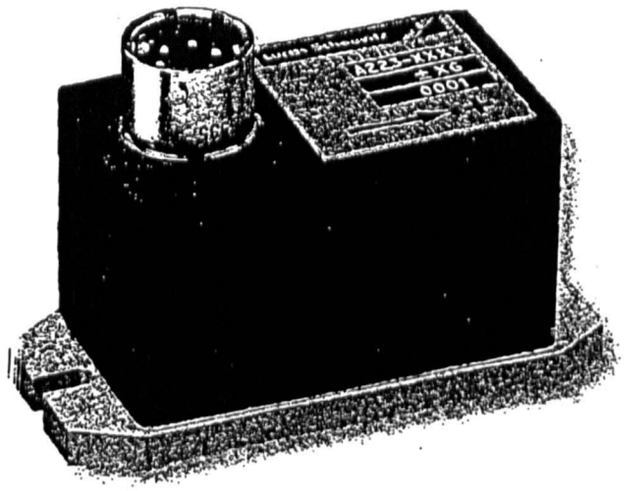

Introduction

The Schaevitz range of Servo Accelerometers measure vector acceleration with high accuracy using a closed loop force balance torquer mechanism.

Typical applications include data acquisition systems, crash recorders, guidance systems for torpedoes, missiles and related military devices; for stabilising platforms on space and ship borne satellite tracking systems; monitoring and controlling deceleration in mass transit systems; road bed analysis and fault detection equipment for high speed railways; military and civil flight simulators; autopilots and low frequency vibration monitoring.

In addition to the instruments offered in this bulletin Schaevitz design accelerometers for specific applications. These custom designed units can be manufactured and tested to conform with military standards.

All A200 Series Accelerometers operate as a closed-loop torque balance servo system. With reference to the illustration below the pendulous mass 'A' develops a torque proportional to the product of its mass unbalance and the applied acceleration.

The movement of mass 'A' is detected by position sensor 'B' whose output signal is connected to an amplifier. The resulting current is fed into the torquer motor 'C' which then develops a torque exactly equal to, but directly opposed to the initial torque from the pendulous mass 'A'. Mass 'A' stops moving, assuming a position minutely differing from its zero 'g' position. Simultaneously, the current to the torquer motor is fed through a stable resistor to provide an output voltage proportional to the applied acceleration.

The system is damped by means of a phase advancing network within the integrated thick film module. The A200 series servo operation can be checked (self test) after installation by applying an independent current input to the torquer motor.

By adjusting the parameters of the servo amplifier and related electronic networks, the operating characteristics of a servo accelerometer can be changed or modified to suit a particular application.

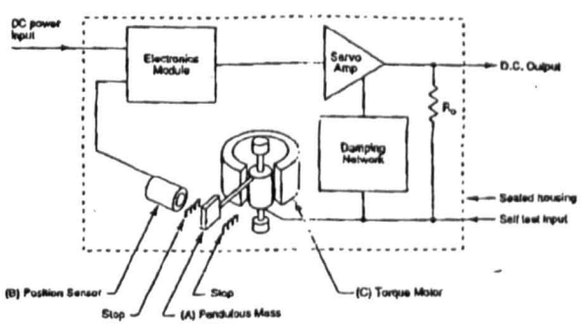

A215/220 Series
DC Operated
Linear Servo
Accelerometers

Designed for operation from a 15-0-15 DC power supply the A200 series is available in 2 versions. The A215 has a volume of approximately one cubic inch and is intended for use where space is limited. Electrical termination is via glass/metal solder pins. The A220's larger size allows for solder pin or connector termination and options such as bias, or low impedance outputs.

General Specification

Input

Ranges (±g)	0.25; 0.5; 1.0; 2.0; 5.0; 10.0; 20.0
Input Voltage	15-0-15V (±10%) dc
Input Current	25mA dc max.

Output at 25°C

FS Range Output	±5V dc ±1%
Zero Offset	≤±0.1% F.R.O.
Nonlinearity	≤±0.05% F.R.O./LMS (ranges to 10g) ±0.10% F.R.O. (ranges above 10g)
Hysteresis	≤0.02% F.R.O.
Resolution	≤0.0005% F.R.O.
Cross Axis Sensitivity	≤±0.002g/g (ranges to ±10g) ≤±0.005g/g (ranges over ±10g)
Noise Output	5mV (RMS) max.
Damping Ratio	0.6 (±0.1)

Range (g)	Natural Frequency (nom.-Hz)	Output Impedance (kilohms)
±0.25	36	20
±0.50	45	10
±1.0	90	5
±2.0	100	2.5
±5.0	115	5
±10.0	130	2.5
±20.0	150	5

Environmental

Temp. Operating	-55°C to +95°C
Storage	-65°C to +105°C
Thermal Sensitivity Shift	≤±0.02% F.R.O./°C
Thermal Zero Shift	≤±0.002% F.R.O./°C
Altitude	-45 to +30,450 metres without damage
Shock	100g for 11m. sec. (½ sine wave)
Acceleration	Will withstand constant 100g in all 3 axis without damage
Humidity/Immersion	IP65
Insulation Resistance	≥20 Meg. ohm at 50V dc

Physical

Sensitive Axis Alignment	Parallel to fixing holes within ±0.2°
Weight	57 grammes – A210 115 grammes – A220

Electrical Connections

Pin Connection (0.6mm dia. x 3mm long)
Pin A – +15V dc excitation
Pin B – 0V dc excitation/output
Pin C – 15V dc excitation
Pin D – ±5V dc output
Pin E – Current output
Pin F – Self Test

DESIGNATION AND ORDERING CODE

A2 □ □ - □ □ 01

Series Number

1. Miniature
2. Standard

*3. Electrical Connector
5. Solder Pin

0. Standard Unit
*3. 1g Bias
0. Standard Unit
1 Customer Special

*Not available for A210 Series

A215 Series Dimensional Drawing (mm)

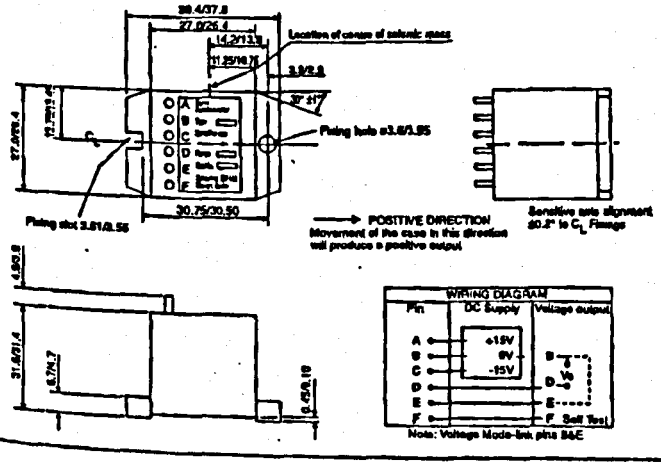

A220 Series Dimensional Drawing (mm)

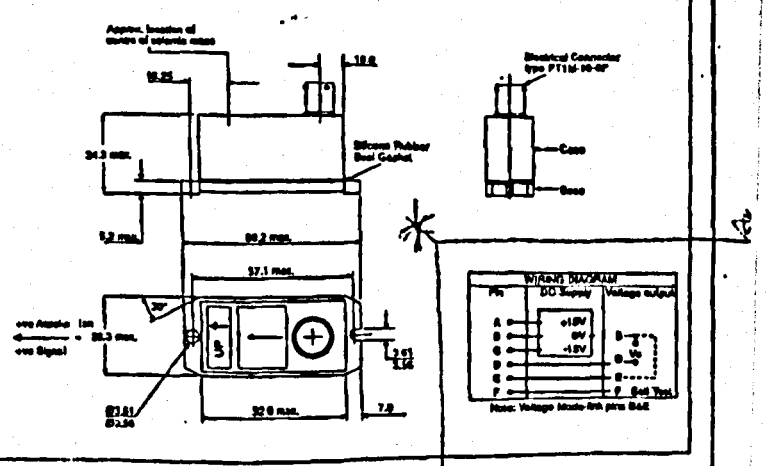

Model 830, 860

Vishay Spectrol

1 - 13/16" (46mm) Three and Ten Turn Wirewound Precision Potentiometer

FEATURES

- 830: 15Ω to 50KΩ, Three-Turn
- 860: 20Ω to 200KΩ, Ten-Turn

ELECTRICAL SPECIFICATIONS

PARAMETER	MODEL 830	MODEL 860
Total Resistance Standard Range Tolerance: 200Ω and above Below 200Ω	 15Ω to 50KΩ Special to 150KΩ STANDARD ± 3% ± 5%	 20Ω to 200KΩ Special to 500KΩ SPECIAL ± 1% ± 3%
Linearity (Independent)	± 0.25% standard	
15Ω to 1KΩ 1KΩ to 5KΩ 5KΩ to 25KΩ 25KΩ and above 20Ω to 50Ω 50Ω to 200Ω 200Ω to 5KΩ 5KΩ and above	± 0.15% ± 0.10% ± 0.075% ± 0.05% – – – –	– – – – ± 0.15% ± 0.10% ± 0.05% ± 0.025%
Noise	100Ω ENR for both models	
Rotation	1080° + 4° - 0°	3600° + 4° - 0°
Power Rating	3.0 watts at 40°C derated to zero at 125°C	8.0 watts at 40°C derated to zero at 125°C
Insulation Resistance	1000MΩ minimum 500VDC	
Dielectric Strength	$1000V_{RMS}$, 60Hz	
Absolute Minimum Resistance	Not to exceed linearity x total resistance or 1Ω, whichever is greater	
End Voltage	0.5% of total applied voltage maximum	
Phasing	CCW End Points sect. 2 phased to sect 1 within 1°	
Taps (Extra)	42 available as special standard tolerance ± 1°	108 available as special standard tolerance ± 1°

ORDERING INFORMATION

Models 830 and 860 can be ordered from this data sheet with a variety of alternate characteristics, as shown. For most rapid service on your order, please state:

830, 860	**1**	**1**	**XXX**
MODEL	BUSHING MOUNT	NUMBER OF SECTIONS	RESISTANCE OF EACH SECTION Beginning with the section nearest the mounting end

Other characteristics will be standard as described on this data sheet. If special characteristics are required, such as: special linearity tolerance, special resistance tolerance, extra taps, non-linear functions, etc., please state these on your order and allow additional lead time for delivery.

Model 830, 860

Vishay Spectrol 1 - 13/16" (46mm) Three and Ten Turn Wirewound Precision Potentiometer

MATERIAL SPECIFICATIONS	
Bushing	Aluminum, nickel plated
Housing and Front Lid	Molded glass filled thermoset plastic
Rear Lid	Molded glass filled nylon
Shaft	Stainless steel, non magnetic, non-passivated
Terminals	Brass, plated for solderability
Mounting Hardware Lock washer: Panel nut:	 Internal tooth Steel, nickel plated Brass, nickel plated

MARKING	
Unit Identification	Units will be marked with Spectrol name and model no, resistance and resistance tolerance, linearity, terminal identification, and date code

ENVIRONMENTAL SPECIFICATIONS	
Vibration	10g thru 500 CPS
Shock	50g
Rotational Life	500,000 shaft revolution
Load Life	900 Hours
Temperature Range	- 55°C to + 125°C
Moisture Resistant	–
Salt Spray	48 hours

POWER RATING CHART

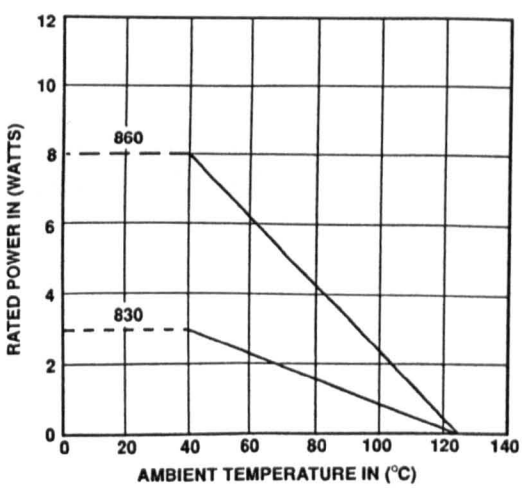

RESISTANCE ELEMENT DATA					
STANDARD RESISTANCE VALUES (Ω)	RESOLUTION (%)	OHMS PER TURN	MAXIMUM CURRENT AT 70°C AMBIENT (mA)	MAXIMUM VOLTAGE ACROSS COIL (V)	WIRE TEMP. COEF. (ppm/°C)
MODEL 860					
20	0.044	0.009	632	13	800
50	0.027	0.014	400	20	800
100	0.024	0.024	283	28	800
200	0.028	0.056	200	40	180
500	0.023	0.115	126	63	20
1K	0.018	0.182	89	89	20
2K	0.020	0.402	63	126	110
5K	0.015	0.754	40	200	20
10K	0.013	1.23	28	283	20
20K	0.010	1.97	20	400	20
50K	0.007	3.69	13	632	20
100K	0.007	6.51	8.9	894	20
200K	0.005	9.63	5.0	1,000	20
500K	0.004	20.0	2.0	1,000	20
MODEL 830					
20	0.094	0.019	387	8	800
50	0.074	0.037	245	12	800
100	0.071	0.071	173	17	180
200	0.072	0.145	122	25	20
500	0.064	0.320	77	39	110
1K	0.050	0.500	55	55	110
2K	0.047	0.948	39	77	20
5K	0.035	1.73	24	125	20
10K	0.029	2.92	17	176	20
20K	0.024	4.80	12	250	20
50K	0.017	8.31	8	375	20
100K	0.015	14.5	5	600	20
150K	0.013	20.0	4	750	20

Digital, Magnetic Pick-Up

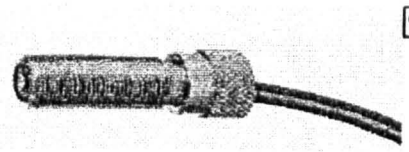

Quick Tip
Click on the picture or this icon to see a better quality image of this product

	stock no.	price each 1+	6+	
Order	304-172	£24.02	£22.35	Tech. Info.

(April 2005 Catalogue page 1-1363)

Miniature magnetic 'pick-up' transducers suitable for use in a very wide range of sensing applications. Each device resp movement of ferrous parts past the pole-piece on the end of the unit. Used extensively in areas such as speed regulatic motors, when sensing, for example, the teeth on a gear wheel. However, magnetic pick-ups may be used to implement and control functions in many fields. Automotive applications include crank angle sensing, ignition timing, anti-skid syste diagnostics. Applications in the computer peripherals area encompass disc drives, line printers, card punches/readers a terminals. The diagrams indicate the two basic modes of using these components. Note especially their small size in rel their high signal output, enabling their deployment where many conventional sensors cannot be fitted. Fully encapsulate construction for reliable operation, but not intended for immersion in liquids.

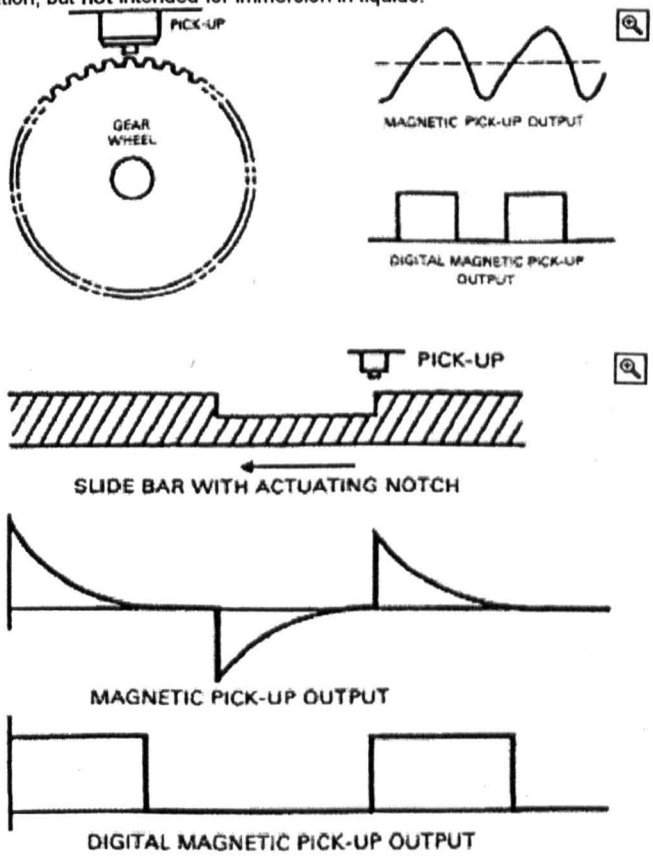

The analogue output style of these transducers is available in three sizes 1/4 in. (std.), 3/8 in. (high o/p) and 5/8 in. heav They offer an inexpensive solution wherever a simple alternating waveform corresponding to movement past the pole p required. They are passive devices requiring no external power. They yield an output voltage in response to variations i induced magnetic field caused by proximity to moving ferrous metal parts. They are steel encased for ruggedness and a supplied with two fixing nuts. The standard model interfaces directly with tachometers IC type 302-047 but the high o/p may overload it at speeds greater than 10 000 r.p.m.

Note: output voltage is given for a load of 100k Ohms with a 0·005in. air gap at 20kHz operation. This corresponds quit the pick up being 0·13mm from a 38mm diameter gear wheel with 30 teeth revolving at 13 000 r.p.m. This output will be with other conditions and will be influenced by the composition of the gear wheel teeth. In unusual conditions it should b determined by experiment noting the following points:

- Use the pick up with a high impedance load
- Position the pick up as close as is safe to the moving parts, clearances up to 2·5mm are quite normal

- In a geared system, use the pick up with the highest speed gear wheel

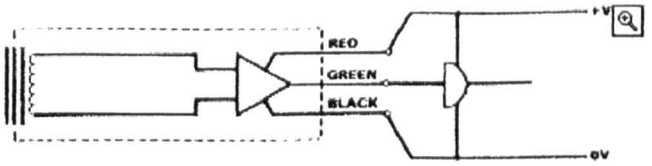

An 'active' version of the standard type (304-166) but incorporating an IC to provide a digital output compatible with mos systems.

- Requires a peripheral speed greater than 250mm per second to operate
- Rise and fall times and amplitude of the output pulse are independent of the characteristics and speed of disco
- Note; NOT polarity protected, any momentary reversal of the supply voltage will destroy the device

technical specification

Supply voltage:	+5V to +15V
Output voltage:	$V_o = \frac{V_S R_L}{R_L + 5000}$
Load resistance:	1 kΩ min.
Output rise time:	1 µs max.
Output fall time:	50 ns max.
Operating temp:	-25°C to +85°C
Clearance from peripherals	Up to 2.5mm

SOLID STATE TECHNOLOGY

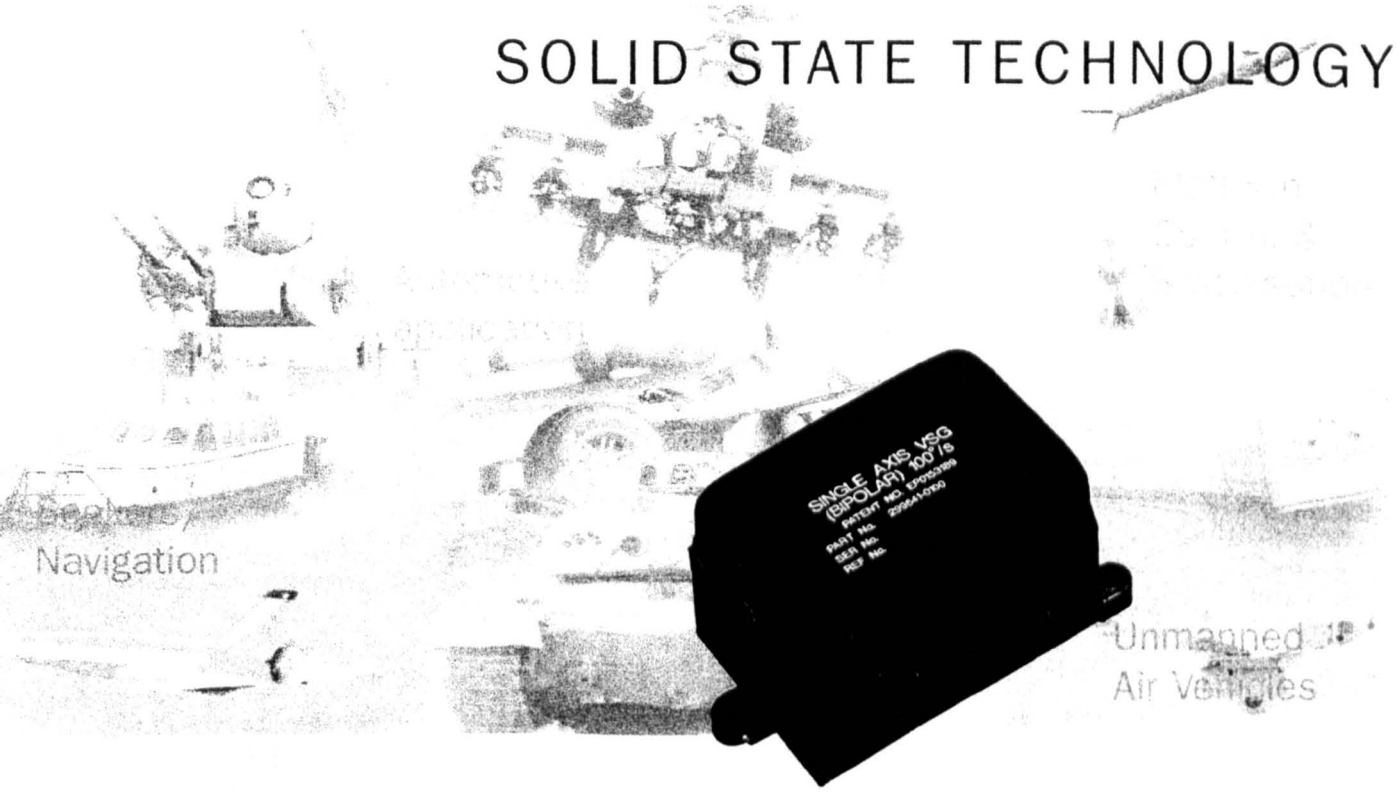

CAPABILITY **BAE SYSTEMS is Europe's leading supplier of precision motion sensors and sensing systems incorporating a full range of technologies. With an 80 year pedigree in this field there is a lifetime commitment to sensor development, innovation, manufacture and support for a wide variety of military and commercial customers globally.**

The company offers a combination of mechanical and solid state motion sensing solutions designed to meet customers needs.

The VSG (Vibrating Structure Gyroscope), is a solid state rate sensor which makes use of the coriolis effect to detect angular rate. It comprises a single axis sensing element and electronics in an easy-to-use package. The sensing element is a shell type vibrating structure, which in this case is a piezoceramic cylinder. The self contained electronics provide the drive, control, demodulation and filtering circuitry for the instrument.

Significant features:

- Low unit price
- Robust, no moving parts
- Long life
- Various rate ranges available
- Self contained analogue unit
- Excellent noise and bias performance
- Low power requirement
- Suitable for harsh environments
- Over 8000 units sold to date
- dc in dc out system

Applications include:

- Unmanned Air Vehicles
- Missile systems
- Platform stabilisation
- Gun fire control systems
- Oceanographic survey equipment
- Robotics
- Tilting trains
- Automotive industry

BAE SYSTEMS

TYPICAL PERFORMANCE GUIDE

Description	Solid State Rate Sensor
Number of Axes	1
Rate Ranges	50, 100, 200, 500, 1000°/s
Output	DC Voltage (Bipolar or Unipolar)
Scale Factor	
Nominal	50mV/°/s
Linearity	0.4% FS
Variation with temperature	+1 to -6%
Repeatability	± 2%
Bias	
Setting (@ 20°C)	± 2°/s
Variation with temperature	± 5°/s
Stability	± 0.3°/s
Repeatability	0.3°/s
g sensitivity	± 0.005°/s/g
Bandwidth (-90° phase shift)	75Hz
Quiescent Noise (1Hz to 100Hz)	0.02°/s rms
Environment	
Operating temperature	-30°C to +60°C
Humidity	70% ± 10% RH
Vibration (operational)	10g rms (20Hz to 2KHz)
Shock (operational)	500g (11ms, 1/2 sine)
Mass	135 grams
Electrical	
Supply voltage	± 15V
Supply current	80mA
General	
Built-in test	No
Start-up time	300ms
Temperature output	2.1mV/°C (630mV @ 25°C)
MTBF	50,000 + hrs

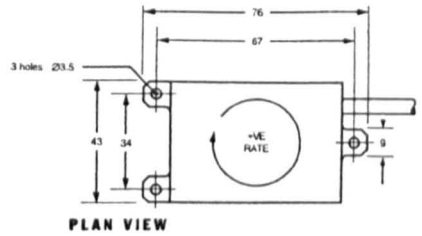

PLAN VIEW

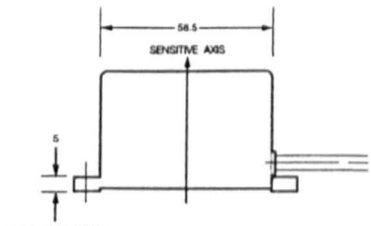

SIDE VIEW

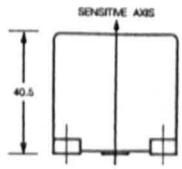

END VIEW

FOR MORE INFORMATION CONTACT

Rest of the World
Sales and Marketing
Rotating Sensors
T +44 (0) 1752 722103
F +44 (0) 1752 695485
E rotating.sensors@baesystems.com

North American Office
Sales and Marketing
T + (817) 738-9980
F + (817) 377-0553
E charlie.hopper@baesystems.com
www.base-usa.com/sensor

BAE SYSTEMS Clittaford Road Southway Plymouth Devon PL6 6DE United Kingdom
Telephone +44 (0) 1752 695695 Fax +44 (0) 1752 695500 www.baesystems.com

Appendix 3

List of Research Publications

(a)- In scientific Journals:

1- **M.Azman**, H. Rahnejat, P.D. King and T.J. Gordon,
"Influence of anti-dive and squat geometry in combined vehicle bounce and pitch dynamics", *Proc. Instn. Mech. Engrs., Part K: Journal of Multi-body Dynamics, Vol. 218, 2004, pp. 231-242.*

2- **M. Azman**, P.D. King and H. Rahnejat,
"Transient analysis of vehicular pitch plane dynamics, subject to road events and driver actions",
Int. J. Veh. Design, submitted, March 2005 (in review process)

(b)- In Conferences

5- **M. Azman**, T.Gordon and H. Rahnejat
"Suspension and road profile effects in vehicle pitch plane response to transient braking and throttle actions",
Proc. 18th IAVSD Conference, Tokyo, Japan, August 2003.